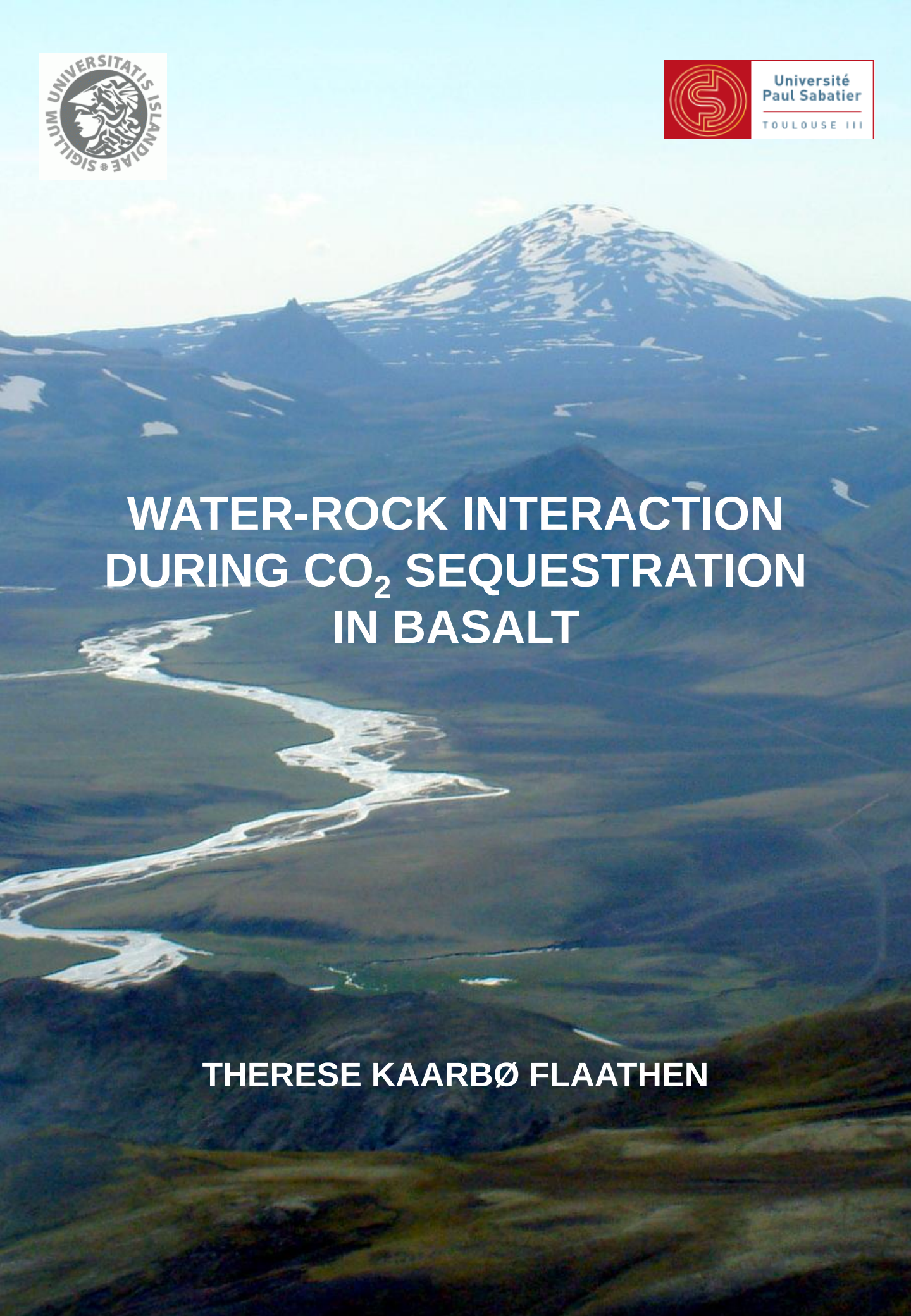

WATER-ROCK INTERACTION DURING CO_2 SEQUESTRATION IN BASALT

THERESE KAARBØ FLAATHEN

Dissertation for the Degree of Doctor of Philosophy

Water-Rock Interaction During CO_2 Sequestration in Basalt

(Étude de l'Interaction Eau-Basaltes Lors d'Injection de CO_2)

Therese Kaarbø Flaathen

Reykjavik, Iceland
September 3rd 2009

University of Iceland
School of Engineering and Natural Sciences,
Faculty of Earth Sciences
&
Université III Toulouse – Paul Sabatier
Laboratoire des Mécanismes et Transferts en Géologie

Academic Dissertation

A Dissertation Presented to the University of Iceland Faculty of Earth Science and to Université III Toulouse, Paul Sabatier, in Candidacy for the Degree of Doctor of Philosophy in Geology

Supervisors

Dr. Sigurður R. Gíslason
School of Engineering and Natural Sciences
Institute of Earth Sciences
University of Iceland, Reykjavik, Iceland

Dr. Eric H. Oelkers
Université III Toulouse, Paul Sabatier
Observatoire Midi-Pyrénées/LMTG

Doctoral Committee

Dr. Sigurður R. Gíslason
School of Engineering and Natural Sciences
Institute of Earth Sciences
University of Iceland, Reykjavik, Iceland

Dr. Eric H. Oelkers
Université III Toulouse, Paul Sabatier
Observatoire Midi-Pyrénées/LMTG

Dr. Stefán Arnórsson
School of Engineering and Natural Sciences
Institute of Earth Sciences
University of Iceland, Reykjavik, Iceland

Opponents

Dr. Halldór Ármannsson
Iceland Geosurvey
Reykjavik, Iceland

Dr. Yousif K. Kharaka
US Geological Survey
Menlo Park, CA, USA

Dr. Luigi Marini
Department for the Study of the Territory and its Resources
University of Genoa, Italy

Jury

Dr. Pierre Agrinier
Institute de Physique de Globe de Paris, France

Dr. Stefán Arnórsson
School of Engineering and Natural Sciences
Institute of Earth Sciences
University of Iceland, Reykjavik, Iceland

Dr. Halldór Ármannsson
Iceland Geosurvey
Reykjavik, Iceland

Dr. Kevin Burton
Université de Toulouse III – Paul Sabatier
Toulouse, France

Dr. Sigurður R. Gíslason
School of Engineering and Natural Sciences
Institute of Earth Sciences
University of Iceland, Reykjavik, Iceland

Dr. Yousif K. Kharaka
US Geological Survey
Menlo Park, CA, USA

Dr. Luigi Marini
Department for the Study of the Territory and its Resources
University of Genoa, Italy

Dr. Eric H. Oelkers
Université III Toulouse, Paul Sabatier
Observatoire Midi-Pyrénées/LMTG

Water-Rock Interaction During CO_2 Sequestration in Basalt

Printed by Oddi, Reykjavik, Iceland, 2009
ISBN 978-9979-9914-1-0

Abstract

The potential dangers with increased concentration of CO_2 in the atmosphere, such as climate changes and sea level rise, have lead to an interest in CO_2 sequestration in geological formations. The thermodynamically most stable way to store carbon is as carbonate minerals. Carbonate mineral formation, however, requires divalent cations originating from a non-carbonate source. One such source is basaltic rocks which contain high concentrations of Ca^{2+}, Mg^{2+} and Fe^{2+}. The potential for forming carbonate minerals through the injection of CO_2 into basalt is under investigation in Iceland and several other places around the world. The aim of this thesis is to help optimize carbonate mineral precipitation in basalts during CO_2 injection through a series of related field and laboratory studies.

A detailed study of the chemical composition of the groundwater surrounding the Mt. Hekla volcano in south Iceland was performed to assess fluid evolution and toxic metal mobility during CO_2-rich fluid basalt interaction. These fluids provide a natural analogue for evaluating the consequences of CO_2 sequestration in basalt. The concentration of dissolved inorganic carbon in these groundwaters decreases from 3.88 to 0.746 mmol/kg with increasing basalt dissolution while the pH increases from 6.9 to 9.2. This observation provides direct evidence of the potential for basalt dissolution to sequester CO_2. The concentrations of toxic metals in these waters are low and reaction path modeling suggests that calcite and Fe(III) (oxy)hydroxides scavenge these metals as the fluid phase is neutralized by further basalt dissolution.

The rate limiting step for mineralization of CO_2 in basalt is thought to be the release of divalent cations to solution through basaltic glass dissolution. The dissolution rate of basaltic glass can be increased by adding ligands which complex aqueous Al^{3+}. Aqueous SO_4^{2-} can complex Al^{3+} and the effect of SO_4^{2-} on the dissolution rate of basaltic glass was studied using mixed flow reactors at $3 < pH < 10$ at 50 °C. Moreover, sulphur is often present in the flue gases of power plants and their disposal also poses an environmental challenge. If possible, co-injection of sulfur with CO_2 could provide a novel cost effective disposal method for industrial generated sulphur. Consistent with current models describing basaltic glass dissolution by aqueous solution composition, results show that SO_4^{2-} increases the dissolution rate of the glass in acidic conditions, while no effect was found in alkaline solutions. These results suggest both that 1) co-injection of sulfate may accelerate CO_2 mineralization in basalts, and 2) existing kinetic models provide an accurate description of basaltic glass dissolution.

To further assess the potential effect of SO_4^{2-} on the precipitation rate of carbonates, steady-state rates of calcite precipitation were measured in mixed flow reactors at 25 °C and pH ~9.1. The results show that 0.005 M Na_2SO_4 decreases the precipitation rate of calcite by ~40%. This result suggests that co-injected sulphate could slow calcite precipitation in the subsurface at pH conditions typical of calcite precipitation. Further experiments are planned to completely define these effects at conditions expected at subsurface CO_2 injection sites.

Ágrip

Áhugi á bindingu koltvíoxíðs í bergi, í svokölluðum karbónat steintegundum eða karbónötum, hefur vaxið hratt undanfarin ár vegna hækkandi styrks koltvíoxíðs í andrúmslofti, sem getur leitt til loftslagsbreytinga og sjávarborðshækkana. Efnavarmafræðilega er binding kolefnis í steini stöðugasta bindingarform kolefnis. Til þess að mynda karbónöt, sem leiðir til bindingar koltvíoxíðs, þarf tvígildar katjónir, og þær þurfa að rekja uppruna sinn til annarra bergtegunda en karbónata. Bergtegundin basalt er ein slík bergtegunda, en basaltið er ríkta af tvígildu katjónunum Ca^{2+} , Mg^{2+} og Fe^{2+}. Möguleikar á bindingu kolefnis í basalti eru nú rannsakaðir á Íslandi og víða annars staðar. Tilgangur þessarar doktorsritgerðar er að rannsaka hvernig best er að mynda karbónat steindir þegar koltvíoxíð er bundið í steini í basalti, með rannsóknum úti í náttúrunni og með tilraunum á rannsóknarstofu.

Grunnvatnskerfið í nágrenni Heklu er náttúruleg hliðstæða við niðurdælingu koltvíoxíðs í basalt. Koltvíoxíðið á Heklusvæðinu er upprunnið úr kviku undir fjallinu, það leitar til yfirborðs og blandast grunnvatninu í nágrenni fjallsins í gosum og milli gosa og gastegundir og málmar berast beint til andrúmslofts í eldgosum. Þarna er hægt að rannsaka hvernig kvikugastegundir hafa áhrif á efnasamsetningu vatns t.d. hvað varðar bindingu koltvíoxíðs og styrks og hreyfanleika mengandi efna í vatninu. Styrkur ólífræns kolefnis í upplausn í lindavatninu á þessum slóðum minnkar frá 3,88 til 0,746 mmol/kg með auknum efnaskiptum vatns og bergs á meðan pH gildi vatnsins hækkar frá 6,9 til 9,2. Þarna má sjá hvernig efnaskipti vatns og bergs í náttúrunni binda kolefni sem er upprunnið úr kviku. Styrkur mengandi efna eins og þungmálma í lindvatninu í nágrenni Heklu er lítill, og líkanareikningar benda til að steindirnar kalsít og járnoxíhydroxíð (FeOOH) bind þungmálmanna samfara efnaskiptum vatns og bergs. Þungmálmarnir geta losnað úr bergi á fyrstu stigum efnaskipta vatns, gastegunda og bergs við lágt pH (minna en 6).

Talið er að losun tvígildra katjóna úr basalti samfara upplausn þess í vatni, stjórni hraða bindingar koltvíoxíðs í berginu. Basalt getur verið bæði kristallað eða glerkennt. Gler myndast þegar basaltkvika kólnar hratt án þess að tími gefist til kristöllunar steintegunda. Leysnihraða basaltglers má auka með því að bæta upplestu efni í vatnið, svokallaðan „ligand“, sem getur gengið í efnasamband við þrígilt ál (Al^{3+}) í vatninu. Súlfat (SO_4^{2-}), sem er oxað form brennisteins, getur haft þessi áhrif. Áhrif súlfats á leysnihraða basaltglers voru rannsökuð á rannsóknarstofu í svokölluðum gegnumflæðishvarfakútum við 50 °C og pH gildi frá 3 til 10.

Brennisteinn er algeng gastegund í útblæstri orkuvera og iðnaðarvera, og losun hans til andrúmsloft getur valdið skaða. Ef brennisteinn hvatar efnahvörfin, gæti verð hagkvæmt að dæla báðum gastegundum samtímis í berg þar sem brennisteinn og kolefni bindast varanlega. Tilraunirnar sýna að súlfat hraða upplaun basaltglers við lágt pH en hefur engin áhrif við hátt pH. Þetta er í góðu samræmi við líkön sem lýsa leysnihraða basaltglers og bendir til að það gæti hraðað bindingu koltvíoxíðs í basalti að dæla oxuðum brennisteinssamböndum og koltvíoxíði samtímis í bergið.

Til þess að rannsaka frekar áhrif brennisteins á bindingu koltvíoxíðs í basalti, voru gerðar tilraunir á rannsóknarstofu með áhrif súlfats á útfellingarhraða karbónatsins kalsíts. Áhrifin á útfellingarhraðann voru mæld í gegnumflæðishvarfakútum við 25°C og pH 9,1. Niðurstöður sýna að súlfat í styrknum 5 mmól/kg minkar útfellingarhraða kalsíts um 40%. Þetta bendir til að samhliða niðurdæling brennisteins og koltvíoxíðs hægi á útfellingu kalsíts við þær aðstæður sem það myndast við í náttúrunni. Frekari tilrauna er þörf til þess að kanna þessi áhrif á útfellingarhraða karbónata og heildaráhrif brennisteins á upplausn basalts og útfellingu karbónata.

Résumé

Les dangers potentiels liés à l'augmentation de la teneur en CO_2 de l'atmosphère, tels que les changements climatiques ou l'élévation du niveau des mers, ont provoqué un grand intérêt pour la séquestration du gaz carbonique dans les formations géologiques. Le moyen thermodynamiquement le plus sûr pour stocker le carbone est sous la forme de minéraux carbonatés, mais il exige une source de cations divalents qui ne soit pas carbonatée. Les roches basaltiques qui présentent de fortes teneurs en calcium, magnésium et fer peuvent être une de ces sources et la possibilité de former des minéraux carbonatés par injection de CO_2 dans les roches basaltiques est en cours d'investigation en Islande et dans d'autres endroits du monde. Dans ce cadre, l'objectif de cette thèse est de contribuer à l'optimisation de la précipitation des carbonates dans les basaltes lors de l'injection de CO_2 grâce à une série d'études de terrain et de laboratoire complémentaires.

Une étude détaillée de la composition chimique des eaux souterraines au pied du volcan Mont Hekla, dans le sud de l'Islande, a d'abord été menée afin d'évaluer l'évolution chimique des fluides et la mobilité des métaux toxiques lors des interactions entre basalte et fluides riches en CO_2. Ces fluides fournissent un analogue naturel pour estimer les conséquences de la séquestration du CO_2 dans les basaltes. La teneur de ces fluides en carbone inorganique dissous diminue de 3,88 à 0,746 mmole/kg avec l'augmentation de la mise en solution du basalte tandis que le pH passe de 6,9 à 9,2. Ces observations fournissent une preuve directe du potentiel qu'offre la dissolution du basalte pour séquestrer le CO_2. Les concentrations des métaux toxiques dans ces eaux sont faibles et la modélisation des chemins réactionnels suggère que la calcite et les (oxy)hydroxydes de fer piègent ces métaux, suite à l'alcalinisation des fluides induite par la dissolution continue du basalte.

On sait que ce sont les cations divalents libérés par la dissolution du verre basaltique qui contrôlent la minéralisation du gaz carbonique dans les basaltes. La vitesse de dissolution du verre basaltique peut être accrue par l'addition de ligands qui se complexent avec Al^{3+}. L'ion $SO4^{2-}$ fait partie de ces ligands et l'étude de son impact sur la vitesse de dissolution du verre basaltique a été conduite dans des réacteurs de type 'mixed flow' à 50°C et $3 < pH < 10$. Le soufre est souvent présent dans les gaz émis par les centrales électriques et son stockage constitue un challenge environnemental. La co-injection avec CO_2, si elle est réalisable, peut donc constituer une nouvelle méthode peu couteuse de stockage du soufre généré par l'industrie.

En accord avec les modèles actuels décrivant la cinétique de dissolution du verre basaltique en fonction de la composition de la solution aqueuse, les résultats de ce travail montrent que SO_4^{2-} augmente la vitesse de dissolution du verre aux conditions acide mais qu'il n'a aucun effet aux pH alcalins. Ces résultats suggèrent à la fois que 1) la co-injection de sulfate peut accélérer la minéralisation du CO_2 dans les basaltes et 2) les modèles cinétiques existant permettent une description précise de la dissolution du verre basaltique.

Afin d'évaluer plus précisément l'impact des ions sulfates sur la vitesse de précipitation des carbonates, la vitesse de précipitation de la calcite en régime stationnaire a été mesurée dans des réacteurs à circulation 'mixed flow' à 25°C et pH ~ 9.1. Les résultats montrent qu'en présence de 0.005 M de Na_2SO_4 la vitesse de précipitation de la calcite est diminuée d'environ 40% et qu'ainsi la co-injection de sulfate peut ralentir la précipitation de la calcite aux pH typiques de la précipitation de ce minéral en subsurface. Des expériences supplémentaires sont prévues pour caractériser définitivement l'effet du sulfate aux conditions attendues aux sites d'injection du CO_2 en subsurface.

Acknowledgment

The first people I would like to thank are of course my supervisors Sigurður R. Gíslason at the University of Iceland and Eric H. Oelkers at Université Paul Sabatier, Toulouse. Thank you so much for your constantly support and all the good advices I have received during this time, both about science and about the important things in life (such as good food and wine). I really appreciate your expertise and I look forward to continue working with you both in the future.

I started working on my thesis in Iceland, and Eydís Salome Eiriksdóttir and Guðmundur Bjarki Ingvarsson were both of great help and assistance when it came to teaching me how to sample springs and rivers, and how to get around in the lab. It was always good to have Eydís nearby when I had questions about my results or just needed some friendly advice. Good discussion with Erik Sturkell, Andri Stefánsson and Stefán Arnórsson were also of great help. I also have to thank The Nordic Volcanological Center for their financial support of my studies and the Carbfix consortment: Wallace S. Broecker, Sigurður R. Gíslason, Eric H. Oelkers, Einar Gunnlaugsson, Jakob Sigurður Friðriksson, Juerg M. Matter, Andri Stefánsson and Hólmfríður Sigurðardóttir, and of course the CarbFix students, Alexander Gysi, Edda Sif Aradóttir, Gabrielle J. Stockmann, Helgi Arnar Alfreðsson and Snorri Guðbrandsson for giving me a good insight into CO_2 sequestration in basalt.

When I came to Toulouse, to perform the experimental part of my thesis, I quickly found out that Giuseppe Saldi was a guy worth being friends with. Eric talks about him as an excellent experimentalist, and I have many times needed his help in the laboratory. One of the good things about Giuseppe is that no matter how busy he is, he is always ready to help me with fixing the backpressure regulator or whatever it is I need help with. So Giuseppe, thank you!

Other people I would like to thank at LMTG are Jacques Schott, Pascale Benezet and Oleg and Gleb Pokrovsky for good discussions along the way, and Alain Castillo, our technician, for always being ready to help when some of the equipment falls apart. I would also like to thank Jacques for translating my abstract into French.

The two last years of mu PhD was founded by the MIN-GRO network. Being a part of this group has been an excellent way of making connections with students and professors from all over Europe. I would like to thank the partners in this project; Eric H. Oelkers, Susan S.

Stipp, Clare Desplats, Liane G. Benning, Nora H. de-Leeuw, Christine and Andrew Putnis, Per Aagaard, Manuel Prieto, Sigurður R. Gíslason and Paul H. Nadeau for the excellent training they have given me during the twice a year workshops of the MIN-GRO and MIR-EST group. Of course all the students in these two networks, which unfortunately are too many to name, also needs to be thanked for making these meetings such great social gatherings.

During my stay in Toulouse, I have learned to appreciate the "French way of life" all thanks to Markus, Chris, Elisa, Giuseppe, Sandra, Teresa, Romain, Sam and others. Our social evenings lifted my spirit when the calcite experiments had failed yet again…

At last I would like to thank my family, my parents and my sister, for their support and encouragement along the way.

Therese Kaarbø Flaathen
Toulouse, France, August 2009

Table of Contents

1 Introduction

The concentration of CO_2 in the atmosphere has increased from ~280 ppm by volume at pre-industrial time to ~385 ppm today mostly due to the combustion of fossil fuels which emits an estimated 29 Gt CO_2 annually into the Earth's atmosphere (Taylor, 1991; Manabe and Stouffer, 1993; Houghton et al., 1995; Retallack, 2002; ICPP, 2005; 2007; Oelkers and Cole., 2008; Broecker, 2008). A large current effort is being made to identify and optimize CO_2 sequestration technologies to address the potential dangers, such as changes in the weather and sea level rise, associated with increased atmospheric CO_2 content (Korbøl and Kaddour, 1995; Hitchon et la., 1999; Bachu and Adams, 2003; Arts et al., 2004; Chadwick et al., 2004; Emberley et al., 2004; IPCC, 2005; Oelkers and Schott, 2005; McGrail et al., 2006; Ármannsson et al., 2007; Bachu et al., 2007; Marini, 2007; Matter et al., 2007; Wiese et al., 2008; Oelkers and Cole, 2008; Broecker, 2008; Kelemen and Matter, 2008; Cantucci et al., 2009; Iding and Ringrose, 2009; Kharaka et al., 2009; Li et al., 2006; Audigane et al., 2007; Gislason et al., 2009; Hermanrud et al., 2009; Kharaka et al., 2009; Matter et al., 2009; Michael, et al., 2009; Renderos, 2009; Schaef and McGrail, 2009; Stenhouse et al., 2009; Schaef et al., 2009). Geological storage of CO_2 together with energy conservation and non-fossil fuel energy sources is thought to be the only way to stem the ongoing buildup of atmospheric CO_2 (IPCC, 2005; Broecker, 2007; 2008). At large point sources of CO_2 emission, like fossil fuel and biomass energy facilities, and at major CO_2 emitting industries, CO_2 can be captured directly and transported to a suitable storage place (ICCP, 2005; Rubin, 2008; Bouillon et al., 2009). Possible storage places for CO_2 are, among others, saline aquifers in deep onshore and offshore sedimentary formations, the deep oceans and in basalts, granitic and ultramafic rocks.

This thesis is a combined field, laboratory and modeling study aimed at optimizing our knowledge about CO_2-water-rock interactions to help scientists succeed in carbon mineralization, which is thought to be the safest and most stable way to store CO_2 (ICCP, 2005). A pilot study investigating the possibility of sequestering CO_2 as carbonate minerals in Icelandic basalts is being performed by the CarbFix research group (Gislason et al., 2009; Matter et al., 2009) and my study looks into the possible release of toxic metals to the surroundings during this

process, and how we can speed up the carbonization process by increasing the dissolution of the basalt.

1.1 Different methods available for carbon storage

CO_2 can be stored in geological formations like deep saline aquifers in onshore and offshore sedimentary formations, spent petroleum reservoirs, the deep sea, and become mineralized in ultramafic rocks and basalts. Sequestration of CO_2 in forestation and soil will not be further addressed.

When CO_2 is being injected into an aquifer, the gas will react with the water present and produce carbonic acid:

$$CO_2 + H_2O = H_2CO_3 \quad (1)$$

The carbonic acid can then dissociate into bicarbonate:

$$H_2CO_3 = HCO_3^- + H^+ \quad (2)$$

When the gas is turned into an aqueous phase (as carbonic acid or bicarbonate), it can no longer escape by buoyancy, and it is captured by so-called solubility trapping (Hitchon et al., 1999). If the minerals present in the aquifer contain divalent cations, like Ca, Mg and Fe, carbonate minerals can precipitate and the CO_2 will be stored by mineral trapping (Hitchon et al, 1999):

$$(Ca^{2+}, Fe^{2+}, Mg^{2+}) + HCO_3^- = (Ca, Fe, Mg)CO_3 + H^+ \quad (3)$$

Some of the details of the different methods to sequester CO_2 in geological formations and in the deep ocean are summarized below.

Large sedimentary basins are well suited for CO_2 storage because they have tremendous pore volume and connectivity, and they are widely distributed. Possible formations include saline aquifers, depleted oil- and gas reservoirs and coal beds (Bachu and Adams, 2003; Emberley et

al., 2004; Benson and Cole, 2008; Cantucci et al., 2009; Iding and Ringrose, 2009). Intergovernmental Panel on Climate Change (IPCC), (2005) reported that three industrial-scale CO_2 storage projects in sedimentary basins were in operation. These are the Sleipner Project in the Utsira formation, outside the coast of Norway, the Weyburn Enhanced Oil Recovery project in Canada and the In Salah project in a gas field in Algeria. In addition to these, CO_2 injection into the Snøhvit field in the Barents Sea started up in 2008 and numerous others projects are under investigation.

The Sleipner Project, run by the oil company StatoilHydro, is the world's first industrial-scale storage operation (Chadwick et al., 2004). Carbon dioxide is being extracted from the produced gas, to meet quality specifications, and stored 1000 meters below ground in the Utsira Formation, offshore the west of Stavanger (Arts et al, 2004; Chadwick et al., 2004; Akervoll et al., 2009). A schematic drawing of the Sleipner field can be seen in Figure 1.1.

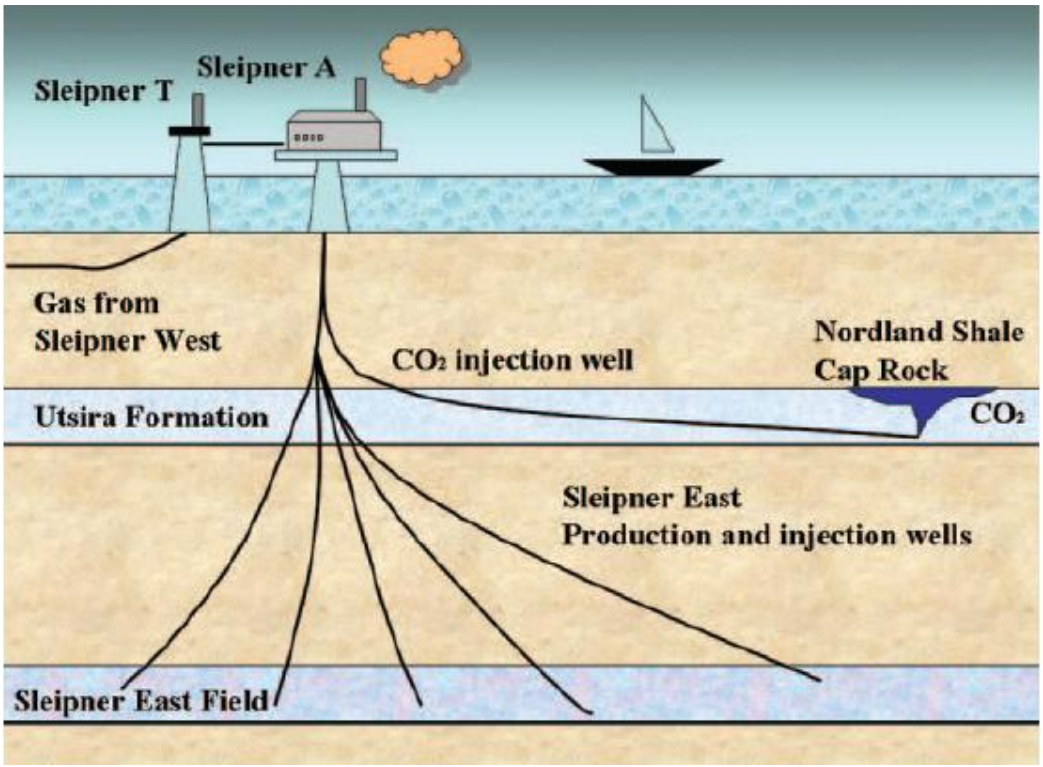

Figure 1.1 Cross section of CO_2 injection in the Utsira formation at Sleipner (from Audigane et al, 2007)

The Utsira Formation consists of sandstones with 90-98% sand content and has an average porosity of 35-40%, and is overlain by the Nordland shale (caprock). The sand is mainly comprised of quartz (75%), K-feldspar (13%) and calcite (3%) (Chadwick et al., 2004). The thickness of the formation varies between 150 and 250 m and the top of the formation is located at ~800 m true vertical depth (Korbøl and Kaddour, 1995). Injection started in 1996 and ~1 million ton CO_2 has been injected per year (Hermanrud et al., 2009). The total accumulated amount of CO_2 through the life time of the field is thought to be approximately 20 million tons (Korbøl and Kaddour, 1995; Chadwick et al., 2004). Figure 1.2 shows time lapse seismic data in the Utsira Formation from before the injection started to 2006 (Hermanrud et al., 2009). The gas has migrated into nine different layers inside the formation. StatoilHydro informs on their web pages that the results from the seismic investigation in 2008 shows that no CO_2 is leaking out of the formation (http://www.statoilhydro.com).

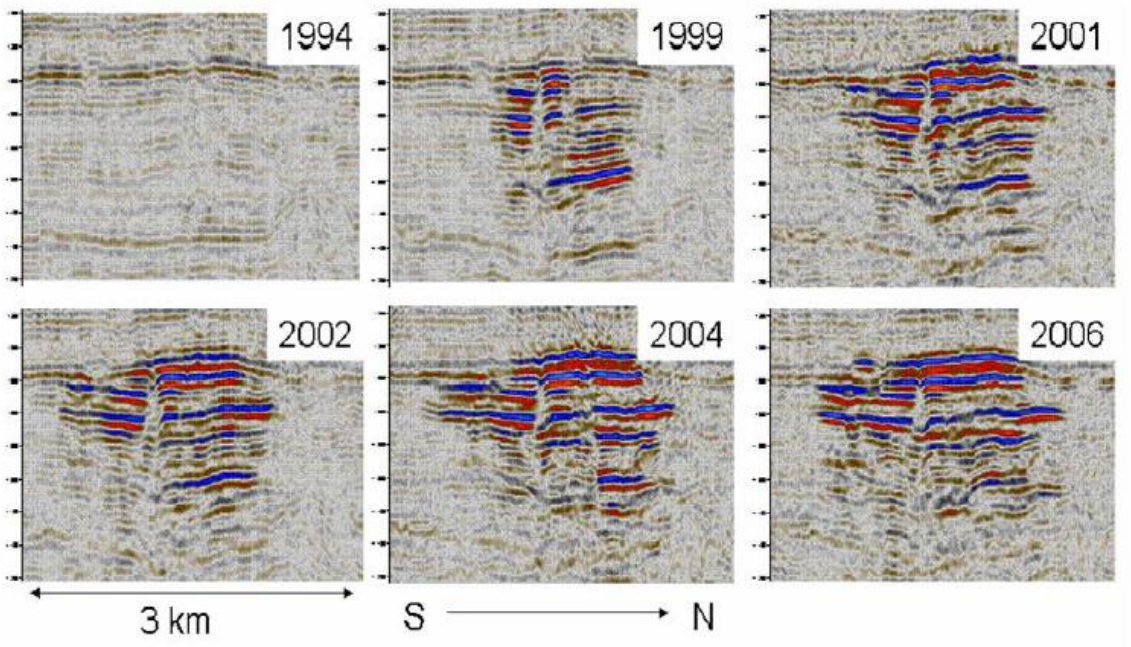

Figure 1.2 Time lapse seismic data in the Utsira Formation. The bright amplitudes reveal the presence of injected CO_2. (From Hermanrud et al., 2009)

Two-dimensional reactive transport modeling of CO_2 injected at the Sleipner site (Audigane et al., 2007) suggests that after 10.000 years, only 5% of the injected gas will be trapped into minerals while 95% will be dissolved in the brine. The small percentage of mineral trapping is due to the low reactivity of the minerals present in the aquifer and relative lack of divalent metal cations.

EnCana started injecting CO_2 into the Weyburn field (Williston Basin Oilfield) in 2000, to combine CO_2 sequestration with enhanced oil recovery by injecting the gas into an almost empty oil field to increase the pressure and in that way enhance the amount of oil which can be extracted (Emberley et al., 2005). The oil field consists of shallow marine carbonate and the injection rate has been ~5000 tons supercritical CO_2 per day, or 3 billion standard m^3 per year. The project is scheduled to continue until 2025-2030, and by then 15-20 Mtons of CO_2 will have been stored (Cantucci et al., 2009). Geochemical modeling and monitoring of the aquifer show that the injected CO_2 reacts with the host rock and dissolves the carbonate minerals present and produces alkalinity (Emberley et al., 2004; 2005; Cantucci, 2009). Geochemical simulations performed by Cantucci et al., (2009) suggests that the CO_2 is partially neutralized by solubility and mineral trapping by dawsonite precipitation due to trace amounts of silicate minerals over a period of thousands of years (Emberley et al., 2004; 2005). Unfortunately, the concentrations of toxic metals in the aquifer prior to, and during injection, were not reported in these studies.

The In Salah Gas Joint Venture CO_2 storage project takes place in the Sahara desert in Algeria and is currently the largest onshore CO_2 storage project in the world (Iding and Ringrose, 2009) where nearly 1 million tons per year of CO_2 are injected into the Krechba field, a saline aquifer, at a depth of 1880 meters. The CO_2 stems from gas production and the project is a joint venture between Sonatrach, British Petroleum and StatoilHydro. It is the world's first industrial scale CO_2 storage project in the water-leg of a depleting gas field (Rutqvist et al., 2009). The Krechba field is composed of sandstones with low to medium permeability with occasional appearance of fractures and small faults in both the reservoir unit and in the adjacent Carboniferous mudstone and siltstone units of the caprock. Despite the evidence of fractures, the thick mudstone caprock sequence provides an effective flow and mechanical seal for the storage system (Iding and Ringrose, 2009).

The Frio formation, in the U.S. Gulf Cost, is being used to investigate the potential for geological storage of CO_2 in saline sedimentary aquifers onshore. The injection zone is a subarkosic, fine-grained moderately sorted quartz and sandstone, with minor amounts of illite/smectite, calcite and oxyhydroxide. The mean porosity is 32% and the permeability is very high (2-3 Darcies) (Kharaka et al., 2009). In 2004, 1600 tons of CO_2 were injected into this formation which led to a decrease in pH and a strong increase in alkalinity. Geochemical modeling suggests that the Frio formation water in contact with the supercritical CO_2 would have a pH of 3 which would make the brine highly undersaturated with respect to minerals like iron oxyhydroxides, carbonates and aluminosilicates (Kharaka et al., 2006a). After injection, the concentrations of metals like Fe, Ca, Mn, Pb, Zn and Mo increased in the pore fluids. The enhanced Fe and Mn concentrations are thought to be due to the dissolution of Fe oxy hydroxides and Mn oxides, or to be a result of corrosion of pipe and well casing (Kharaka et al, 2006b; 2009). Since iron oxy hydroxides are known to scavenge toxic metals by sorption or coprecipitation, the increased concentration of Pb, Zn and Mo can be due to the dissolution of this phase. The increase in Ca concentration is most likely due to dissolution of calcite in the host rock (Kharaka et al., 2009). This field test demonstrated that CO_2 can relatively easily be injected and stored in saline aquifers.

One of the main challenges for CO_2 storage in saline aquifers is to prevent brine leakage into overlying drinking water supplies (Stenhouse et al., 2009). It is common to believe that the caprock, which has sealed the original hydrocarbon in the reservoirs for millions of years, is sufficient to prevent the injected CO_2 from migrating into the upper formations. However, the much lower interfacial tension of the CO_2/water system, compared to that of the original hydrocarbon/water system, reduces the sealing capacity of the caprock significantly (Li et al., 2006). In addition, the high mineral dissolution rates in the system during and after CO_2 injection could dissolve the caprock and let water with high concentrations of toxic metals, from the dissolution of iron oxyhydroxide, escape together with CO_2 (Kharaka et al., 2006b; Stenhouse et al., 2009). Since sedimentary basins have very low concentrations of minerals containing divalent cations, which are needed for the carbonization process, there is little chance to mineralize the CO_2 injected. As shown in the Sleipner field, the injected CO_2 tends to migrate

upwards due to buoyancy. A failure in the caprock sealing the reservoir can lead to migration of highly acidic and toxic water into surrounding aquifers and possibly to the surface.

The deep ocean could be a sink for anthropogenic CO_2 due to its vast uptake capacity. Today, the ocean naturally contains 50 times more carbon than the atmosphere and 20 times more carbon than is found in the land biosphere (Adams and Caldeira, 2008). The idea behind this type of storage is to inject the CO_2 into the deep ocean where it will be sealed off from the ocean surface water and the atmosphere for a few hundred years. After this time, the ocean will have turned and the CO_2 will equilibrate with the atmosphere putting us exactly where we would have been in the first place. This method will only buy us some time to come up with safe and effective ways of CO_2 sequestration. However, by continuing emitting the CO_2 directly into the atmosphere, the concentration of CO_2 in the ocean surface waters will increase dramatically, reducing the pH, which will have a harmful effect on coral reefs and other organisms that consist of calcium carbonate.

Recently, the interest of mineralization of CO_2 has increased (McGrail et al., 2006; Marini, 2007: Matter et al., 2007; Kelemen and Matter, 2008; Schaef and McGrail, 2009; Schaef et al., 2009; Gislason et al., 2009; Matter et al., 2009). Geochemical modeling suggests that rock types like basalt, ultramafic rocks and granitic rocks can be used to safely store CO_2 as carbonates over a geological timescale. This type of CO_2 sequestration in explained in detail below.

1.2 Mineralization of CO_2

The IPCC (2005) stated that mineral trapping is the most stable and secure form of CO_2 sequestration (Figure 1.3). By mineralization, the CO_2 is stored as carbonate minerals which thermodynamically is the most stable phase for carbon. Granitic, basaltic and ultramafic rocks are being investigated for their carbonization potential at different locations around the world. In Japan, CO_2 is being injected into granitic rocks in the Ogachi hydrothermal area (Kaieda et al., 2009), while the Deccan Traps in India (Garg and Shukla, 2009) and the big flood basalt in the southeast of US (McGrail et al., 2006; Schaef et al., 2009; Schaef and McGrail, 2009) are under

investigation for CO_2 sequestration. Also CO_2 injection into deep-sea basalt is being explored (Goldberg et al., 2008).

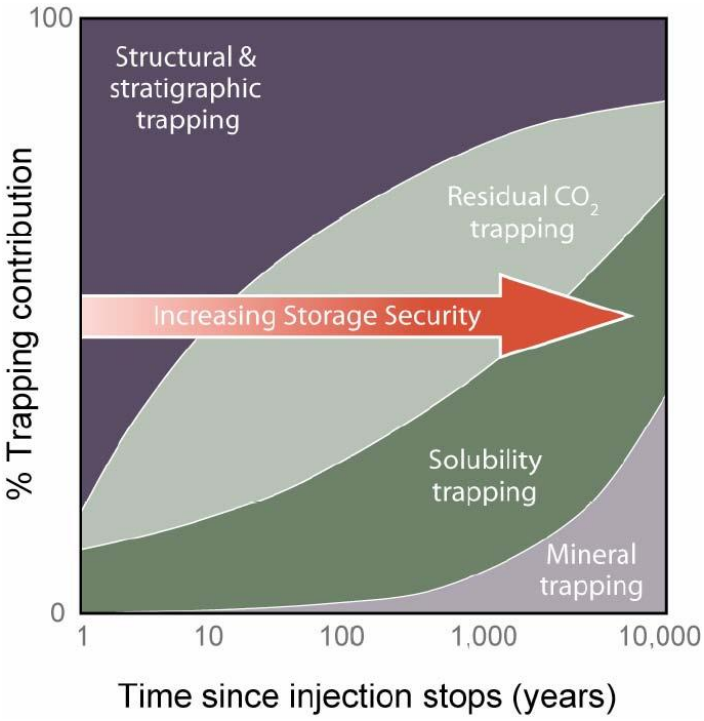

Figure 1.3. Storage security (IPCC, 2005)

In Iceland, the CarbFix project group, an international group where the main partners are Reykjavik Energy, University of Iceland, The Earth Institute at Colombia University in New York, and the Centre National de la Recherche Scientifique, Université Paul Sabatier in France, has been created to develop and optimize practical and cost-effective technology for in-situ carbon mineralization in Icelandic basalts (Gislason et al, 2009; Matter et al., 2009).

1.2.1 In-situ mineral sequestration in basalt

The dissolution rate of basaltic glass is fast compared to other minerals and glasses (Oelkers and Schott, 1995; Oelkers 2001; Pokrovski and Schott, 2000; Wolff-Boenisch et al., 2004a) and the high concentration of divalent anions, like Fe, Mg and Ca which can be used to form

carbonates, makes CO_2 sequestration in basalt promising. The potential of CO_2 sequestration in basalt is supported by the fact that while basalt only covers ~10% of the terrestrial surface it consumes ~30-35% of all CO_2 produced during natural weathering of silicates at the Earth's surface (Dessert et al., 2003). The carbonates which can precipitate are calcite ($CaCO_3$), dolomite ($(Ca_{0.5}Mg_{0.5})CO_3$), magnesite ($MgCO_3$), siderite ($FeCO_3$) and Mg-Fe carbonate solid solutions.

During in-situ mineral sequestration, CO_2 is injected into an aquifer where it dissolves in water and produces carbonic acid (Eqn. 1). The dissociation into bicarbonate (Eqn. 2) releases a proton (H^+) which is free to react with the host rock, here shown with basaltic glass from Stapafell, Iceland (Oelkers and Gislason, 2001):

$$SiAl_{0.36}Ti_{0.02}Fe(III)_{0.02}Ca_{0.26}Mg_{0.28}Fe(II)_{0.17}Na_{0.08}K_{0.008}O_{3.45} + 2.82H^+ =$$
$$SiO_{2(aq)} + 0.36Al^{3+} + 0.02TiO_{2(aq)} + 0.02Fe^{3+} + 0.26Ca^{2+} +$$
$$0.28Mg^{2+} + 0.17Fe^{3+} + 0.08Na^+ \; 0.\; 008K^+ + 1.41H_2O \qquad (4)$$

This reaction releases carbonate forming cations, Ca, Fe and Mg, into the solution at the same time as it consumes protons. Proton consummation increases the pH in the water promoting the precipitation of secondary minerals, including carbonates, according to Eqn. 3. The precipitation of carbonates only proceeds if the protons which are produced are being consumed by dissolution reactions like the one with basaltic glass or other common minerals in basalts, like plagioclase and forsterite.

1.2.2 Optimizing the carbonization process

One of the main challenges of carbonization is to optimize the process so that most CO_2 is mineralized with the least amount of energy and money. The slowest, and therefore the rate limiting step, in this process has been shown by experimental and field studies to be the dissolution of the host rock and the following release of divalent cations. A number of methods exist to accelerate divalent cation release rates including choosing the correct type of host rock,

by increasing the surface area where the mineral and fluid can react and by optimizing the composition of the injected fluid and the temperature.

The correct choice of host rock is a rock which has a high dissolution rate and which contains high concentrations of divalent cations, like Ca, Fe and Mg. Oelkers and Schott (1995), Oelkers (2001), Pokrovsky and Schott (2000), Wolff-Boenisch et al. (2004a) among others observed that the dissolution rate of basaltic glass, Ca-plagioclase and forsterite are high compared to other silicate minerals. Wolff-Boenisch et al. (2006) showed that the release rate of Ca^{2+} increases with decreasing silica content of the rock. Gabbro and basaltic glass have a high concentration of divalent cations and are poor in silica which gives them release rates of Ca^{2+} which are about 2 orders of magnitude higher than those of granite and rhyolite. They also demonstrated that crystalline rock has a lower release rate than glassy rock, as shown in Figure 1.4.

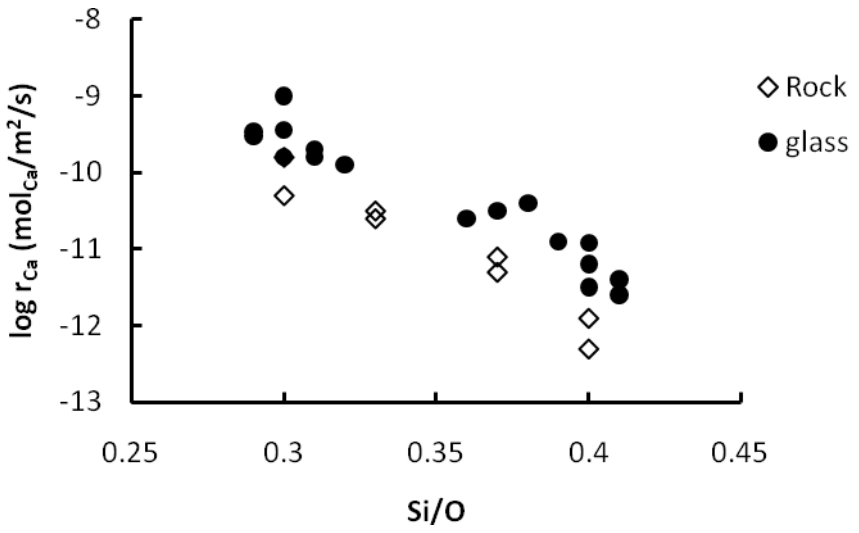

Figure 1.4. Far-from–equilibrium Ca-release rates calculated from granite, granodiorite, diorite, gabbro and natural glasses at pH 4 and 25 °C (modified from Wolff-Boenisch et al., 2006) plotted as a function of the Si/O atomic ratio of the solid.

To maximize the surface area for mineral-fluid interactions, it is important to choose porous rock formations with fractures so that the injected CO_2 can migrate downstream. Close to the injection well, the pH of the water will be low and the host rock will be highly undersaturated

which will lead to dissolution and most likely increased reactive surface area. Further downstream, the pH will be higher (as shown in reaction 4) and the precipitation of secondary minerals might decrease the reactive surface area and finally clog parts of the aquifer (Cubillas et al., 2005; Stockman et al., 2008).

At far from equilibrium conditions, the dissolution rate equation of basaltic glass can be described as (Gislason and Oelkers, 2003):

$$r_{+,geo} = A_A \exp^{-\frac{E_A}{RT}\left(\frac{a^3_{H^+}}{a_{Al^{3+}}}\right)^{1/3}} \quad (5)$$

where $r_{+,geo}$ signifies the geometric surface area normalized steady-state basaltic glass dissolution rate at far-from-equilibrium conditions, A_A refers to a constant equal to $10^{-5.6}$ (mol of Si) cm^2/s, E_A designates a pH independent activation energy equal to 25.5 kJ/mol, R stands for the gas constant, T signifies temperature in K and a_i represents the activity of the subscripted aqueous species. As can be seen from equation 5, the dissolution rate can be increased either by increasing the H^+/Al^{3+} ratio, by operating at far from equilibrium conditions, or by increasing the temperature.

Gislason and Oelkers (2003) calculated that the dissolution rate of basaltic glass could be increased by a factor of 60 by increasing the temperature from 0 to 100 °C in a solution containing 10^{-6} mol/kg aluminium at pH 3.5. The temperature effect is much higher at basic conditions where the same increase in temperature is estimated to increase the dissolution rate by 4.5 orders of magnitude at pH 9. To benefit from this, the injection site can be located in areas with a high geothermal gradient or at large depth. The drawbacks with using high temperature is that the pore spaces in the host rock tend to already be filled up with secondary minerals, which means that the reactive surface area is low, and also that CO_2 becomes less soluble in water with increasing temperature.

The composition of the fluid strongly influences the rates. As can be seen from Equation 5, the higher the activity of H^+ (e.g. the lower the pH), the higher the dissolution rate. The Al^{3+} species inhibits the dissolution rates and the concentration of this species depends on the pH; at

pH below 4.3, Al^{3+} is the dominating specie and its concentration decreases to almost 0 at pH 6. In acid solutions containing 10^{-6} mol/kg aluminum, the 3rd power of the proton activity decreases faster than the activity of Al^{3+}, which results in a decrease in rate when increasing from pH 0 to 7. At basic conditions, the dissolution rate increases again because the concentration of Al^{3+} decreases faster than the 3rd power of the proton activity. As a result, the dissolution rate of basaltic glass is highest at low pH, reaches a minimum between pH 6 and 7, and then increases again at basic conditions, as shown in Figure 1.5.

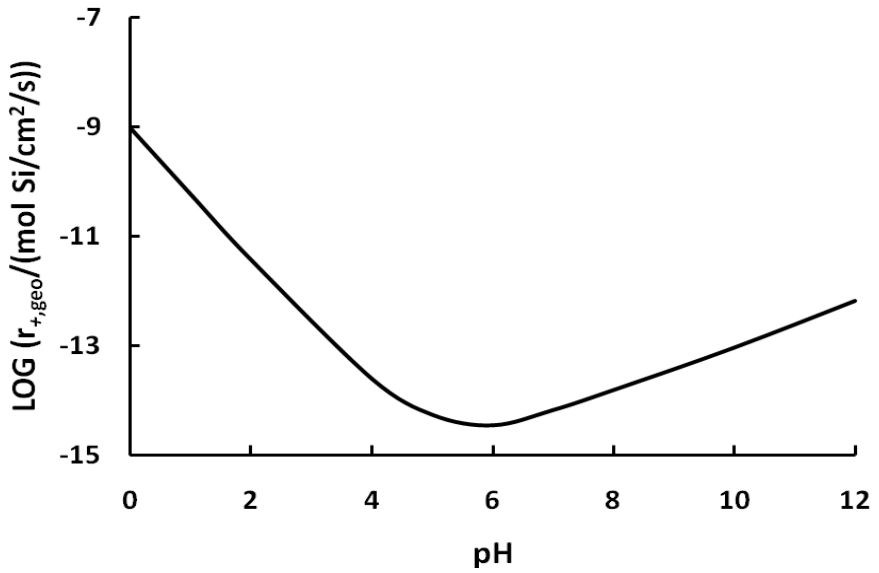

Figure 1.5. Predicted dissolution rate of basaltic glass, $r_{+,geo}$ versus pH, using Eqn. 5, in a solution containing 10^{-6} M Al.

It is possible to increase the rates by adding a ligand which complex aqueous Al^{3+}. According to Wolff-Boenisch et al. (2004b), fluorine is a ligand which can enhance the dissolution rate by 2 orders of magnitude by complexing Al^{3+}:

$$Al^{3+} + F^- = AlF^{2+} \quad (6)$$

$$AlF^{2+} + F^- = AlF_2^+ \quad (7)$$

1.2.3 Challenges during in-situ mineralization of CO_2

The two main challenges for successful CO_2 mineralization are to inhibit secondary minerals containing divalent cations, other than carbonates, to precipitate and to avoid the release of toxic metals into the environment. Common secondary minerals in basalt containing these cations are smectites, zeolites and iron and manganese oxides (Gislason and Eugster, 1987a; Gislason and Eugster, 1987b; Crovisier et al., 1992; Gislason et al., 1993; Neuhoff et al., 1999; Rogers et al., 2006).

The possible mobilization of toxic metals during injection of CO_2 rich water into basalt poses a potential risk for CO_2 sequestration in these rocks. Moune et al. (2006) reported the concentrations of toxic metals, like Pb, Mn, Cd, Sr and Cu, in the Hekla 2000 lava which has a basaltic andesitic composition. When CO_2 rich water dissolves the basalt, these toxic metals will be released in the aquifer. If they escape into surface and drinking waters, they may have a harmful effect on the biota. Kharaka et al. (2006b) comment on this problem in the Frio project, where high concentrations of toxic metals were released after injection of CO_2.

1.3 Aims and structure of this thesis

This thesis is a combined field, laboratory and modeling study aimed at optimizing our knowledge about CO_2-water-rock interactions to help scientists succeed in carbon mineralization. In addition to introduction and conclusions, the thesis comprises four parts. The first part, Chapter 2, contains the paper *Flaathen and Gislason, 2007. The effect of volcanic eruptions on the chemistry of surface waters: The 1991 and 2000 eruptions of Mt. Hekla, Iceland* which was published in Journal of Volcanology and Geothermal Research. The second part, Chapter 3, contains the paper *Flaathen et al., 2009. Chemical evolution of the Mt. Hekla, Iceland, groundwaters: A natural analogue for CO_2 sequestration in basaltic rocks*, which was published in Applied Geochemistry. Parts number three and four, Chapter 4 and 5, are unpublished manuscripts dealing with the effect of aqueous sulphate on basaltic glass dissolution rates and the effect of aqueous sulphate on the precipitation rates of calcite, respectively. These manuscripts are prepared to be submitted for publication in Geochimica et Cosmochimica Acta and Chemical Geology, respectively. These chapters are summarized below.

In addition to this, there are two appendices. Appendix I is the extended abstract *Flaathen et al., 2008. The effect of aqueous sulphate on basaltic glass dissolution rates* which was published in Mineralogical Magazine 72, and Appendix II is the chemistry of spring water samples from Flaathen et al., (2009).

In Chapter 2, the effects of toxic metal release from fresh volcanic ash on four different kinds of surface waters are described, with a strong emphasis on the effect of aqueous Al-F complexation on this process. The ash stems from the Hekla volcano, Iceland, which is of basaltic andesitic composition. The different types of surface waters investigated were rain water, sea water and high and low alkalinity river waters.

Natural analogues allow us to better understand the carbonization processes in basalt, and this is the topic of Chapter 3. The groundwater surrounding the Hekla volcano is ideal for such a study because it is constantly fed with CO_2 from depth and flows through basaltic rocks. A detailed study of the chemical composition of the groundwater was performed to assess fluid evolution and toxic metal mobility during CO_2-rich fluid basalt interaction. This study was performed using both field data and reaction path modeling with the computer code PHREEQC (Parkhurst and Appelo, 1999).

The theme of Chapter 4 is exploration of the potential to enhance the dissolution rate of basaltic glass by adding aqueous sulphate. As shown in Eq. 5, the dissolution rate can be increased by decreasing the concentration of free Al^{3+} ions in solution. In the same way as F^-, SO_4^{2-} can complex Al^{3+} and make Al-SO_4 complexes:

$$Al^{3+} + SO_4^{2-} = Al(SO_4)^+ \quad (8)$$

$$Al^{3+} + 2SO_4^{2-} = Al(SO_4)_2^- \quad (9)$$

Power plants and aluminum smelters often emit flue gases containing SO_2 which is a very reactive gas and therefore difficult to store safely on-land. After oxidation into SO_4^{2-}, sulphate in aqueous form could be co-injected with CO_2, to possibly increase the dissolution rate of the basalt and at the same time store SO_4^{2-} safely in the ground. Flow-through experiments have

been performed at pH ranging from 3 to 10 with a concentration of SO_4^{2-} ranging from 0 to 100 mM at 50 °C to assess these effects.

The presence of dissolved sulphate could potentially hinder CO_2 sequestration efforts if the sulphate injected inhibits carbonate mineral precipitation. Therefore, a study of the effect of aqueous sulphate on the precipitation rates of calcite is examined in Chapter 5. Flow-through reactors were used to measure the precipitation rate of calcite from a mixed $NaHCO_3/Na_2CO_3$ and $CaCl_2$ solution containing 0 to 25 mM SO_4^{2-} at 25 °C.

REFERENCES

Akervoll, I., Lindeberg, E., Lackner, A., 2009. Feasibility of Reproduction of Stored CO_2 from the Utsira Formation at the Sleipner Gas Field. Energy Procedia 1, 2557-2564.

Adams, E.E., Caldeira, K., 2008. Ocean Storage of CO_2. Elements 4, 319-324.

Ármannsson, H., Frisdriksson, T., Wiese, F., Hernández, P., Pérez, N., 2007. CO_2 budget of the Krafla geothermal system, NE-Iceland. In: Water-rock Interaction, (Ed.: Bullen, T.B. and Wang, Y.), Taylor & Francis Group, London, 189-192.

Arts, R., Eiken, O., Chadwick, A., Zweigel, P., ver der Meer, L., Zinszner, B., 2004. Monitoring of CO2 injected at Sleipner using time-lapse seismic data. Energy 29, 1383-1392.

Audigane, P., Gaus, I., Czernichowski-Lauriol, I., Pruess, K., Xu, T., 2007. Two dimensional reactive transport modelling of CO_2 injection in a saline aquifer at the Sleipner site, North Sea. American Journal of Science 307, 974-1008.

Bachu, S., Adams, J.J., 2003. Sequestration of CO_2 in geological media in response tp climate change: capacity of deep saline aquifers to sequester CO_2 in solution. Energy Conversion and Management 44, 3151-3175.

Bachu, S., Bonijoly, D., Bradshaw, J., Burruss, R., Holloway, S., Christensen, N.P., Mathiassen, O.M., 2007. CO_2 storage capacity estimation: Methodology and gaps. International Jouranla of Greenhouse Gas Control 1, 430-443.

Benson, S.M., Cole, D.R., 2008. CO_2 sequestration in Deep Sedimentary Formations. Elements 4, 325-331.

Bouillon, P.A., Hennes, H., Mahieux, C., 2009. ECO_2: Post combustion or Oxyfuel – A comparison between coal power plants with integrated CO_2 capture. Energy Procedia 1, 4015-4022.

Broecker, W.S., 2007. CO_2 Arithmetic. Science 315, 1371.

Broecker, W.S., 2008. CO_2 capture and storage: Possibilities and perspectives. Elements 4, 295-297.

Cantucci, B., Montegrossi, G., Vaselli, O., Tassi, F., Quattrocchi, F., Perkins, E.H., 2009. Geochemical modeling of CO_2 storage in deep reservoirs ; The Weyburn Project (Canada) case study. Chemical Geology. In Press.

Chadwick, R.A., Zweigel, P., Gregersen, U., Kirby, G.A., Holloway, S., Johannessen, P.N., 2004. Geological reservoir characterization of a CO_2 storage site: The Utsira Sand, Sleipner, northern North Sea. Energy 29, 1371-1381.

Crovisier, J.L., Honnorez, J., Fritz, B., 1992. Dissolution of subglacial volcanic glasses from Iceland: laboratory study and modelling.

Cubillas, P., Köhler, S., Prieto, M., Causserand, C., Oelkers, E.H., 2005. How do mineral coatings affect dissolution rates? An experimental study of coulpled $CaCO_3$ dissolution–$CdCO_3$ precipitation. Geochimica et Cosmochimica Acta 69, 5459-5476.

Dessert, C., Dupré, B., Gaillardet, J., François, L.M., Allègre, C.J., 2003. Basalt weathering laws and the impact of basalt weathering on the global carbon cycle. Chemical Geology 202, 257-273.

Emberley, S., Hutcheon, I., Shevalier, M., Durocher, K., Mayer, B., Gunter, W.D., Perkins, E.H., 2004. Geochemical monitoring of fluid-rock interaciton and CO_2 storage at the Weyburn CO_2-injection enhanced oil recovery site, Saskatchewan, Canada. Energy 29, 1393-1401.

Emberley, S., Hutcheon, I., Shevalier, M., Durocher, K., Mayer, B., Gunter, W.D., Perkins, E.H., 2005. Monitoring of fluid-rock interaction and CO2 stoarge through produced fluid sampling at the Weybrun CO^2-injection enhanced oil recovery site, Saskatchewan, Canada. Applied Geochemistry 20, 1131-1157.

Flaathen, T.K., Gislason, S.R, 2007. The effect of volcanic eruptions on the chemistry of surface waters: The 1991 and 2000 eruptions of Mt. Hekla, Iceland. Journal of Volcanology and Geothermal Research 164, 293-316.

Flaathen, T.K., Oelkers, E.H., Gislason, S.R., 2008. The effect of aqueous sulphate on basaltic glass dissolution rates. Mineralogical Magazine 72, 39-41.

Flaathen, T.K., Gislason, S.R., Oelkers, E.H., Sveinbjörnsdóttir, Á.E., 2009. Chemical evolution of the Mt. Hekla, Iceland, groundwaters: A natural analogue for CO_2 sequestration in basaltic rocks. Applied Geochemistry 24, 463-474.

Garg, A., Shukla, P.R., 2009. Coal and energy security for India: Role of carbon dioxide (CO2) capture and storage (CCS). Energy doi:10.1016/j.energy.2009.01.005

Gislason, S.R., Eugster, H.P., 1987a. Meteoric water-basalt interactions. I: A laboratory study. Geochimica et Cosmochimia Acta 51, 2827-2840.

Gislason, S.R., Eugster, H.P., 1987b. Meteoric water-basalt interactions. II: A field study in N.E. Iceland. Geochimica et Cosmochimica Acta 51, 2841-2855.

Gislason, S.R., Veblen, D.R., Livi, K.J.T., 1993. Experimental meteoric water-basalt interactions: Characterization and interpretation of alteration products. Geochimica et Cosmochimica Acta 57, 1459-1471.

Gislason, S.R., Oelkers, E.H., 2003. Mechanism, rates and consequences of basaltic glass dissolution: II. An experimental study of the dissolution rates of basaltic glass as a function of pH and temperature. Geochimica et Cosmochimica Acta 67, 3817-3832.

Gislason, S.R., Wolff-Boenisch, D., Stefansson, A., Oelkers, E., Gunnlaugsson, E., Sigurdardóttir, H., Sigfússon, Broecker, W., Matter, J., Stute, M., Axelsson, G., Fridriksson, T., 2009. Mineral sequeatration of carbon dioxide in basalt; The CarbFix project. International Journal of Greenhouse Gas (Submitted).

Goldberg, D.S., Takahashi, T., Slagle, A.L., 2008. Cabon dioxide sequestration in deep-sea basalt. Proceedings of the National Academy of Scienes 105: 9920-9925.

Hitchon, B., Gunter, W.D., Gentzis, T., Bailey, R.T., 1999. Sedimentary basins and greenhouse gases; a serendipitous association. Energy Conversion & Management 40, 825-843.

Hermanrud, C., Andresen, T., Eiken, O., Hansen, H., Janbu, A., Lippard, J., Bolås, H.N., Simmenes, T.H., Teige, G.M.T., Østmo, S., 2009. Storage of CO_2 in saline aquifers – lessons learned from 10 years of injection into the Utsira Formation in the Sleipner area. Energy Procedia 1, 1997-2004.

Houghton, J.T., Meira Filho, L.G., Callander, B.A., Harris, N., Kattenberg, A., Maskell, K., 1996. Climate Change. The science of climate change, Cambridge University Press, UK, pp 572.

Iding, M., Ringrose, P., 2009. Evaluating the impact of fractures on the long-term performance od the In-Salah CO_2 storage site. Energy Procedia 1, 2021-2028.

Intergovernmental panel on Climate Change (IPCC), 2005. Summary for Policymakers. In: Metz, B., Davidson, O., Coninck, H., Loos, M., Meyer, L. (eds) IPCC Special Report on Carbon Dioxide Capture and Storage, prepared by Working Group III of the Intergovernmental Panel on Climate Change. Cambridge University Press, Cambridge, UK, and New York, USA, pp 3-15.

Intergovernmental panel on Climate Change (IPCC), 2007. Climate Change 2007; Synthesis Report. Contribution of working Groups I, II and III to the Fourth Assessment Report of the Intergovernmental Panel on Climate Change (Eds.) Pachauri, R.K., Reisinger, A. IPCC, Geneva, Switzerland, 104 pp.

Kaieda, H., Ueda, A., Kubota, K., Wakahama, H., Mito, S., Sugiyama, K., Ozawa, A., Kuroda, Y., Sato, H., Yajima, T., Kato, K., Ito, H., Ohsumi, T., Kaji, Y., Tokumaru, T., 2009. Field experiments for studying on CO_2 sequestration in solid minerals at the Ogachi HDR geothermal site, Japan. PROCEEDINGS, Thirty-Fourth Workshop on Geothermal Reservoir Engineering, Stanford University, Stanford, California, February 9-11, 2009. SGP-TR-187.

Kelemen, P.B., Matter, J., 2008. In situ carbonation of peridotite for CO_2 storage. Proceedings of the National Academy of Science 105, 17295-17300.

Kharaka, Y.K., Cole, D.R., Thordsen, J.J., Kakouros, E., Nance, H.S, 2006a. Gas-water-rock interactions in sedimentary basins: CO_2 sequestration in the Frio Formation, Texas, USA. Journal of Geochemical Exploration 89, 183-186.

Kharaka, Y.K., Cole, D.R., Hovorka, S.D., Gunter, W.D., Knauss, K.G., Freifeld, B.M., 2006b. Gas-water-rock interaction in Fro Formation following CO2 injection: Implications for the storage of greenhouse gases in sedimentary basins. Geological Society of America 34, 577-580.

Kharaka, Y.K., Thordsen, J.J., Hovorka, S.D., Nance, H.S., Cole, D.R., Phelps, T.J., Knauss, K.G., 2009. Potential environmental issues of CO_2 storage in deep saline aquifers: Geochemical results from the Frio-I Brine Pilot test, Texas, USA. Applied Geochemistry 24, 1106-1112.

Korbøl, R., Kaddour, A., 1995. Sleipner West CO_2 disposal – Injection of removed CO_2 into the Utsira Formation. Energy Conversion and Management 36, 509-512.

Li, Z., Dong, M., Li, S., Huang, S., 2006. CO_2 sequestration in depleted oil and gas reservoirs – caprock sharacterization and storage capacity. Energy Conversion and Management 47, 1372-1382.

Manabe, S., Stouffer, R.J., 1993. Century-scale effects of increased atmospheric CO_2 on the ocean-atmosphere system. Nature 364, 215-218.

Marini, L., 2007. Geological Sequestration of Carbon Dioxide: Thermodynamics, Kinetics and Reaction Path modeling. Elsevier, Amsterdam, 470 pp.

Matter, J.M., Takahashi, T., Goldberg, D., 2007. Experimental evaluation of in situ CO_2-water-rock reactions during CO_2 injection in basaltic rocks: Implications for geological CO_2 sequestration. Geochemistry, Geophysics, Geosystems 8, Q02001, doi: 10.1029/2006GC001427.

Matter, J.M., Broecker, W.S., Stute, S., Gislason, S.R., Oelkers, E.H., Stefánsson, A., Wolff-Boenisch, D., Gunnlaugsson, E., Axelsson, G., Björnsson, G., 2009. Permanent Carbon Dioxide Storage into Basalt: The CarbFix Pilot Project, Iceland. Energy Procedia 1, 3641-3646.

McGrail, B.P., Schaef, H.T, Ho, A.M., Chien, Yi-Ju, Dooley, J.J., Davidson, C.L., 2006. Potential for carbon dioxide sequestration in flood basalts. Journal of Geophysical Research, vol 111. B12201, doi:10.1029/2005JB004169.

Michael, K., Arnot, M., Cook, P., Ennis-King, J., Funnell, R., Kaldi, J., Kirste, D., Paterson, L., 2009. CO_2 storage in saline awuifers I – current state of scientific knowledge. Energy Procedia 1, 3197-3204.

Moune, S., Gauthier, P.J., Gislason, S.R., Sigmarsson, O., 2006. Trace element degassing and enrichment in the eruptive plume of the 2000 eruption of Hekla volcano, Iceland. Geochimica et Cosmochimica Acta 70, 461-479.

Neuhoff, P.S., Fridriksson, T., Arnórsson, S., Bird, D.K., 1999. Porosity evolution and mineral paragenesis during low-grade metamorphism of basaltic lavas at Teigarhorn, Eastern Iceland. American Journal of Science 299, 467-501.

Oelkers, E.H., Schott, J., 1995. Experimental study of anorthite dissolution and the relative mechanism of feldspar hydrolysis. Geochimica et Cosmochimica Acta 59, 5039-5053.

Oelkers, E.H., 2001. An experimental study of forsterite dissolution rates as a function of temperature and aqueous Mg and Si concetnration. Chemical Geology 175, 485-494.

Oelkers, E.H., Gislason, S.R., 2001. The mechansim, rates and consequences of basaltic glass dissolution: I. An experimental study of the dissolution rates of basaltic glass as as function of aqueous Al, Si and oxalic acid concentration at 25 °C and pH = 3 and 11.

Oelkers, E.H., Schott, J., 2005. Geochemical aspects of CO_2 sequestration. Chemical Geology 217, 183-186.

Oelkers, E.H., Cole, D.R., 2008. Carbon dioxide sequestration: A solution to a global problem. Elements 4, 305-310.

Parkhurst D.L. and Appelo C.A.J. (1999). User's guide to PHREEQC (Version 2) – A computer program for speciation, batch-reaction, one-dimensional transport, and inverse geochemical calculations. USGS-Report 99-4259.

Pokrovski, O.S., Schott, J., 2000. Kinetics and mechanism of forsterite dissolution at 25 °C and pH from 1 to 12. Geochimica et Cosmochimica Acta 64, 3313-3325.

Renderos, R.E., 2009. Carbon dioxide fixation by calcite and diffusive degassing in the southern region of the Berlín Geothermal system, El Salvador. M.Sc. Thesis, Faculty of Earth Sciences, University of Iceland, 54 pp.

Retallack, G.J., 2002. Carbon dioxide and climate over the past 300 myr. Philosophical transactions. Series A, Mathematical, physical and engineering sciences 360, 659-673.

Rogers, K.L., Neuhoff, P.S., Pedersen, A.K., Bird, D.K., 2006. CO2 metasomatism in a basalt-hosted petroleum reservoir, Nuussuaq, West Greenland. Lithos 92, 55-82.

Rubin, E.S., 2008. CO_2 Capture and Transport. Elements 4, 311-317.

Rutqvist, J., Vasco, D.W., Myer, L., 2009. Coupled reservoir-geomechanical analysis of CO_2 injection at In Salah, Algeria. Energy Procedia 1, 1847-1854.

Shaef, H.T., McGrail. B.P., Owen, A.T., 2009. Basalt-CO_2-H_2O Interactions and Variability in Carbonate Mineralization Rates. Energy Procedia 1, 4899-4906.

Schaef, H.T., McGrail. B.P,, 2009. Dissolution of Columbia River Basalt under mildly acidic conditions as a function of temperature: Experimental results relevant to the geological sequestration of carbon dioxide. Applied Geochemistry 24, 980-987.

Stenhouse, M., Arthur, R., Zhou, W., 2009. Assessing environmental impacts from geological CO_2 storage. Energy Procedia 1, 1895-1902.

Stockman, G., Wolff-Boenisch, D., Gislason, S.R., Oelkers, E.H., 2008. Dissolution of diopside and basaltic glass; the effect of carbonate coating. Min. Mag. 72, 135-139.

Taylor, F.W., 1991. The Greenhouse effect and climate change. Reports on Progress in Physics 54, 881-918.

Wiese, F., Fridriksson, T., Ármannsson, H., 2008. CO_2 fixation by calcite in high-temperature geothermal systems in Iceland. Report from the Iceland Geosurvey (Ísor), Ísor-2008/003, Reykjavik, 68 pp.

Wolff-Boenisch, D., Gislason, S.R., Oelkers, E.H., Putnis, C.V., 2004a. The dissolution rates of natural glasses as as function of their composition at pH 4 and 10.6, and temperatures from 25 to 74 C. Geochimica et Cosmochimica Acta 68, 4843-4858.

Wolff-Boenisch, D., Gislason, S.R., Oelkers, E.H., 2004b. The effect of fluoride on the dissolution rates of natural glasses at pH 4 and 25 °C. Geochimica et Cosmochimica Acta 68, 4571-4582.

Wolff-Boenisch, D., Gislason, S.R., Oelkers, E.H., 2006. The effect of crystallinity on dissolution rates and CO_2 consumption capacity of silicates. Geochimica et Cosmochimica Acta 70, 858-870.

Available online at www.sciencedirect.com
ScienceDirect
Journal of Volcanology and Geothermal Research 164 (2007) 293–316
Journal of volcanology and geothermal research
www.elsevier.com/locate/jvolgeores

The effect of volcanic eruptions on the chemistry of surface waters: The 1991 and 2000 eruptions of Mt. Hekla, Iceland

Therese K. Flaathen [a,*], Sigurdur R. Gislason [b]

[a] Nordic Volcanological Center, Institute of Earth Sciences, University of Iceland, Sturlugata 7, 101 Reykjavík, Iceland
[b] Institute of Earth Sciences, University of Iceland, Sturlugata 7, 101 Reykjavík, Iceland

Received 8 December 2006; received in revised form 12 May 2007; accepted 16 May 2007
Available online 31 May 2007

Abstract

The Mt. Hekla eruptions in 1991 and 2000 have provided a unique opportunity to study the local environmental effects of high latitude volcanic eruptions in the middle of winter. Both eruptions started around sunset at sub-zero temperatures. In order to define better these effects we studied the chemistry of surface waters in the vicinity of the volcano. Additionally, we describe and predict the environmental consequences of these volcanic eruptions on the chemistry of surface waters on land and in the ocean.

Several dissolved elements in the polluted snow melt from the 2000 eruption (Cl, F, Al, Fe, Mn, As, Cd, Pb, Zn, and U) exceeded the limits for water intended for human consumption. The volcanic ash, the primary minerals and secondary mineral phases that commonly form in the weathering environment of Iceland were undersaturated in the polluted snow melts with the exception of fluorite, barite, goethite and amorphous FeOOH. These minerals can constrain the maximum initial concentration of the respective dissolved constituents in the meltwaters. It took few days after the first rainfall on the volcanic ash to flush out the readily soluble constituents in the vicinity of the headwaters of the Ytri–Rangá River. The polluted river waters were oversaturated with respect to several secondary minerals, resulting in precipitation of amorphous Al hydroxide and FeOOH and further, scavenging of some trace elements on the Al and Fe surfaces. Dissolved Al and F were the main contaminants in the Ytri–Rangá river water. Previous studies have shown that combined Al–F toxicity is directly related to the predominance of specific Al–F species in solution. Model calculations for mixing of a Hekla-type volcanic cloud with 4 surface water end-members shows Al–F species to be most important in rain and dilute river waters. This makes Al and F phyto-available but diminishes the concentration of the Al^{3+} species, the most toxic Al species. Mixing with high alkalinity river waters or seawater results in the domination of non toxic $Al(OH)_4^-$ species at dilutions greater than 800, thus hindering Al toxicity and bioavailability.

This study indicates that H_2SO_4 contamination from volcanic eruptions is time and place dependent. Volcanic eruptions that take place during winter at high latitudes result in relatively high global sulfur contamination and relatively low local sulfur contamination due to the low oxidation rate of SO_2 into H_2SO_4 because of the low solar radiation.

Keywords: Al–F complexes; volcanic gases; volcanic aerosols; tephra; sulfur contamination

1. Introduction

Volcanoes contribute to atmospheric and stratospheric contamination by increasing the amount of greenhouse gases, sulfur species and aerosols which affect the climate and lead to acidification of the precipitation (e.g.

* Corresponding author. Tel.: +354 525 4800; fax: +354 525 4499.
E-mail addresses: therese@hi.is (T.K. Flaathen), sigrg@raunvis.hi.is (S.R. Gislason).

0377-0273/$ - see front matter © 2007 Elsevier B.V. All rights reserved.
doi:10.1016/j.jvolgeores.2007.05.014

Rampino and Self, 1992; Robock, 2000; Chiodini and Frondini, 2001; Thordarson et al., 2001; Gislason et al., 2002; Robock, 2003; Oppenheimer, 2003; Delmelle et al., 2003; Grattan, 2004; Chenet et al., 2005; Grattan et al., 2005). Salt particles bound to the surface of tephra, airborne volcanic ash, can have a major effect on surface waters. The salt particles are highly soluble and dissolve rapidly when exposed to surface waters, releasing the metals and protons that were bound in the salts (e.g. Frogner et al., 2001). The anions and protons released from the salts can affect the dissolution rates of the tephra itself, adding to the transient flux of metals to surface waters (Gislason and Oelkers, 2003; Wolff-Boenisch et al., 2004a). Some of these metals are toxic, others are essential for life, and some metals can be both essential and toxic depending on their concentration and speciation. Thus, whether surface waters become fertilized or polluted by volcanic ash depends on the amount and type of tephra and the proton and buffering capacity of the waters. Furthermore, at high latitudes, timing of the eruptions can be crucial for the environmental effect. Volcanic eruptions that take place in the middle of winter will not fertilize surface waters due to lack of biotic activity (Gislason et al., 2002).

The Hekla eruptions in 1991 and 2000 provided a unique opportunity to study the local environmental effect of high latitude eruptions in the middle of winter, as both eruptions started around sunset, and the initial energetic sub-Plinian phase occurred during the night. During the eruptions and for a few days afterwards the temperature in the vicinity of the volcano was below zero, thus hindering dissolution of the metal and proton salts. This study accordingly measured the effect of these eruptions on the chemistry of surface waters in the vicinity of the volcano. In addition, we describe and predict the environmental consequences of these eruptions on the chemistry of surface waters on land and in the ocean.

2. Geological background

2.1. Hekla volcano and the ground-water system

The Mt. Hekla volcano (63.98° N, 19.70° W) is a ridge built up by repeated fissural eruptions (Fig. 1). The

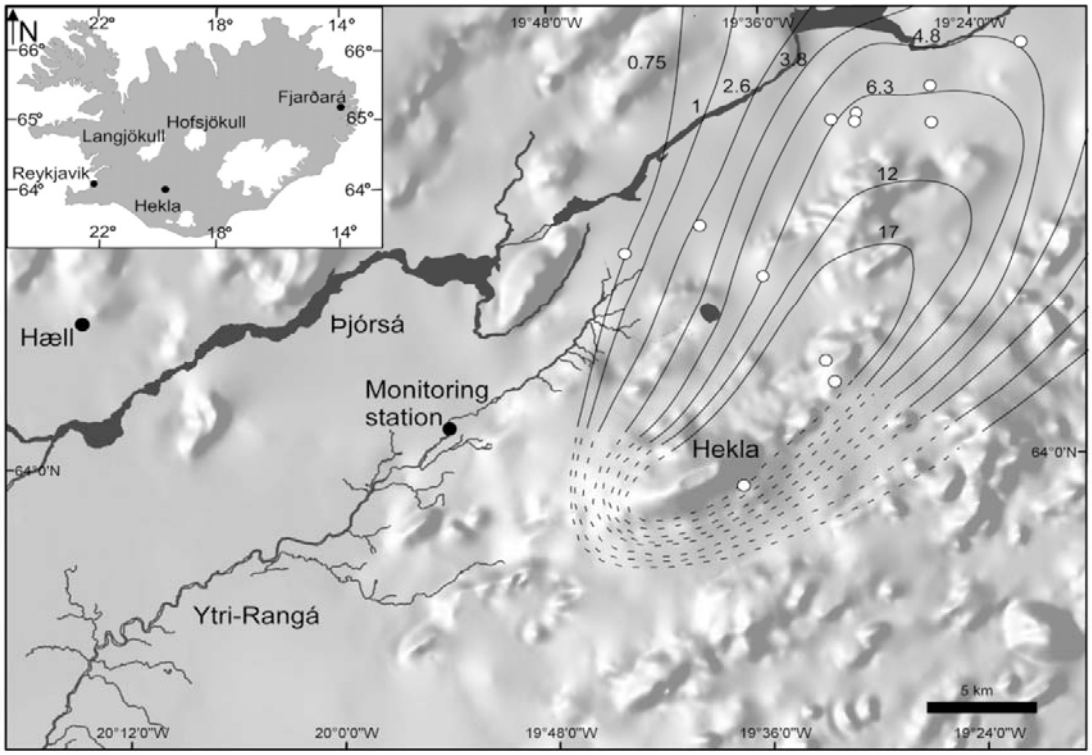

Fig. 1. Location of the Hekla volcano and Ytri–Rangá River in south Iceland. Superimposed on the map are isolines (kg/m^2) of tephra of the ash fall after the 1991 Mt. Hekla eruption (Larsen et al., 1992), the monitoring station in the Ytri–Rangá River, the meteorological station at Haell, and the location of snow and ash samples (white circles).

volcano strikes N 65° E and is located where the eastern volcanic zone, a propagating rift, meets the South Iceland seismic zone, a transform zone (Gudmundsson et al., 1992). The volcano has erupted 18 times since 1104 (Gronvold et al., 1983). The lava fields surrounding Mt. Hekla host a large ground-water body, with the general ground-water movement flowing from the northeast to the southwest along the volcanic zone. Ground-water discharge is evident at the headspring of the Ytri–Rangá River, northwest of the volcano, as well as the springs west, south and southeast of the volcano (Árnason, 1976). Due to long-term influx of magmatic gases from Hekla to the ground-water system and the high reactivity of the volcanic rocks, the concentration of dissolved solids and alkalinity is high in the Ytri–Rangá River (Fig. 1; TDS: 170–180 mg/kg, alkalinity about 1.5 meq/kg). This is one of the highest alkalinities measured in Icelandic rivers (e.g. Gislason et al., 1996) and makes this river capable of neutralizing a greater acid load than other rivers in Iceland. The discharge rate of the Ytri–Rangá River at the bridge north of Galtalaekur (Fig. 1) is about 15.5 m^3/s and is very stable since it is primarily fed by springs (The Hydrological Services of the National Energy Authority, 2006).

2.2. The 1991 eruption

On 17 January 1991 at 17:00 UT, 42 min after sunset, Hekla started to erupt. The eruption lasted until March 11th and produced 0.02 km^3 of tephra and 0.15 km^3 of lava (Gudmundsson et al., 1992). The main tephra fall occurred during the first 8 hours of the eruption and most of the ash fell in the area north-northeast of the volcano (Larsen et al., 1992; Fig. 1). The average content of soluble fluorine was 1600 mg F from 1 kg of tephra (Gudmundsson et al., 1992). Snowfall during the eruption made it possible to collect snow with enclosed volcanic aerosols and ash (Gislason et al., 1992).

2.3. The 2000 eruption

The Hekla eruption in 2000 started on the 26th of February, at 18:17 UT, 9 min before sunset. A 4.5 km long fissure opened on the crest and on the southeast flank of the Hekla ridge (Fig. 2; Lacasse et al., 2003).

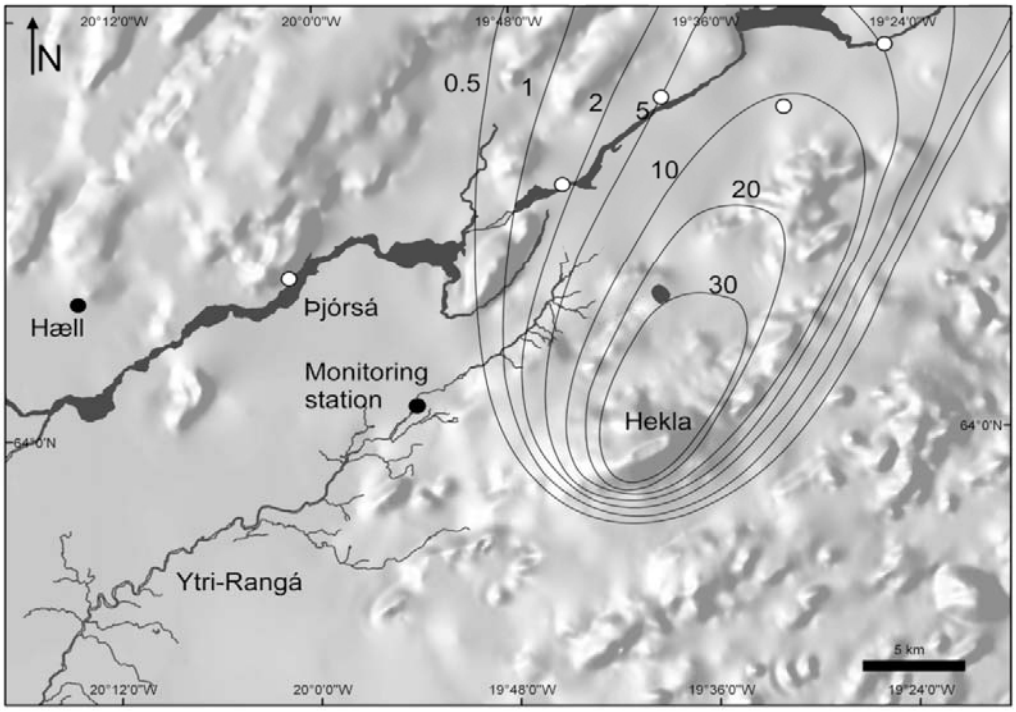

Fig. 2. The Hekla volcano and the Ytri–Rangá River in south Iceland. Superimposed on the map are isolines (kg/m^2) of the ash fall after the 2000 eruption (Haraldsson, 2001), the monitoring station in the Ytri–Rangá River, the meteorological station at Haell and the location of snow and ash samples (white circles).

After a few minutes, the eruption produced a cloud that rose to 11–12 km a.s.l. and was carried north by light winds. Seismic and weather radar data indicate that the most intense explosive activity lasted until about 22:00 UT, after which the activity in the summit area decreased to a level of intense fire fountaining and phreatomagmatic explosions (S Karlsdottir and H Mattson as quoted by Rose et al., 2003). Remote sensing data (Rose et al., 2003) suggest that ice mass in the volcanic cloud peaked at about 1 Tg about 10 hours after the beginning of the eruption. The volcanic cloud contained up to 0.2 Tg of SO_2, up to 0.003–0.008 Tg of sulfate aerosols and about 0.1 Tg of ash (tephra) (Rose et al., 2003). A recent study by Moune et al. (2007) states that the amount of degassed SO_2 may easily be an order of magnitude higher than the amount estimated by remote sensing techniques. The 2000 eruption is the shortest and smallest Hekla eruption on record in terms of its duration, 11 days, and of the total volume of unconsolidated tephra, 0.01 km^3 (Haraldsson et al., 2002), and lava, 0.17 km^3 (Ólafsdóttir et al., 2002). The tephra was transported by the prevailing winds north-northeast across central and northern Iceland and off the north coast (Haraldsson, 2001; Lacasse et al., 2003). The ash load on the headwaters of the Ytri–Rangá River was up to 5 kg/m^2 (Haraldsson, 2001; Fig. 2). Snow that fell during the sub-Plinian phase after February 26 at 22:00 UT made it possible to collect snow samples containing ash.

3. Material and methods

3.1. River samples 1991 and 2000

Samples of the Ytri–Rangá River were collected at the monitoring station (N 64°00.945′ W 19°53.810′) right after the beginning of both eruptions, as shown in Figs. 1 and 2. The water samples were filtered immediately after sampling through 0.2 μm Millipore membranes (cellulose acetate). Samples intended for major and trace element analyses were acidified by concentrated suprapure HNO_3 (1/100). Alkalinity/DIC and pH were determined in the laboratory at ambient temperature 1 to 5 days after sampling. For the 1991 samples, pH, F and Cl were measured with an ion-selective electrode. SiO_2, Na, K, Ca, Mg, SO_4, Fe, Mn, Ti, Al and Sr were measured by inductively-coupled plasma emission spectrometry (ICP-AES). The dissolved inorganic nutrients PO_4, NO_3, and NH_4 were measured by a spectrophotometer. In 2000, F, Cl and SO_4 were measured by ion-chromatography (IC). The rest of the dissolved elements were analyzed by a combination of ICP-AES, inductively coupled plasma sector mass spectrometry (ICP-SMS), and atomic fluorescence spectrometry (AFS).

3.2. Snow samples

Fresh snow containing ash was collected on the ground 18–23 h after the beginning of the 2000 eruption at sampling sites located 10–20 km north and west of Hekla (Fig. 2). The presence of tephra in snow layers acted as indicators of whether the snow layers fell during, before or after the early hours of the eruption. The mixture of tephra and snow was sampled into heavy-walled 30-liter plastic bags which had been washed with 0.1 M hydrochloric acid for more than an hour and then carefully rinsed several times with DI water. At each sampling site about one square meter was cleared of the first few centimeters of snow that fell after the deposition of the sub-Plinian unit. Sampling bags were packed into insulation boxes to ensure no melting of the snow samples during their transport to the laboratory.

Samples were kept in a freezer at −18 °C until they were melted by immersing the plastic bags in hot water (60–95 °C) in the laboratory for 30 min. Once all snow was melted, solutions were immediately filtered through 0.2 μm cellulose acetate filters. Filtered solutions were then treated similarly to the river water samples described in 3.1. The snow samples from the 2000 eruption have been used for calculation of trace element degassing and enrichment in the eruptive plume of Mt. Hekla (Moune et al., 2006).

3.3. PHREEQC2

3.3.1. Speciation and mixing calculations

Speciation, saturation-state calculations and mixing simulations were performed by the PHREEQC 2.11 computer code (Parkhurst and Appelo, 1999). The database Wateq4f was used with some changes: thermodynamic data for the primary minerals of basalt are from Stefánsson (2000); thermodynamic data for Hekla 1991 and 2000 glasses are from Gudmundsson et al. (1992) and Wolff-Boenisch et al. (2004b), respectively. Thermodynamic data for secondary minerals are from Stefánsson and Gislason (2001), thermodynamic data for aqueous aluminum species are from Arnórsson and Andrésdóttir (1999); thermodynamic data for Fe^{2+}, $Fe(OH)_4^-$ and H_4SiO_4 are from Shock et al. (1997), Diakonov et al. (1999) and Gunnarson and Arnórsson (2000), respectively.

To simulate the chemical reactions that take place when melted snow that is highly contaminated with

volcanic ash comes in contact with various surface waters, the melted snow samples from the 2000 eruption between the 10 and 20 kg/m^2 isolines which had the lowest pH and were most contaminated (sample 00-HE014 in Table 3; Fig. 2) were mixed with increasingly greater proportions of: (1) uncontaminated precipitation from the Langjökull Glacier (Fig. 1), (2) water from Fjardará River (Fig. 1), (3) uncontaminated river water from the Ytri–Rangá, and (4) seawater. The mixing was performed at in situ temperatures and the mixtures were equilibrated with atmospheric O_2 and CO_2. For seawater and river water, measured alkalinity was used instead of atmospheric CO_2 concentrations. Calcite, fluorite, amorphous $Al(OH)_3$ and amorphous FeOOH were allowed to precipitate when supersaturated.

3.3.2. ΔG_r for the dissolution of minerals and glasses in snow and water

The melted snow/ash samples and water samples from both eruptions were modeled with PHREEQC to define the saturation state of primary and secondary minerals at the in situ temperature (0.1 °C for the snowmelt samples). The saturation state is given as the Gibbs free energy of the reaction, ΔG_r (Gislason and Arnórsson, 1990, 1993). Most often saturation state is given as the logarithm of the ratio between the equilibrium constant K and the reaction quotient Q, sometimes referred to as the ion activity product: SI = log Q/K. The relationship between the ΔG_r and SI is as follows:

$$\Delta G_r = \frac{R*T*2.303*SI}{1000},$$

where R=8.3145 J K^{-1} mol^{-1}, T (K) and 2.303 is a conversion factor. The Gibbs free energy of reaction is equal to zero at equilibrium. If $\Delta G_r < 0$, the mineral is unstable, i.e. dissolving. Dissolution rate equations for minerals and glasses are written in terms of the ΔG_r and not the SI (e.g. Gislason and Oelkers, 2003). Thus it is of advantage to use ΔG_r rather than the conventional SI. The numerical value of the ΔG_r for undersaturated minerals will tell whether the saturation state slows down the dissolution rate of undersaturated minerals and volcanic glasses. At 0 to 25 °C, the dissolution rate is dependent on the saturation state when ΔG_r ranges from <0 to −10 kJ/mol. At higher undersaturation, when the ΔG_r is a greater negative number than −10 kJ/mol, the dissolution rate is independent of the saturation state. The saturation state of both end-members and solid solution primary minerals was investigated. Both end-members for olivine and typical phenocryst ($Fo_{0.43}Fa_{0.57}$) and groundmass ($Fo_{0.80}Fa_{0.20}$) compositions were investigated, together with two ortho- and three clinopyroxenes, four different plagioclases, and volcanic glass of basaltic (Stapafell) and basaltic–andesitic composition (Hekla, 1991–2000). As secondary minerals, gibbsite, amorphous $Al(OH)_3$, three different allophanes, imogolite (natural gel and synthetic gel), laumontite, montmorillonite from Aberdeen and Belle Fourche and Ca montmorillonite, cryptocrystalline goethite, amorphous FeOOH, amorphous silica, quartz, chalcedony, moganite, fluorite, anhydrite, gypsum, barite and calcite were considered.

4. Results

4.1. Results from the 1991 eruption

Fig. 1 shows the ash load from the 1991 eruption and locations of snow samples and the monitoring station. Since the eruptive plume was transported in a north-northeasterly direction, only the upper part of the Ytri–Rangá River was affected by ash deposition from the sub-Plinian column (between 0.75 and 1.5 kg/m^2 of ash in the 12 first hours or so). Table 1 shows analyses of snow samples containing ash from the 1991 eruption. The samples were taken during the later stage and after the eruption and, with one exception, are not representative of the initial explosive sub-Plinian phase. The highest measured concentrations of Fe, Al and F in the snow/ash samples were 44.0, 440 and 1753 μmol/kg, respectively.

The weather conditions in the Hekla area from the beginning of the eruption and for the following 9 days were measured at the Haell weather station (Fig. 1; 64°03.904′ N 20°14.471′ W, 121 m.a.s.l.) and are shown in Fig. 3. The headsprings of the Ytri–Rangá River are about 220 m.a.s.l., with the temperature there probably one degree lower than at the Haell station. The first period of rain occurred on the fourth, fifth and sixth days of the eruption and there was another period with rain on days seven and eight.

The chemistry of the Ytri–Rangá River was monitored at the bridge over the river north of Galtalaekur (Figs. 1 and 2). The first water sample was taken ca 1.5 h after the beginning of the eruption. Samples were then taken 3–4 times a day during the eruption and then every second day, weekly, and finally monthly for ca 500 days.

Time series results for pH and selected dissolved elements are shown in Fig. 4 and all data are shown in Table 2. A sample collected in 1988 at the monitoring station is shown in Table 2 for comparison. The F concentration is shown for 3 different time scales: 6 days, 30 days and 300 days from the beginning of the eruption, Jan. 17 at 17:00 UT. Thus 4 days from the

Table 1
Analyses of snow samples collected during the later stage of the 1991 eruption

Sample number	Location	Date and time	pH	T °C (titration)	Charge balance (% error) (PHREEQC)	SiO_2 (mmol/kg) (ICP-AES)	Na (mmol/kg) (ICP-AES)	K (mmol/kg) (ICP-AES)	Ca (mmol/kg) (ICP-AES)	Mg (mmol/kg) (ICP-AES)	S (mmol/kg) (ICP-AES)
Drinking water limits							8.70	0.307	2.50	2.06	2.60
91-3051	64.012° N, 19.903° W	1/25/1991 13:10	5.13	21.6	−2.6	0.0469	0.0983	0.00332	0.0205	0.0169	0.00895
91-3052	64.449° N, 19.438° W	1/28/1991 17:10	5.01	20.1	4.7	0.149	0.236	0.0110	0.189	0.0745	0.0582
91-3053	64.151° N, 19.511° W	1/28/1991 16:20	5.91	21.6	9.6	0.293	0.440	0.0233	0.392	0.183	0.120
91-3054	64.105° N, 19.658° W	1/28/1991 15:30	6.17	20.1	6.2	0.180	0.281	0.0115	0.184	0.110	0.0707
91-3062	63.988° N, 19.623° W	1/29/1991 18:15	3.25	17.0	n.m.	n.m.	n.m.	n.m.	n.m.	n.m.	n.m
91-3063	63.988° N, 19.623° W	2/1/1991 15:20	3.32	19.9	−1.2	0.176	0.237	0.0120	0.140	0.0518	0.0574
91-3064	63.988° N, 19.623° W	2/1/1991 15:20	3.49	18.3	−2.4	0.0834	0.176	0.00639	0.0569	0.0309	0.0255
91-3065	63.988° N, 19.623° W	2/1/1991 15:40	3.52	20.9	−1.5	0.102	0.208	0.00716	0.0764	0.0379	0.0356
91-3066	64.185° N, 19.351° W	1/28/1991 17:20	3.61	20.7	3.2	0.031	0.214	0.00537	0.0414	0.0239	0.0266
91-3067	64.034° N, 19.535° W	1/29/1991 13:35	4.77	22.7	−8.4	0.00333	0.0874	0.00230	0.00499	0.00987	0.00979
91-3068	64.093° N, 19.729° W	1/28/1991 14:48	5.3	24.8	−13	0.00150	0.0405	0.00230	0.00175	0.00453	0.00541
91-3069	64.166° N, 19.438° W	1/28/1991 17:10	3.48	22.6	2.3	0.0662	0.388	0.0105	0.0826	0.0440	0.0644
91-3070	64.043° N, 19.543° W	1/29/1991 14:05	4.81	23.0	−6.1	0.00216	0.0913	0.00153	0.00299	0.00987	0.00885
91-3071	64.082° N, 19.600° W	1/29/1991 16:10	5.06	22.4	0.69	0.00150	0.144	0.00230	0.00424	0.0160	0.0122
91-3097	64.151° N, 19.532° W	2/13/1991 14:50	5.16	22.8	2.6	0.0245	0.188	0.00512	0.0424	0.0366	0.0325
91-3098	64.154° N, 19.509° W	2/13/1991 15:15	4.62	21.5	3.3	0.112	0.291	0.00870	0.0736	0.0683	0.0512
91-3106		1/22/1991	6.64	21.3	28	0.240	0.165	0.00870	0.0539	0.00658	0.0270
91-3107		1/26/1991	5.96	21.8	3.4	0.130	0.267	0.00501	0.0412	0.0263	0.0344
91-3108		1/22/1991	6.32	22.4	11	0.181	0.291	0.0149	0.0938	0.0255	0.0427
91-3109		1/22/1991	6.06	21.0	5.7	0.371	0.301	0.0100	0.138	0.0687	0.0363
91-3110		1/28/1991	6.67	21.7	20	0.00749	0.101	0.00803	0.0202	0.00288	0.0230
91-3111		1/28/1991	6.46	22.2	15	0.0118	0.118	0.00911	0.0227	0.00370	0.0262
91-3115	64.809° N, 18.869° W	2/24/1991	3.89	25.8	−15	0.0673	0.109	0.0106	0.119	0.0555	0.0453
91-3116		1/22/1991	5.85	22.0	7.2	0.106	0.119	0.0159	0.0499	0.0218	0.00854
91-3117		1/22/1991	6.42	21.0	7.4	0.106	0.110	0.00997	0.0479	0.0214	0.00833
91-3119		2/16/1991 16:35	5.31	20.6	−19	0.000832	0.0452	0.00179	0.0115	0.00494	0.0149
91-3121		2/16/1991 17:40	4.69	25.0	−6.2	0.00166	0.0161	0.000767	0.00424	0.00288	0.00770
91-3122		2/15/1991	4.06	22.9	1.8	0.0113	0.0426	0.00486	0.0237	0.00782	0.0204

Sample number	Cl (mmol/kg) (Ion-selective elektrode)	F (µmol/kg) (Ion-selective elektrode)	Al (µmol/kg) (ICP-AES)	Fe (µmol/kg) (ICP-AES)	P (µmol/kg) (ICP-AES)	PO_4 (µmol/kg) (Spectro photometer)	NO_3 (µmol/kg) (Spectro photometer)	NH_4 (µmol/kg) (Spectro photometer)	Sr (µmol/kg) (ICP-AES)	Mn (µmol/kg) (ICP-AES)	Ti (nmol/kg) (ICP-AES)
Drinking water limits	7.05	78.6	7.41	3.58			806	18.336		0.91	
91-3051	0.151	57.0	12.1	1.59	0.515	n.m.	0.2	0.262	0.0299	0.191	0.276
91-3052	0.349	778	170	15.0	n.m.	0.00948	0.1	0.208	0.316	2.80	0.349
91-3053	0.676	1753	440	7.91	n.m.	n.d.	0.3	0.502	0.580	7.79	0.104
91-3054	0.389	773	176	0.861	0.00	n.d.	1.5	0.274	0.256	2.46	0.217
91-3062	0.447	859	n.m.	n.m.	n.m.	12.22	0.00161	1.83	n.m.	n.m.	n.m.
91-3063	0.809	944	99.8	73.8	12.0	12.65	0.9	2.45	0.267	2.39	11.9
91-3064	0.502	480	43.9	33.3	5.39	5.59	0.681	2.07	0.108	1.08	5.58
91-3065	0.524	564	56.6	44.0	6.03	6.79	0.579	2.56	0.143	1.42	6.95
91-3066	0.486	142	27.3	8.35	5.74	5.30	0.568	0.234	0.0874	0.444	0.862
91-3067	0.118	11.3	2.03	0.544	n.m.	0.0253	0.0500	0.130	0.0167	0.0364	0.0605
91-3068	0.062	1.58	0.274	0.102	0.00	n.d.	0.0177	0.165	0.00728	0.0164	0.0209
91-3069	0.694	427	57.0	20.1	9.71	10.7	0.0161	0.161	0.162	0.825	2.62
91-3070	0.111	7.74	0.701	0.174	0.00	0.00948	2.09	0.0573	0.0117	0.0200	0.0230
91-3071	0.159	1.89	0.300	0.116	n.m.	0.0558	0.0613	0.177	0.0240	0.0255	0.0376
91-3097	0.271	34.2	11.2	1.31	0.380	0.0453	0.0742	0.268	0.0823	0.617	0.00418
91-3098	0.420	46.6	6.77	0.637	0.466	0.0400	6.29	0.199	0.109	0.564	0.0397
91-3106	0.078	27.2	0.107	0.0859	2.83	n.m.	n.m.	n.m.	0.0451	0.186	0.0146
91-3107	0.231	86.3	0.789	0.152	1.24	n.m.	n.m.	n.m.	0.0488	0.661	0.0146
91-3108	0.129	253	10.3	0.134	3.54	n.m.	n.m.	n.m.	0.0845	1.02	0.0125
91-3109	0.154	611	61.5	0.161	4.42	n.m.	n.m.	n.m.	0.136	3.15	0.0104
91-3110	0.0530	4.79	0.719	0.0788	n.m.	n.m.	n.m.	n.m.	0.0182	0.0783	0.0209
91-3111	0.0629	19.3	0.460	0.206	0.00	n.m.	n.m.	n.m.	0.0262	0.167	0.255
91-3115	0.262	0.941	0.134	0.105	n.m.	n.m.	n.m.	n.m.	n.m.	4.00	11.5
91-3116	0.083	256	40.9	0.109	2.33	n.m.	n.m.	n.m.	0.0524	0.573	0.0209
91-3117	0.105	230	43.4	0.113	2.63	n.m.	n.m.	n.m.	0.0517	0.653	0.0251
91-3119	0.0886	42.7	12.2	0.528	n.m.	n.m.	n.m.	n.m.	0.0255	0.158	0.0146
91-3121	0.0279	32.5	4.23	1.65	n.m.	n.m.	n.m.	n.m.	0.00728	0.0837	0.228
91-3122	0.129	105	17.2	11.2	0.500	n.m.	n.m.	n.m.	0.0481	0.482	0.908

n.m.= not measured.

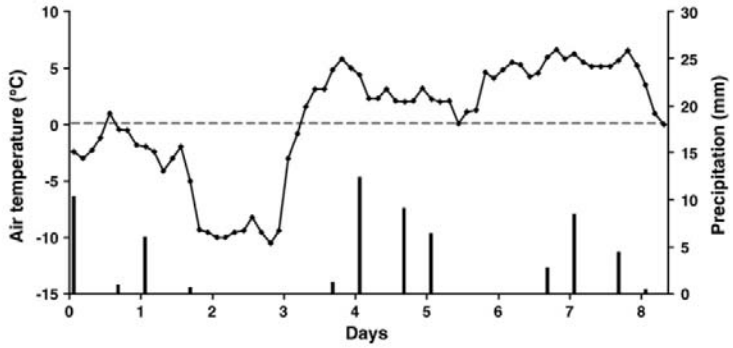

Fig. 3. Air temperature (°C) and precipitation (mm) during the first days after the 1991 eruption as measured at the Haell meteorological station.

beginning of the eruption translates to Jan. 22 at 17:00. The time series for the rest of the elements is for the first 30 days (Fig. 4). Fluorine concentration was stable during the first days of the eruption; starting 3–4 days after the eruption onset, it sharply increased, reaching a maximum on Jan. 21 at 16:52 UT (Fig. 4 and Table 2). Right after the sample was taken over 10 mm of rain fell, resulting in a decrease in the F concentration in the sample collected later in the day (Jan. 21, 22:49; Table 2, Figs. 3 and 4). This decrease could have been due to dilution and/or exhaustion of the readily soluble fluorine source. Six days after the beginning of the eruption (Jan. 23 17:45 UT) the F concentration had decreased to values similar to those observed before the first rain and in the weeks and months after the eruption (top of Fig. 4 and Table 2). Thus it took a little less than 2.5 days to flush out the readily soluble F in the snow and for it to be adsorbed on the tephra in the vicinity of the headsprings of the Ytri–Rangá (Figs. 1 and 4). The Cl and proton concentrations show behavior similar to that of F (Fig. 4) reaching a peak concentration about 4 days from the beginning of the eruption, but the DIC (mostly bicarbonate) and SO_4 concentrations decreased when the snow melt was flushed into the river. This is a very important observation since the eruption cloud consisted mostly of ice, CO_2, SO_2 and some tephra, as observed in the 2000 eruption (Rose et al., 2003). Thus very little SO_2 was oxidized in the vicinity of the volcano. The SO_4 concentration decreased because of dilution and in the case of DIC, as will be discussed later, some degassing of CO_2 occurred in the river water because of a decrease in pH. Mn reached a peak concentration 4 days from the eruption concordantly with the F, while Al and Fe concentrations reached their highest concentrations a few days later, as can be seen in Fig. 4 and Table 2. The concentrations of F, Al, Fe and Mn in the snow/ash samples exceeded allowable drinking water limits in many samples (Table 1). Three samples of the river water exceeded the drinking water limits for F, while only one sample had too high a concentration of Al (Fig. 4; Table 2).

4.2. Results from the 2000 eruption

An isoline map of the ash fall from the 2000 eruption is shown in Fig. 2, together with the location of snow samples and the monitoring station. During this eruption, the wind direction was more to the north than in the 1991 eruption (Fig. 1), which caused a higher load of ash to fall into the Ytri–Rangá River and its catchments (Figs. 1 and 2). Maximum ash load in the river was ca 5 kg/m^2 in the northeastern parts (Haraldsson, 2001).

Analyses of snow samples containing ash taken during the 2000 eruption are shown in Table 3. All the melted snow samples were affected by volcanic aerosols, as reflected in the pH of the waters, which ranged from 2.6 to 4.5. The average 1998–1999 winter precipitation from the Langjökull Glacier (Gíslason et al., 2000) (Fig. 1) is shown for comparison in Table 3. The highest concentrations were measured in sample 00-HEO14 from the main axis of the fallout (Fig. 2; Table 3). In this sample the concentrations of dissolved F, Al and Fe in the melted snow were 66.2, 6.04 and 4.15 mmol/kg, respectively. The highest concentrations of Pb, Cd and Co were 282, 9879 and 725 nmol/kg, respectively, while the highest measured Cu concentration was 3729 nmol/kg. The measured concentrations of Cl, F, Al, Fe, Mn, As, Cd and Pb all exceeded the drinking water limits given by the European Community (1998) in one or more snow samples (Table 3).

Weather reports from the Haell weather station (Fig. 5) show that the first period of rain after the onset of the eruption started on day 7. Fig. 6 and Table 4 show the time series of pH as well as the dissolved major and trace elements in the Ytri–Rangá River at the monitoring station (Fig. 2). The first sample was taken 30 min after

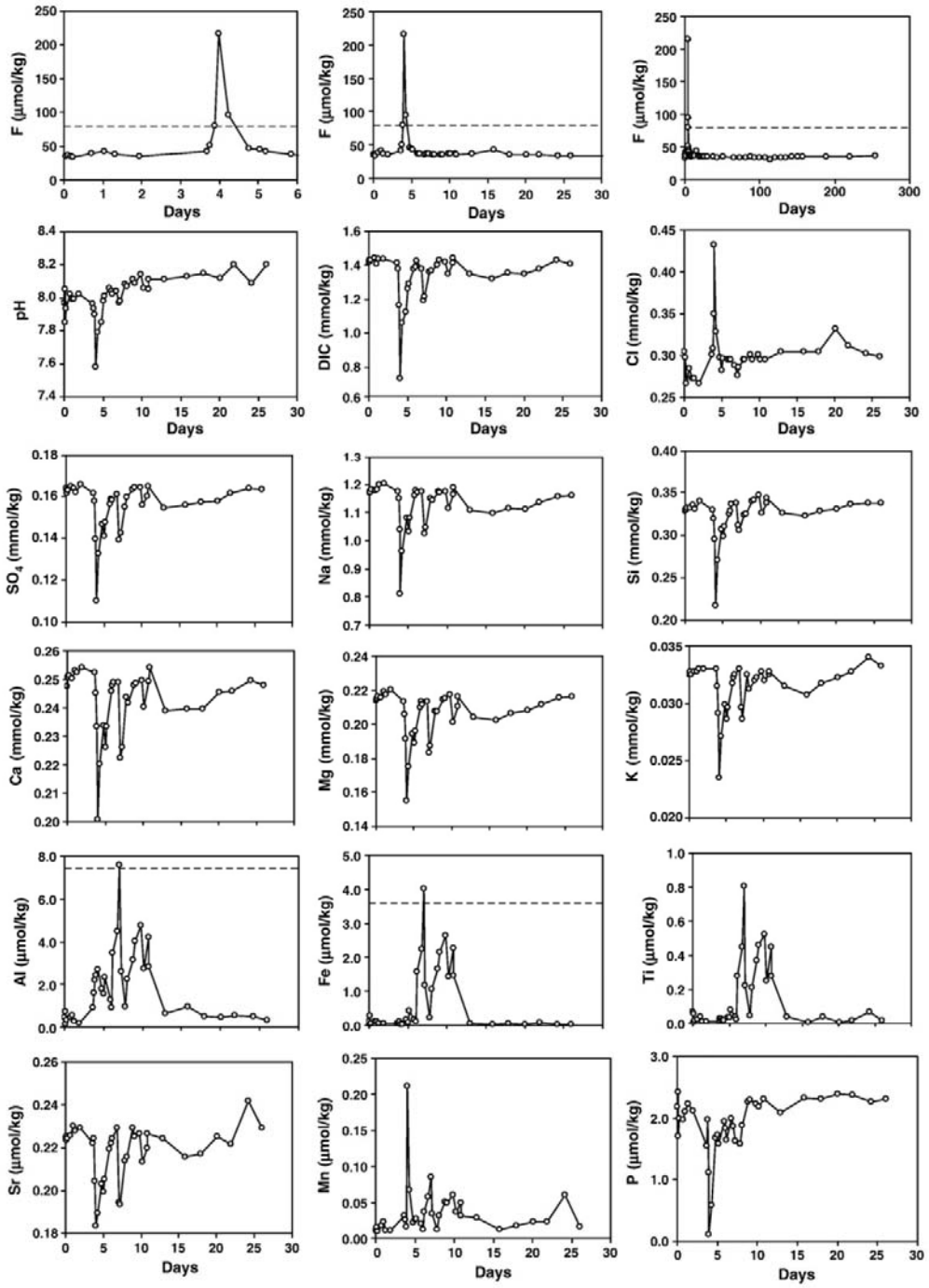

Fig. 4. Dissolved constituents in the Ytri–Rangá River versus time during and after the 1991 eruption. Note the various time scales for the F concentrations at 6, 30 and 300 days. All other concentrations are shown for the 30 day period. The hatched horizontal line on some diagrams is the upper limit for drinking water (European Communities, 1998). No horizontal line is shown if concentrations were below this upper limit.

the beginning of the eruption, and samples were taken frequently during the first day because tephra fell directly into the river during the initial sub-Plinian phase of the eruption (Fig. 2). Frequent sampling was resumed following the first rain on the tephra. The monitoring continued for two months with a total of 18 samples. The

Table 2
The chemical composition of river water sampled during and after the 1991 eruption

Sample number	Date and time	T °C (in situ)	pH (titration)	T °C (titration)	Charge balance (% error) (PHREEQC)	SiO_2 (mmol/kg) (ICP-AES)	Na (mmol/kg) (ICP-AES)	K (mmol/kg) (ICP-AES)	Ca (mmol/kg) (ICP-AES)	Mg (mmol/kg) (ICP-AES)	DIC (mmol/g)	Alk. (meq-kg)	S (mmol/kg) (ICP)	Cl (mmol/kg) (Ion-selective electrode)	F (μmol/kg) (Ion-selective electrode)	Al (μmol/kg) (ICP-AES)	Fe (μmol/kg) (ICP-AES)	PO_4 (μmol/kg) (Spectrophotometer)	Sr (μmol/kg) (ICP-AES)	Mn (μmol/kg) (ICP-AES)	Ti (μmol/kg) (ICP-AES)
Drinking water limits							8.7	0.307	2.5	2.0568			2.6	7.05	78.6	7.41	3.58			0.91	
88-3019	6/30/1988 19:15	6.0	8.44	6.4	−1.9	0.747	1.20	0.039	0.243	0.236	1.60	1.58	0.187	0.299	32.9	n.m.	n.m.	n.m.	n.m.	n.m.	n.m.
91-3018	1/17/1991 18:22	n.m.	7.97	20.5	1.9	0.329	1.17	0.0325	0.248	0.214	1.42	1.38	0.164	0.305	34.9	0.478	0.125	2.19	0.224	0.0109	0.0710
91-3019	1/17/1991 19:18	n.m.	8.05	19.9	2.1	0.330	1.17	0.0327	0.251	0.215	1.42	1.39	0.163	0.298	35.7	0.719	0.286	2.43	0.225	0.0146	0.0564
91-3020	1/17/1991 21:20	n.m.	7.85	19.4	2.4	0.329	1.17	0.0327	0.251	0.215	1.43	1.38	0.161	0.298	35.3	0.137	0.025	1.70	0.224	0.0091	0.00418
91-3021	1/17/1991 22:12	n.m.	7.93	20.0	3.2	0.332	1.18	0.0325	0.251	0.216	1.43	1.39	0.163	0.267	33.3	0.319	0.068	2.00	0.224	0.00910	0.0146
91-3022	1/18/1991 9:50	n.m.	8.02	19.4	2.0	0.332	1.18	0.0327	0.250	0.216	1.45	1.41	0.165	0.284	38.6	0.460	0.111	1.98	0.226	0.0182	0.0230
91-3023	1/18/1991 18:01	n.m.	7.99	20.3	3.5	0.336	1.18	0.0327	0.253	0.219	1.41	1.37	0.164	0.272	41.7	0.526	0.104	2.11	0.230	0.0237	0.0376
91-3024	1/19/1991 15:19	n.m.	8.02	19.6	3.5	0.340	1.20	0.0330	0.254	0.220	1.44	1.40	0.166	0.267	35.4	0.189	0.047	2.12	0.229	0.0109	0.0125
91-3025	1/19/1991 0:33	n.m.	7.99	20.0	3.3	0.331	1.20	0.0330	0.253	0.217	1.44	1.40	0.162	0.272	37.3	0.293	0.063	2.23	0.228	0.0109	0.0125
91-3029	1/21/1991 9:03	9.1	7.96	19.7	2.6	0.330	1.18	0.0330	0.252	0.213	1.41	1.37	0.162	0.301	42.0	0.901	0.047	1.55	0.222	0.0309	0.0104
91-3030	1/21/1991 11:24	5.7	7.93	20.7	1.8	0.319	1.15	0.0315	0.245	0.206	1.38	1.34	0.158	0.308	50.5	1.61	0.068	1.98	0.224	0.0255	0.0271
91-3031	1/21/1991 14:16	4.9	7.90	20.0	2.3	0.295	1.04	0.0292	0.233	0.191	1.16	1.13	0.139	0.349	79.9	2.21	0.116	1.12	0.205	0.0164	0.0271
91-3032	1/21/1991 16:52	3.6	7.58	20.8	−0.2	0.217	0.81	0.0235	0.201	0.155	0.74	0.693	0.110	0.432	216	2.43	0.016	0.10	0.183	0.2111	0.0188
91-3033	1/21/1991 22:49	3.4	7.79	20.7	2.2	0.270	0.96	0.0271	0.220	0.175	1.06	1.02	0.133	0.328	95.3	2.69	0.032	0.59	0.189	0.0673	0.0146
91-3034	1/22/1991 11:33	3.8	7.85	21.6	6.7	0.306	1.08	0.0299	0.234	0.195	1.12	1.09	0.146	0.298	45.8	1.76	0.170	1.68	0.203	0.0218	0.0355
91-3035	1/22/1991 18:01	3.8	7.98	21.6	1.5	0.299	1.03	0.0286	0.226	0.189	1.27	1.23	0.141	0.282	44.5	1.53	0.079	1.73	0.200	0.0255	0.0313
91-3036	1/22/1991 21:30	3.6	8.01	20.5	2.1	0.310	1.08	0.0297	0.234	0.196	1.29	1.26	0.148	0.296	42.4	2.33	0.417	1.58	0.205	0.0273	0.079
91-3037	1/23/1991 13:30	4.0	8.06	20.5	2.8	0.325	1.16	0.0317	0.246	0.210	1.38	1.35	0.156	0.295	37.3	1.29	0.172	1.94	0.219	0.0200	0.0397
91-3038	1/23/1991 17:45	4.4	8.04	19.6	3.1	0.329	1.18	0.0322	0.248	0.214	1.39	1.36	0.159	0.295	36.5	0.93	0.104	1.83	0.222	0.0127	0.0251
91-3039	1/23/1991 21:00	4.7	8.02	20.0	2.4	0.337	1.17	0.0325	0.249	0.212	1.42	1.39	0.158	0.295	36.4	3.46	1.572	1.64	0.224	0.0364	0.276
91-3040	1/24/1991 11:30	5.2	8.04	19.2	3.8	0.337	1.17	0.0330	0.249	0.213	1.38	1.34	0.161	0.288	36.0	4.47	2.249	1.99	0.229	0.0582	0.451
91-3041	1/24/1991 18:20	4.8	7.97	20.3	3.9	0.311	1.02	0.0297	0.223	0.184	1.19	1.16	0.139	0.276	36.5	7.57	4.030	1.86	0.194	0.0855	0.808
91-3042	1/24/1991 22:34	4.8	7.98	19.0	3.3	0.305	1.05	0.0286	0.226	0.188	1.22	1.19	0.142	0.285	36.4	2.60	1.166	1.63	0.194	0.0346	0.219
91-3043	1/25/1991 13:10	4.6	8.08	19.8	2.9	0.324	1.15	0.0325	0.244	0.207	1.36	1.33	0.155	0.295	35.2	0.945	0.242	1.58	0.214	0.0127	0.0438
91-3044	1/25/1991 18:54	3.9	8.07	19.9	2.1	0.325	1.14	0.0312	0.242	0.207	1.37	1.34	0.160	0.295	36.0	2.24	1.060	1.88	0.216	0.0309	0.213
91-3045	1/26/1991 13:21	4.8	8.11	20.1	2.3	0.340	1.17	0.0320	0.248	0.214	1.40	1.38	0.163	0.301	34.9	3.14	1.663	2.27	0.229	0.0510	0.370
91-3046	1/26/1991 19:07	4.9	8.09	21.6	2.1	0.341	1.17	0.0322	0.249	0.215	1.43	1.40	0.164	0.295	34.9	4.00	2.152	2.29	0.225	0.0491	0.459
91-3047	1/27/1991 13:08	5.0	8.14	20.0	2.4	0.347	1.17	0.0327	0.250	0.218	1.42	1.39	0.164	0.301	36.3	4.74	2.645	2.24	0.226	0.0601	0.524
91-3048	1/27/1991 21:39	5.1	8.06	21.6	2.0	0.326	1.12	0.0320	0.240	0.201	1.35	1.32	0.156	0.295	36.5	2.75	1.450	2.18	0.213	0.0364	0.253
91-3049	1/28/1991 12:45	3.8	8.05	20.1	2.2	0.338	1.16	0.0325	0.249	0.210	1.41	1.38	0.160	0.295	37.4	4.21	2.269	2.32	0.220	0.0491	0.447
91-3050	1/28/1991 13:20	2.7	8.11	21.4	2.2	0.343	1.19	0.0327	0.254	0.216	1.45	1.42	0.165	0.295	35.9	2.84	1.470	2.32	0.326	0.0309	0.276
91-3099	1/30/1991 15:20	3.6	8.11	21.2	1.5	0.326	1.11	0.0315	0.239	0.204	1.35	1.32	0.154	0.305	36.4	0.623	0.045	2.10	0.224	0.0291	0.0397
91-3100	2/2/1991 13:32	3.4	8.13	22.4	1.7	0.323	1.10	0.0307	0.240	0.202	1.32	1.29	0.156	0.305	43.5	0.960	0.030	2.32	0.216	0.0127	0.00835
91-3101	2/4/1991 15:23	2.8	8.15	21.3	1.3	0.329	1.11	0.0317	0.240	0.207	1.36	1.33	0.157	0.305	35.8	0.511	0.054	2.32	0.217	0.0182	0.0397

Sample number	Date and time	T °C water	pH	T °C (titration)	Charge balance (% error) (PHREEQC)	SiO_2 (mmol/kg) (ICP-AES)	Na (mmol/kg) (ICP-AES)	K (mmol/kg) (ICP-AES)	Ca (mmol/kg) (ICP-AES)	Mg (mmol/kg) (ICP-AES)	DIC (mmol/kg)	Alk (meq./kg)	S (mmol/kg) (ICP-AES)	Cl (mmol/kg) (ion-selective electrode)	F (μmol/kg) (ion-selective electrode)	Al (μmol/kg)	Fe (μmol/kg)	PO_4 (μmol/kg)	Sr (μmol/kg)	Mn (μmol/kg)	Ti (μmol/kg)
91-3102	2/6/1991 19:16	4.5	8.12	22.2	0.92	0.331	1.11	0.0322	0.246	0.208	1.35	1.33	0.158	0.332	34.8	0.460	0.023	2.39	0.225	0.0237	0.00626
91-3103	2/8/1991 13:56	4.3	8.20	21.1	1.4	0.337	1.14	0.0327	0.246	0.211	1.38	1.36	0.161	0.311	35.4	0.537	0.091	2.37	0.221	0.0237	0.0188
91-3104	2/10/1991 22:40	4.3	8.09	22.1	1.5	0.337	1.16	0.0340	0.250	0.216	1.43	1.40	0.164	0.302	34.1	0.497	0.039	2.27	0.242	0.0691	0.0668
91-3105	2/12/1991 17:30	4.4	8.20	21.0	2.0	0.337	1.16	0.0332	0.248	0.216	1.41	1.38	0.163	0.298	34.3	0.322	0.043	2.32	0.229	0.0164	0.0167
91-3150	2/16/1991 18:53	3.9	8.11	22.8	0.074	0.332	1.19	0.0330	0.253	0.220	1.53	1.50	0.162	0.307	34.6	0.278	0.052	1.60	0.227	0.00182	0.00418
91-3151	2/16/1991 18:53	2.9	8.17	22.8	0.22	0.335	1.21	0.0335	0.257	0.222	1.55	1.52	0.165	0.307	34.7	0.285	0.090	1.88	0.231	0.00182	0.00418
91-3152	2/24/1991 17:08	2.6	8.17	22.8	1.3	0.331	1.20	0.0332	0.255	0.222	1.50	1.47	0.167	0.291	34.5	0.237	0.009	1.96	0.228	0.00182	n.d.
91-3153	3/2/1991 13:52	4.0	8.30	20.8	0.48	0.334	1.21	0.0335	0.256	0.227	1.53	1.51	0.172	0.301	33.8	0.363	0.030	1.39	0.237	0.00910	0.0251
91-3154	3/9/1991 18:17	3.4	8.18	21.0	−0.19	0.334	1.21	0.0332	0.259	0.230	1.57	1.55	0.172	0.301	33.9	0.267	0.018	2.06	0.234	0.00364	0.00626
91-3155	3/24/1991 19:35	4.3	8.27	21.2	−0.97	0.325	1.21	0.0343	0.253	0.226	1.58	1.56	0.170	0.313	33.3	0.415	0.011	0.47	0.229	0.00000	0.00209
91-3156	3/31/1991 14:26	4.6	8.26	21.4	0.26	0.328	1.20	0.0327	0.250	0.222	1.52	1.50	0.170	0.294	33.1	0.549	0.009	0.75	0.219	0.00182	0.00000
91-3157	4/8/1991 14:24	4.9	8.20	21.6	0.37	0.326	1.24	0.0330	0.256	0.229	1.55	1.53	0.180	0.305	33.4	0.437	0.027	0.25	0.229	0.00000	0.00209
91-3159	4/20/1991 14:06	5.0	8.29	22.3	4.6	0.342	1.27	0.0348	0.273	0.242	1.47	1.45	0.178	0.294	33.6	0.130	n.d.	1.52	0.248	0.00182	0.0626
91-3160	4/26/1991 19:35	4.3	8.15	22.4	0.17	0.321	1.21	0.0338	0.267	0.235	1.60	1.56	0.176	0.294	33.8	0.345	0.0179	1.99	0.243	0.00182	0.00418
91-3161	5/4/1991 20:43	5.3	8.20	21.8	−0.98	0.322	1.20	0.0338	0.267	0.235	1.61	1.58	0.174	0.319	33.8	0.230	0.0215	1.72	0.243	0.00182	0.00209
91-3162	5/11/1991 19:24	5.3	8.35	22.0	−4.8	0.326	1.12	0.0338	0.225	0.188	1.57	1.55	0.148	0.300	30.8	0.319	0.0269	1.30	0.197	0.00182	0.00209
91-3163	5/17/1991 16:20	6.1	8.47	23.5	2.1	0.322	1.21	0.0343	0.267	0.233	1.47	1.45	0.177	0.317	33.8	0.274	0.0179	1.91	0.244	0.00910	0.0188
91-3164	5/25/1991 23:08	6.4	8.05	23.4	1.5	0.322	1.22	0.0343	0.269	0.239	1.53	1.50	0.178	0.313	33.8	0.148	0.0233	2.05	0.248	0.00182	0.00209
91-3165	6/1/1991 22:00	6.2	8.18	23.5	1.2	0.330	1.22	0.0340	0.263	0.230	1.52	1.50	0.173	0.307	33.5	0.193	0.0304	2.17	0.240	0.00546	0.00626
91-3166	6/9/1991 21:56	4.3	8.13	23.3	1.7	0.334	1.23	0.0345	0.271	0.241	1.54	1.51	0.179	0.309	34.3	0.182	0.0107	1.75	0.247	0.00364	0.0710
91-3167	6/16/1991 23:10	5.8	8.09	23.5	0.87	0.331	1.23	0.0350	0.271	0.242	1.57	1.54	0.182	0.313	34.5	0.267	0.00716	1.94	0.251	0.00364	0.00209
91-3149	6/23/1991 15:30	10.6	8.31	21.9	2.6	0.328	1.25	0.0343	0.272	0.241	1.52	1.49	0.177	0.317	34.3	0.219	0.00895	2.24	0.250	0.00728	0.00209
91-3210	7/25/1991 16:30	6.0	7.90	20.1	2.6	0.338	1.22	0.0353	0.265	0.236	1.47	1.43	0.179	0.327	34.6	2.398	1.41	2.30	0.248	0.0291	0.447
91-3211	8/25/1991 14:30	4.7	7.92	20.2	4.5	0.334	1.22	0.0350	0.264	0.236	1.40	1.36	0.179	0.310	35.3	0.993	0.514	1.95	0.244	0.0164	0.150
91-3212	9/29/1991 8:00	5.1	8.26	20.2	1.1	0.328	1.20	0.0340	0.257	0.230	1.48	1.46	0.179	0.309	35.8	0.652	0.251	1.85	0.237	0.0109	0.117
92-3017	11/2/1991 16:50	4.2	8.11	22.2	7.6	0.352	1.12	0.0238	0.253	0.234	1.51	1.48	0.171	n.m.	n.m.	0.385	0.0985	2.34	0.230	0.0164	0.084
92-3018	12/15/1991 15:30	4.0	8.08	22.3	11	0.355	1.12	0.0237	0.250	0.230	1.38	1.35	0.176	n.m.	n.m.	1.78	0.976	2.48	0.226	0.0309	0.319
92-3019	1/15/1992 12:00	4.9	7.80	22.5	5.3	0.342	1.01	0.0218	0.223	0.204	1.45	1.39	0.154	n.m.	n.m.	0.593	0.0645	2.07	0.196	0.0127	0.0104
92-3020	2/27/1992 16:30	2.8	8.07	22.6	6.4	0.353	1.09	0.0231	0.241	0.223	1.50	1.47	0.164	n.m.	n.m.	0.345	0.0376	2.14	0.213	0.0146	0.100
92-3021	4/7/1992 11:20	4.1	8.13	22.7	5.1	0.329	1.08	0.0241	0.251	0.232	1.55	1.52	0.176	n.m.	n.m.	0.371	0.0895	1.91	0.235	0.0109	0.023
92-3022	5/13/1992 16:55	5.8	8.10	22.7	8.0	0.333	1.16	0.0246	0.269	0.234	1.55	1.52	0.175	n.m.	n.m.	0.345	0.0483	2.29	0.239	0.0127	0.075

n.m. = not measured, n.d. = not detected.

Table 3
Analyses of snow samples collected during the sub-Plinian phase of the 2000 eruption

Sample number	Location	Date and time	pH	T °C (titration)	Charge balance (% error)	SiO_2 (mmol/kg) (ICP-AES)	Na (mmol/kg) (ICP-SMS)	K (mmol/kg) (ICP-SMS)	Ca (mmol/kg) (ICP-SMS)	Mg (mmol/kg) (ICP-SMS)	S (mmol/kg) (ICP-AES)	SO_4 (mmol/kg) (IC)	Cl (mmol/kg) (IC)	F (μmol/kg) (IC)
Drinking water limits														
99-L2	64.809° N, 18.869° W	3/28/2005	5.73	19.7	−14	<0.0011	0.04	<0.01	<0.0025	0	0	0	0.06	0.34
00-HE025	64.076° N, 20.027° W	2/27/2000 12:56	3.50	21.8	−11	0.262	0.670	0.104	0.462	0.309	0.0817	0.0795	2.08	5.606
00-HE027	64.119° N, 19.748° W	2/27/2000 14:07	3.10	20.2	−10	2.81	5.31	0.826	1.94	1.93	0.204	0.216	14.5	43.783
00-HE028	64.160° N, 19.648° W	2/27/2000 14:56	3.51	18.7	1.7	2.94	6.66	0.752	2.04	1.73	0.873	0.807	14.4	23.586
00-HE30	64.183° N, 19.419° W	2/27/2000 18:02	4.46	20.7	−12	0.224	1.41	0.102	0.923	0.588	0.264	0.267	3.67	4.520
00-HE014	64.155° N, 19.523° W	2/7/2000 15:52	2.55	20	−13	6.59	4.70	0.795	2.49	2.40	0.146	0.157	16.6	66.187

Sample number	Al (μmol/kg) (ICP-SMS)	Fe (μmol/kg) (ICP-SMS)	P (μmol/kg) (ICP-SMS)	B (μmol/kg) (ICP-SMS)	Mn (μmol/kg) (ICP-SMS)	Sr (μmol/kg) (ICP-SMS)	As (nmol/kg) (ICP-SMS)	Ba (nmol/kg) (ICP-SMS)	Cd (nmol/kg) (ICP-SMS)	Co (nmol/kg) (ICP-SMS)	Cr (nmol/kg) (ICP-SMS)	Cu (nmol/kg) (ICP-SMS)	Ni (nmol/kg) (ICP-SMS)	Pb (nmol/kg) (ICP-SMS)
Drinking water limits	7.41	3.58	n.m.	92.51	0.910		133.5	730	44.5	n.m.	962	31471	341	48.3
99-L2	0.027	<0.007	0.066		0.001	0.009	<0.134	0.146	0.694	0.049	<0.192	<1.57	3.135	0.088
00-HE025	730	580	57.5	0.443	20.7	0.588	89.8	634	112	97.4	1.31	190	3.82	27.0
00-HE027	4818	4816	103	1.62	184	2.20	83.2	816	742	725	2.12	1493	11.6	62.7
00-HE028	2116	4423	16.4	2.56	211	1.97	64.9	704	987	675	2.81	3729	24.9	61.8
00-HE30	701	276	2.51	0.570	45.9	0.947	<1.33	485	229	145	0.462	634	<1.70	1.41
00-HE014	6042	4154	975	2.39	153	2.26	639	4624	952	519	2.885	2109	8.36	282

Sample number	Zn (nmol/kg) (ICP-SMS)	Hg (nmol/kg) (AFS)	Mo (nmol/kg) (ICP-SMS)	Ti (nmol/kg) (ICP-SMS)	Se (nmol/kg) (ICP-SFMS)	Ge (nmol/kg) (ICP-SFMS)	Ce (nmol/kg) (ICP-SFMS)	Dy (nmol/kg) (ICP-SFMS)	Er (nmol/kg) (ICP-SFMS)	Eu (nmol/kg) (ICP-SFMS)	Gd (nmol/kg) (ICP-SFMS)	Ho (nmol/kg) (ICP-SFMS)	La (nmol/kg) (ICP-SFMS)	Lu (nmol/kg) (ICP-SFMS)
Drinking water limits	1530	5.00	730		127									
99-L2	20.8	<0.011	<0.104	0.668	n.m.	n.m.	n.m.	n.m.	n.m.	n.m.	n.m.	n.m.	n.m.	n.m.
00-HE025	1250	<0.011	5.19	54.489	n.m.	1.90	45.6	14.8	8.85	2.60	10.2	3.00	18.1	1.09
00-HE027	1217	0.0344	15.0	256.785	n.m.	21.8	133	36.2	20.9	6.79	26.2	7.28	53.5	2.49
00-HE028	226	0.0234	15.6	290.188	n.m.	43.4	15.6	3.23	2.09	0.712	2.42	0.673	6.59	0.320
00-HE30	1881	0.0653	2.43	27.140	n.m.	n.m.	17.8	4.10	2.36	1.17	3.67	0.788	7.27	0.238
00-HE014	10,875	<0.011	90.6	427.975	54.3	n.m.	935	334	205	45.2	197	66.7	419	24.9

Sample number	Nd (nmol/kg) (ICP-SFMS)	Pr (nmol/kg) (ICP-SFMS)	Sb (nmol/kg) (ICP-SFMS)	Sm (nmol/kg) (ICP-SFMS)	Sn (nmol/kg) (ICP-SFMS)	Tb (nmol/kg) (ICP-SFMS)	Tm (nmol/kg) (ICP-SFMS)	U (nmol/kg) (ICP-SFMS)	V (nmol/kg) (ICP-SFMS)	Yb (nmol/kg) (ICP-SFMS)	Be (nmol/kg) (ICP-SFMS)	Li (nmol/kg) (ICP-SFMS)	Th (nmol/kg) (ICP-SFMS)
Drinking water limits								8.40					
99-L2	<0.00347	<0.00355	n.m.	<0.00333	n.m.	<0.00315	<0.00296	n.m.	0.2	<0.00289	n.m.	n.m.	<0.00431
00-HE025	25.8	6.34	0.583	7.65	11.1	2.06	1.28	3.61	550	8.09	147	1686	3.37
00-HE027	89.4	19.7	4.11	21.5	17.1	4.98	2.97	31.76	4653	18.8	1199	14841	2.42
00-HE028	8.94	2.18	3.22	2.15	55.4	0.447	0.326	28.3	4731	2.25	950	32709	1.03
00-HE30	9.64	2.74	<0.821	2.75	<4.21	0.724	0.345	3.77	52.41	2.03	n.m.	n.m.	n.m.
00-HE014	513.0	136	7.59	142	169	50.5	32.8	31.3	4005	160	n.m.	n.m.	n.m.

n.m. = not measured.

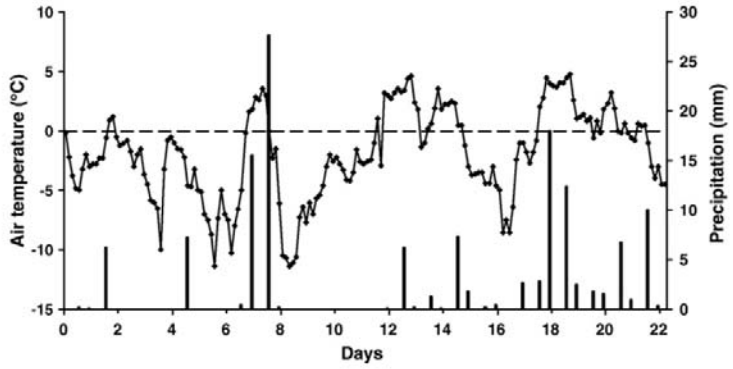

Fig. 5. Air temperature (°C) and precipitation (mm) at the Haell meteorological station during the first days after the 2000 eruption.

results for the first month are shown in Fig. 6. The F concentration rose to 151 μmol/kg at 22:40 UT, 4 h and 23 min after the beginning of the eruption (Fig. 6 and Table 4). It took between 2 to 4 h for the river water to travel from the headsprings of the Ytri–Rangá to the monitoring station at an average velocity of 1 to 2 m/s (Fig. 2).The concentration dropped to 47 μmol/kg at 07:50 UT the morning after the eruption (Table 4 and Fig. 6). The F concentration became very high following the first period of rainfall 7 days after the onset of the eruption (Fig. 6). The concentration was more than 3 times higher than the highest F concentration following the 1991 eruption (Fig. 4). The concentrations were also high following the rain on day 15 and days 18–19 (Fig. 6). The concentrations of Cl, protons, Al, Fe, Mn, Zn, Cu and Cd all increased conspicuously during day 7 of the eruption, following the first rainfall on the tephra (Fig. 6). Elements like Mg, Ca, Sr, Si and K showed some increase in concentration; this contrasts with observations in 1991, when these elements decreased in concentration in the river following the first rainfall on the tephra (Figs. 4 and 6). At the same time, the concentrations of SO_4, P and DIC decreased. The decrease in the SO_4 load of the river water following the first rain on the tephra in 2000 was smaller than in 1991 (Figs. 4 and 6). The concentrations of F, Al, Fe and Mn exceeded the drinking water limits given by the European Community (1998) with concentrations as high as 0.70 mmol/kg, 56 μmol/kg, 5.2 μmol/kg and 1.84 μmol/kg, respectively.

4.3. Saturation state (ΔG_r) of minerals and volcanic glass in the melted snow samples from the 1991 and 2000 eruptions

The saturation states of minerals and glasses are a quantitative constraint on their tendency to dissolve or precipitate, thereby affecting the overall water composition. The most common primary minerals of basalt and andesite – olivines, pyroxenes and plagioclase, both as end-member and solid solution compositions – were all undersaturated in the melted snow samples, together with volcanic glasses of basaltic to andesitic composition. The dissolution rate of the Hekla glass was dependent on the saturation state in 7 samples (Fig. 7; ΔG_r −9.9 to −7.8 kJ/mol) translating to a slowdown of less than 5% of the dissolution rate. The saturation states of Hekla glass in the melted snow samples are shown versus the in situ pH in the upper left corner of Fig. 7. The figures indicate that primary minerals and glasses tended to dissolve in the meltwaters, though it is unclear how much dissolved at the low temperatures (0 to 5 °C) and in the short time (2–4 h) between the beginning of the rain to the arrival of the contamination at the monitoring station.

Secondary minerals can form as a result of the high concentration of dissolved solids in the meltwaters and therefore may constrain dissolved contamination. The first secondary minerals to reach oversaturation during meteoric water-basaltic glass interactions are phases of Fe and Al (Stefánsson and Gislason, 2001). Secondary minerals, especially Fe phases, can scavenge trace metals and nutrients on particle surfaces and thereby affect the composition of surface waters. The saturation states in the snow/ash samples of the most important Al and Fe secondary phases in Icelandic soils are shown in Fig. 7 at 0.1 °C as well as the in situ pH. Amorphous or cryptocrystalline phases are more likely to form than the fully crystalline gibbsite and goethite. All the secondary Al-bearing phases were undersaturated in all meltwater samples, even at the very high Al concentrations typical of some samples from the 2000 eruption (0.7 to 6 mmol/kg, Table 3). This was primarily because of the formation of

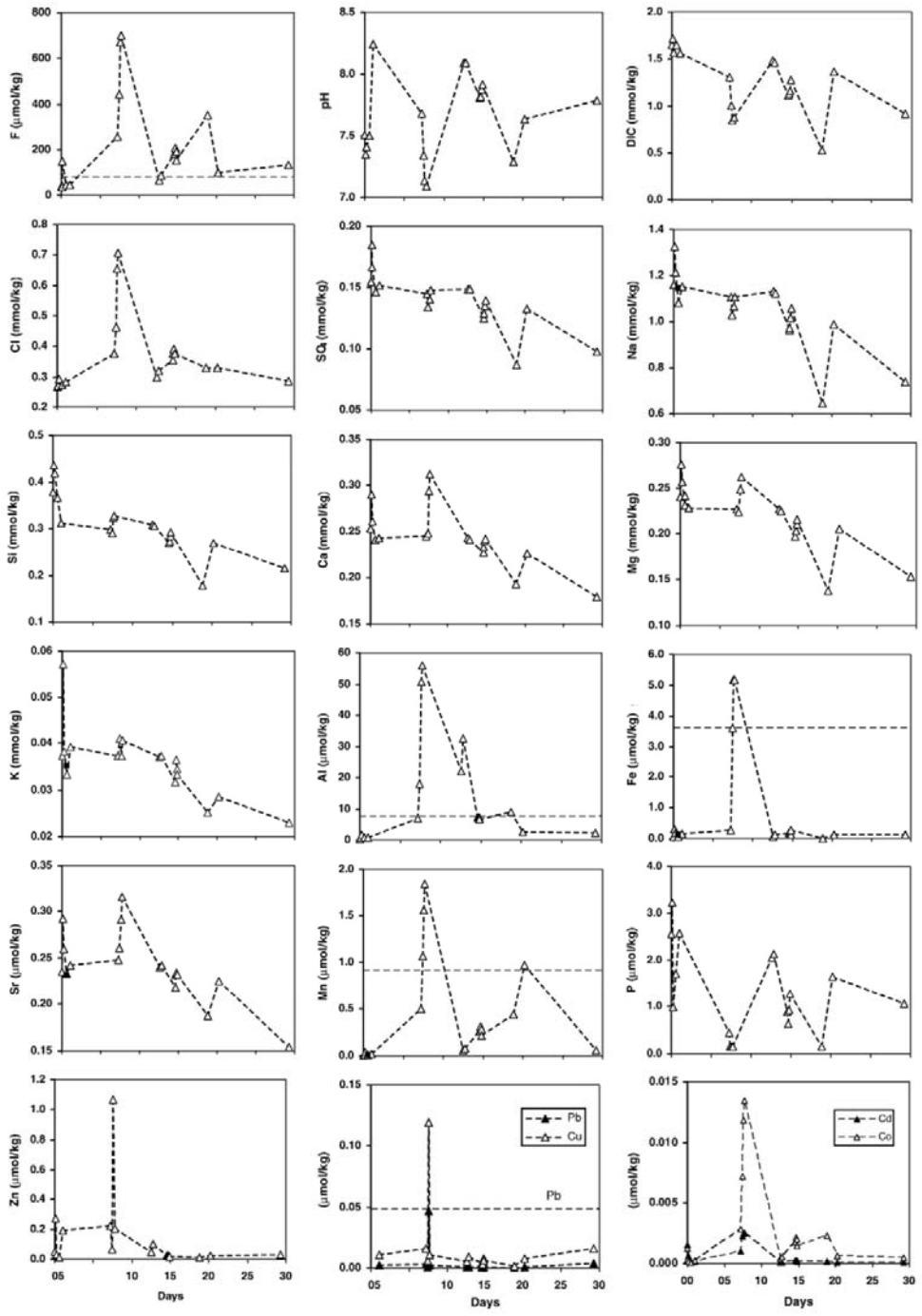

Fig. 6. Dissolved constituents in the Ytri–Rangá River versus time during and after the 2000 eruption. All concentrations are shown for the 30 day period. The hatched horizontal line on some diagrams is the upper limit for drinking water (European communities, 1998). No horizontal line is shown if concentrations were below this upper limit.

soluble Al–F species. Cryptocrystalline goethite was saturated or oversaturated in the meltwaters at every pH, while only meltwaters above the pH of 4 were close to saturation with respect to amorphous FeOOH. Thus it is likely that Fe concentrations in the meltwaters were controlled by the formation of a secondary Fe phase.

Table 4
The chemical composition of river water sampled during and after the 2000 eruption

Sample number	Date and time	T °C (in situ)	pH	T °C (titration)	Charge balance (% error) (PHREEQC)	SiO_2 (mmol/kg) (ICP-AES)	Na (mmol/kg) (ICP-AES)	K (mmol/kg) (ICP-AES)	Ca (mmol/kg) (ICP-AES)	Mg (mmol/kg) (ICP-AES)	DIC (mmol/kg)	Alk (meq/kg)	S (mmol/kg) (ICP-AES)	SO_4 (mmol/kg) (IC)	Cl (mmol/kg) (IC)	F (μmol/kg) (IC)	Al (μmol/kg) (ICP-SMS)
Drinking water limits							8.70	0.307	2.50	2.06				2.60	7.05	78.6	7.41
00-HE001	2/26/2000 18:50	n.m.	7.51	n.m.	1.5	0.379	1.16	0.0373	0.253	0.240	1.65	1.53	0.154	0.143	0.267	39.1	0.420
00-HE002	2/26/2000 19:50	n.m.	7.35	n.m.	8.5	0.436	1.33	0.0572	0.290	0.276	1.72	1.53	0.185	0.146	0.273	38.6	0.894
00-HE003	2/26/2000 22:40	n.m.	7.41	n.m.	2.8	0.418	1.21	0.0383	0.261	0.257	1.57	1.43	0.166	0.147	0.292	151	1.65
00-HE004A	2/27/2000 7:50	n.m.	7.50	n.m.	−1.7	0.367	1.08	0.0332	0.241	0.231	1.65	1.52	0.146	0.145	0.273	47.1	1.00
00-HE004B	2/27/2000 7:50	n.m.	7.50	n.m.	0.9	0.381	1.14	0.0351	0.252	0.242	1.65	1.52	0.155				1.15
00-HE005	2/27/2000 19:33	2.3	8.24	19.2	−0.66	0.311	1.15	0.0394	0.243	0.228	1.56	1.53	0.152	0.156	0.282	45.8	0.819
00-HE008	3/4/2000 23:43	2.9	7.68	14.2	−1.4	0.298	1.10	0.0373	0.245	0.227	1.31	1.24	0.145	0.148	0.375	259	7.04
00-HE009	3/5/2000 4:46	3.5	7.34	20.6	−0.018	0.291	1.03	0.0412	0.248	0.224	1.00	0.904	0.134	0.125	0.463	442	17.9
00-HE010	3/5/2000 9:02	2.5	7.14	21.1	0.93	0.323	1.07	0.0373	0.294	0.249	0.852	0.727	0.140	0.134	0.654	671	50.8
00-HE011	3/5/2000 12:00	2.1	7.09	21.0	0.69	0.328	1.10	0.0407	0.312	0.262	0.874	0.733	0.148	0.142	0.708	700	56.0
00-HE013	3/10/2000 8:04	3.9	8.09	16.5	1.5	0.308	1.13	0.0371	0.243	0.227	1.49	1.45	0.149	0.145	0.299	65.8	22.0
00-HE015	3/10/2000 13:50	5.1	8.09	23.6	0.98	0.306	1.12	0.0373	0.241	0.225	1.47	1.44	0.148	0.146	0.322	89.0	32.6
00-HE016	3/12/2000 8:19	3.0	7.81	22.2	−0.19	0.270	0.96	0.0317	0.227	0.197	1.12	1.08	0.125	0.123	0.355	184	7.19
00-HE017	3/12/2000 11:00	2.7	7.82	22.3	−0.72	0.273	0.97	0.0366	0.233	0.204	1.13	1.09	0.129	0.124	0.375	208	7.38
00-HE018	3/12/2000 13:00	2.7	7.88	22.2	0.13	0.285	1.02	0.0345	0.240	0.211	1.16	1.12	0.135	0.132	0.392	192	7.12
00-HE019	3/12/2000 15:15	2.7	7.92	21.9	−0.44	0.293	1.06	0.0332	0.242	0.216	1.28	1.24	0.139	0.134	0.375	154	6.52
00-HE020	3/16/2000 14:00	2.2	7.29	22.1	1.3	0.178	0.644	0.0251	0.193	0.138	0.525	0.469	0.0870	0.082	0.330	353	8.97
00-HE021	3/18/2000	2.0	7.64	25.0	−2.8	0.270	0.987	0.0286	0.226	0.205	1.36	1.30	0.133	0.125	0.330	98.4	2.48
00-HE022	3/27/2000	3.9	7.79	25.0	−2.5	0.215	0.739	0.0229	0.179	0.153	0.921	0.888	0.0979	0.0947	0.288	134	2.35

Sample number	Fe (μmol/kg) (ICP-AES/ICP-SMS)	P (μmol/kg) (ICP-SMS)	Sr (μmol/kg) (ICP-AES)	Mn (nmol/kg) (ICP-SMS)	Ti (nmol/kg) (ICP-SMS)	B (nmol/kg) (ICP-SMS)	As (nmol/kg) (ICP-SMS)	Ba (nmol/kg) (ICP-SMS)	Cd (nmol/kg) (ICP-SMS)	Co (nmol/kg) (ICP-SMS)	Cr (nmol/kg) (ICP-SMS)	Cu (nmol/kg) (ICP-SMS)	Ni (nmol/kg) (ICP-SMS)	Pb (nmol/kg) (ICP-SMS)	Zn (nmol/kg) (ICP-SMS)	Hg (nmol/kg) (AFS)	Mo (nmol/kg) (ICP-SMS)
Drinking water limits	3.58			0.910		92.51	133.5	730	44.5		962	31471	341	48.3	1530	5.00	730
00-HE001	0.0743	2.55	0.235	3.72	8.54	1814	5.73	2.48	*0.228*	0.299	4.87	*18.7*	*1.89*	*0.67*	*46.6*	<0.0558	17.9
00-HE002	0.310	3.23	0.293	8.36	17.2	5174	22.4	5.29	*1.52*	1.23	11.7	*163*	*7.06*	*10.93*	*271*	<0.0144	21.1
00-HE003	0.171	0.979	0.260	40.4	22.5	1921	11.1	6.12	*0.641*	0.187	3.21	*9.51*	*1.77*	*0.48*	*31.0*	0.0518	16.8
00-HE004A	0.0698	1.70	0.233	9.61	16.2	1730	8.01	4.29	*0.185*	0.110	3.85	*1.61*	*0.852*	*0.12*	*13.0*	0.0150	16.9
00-HE004B	0.109	1.82	0.231	9.93	13.4	1731	7.75	4.50	*0.312*	0.128	4.19	*53.2*	*1.24*	*0.78*	*65.7*	0.0188	16.6
00-HE005	0.140	2.57	0.242	21.7	22.3	2322	2.79	10.8	0.148	0.209	3.96	10.7	4.26	2.08	196	<0.011	18.2
00-HE008	0.285	0.436	0.248	497	43.2	2155	0.87	7.94	0.979	2.88	0.888	16.2	4.11	2.86	223	<0.011	16.1
00-HE009	3.60	<0.161	0.261	1072	195	1924	0.39	9.68	2.24	7.23	0.760	5.90	4.46	0.57	68.8	<0.011	13.6
00-HE010	5.17	<0.161	0.292	1558	228	1850	0.43	8.16	2.46	11.8	0.671	119	5.20	46.33	1068	<0.011	12.4
00-HE011	5.19	<0.161	0.316	1838	165	1859	0.49	7.94	2.54	13.4	0.740	10.8	5.30	2.52	208	<0.011	12.4
00-HE013	0.0591	2.04	0.240	58.6	12.0	2155	2.11	2.48	0.107	0.423	3.71	5.60	3.48	0.811	47.1	<0.011	16.5
00-HE015	0.109	2.12	0.242	75.4	15.6	2183	2.51	2.61	0.105	0.533	3.46	9.10	5.04	0.758	106	<0.011	16.6
00-HE016	0.190	0.891	0.218	260	45.7	1721	1.39	2.81	0.212	1.80	2.29	4.14	3.71	0.449	24.8	<0.011	12.8
00-HE017	0.184	0.643	0.232	319	39.2	1748	1.47	3.00	0.270	2.16	2.08	3.37	3.78	0.241	26.0	<0.011	12.9
00-HE018	0.120	0.927	0.234	286	30.3	1896	1.25	2.84	0.219	2.02	2.40	7.63	3.85	3.81	26.2	<0.011	14.0
00-HE019	0.269	1.28	0.232	218	51.4	1859	1.66	2.65	0.182	1.47	2.77	5.96	3.27	0.81	20.0	<0.011	13.9
00-HE020	0.00716	<0.161	0.188	444	2.32	1073	0.45	2.40	0.165	2.31	1.23	1.57	1.47	0.05	11.8	<0.011	7.57
00-HE021	0.115	1.64	0.225	967	18.8	934	7.94	1.89	0.0480	0.606	3.52	7.55	4.45	0.39	26.2	<0.011	15.2
00-HE022	0.111	1.07	0.154	61	21.5	623	6.70	1.43	0.0400	0.480	2.40	16.1	3.90	4.10	32.6	<0.011	11.2

n.m. = not measured.

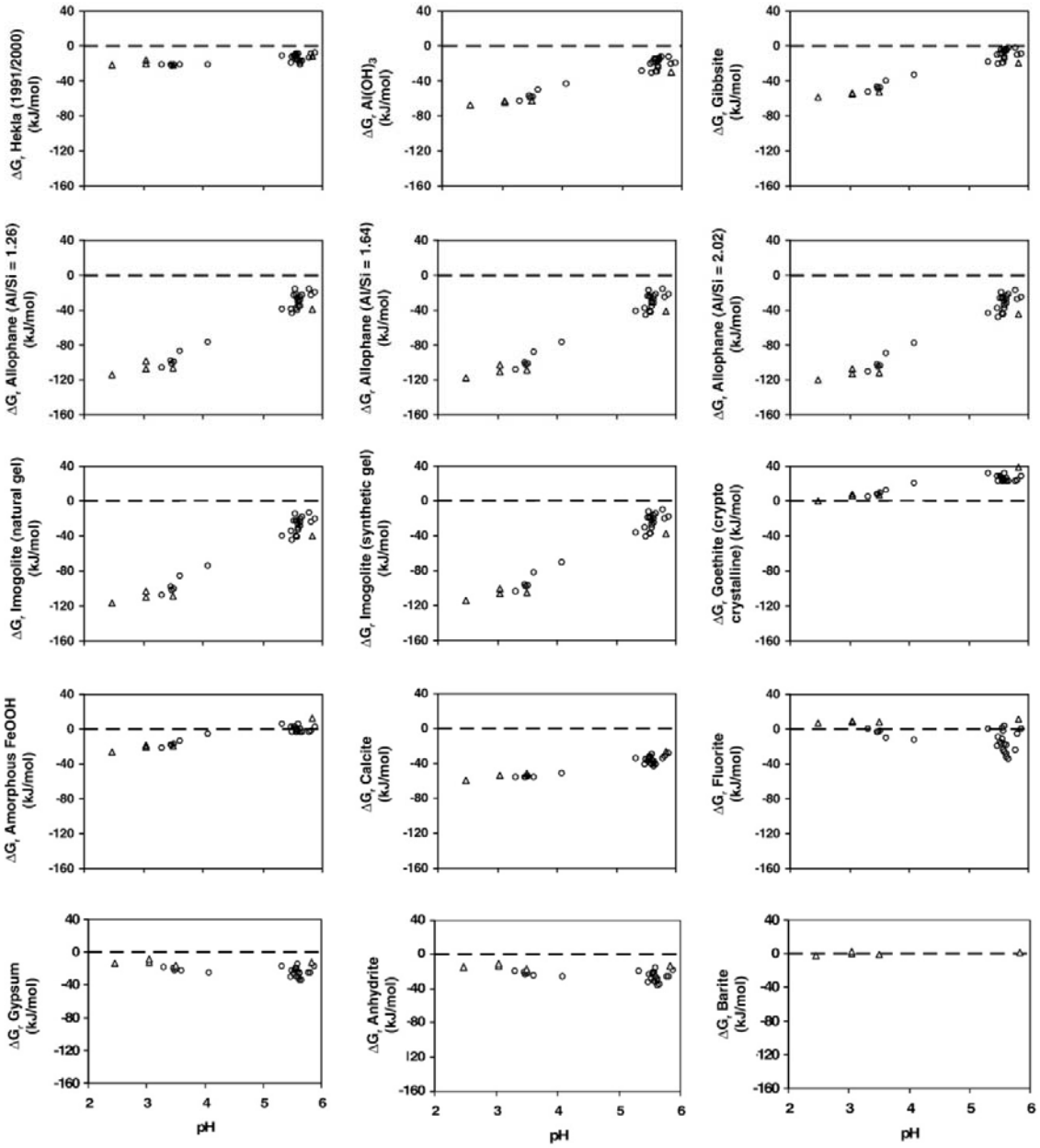

Fig. 7. The pH dependence of the saturation state of selected minerals and glasses in snow samples containing ash collected during and after the 1991 (open circles) and 2000 (open triangles) eruptions of Mt. Hekla, depicted in terms of Gibbs free energy of the dissolution reactions of the respective minerals and glasses. The dashed line shows equilibrium conditions: $\Delta G_r = 0$.

Many of the meltwaters were saturated with respect to fluorite (Fig. 7). Thus fluorite potentially controls the concentration of F and Ca in the meltwaters. Both gypsum and anhydrite were undersaturated in the meltwaters while barite was saturated. The concentration of Ba in the meltwater was so low that SO_4 was practically unconstrained.

4.4. Saturation state (ΔG_r) of minerals and volcanic glasses in Ytri–Rangá River during and after the 1991 and 2000 eruptions

The most common primary minerals of basalt to andesite and volcanic glasses of basaltic to andesitic composition were all undersaturated in the river water

samples, as shown for example for the Hekla glass versus the in situ pH in the upper left corner of Fig. 8. Exceptions to this were some samples that were oversaturated with respect to plagioclase. The river waters were less undersaturated with respect to the primary phases, minerals and glasses than were the meltwaters (Figs. 7 and 8). The relatively high saturation state of the tephra ($\Delta G_r > -10$ kJ/mol) slowed down the dissolution rate in the river water by 10–80%. Thus primary minerals and glasses had the potential to dissolve in the river waters, but probably did not substantially contribute to the river composition because of the short residence time of the waters in the river channel (2–4 h).

Secondary minerals could have formed as a result of oversaturation during the mixing of polluted meltwaters with the river water following the 1991 and 2000

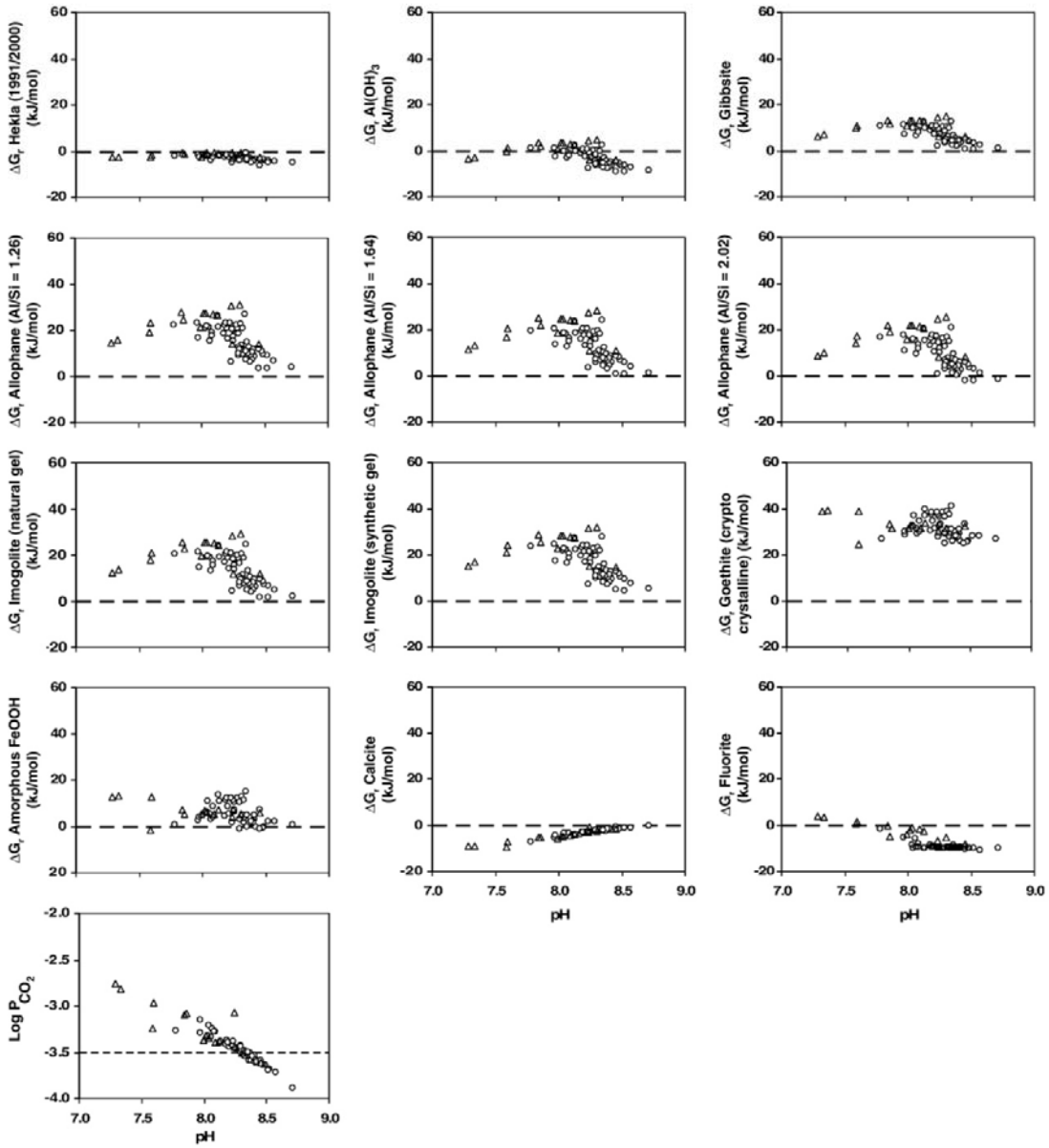

Fig. 8. The pH dependence of the saturation state of selected minerals and glasses in water samples collected during and after the 1991 (open circles) and 2000 (open triangles) eruptions of Mt. Hekla in the Ytri–Rangá River, depicted in terms of Gibbs free energy of the dissolution reactions. The dashed line shows equilibrium conditions: $\Delta G_r = 0$.

eruptions. The saturation states of the most important Al and Fe secondary phases in the river waters are shown in Fig. 8 versus the in situ pH. All the secondary Al phases except amorphous $Al(OH)_3$ were oversaturated or saturated in the river waters following both eruptions, as shown in Fig. 8. The river waters with in situ pH below 8.4 were all very close to the equilibrium with amorphous Al $(OH)_3$. Thus it is likely that this phase constrained the concentration of Al in these waters. Cryptocrystalline goethite was highly oversaturated in the river waters and amorphous FeOOH was supersaturated or saturated. Thus it is likely that the concentration of Fe was constrained in the meltwaters by the formation of amorphous Fe hydroxide. Fluorite was only supersaturated in 3 of the Hekla 2000 river samples (Fig. 8), while fluorapatite was supersaturated in all the waters. Anhydrite, gypsum and barite were undersaturated in all the water samples.

5. Mixing

5.1. Mixing of melted snow/ash with surface waters

Evidence presented in previous sections shows a drastic change in pH and saturation state between the meltwaters and the river water, resulting in oversaturation with respect to some secondary minerals. This mixing resulted in formation of amorphous Al hydroxide and amorphous FeOOH and the ensuing consumption of dissolved Fe and Al as well as scavenging of some trace elements on the Al and Fe surfaces. Furthermore, the concentrations of Al and F are the only dissolved chemical constituents analyzed for which exceeded the maximum allowed dissolved concentrations in drinking water (European Community, 1998) in more than four river water samples (Figs. 4 and 6). The toxicity and bioavailability of total dissolved Al is dictated by the speciation, Al^{3+} being the most toxic species (Gensemer and Playle, 1999). It is therefore important to study the distribution of dissolved Al species in Hekla-type contamination during mixing with surface waters, as well as the saturation state of the mixture with respect to solid Al and Fe hydroxides and fluorite. Mixing of Hekla-type volcanic cloud material with surface waters has been simulated with four end-members: (1) Unpolluted average 1998–1999 winter precipitation on the Langjökull Glacier (Fig. 1 and Table 3; Gislason et al., 2000); (2) the Fjardará river (Fig. 1; Gislason et al., 2004) ; (3) the Ytri–Rangá River not affected by tephra fallout (Table 2); and (4) seawater (Nordstrom et al., 1979) with F^- concentration from Riley and Skirrow (1965) and Al concentration from Frogner Kockum et al. (2006). This is similar to the approach by Frogner Kockum et al. (2006) but the present study used a different thermodynamic database for the Al species, as described in the section on material and methods. As described previously in Section 2.1, the alkalinity of the Ytri–Rangá River was unusually high for Icelandic rivers at 1.5 meq/kg, compared to the 0.181 meq/kg alkalinity of the Fjardará river and the 2.27 meq/kg alkalinity of seawater. The snow sample with the lowest pH and highest F concentration, collected close to the 10 kg/m^2 isoline, was chosen as the starting material for the dilution simulations (Fig. 2; sample 00-HE014 in Table 1). The ash-rich meltwaters reflected the composition of the metal and proton salts adsorbed on the surface of the ash and embedded in the snow. The snow-ash mixture was melted in the laboratory under controlled conditions in less than 30 min. It was therefore an ideal candidate for testing for volcanic ash and aerosol end-member composition.

5.2. Results from mixing modeling of snow with four surface waters

The pH and F concentration dictate the Al speciation in the mixing between contaminated snow and surface waters. At low pH and high F concentration, Al–F complexes were the main Al species in all the surface waters (Fig. 9). During mixing, the pH increased faster up to normal levels in waters with high alkalinity due to the greater buffering capacity of these systems.

The natural low pH (5.6) of unpolluted precipitation caused the Al to bind with available F, even at high levels of dilution. Fluorite was supersaturated and precipitated only until the snow melt had been diluted one to four, meaning that F was mainly unconstrained, causing high contamination to the areas which received ash fall (Fig. 9A) while amorphous FeOOH and aluminum hydroxide were undersaturated during all dilutions.

When mixed with the waters of the Fjardará River (alkalinity: 0.181 meq/kg) non-Al–F complexes became the dominant Al species after 3500 dilutions. Fluorite precipitated out until the snow sample had been diluted ca 60 times, thus decreasing the contamination of the river water (Fig. 9B). Amorphous FeOOH and aluminum hydroxide precipitated out between 200–200 000 and 2000–20 000 times dilutions, respectively.

After diluting snow melt with the water of the Ytri–Rangá River 15 000 times, the pH was predicted to rise to normal levels (8.4). The $Al(OH)_4^-$ species dominated the mixture after 500 dilutions (Fig. 9C). Table 5 shows the modeled Al-speciation in the Ytri–Rangá River during peak concentrations of F after both eruptions and during normal concentrations. Fluorite was oversaturated and

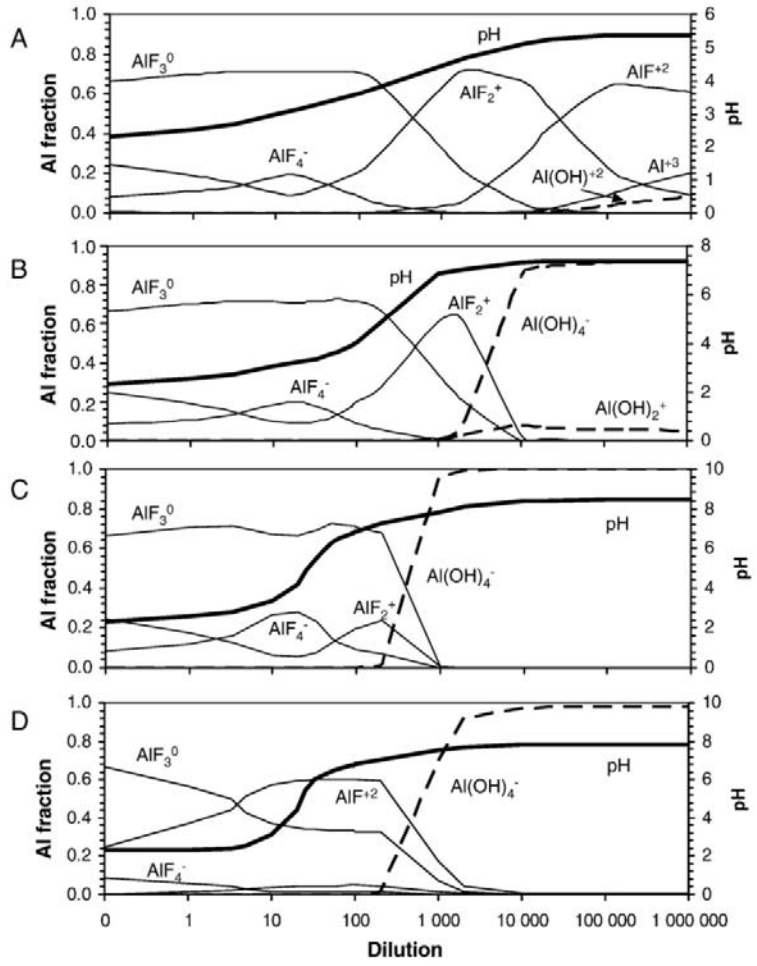

Fig. 9. Speciation of dissolved Al during increasing dilution of the most polluted snow/ash sample (00-HE014) with four end-members: (A) unpolluted precipitation from Langjökull Glacier (alkalinity ~0 meq/kg); (B) water from the Fjardará River (alkalinity=0.181 meq/kg); (C) water from the Ytri–Rangá River (alkalinity=1.48 meq/kg); and (D) seawater (alkalinity=2.27 meq/kg).

precipitated out until the snow melt had been diluted 200 times and thereby decreasing the water contamination. Amorphous FeOOH and aluminum hydroxide precipitated out after 25 times dilution and onwards and between 200 and 10000 times, respectively. After a dilution of 100000 times, the concentration of F was down to a normal level (35.8 μmol/kg) while Al had to be diluted 200000 times to drop to normal concentration in the river water (0.652 μmol/kg). These required levels of dilution indicate that a significant amount of F and Al had precipitated in the field.

After the snow melt had been diluted with seawater 6000 times, the pH was predicted to have risen to normal seawater levels (7.8–8.2). The saturation state of fluorite showed that the mineral may precipitate until being diluted 660 times. Amorphous FeOOH was precipitated

Table 5
Speciation of aluminum in unpolluted river water from the Ytri–Rangá and at peak concentrations of F during the 1991 and 2000 eruptions

	Sample number	Al (μmol/l)	$Al(OH)_4^-$ (%)	AlF_2^+ (%)	AlF_3 (%)	AlF_4^- (%)	Sum (%)
Normal concentration	91-3212	0.652	99.8	0.0005	0.0002	0	99.8
F-peak 1991	91-3032	2.43	64.6	9.57	22.7	1.91	98.8
F-peak 2000	00-HE011	56	0.101	12.6	72.2	15	99.9

out after 20 dilutions while aluminum hydroxide precipitated out after diluting between 200 and 2000 times. After ca 800 dilutions, the concentration of Al–OH complexes exceeded the concentration of Al–F complexes (Fig. 9D).

6. Discussion

6.1. Dissolution of salt particles from tephra

Volcanic activity has been shown to have a fertilizing effect on the environment (e.g. Sarmiento, 1993; Frogner et al., 2001; Gislason et al., 2002). This is due to emission of volcanic gases and, in the case of subaerial eruptions, the very reactive salt particles that are formed on the surface of the ash (Óskarsson, 1980, 1981; Varekamp et al., 1984). The most common volcanic salt particles are the chlorides, fluorides and sulfates of the alkali metals and calcium (Óskarsson, 1980, 1981).

For both eruptions, when the first rain hit the pristine volcanic Hekla ash of this study the concentration of elements in the Ytri–Rangá River changed rapidly. In 1991, the rain caused an increase in the concentrations of F, Cl and Mn but a decrease in the concentrations of SO_4, Na, Si, Ca Mg, K, Sr and PO_4. In 2000, the rain caused an increase in the concentrations of F, Cl, Si, K, Ca, Mg, Al, Fe, Mn and Sr and a decrease in the concentrations of SO_4, Na and PO_4. The high concentrations of F, Cl and Mn were due to the leaching of reactive salt particles bound on the surface of the ash (Óskarsson, 1980; Frogner et al., 2001), while the decreases in concentrations were caused by dilution of the river with snow melt and rainwater that had lower concentrations than the river water.

The low pH and the extremely high concentrations of F in the melted snow/ash mixture from the 2000 eruption might have enhanced the dissolution rate of the Hekla glass itself (Wolff-Boenisch et al., 2004a) and therefore increased the concentration of elements like Na, Si, Ca, Mg, Al, Fe and Sr in the meltwaters during this eruption.

6.2. Al–F contamination in surface waters

The high concentration of F, Al and Mn in the river during the first periods of rain after the onset of the eruptions caused a threat to biota. As described in detail in Frogner Kockum et al. (2006) and references cited therein, fluorine is not an essential element for plant growth, but plants may accumulate it when it is readily available. In addition to harming the plants, livestock ingesting these plants may be afflicted by chronic fluorosis. Aluminum is the third most abundant element in the Earth's crust, but it has no useful biological function. On the contrary, it is recognized as a toxic metal with Al^{3+} as the main rhizotoxic species (Kinraide, 1997; Stevens et al., 1997). At low pH, Al and F become more available for plant uptake and Al^{3+} binds strongly to F^- and makes aluminofluoride complexes. The main F–Al species toxic to plants are AlF^{+2} and AlF_2^+ (Stevens et al., 1997; Kinraide, 1997; Manoharan et al., 2007). In precipitation contaminated by volcanic clouds, F is phyto-available through complexation as soluble aluminum–fluoride compounds (Fig. 9a; Stevens et al., 1997). In highly alkaline rivers (>1.5 meq) and seawater, the least toxic $Al(OH)_4^-$ species exceeds the concentration of Al–F species after 800 dilutions (Fig. 9C and D). Thus neither Al nor F is phyto-available in these environments at dilutions greater than 800 times. According to the modeling of the present study, the most toxic Al^{3+} species (Gensemer and Playle, 1999) is never an important species in a highly alkaline environment (Fig. 9).

The normal Al-speciation in Ytri–Rangá River consists of only $Al(OH)_4^-$ (Table 5). During the highest concentration of F after the 1991 eruption (sample 91-3032, Fig. 4; Table 2) only 65% of the Al was bound as aluminum hydroxide while the rest was bound into Al–F complexes. During the peak in 2000 (sample 00-HE011, Fig. 6; Table 4) all of the Al was bound into aluminum fluoride complexes. In other words, the river became more toxic to biota during the 2000 eruption. The relative abundance of $Al(OH)_4^-$ vs. Al^{3+} and Al–F complexes was dependent only on the pH and the F concentration.

The most polluted snow sample (00-HE014) had a F concentration of 66.2 mmol/kg. To increase the concentration of F in the Ytri–Rangá (discharge of 15.5 m^3/s) from 35.8 μmol/kg (normal level) to 700 μmol/kg (peak in 2000), assuming conservation of mass, a snow melt discharge of 0.157 m^3/s is needed. This translates to a 1/99 dilution. The PHREEQC-modeling, on the other hand, shows that you need 0.242 m^3/s of snow melt into the river (a 1/64 dilution) to account for the observed F concentration. This increased amount of snow melt in the modeling compared to simple mass balance calculations is due to precipitation of fluorite in the model, which removes F from the solution. These dilutions of the most polluted snow sample yielded calculated dissolved Al concentrations at maximum contamination in the Ytri–Rangá ranging from 61–94 μmol/kg and Fe concentrations of 42–65 μmol/kg. The calculated Al concentration was slightly higher than the observed 55 μmol/kg (Fig. 6, Table 4), but the calculated Fe concentration was much

higher than the observed 5.19 μmol/kg (Fig. 6, Table 4), indicating some precipitation of an Al-containing phase but a significant precipitation of an Fe-containing phase. This is consistent with the saturation state modeling shown in Fig. 8. The precipitation might hinder toxicity of the water by consuming and or scavenging toxic metals (Dong et al., 2001; Kumpiene et al., in press). This could also limit the fertilization of surface waters of essential macro- and micronutrients, as demonstrated in Fig. 10 where the dissolved concentration of P is shown versus the saturation state of amorphous FeOOH in the melted snow samples. The concentration of P was high in all samples that were undersaturated with respect to amorphous FeOOH, but low in all samples that were saturated.

6.3. Oxidation of SO_2 into SO_4^{2-}

SO_2 is one of the main gases emitted during volcanic eruptions and one of the main gases formed during the 2000 Hekla eruption (Rose et al., 2003; Moune et al., 2007). When sulfur dioxide is released into the atmosphere, gaseous SO_2 is oxidized by the OH radical in air to form sulfurous acid (SO_3), which then reacts with water to produce sulfuric acid particles (e.g. McCormick et al., 1995). The lifetime of SO_2 in the troposphere is around a week (Oppenheimer, 2003), which is a substantially shorter time than in the stratosphere (Mills, 2000). The lack of sunlight in the arctic for large parts of the year limits the production of the OH radical so that the lifetime of SO_2 in the arctic winter atmosphere becomes significantly longer than in other regions of the atmosphere (Hunton et al., 2005).

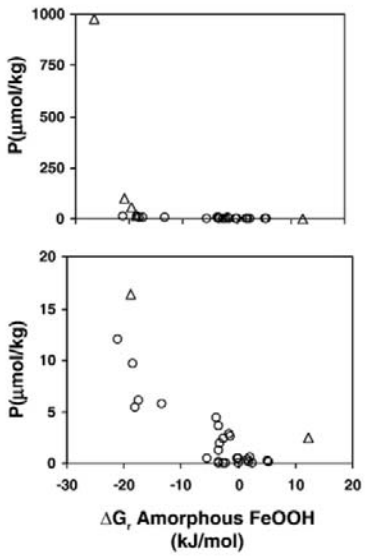

Fig. 10. Concentration of dissolved inorganic phosphorus versus the saturation state of the same samples with respect to amorphous FeOOH in the snow melts from 1991 (open circles) and 2000 (open triangles).

During the 2000 Hekla eruption, an instrumented NASA aircraft made in situ measurements of trace gas concentrations and aerosol properties (Hunton et al., 2005). The estimated SO_2 mass for the entire Hekla cloud based on the various algorithms has been evaluated at 0.13 to 0.37 Tg (Rose et al., 2003). The peak concentrations of gaseous H_2SO_4 were on the order of 0.4 ppbv or 0.04% of the SO_2 values, indicating that little or none of the volcanic sulfur occurred as the gas phase of H_2SO_4. However, the concentration of the H_2SO_4 aerosols was significantly higher or 7% (Rose et al., 2003). The percent concentration of the H_2SO_4 aerosols in the vicinity of the Hekla volcano was calculated by the total amount of the 2000 ash fall (0.01 km^3), the measured concentration of SO_4 in the snow samples associated with a known mass of pristine ash, and the estimated SO_2 emission as given by Rose et al. (2003). The percent concentration lies in the range of 0.001 weight % to 0.38 weight % depending on: 1) density of ash; 2) sample used (Table 3); and 3) the total amount of emitted SO_2 (Rose et al., 2003). These calculations suggest a trivial amount of H_2SO_4 emitted directly from the volcano and a trivial amount of SO_2 oxidized in the vicinity of the volcano.

Analyses from the Ytri–Rangá River show that the concentration of SO_4 decreased during the first periods of rain after both the 1991 and the 2000 eruptions because of dilution by rain and snow melt. The fact that both eruptions happened after sunset in January and February at 64° N, when the concentrations of OH radicals were low in the atmosphere may explain the lack of SO_4 in the polluted river water and snow samples. We suggest that H_2SO_4 contamination from volcanic eruptions is time and place dependent where high altitude and low solar radiation during the day (winter time) give a global SO_2 contamination and small local H_2SO_4 contamination due to the slow oxidation rate of SO_2 into SO_4^{2-}. In contrast, the opposite probably applies for volcanic eruptions in the summer time at high latitudes.

7. Conclusions

Wind directions dictate the distribution of airborne local pollution during volcanic eruptions, as can be seen in Figs. 1 and 2. Air temperature affects the timing of pollution. At subzero temperatures water-soluble metal

and proton salts are stable in the terrestrial environment. In the present study such salts dissolved rapidly during the first rain on the snow/ash mixture. The majority of the readily soluble and mobile salts were flushed out during a very few rainy days (Figs. 5 and 6). Metals like Fe are not mobile; most of the released Fe was consumed by precipitation of amorphous FeOOH. Dissolved Al and F were the main contaminants in the river waters close to the Hekla volcano following the 1991 and 2000 eruptions. Model calculations for mixing of a Hekla-type volcanic cloud with the end-members of 4 surface waters show Al–F species to be most important in rain and dilute river waters (Fig. 9). This makes Al and F phyto-available and diminishes the concentration of the Al^{3+} species, the most toxic Al-species. Mixing with highly alkaline river waters or seawater results in the domination of non-toxic $Al(OH)_4^-$ species at dilutions greater than 800, hindering Al toxicity and bioavailability.

This study indicates that H_2SO_4 contamination from volcanic eruptions is time and place dependent. Volcanic eruptions that take place during winter at high latitudes results in relatively high global sulfur contamination and relatively low local sulfur contamination due to the low oxidation rate of SO_2 into H_2SO_4 because of the low solar radiation.

Acknowledgements

We are grateful to many friends and colleagues for their help. Specifically we would like to thank Sveinn Sigurjónsson and Sigurbjörg Elimarsdóttir at the Galtalaekur farm, and Svala Gudmundsdóttir, Sverrir Haraldsson, and Gudmundur Gíslason at the Selsund farm, for their hospitality, help and enthusiasm for this study. We also thank Oddur Sigurdsson and Thorvaldur Thordarson for providing snow samples from the 1991 eruption. Gudmundur Bjarki Ingvarsson and Eydís Salome Eiríksdóttir helped with model calculations and Rósa Ólafsdóttir with GIS. This study was funded by The Nordic Volcanological Center Fellowship and the Science Institute, University of Iceland.

References

Árnason, B., 1976. Groundwater systems in Iceland traced by deuterium. Societas Scientarium Islandica, Reykjavík.

Arnórsson, S., Andrésdóttir, A., 1999. The dissociation constants of Al-hydroxy complexes at 0–350 °C and Psat. In: Ármannsson, H. (Ed.), Geochemistry of the Earth's Surface. Balkema, Rotterdam, pp. 425–428.

Chenet, A.L., Fluteau, F., Courtillot, V., 2005. Modelling massive sulphate aerosol pollution, following the large 1783 Laki basalt eruption. Earth and Planetary Science Letters 236, 721–731.

Chiodini, G., Frondini, F., 2001. Carbon dioxide degassing from the Albani Hills volcanic region, Central Italy. Chemical Geology 177, 67–83.

Delmelle, P., Delfosse, T., Delvaux, B., 2003. Sulfate, chloride and fluoride retention in Andesols exposed to volcanic acid emissions. Environmental Pollution 126, 445–457.

Diakonov, I., Schott, J., Martin, F., Harrichourry, J.-Cl., Escalier, J., 1999. Iron(III) solubilities and speciation in aqueous solutions. Experimental study and modelling: Part 1. Hematite solubility from 60 to 300 °C in NaOH–NaCl solutions and thermodynamic properties of $Fe(OH)_{4\ (aq)}^-$. Geochimica et Cosmochimica Acta 63 (15), 2247–2261.

Dong, D., Li, Y., Hua, X., 2001. Investigation of Fe, Mn oxides and organic material in surface coatings and Pb, Cd adsorption to surface coatings developed in different natural waters. Microchemical Journal 70, 25–33.

European Community, 1998. Council directive 98/83 Official Journal of the European Communities.

Frogner, P., Gislason, S.R., Oskarsson, N., 2001. Fertilizing potential of volcanic ash in ocean surface waters. Geology 29 (6), 487–490.

Frogner Kockum, P.C., Herbert, R.B., Gislason, S.R., 2006. A diverse ecosystem response to volcanic aerosols. Chemical Geology 231 (1–2), 57–66.

Gensemer, R.W., Playle, R.C., 1999. The bioavailability and toxicity of aluminium in aquatic environments. Critical Reviews in Environmental Science and Technology 29 (4), 315–450.

Gislason, S.R., Arnórsson, S., 1990. Saturation state of natural waters in Iceland relative to primary and secondary minerals in basalts I. In: Spencer, R.J., Chou, I-Ming (Eds.), Fluid–Mineral Interactions: A Tribute to H.P. Eugster. Geochemical Society, Special Publication, vol. 2, pp. 373–393.

Gislason, S.R., Arnórsson, S., 1993. Dissolution of primary basaltic minerals in natural waters: saturation state and kinetics. Chemical Geology 105, 117–135.

Gislason, S.R., Oelkers, E., 2003. Mechanism, rates, and consequences of basaltic glass dissolution; II. An experimental study of the dissolution rates of basaltic glass as a function of pH and temperature. Geochimica et Cosmochimica Acta 67 (20), 3817–3832.

Gislason, S.R., Andrésdóttir, A., Sveinbjörnsdóttir, Á.E., Óskarsson, N., Thordarson, Th., Torssander, P., Novâk, M., Zâk, K., 1992. Local effects of volcanoes on the hydrosphere: example from Hekla, southern Iceland. In: Kharaka, Y.K., Maest, A.S. (Eds.), Water–Rock Interaction. Balkema, Rotterdam, pp. 477–480.

Gislason, S.R., Arnórsson, S., Ármannsson, H., 1996. Chemical weathering of basalt in southwest Iceland: effects of runoff, age of rocks and vegetative/glacial cover. American Journal of Science 296, 837–907.

Gislason, S.R., Stefánsdóttir, M.B., Eiríksdóttir, E.S., 2000. ARCTIS, Regional Investigation of Arctic Snow Chemistry: Results from the Icelandic Expeditions, 1997–1999. Raunvísindastofnun, RH-05-2000.

Gislason, S.R., Snorrason, Á., Kristmannsdóttir, H.K., Sveinbjörnsdóttir, Á.E., Torsander, P., Ólafsson, J., Castet, S., Durpé, B., 2002. Effects of volcanic eruptions on the CO_2 content of the atmosphere and the oceans: The 1996 eruption and flood within the Vatnajökull Glacier, Iceland. Chemical Geology 190, 181–205.

Gislason, S.R., Snorrason, Á., Eiríksdóttir, E.S., Sigfússon, B., Elefsen, S.Ó, Harðardóttir, J., Gunnarsson, Á., Hreinsson, E.Ö., Torssander, P., Óskarsson, N.Ö., Oelkers, E.H., 2004. Chemical composition, discharge and suspended material in rivers in East-Iceland, V. Database of Science Institute and National Energy Authority. Science Institute, RH-05-2004. (In Icelandic).

Grattan, J., 2004. Pollution and paradigms: Lessons from Icelandic volcanism for continental flood basalt studies. Lithos 79, 343–353.

Grattan, J., Rabartin, R., Self, S., Thordarson, T., 2005. Volcanic air pollution and mortality in France 1783–1784. Comptes Rendus Geoscience 337, 641–651.

Gronvold, K., Larsen, G., Einarsson, P., Thorarinsson, S., Saemundsson, K., 1983. The Hekla eruption 1980–1981. Bulletin of Volcanology 46 (4), 349–363.

Gudmundsson, A., Oskarsson, N., Gronvold, K., Saemundsson, K., Sigurdsson, O., Stefansson, R., Gislason, S.R., Einarsson, P., Brandsdottir, B., Larsen, G., Johannesson, H., Thordarson, T., 1992. The 1991 eruption of Hekla, Iceland. Bulletin of Volcanology 54, 238–246.

Gunnarson, I., Arnórsson, S., 2000. Amorphous silica solubility and the thermodynamic properties of $H_4SiO_4^0$ in the range of 0° to 350 °C at Psat. Geochimica et Cosmochimica Acta 64 (13), 2295–2307.

Haraldsson, K.Ö., 2001. Heklugosid 2000 -Dreifing gjósku frá fyrsta gosdegi á landi (The Hekla 2000 eruption- distribution of ash from the first days of the eruption). BSc Thesis, University of Iceland (In Icelandic).

Haraldsson, K.Ö., Árnason, S.G., Larsen, G., Eiriksson, J., 2002. The Hekla eruption of 2000 — The tephra fall. Proceedings of the 5th Nordic winter Meeting, Abstracts volume, Reykjavik 2002, p. 71.

Hunton, D.E., Viggiano, A.A., Miller, T.M., Ballenthin, J.O., Reeves, J.M., Wilson, J.C., Shan-Hu- Lee, Anderson, B.E., Brune, W.H., Harder, H., Simpas, J.B., Oskarsson, N., 2005. In situ aircraft observations of the 2000 Mt. Hekla volcanic cloud: Composition and chemical evolution in Arctic lower stratosphere. Journal of Volcanology and Geothermal Research 145, 23–34.

Kinraide, T.B., 1997. Reconsidering the rhizotoxicity of hydroxyl, sulphate, and fluoride complexes of aluminium. Journal of Experimental Botany 48 (310), 1115–1124.

Kumpiene, J., Lagerkvist, A., Maurice, C., in press. Stabilization of As, Cr, Cu, Pb and Zn in soil using amendments — A review. Waste Management. doi:10.1016/j.wasman.2006.12.012.

Lacasse, C., Karlsdottir, S., Larsen, G., Soosalu, H., Rose, W.I., Ernst, G.G.J., 2003. Weather radar observations of the Hekla 2000 eruption cloud, Iceland. Bulletin of Volcanology 66, 457–473.

Larsen, G., Vilmundardóttir, E.G., Thorkelsson, B., 1992. The Hekla eruption of 1991 — The tephra fall. Náttúrufræðingurinn 61 (3–4), 159–176. (In Icelandic).

Manoharan, V., Loganathan, P., Tillman, R.W., Prafitt, R.L., 2007. Interactive effects of soil acidity and fluoride on soil solution aluminium chemistry and barley (*Hordeum vulgare L.*) root growth. Environmental Pollution 145, 778–786.

McCormick, M.P., Thomason, L.W., Trepte, C.R., 1995. Atmospheric effects of the Mt Pinatubo eruption. Nature 373, 399–404.

Mills, M.J., 2000. Volcanic aerosol and global atmospheric effects. In: Sigurdsson, H., Houghton, B., McNutt, S.R., Rymer, H., Stix, J. (Eds.), Encyclopedia of Volcanoes. Academic Press, pp. 931–943.

Moune, S., Gauthier, P.J., Gislason, S.R., Sigmarsson, O., 2006. Trace element degassing and enrichment in the eruptive plume of the 2000 eruption of Hekla volcano, Iceland. Geochimica et Cosmochimica Acta 70, 461–479.

Moune, S., Sigmarsson, O., Thordarson, T., Gauthier, P.J., 2007. Recent volatile evolution in the magmatic system of Hekla volcano, Iceland. Earth and Planetary Science Letters 255, 373–389.

Nordstrom, D.K., Plummer, L.N., Wigley, T.M.L., Wolery, T.J., Ball, J.W., Jenne, E.A., Bassett, R.L., Crerar, D.A., Florence, T.M., Fritz, B., Hoffmann, M., Holden Jr., G.R., Lafon, G.M., Mattigod, S.V., McDuff, R.E., Morel, F., Reddy, M.M., Sposito, G., Thrailkill, J., 1979. A comparison of computerized chemical models for equilibrium calculations in aqueous systems. In: Jenne, E.A. (Ed.), Chemical Modeling in Aqueous Systems. American Chemical Society Symposium Series, vol. 93. American Chemical Society, Washington, D.C., pp. 857–892.

Ólafsdóttir, R., Höskuldsson, Á., Grönvold, K., 2002. The evolution of the flow from Hekla eruption 2000. 25th Nordic Geological Winter Meeting, Abstract Volume.

Oppenheimer, C., 2003. Volcanic degassing. In: Lollar, B.S., Holland, H.D., Turekian, K.K. (Eds.), Treatise in Geochemistry, Environmental Geochemistry. Elsevier, pp. 123–166.

Óskarsson, N., 1980. The interaction between volcanic gases and tephra: fluorine adhering to tephra of the 1970 Hekla eruption. Journal of Volcanology and Geothermal Research 8, 251–266.

Óskarsson, N., 1981. The chemistry of Icelandic lava incrustations and the latest stages of magma degassing. Journal of Volcanology and Geothermal Research 10 (1–3), 93–111.

Parkhurst, D.L., Appelo, C.A.J., 1999. User's guide to PHREEQC (Version 2) — A computer program for speciation, batch-reaction, one-dimensional transport, and inverse geochemical calculations. USGS-Report 99-4259.

Rampino, M.R., Self, S., 1992. Volcanic winter and accelerated glaciation following the Toba super-eruption. Nature 359, 50–52.

Riley, J.P., Skirrow, G., 1965. Chemical Oceanography, vol. 1. Academic Press, pp. 197–322.

Robock, A., 2000. Volcanic eruptions and climate. Reviews of Geophysics 38, 191–219.

Robock, A., 2003. Mount Pinatubo as a test of climate feedback mechanisms. In: Robock, A., Oppenheimer, C. (Eds.), Volcanism and the Earth's Atmosphere. Geophysical Monograph, vol. 139. American Geophysical Union, pp. 1–8.

Rose, W.I., Gu, Y., Watson, I.M., Yu, T., Bluth, G.J.S., Prata, A.J., Krueger, A.J., Krotkov, N., Carn, S., Fromm, M.D., Hunton, D.E., Ernst, G.G.J., Viggiano, A.A., Miller, T.M., Ballenthin, J.O., Reeves, J.M., Wilson, J.C., Anderson, B.E., Flittner, D.E., 2003. The February–March 2000 eruption of Hekla, Iceland from a satellite perspective. In: Robock, A., Oppenheimer, C. (Eds.), Volcanism and the Earth's Atmosphere. Geophysical Monograph, vol. 139. American Geophysical Union, pp. 107–132.

Sarmiento, J.L., 1993. Atmospheric CO_2 stalled. Nature 365, 697–698.

Shock, E.L., Sassani, D.C., Willis, M., Sverjemsky, D.A., 1997. Inorganic species in geological fluids: correlations among standard molal thermodynamic properties of aqueous ions and hydroxide complexes. Geochimica et Cosmochimica Acta 61 (5), 907–950.

Stefánsson, A., 2000. Dissolution of primary minerals of basalt in natural waters I. Calculation of mineral solubilities from 0 °C to 350 °C. Chemical Geology 172, 225–250.

Stefánsson, A., Gislason, S.R., 2001. Chemical weathering of basalts, southwest Iceland: effect of rock crystallinity and secondary minerals on chemical fluxes to the ocean. American Journal of Science 301, 513–556.

Stevens, P.D., McLaughin, M.J., Alston, A.M., 1997. Phytotoxicity of aluminium–fluoride complexes and their uptake from solution culture by *Avena sativa* and *Lycopersicon esculentum*. Plant and Soil 192, 81–93.

The Hydrological Services of the National Energy Authority, 2006. The Data Repository of the Hydrological Services of the National Energy Authority, Permission number 2006/48.

Thordarson, T., Miller, D.J., Larsen, G., Self, S., Sigurdsson, H., 2001. New estimates of sulfur degassing and atmospheric mass-loading

by the 934 AD Eldgjá eruption, Iceland. Journal of Volcanology and Geothermal Research 108, 33–54.

Varekamp, J.C., Luhrb, J.F., Prestegaard, K.L., 1984. The 1982 eruptions of El Chichón Volcano (Chiapas, Mexico): Character of the eruptions, ash-fall deposits, and gas phase. Journal of Volcanology and Geothermal Research 23 (1–2), 39–68.

Wolff-Boenisch, D., Gislason, S.R., Oelkers, E.H., 2004a. The effect of fluoride on the dissolution rates of natural glasses at pH 4 and 25 °C. Geochimica et Cosmochimica Acta 68 (22), 4571–4582.

Wolff-Boenisch, D., Gislason, S.R., Oelkers, E.H., Putnis, C.V., 2004b. The dissolution rates of natural glasses as a function of their composition at pH 4 and 10.6, and temperatures from 25 to 74 °C. Geochimica et Cosmochimica Acta 68, 4843–4858.

Applied Geochemistry 24 (2009) 463–474

Contents lists available at ScienceDirect

Applied Geochemistry

journal homepage: www.elsevier.com/locate/apgeochem

Chemical evolution of the Mt. Hekla, Iceland, groundwaters: A natural analogue for CO_2 sequestration in basaltic rocks

Therese K. Flaathen [a,b,c,*], Sigurður R. Gislason [d], Eric H. Oelkers [a,b,c], Árný E. Sveinbjörnsdóttir [d]

[a] Université de Toulouse; UPS (OMP); LMTG; 14 Avenue Edouard Belin, F-31400 Toulouse, France
[b] CNRS; LMTG; F-31400 Toulouse, France
[c] IRD; LMTG; F-31400 Toulouse, France
[d] Institute of Earth Sciences, University of Iceland, Sturlugata 7, 101 Reykjavík, Iceland

ARTICLE INFO

Article history:
Received 11 July 2008
Accepted 18 December 2008
Available online 29 December 2008

Editorial Handling by Dr. R. Fuge

ABSTRACT

A detailed study of the chemical composition of the groundwater surrounding the Mt. Hekla volcano in south Iceland was performed to assess fluid evolution and toxic metal mobility during CO_2-rich fluid basalt interaction. These fluids provide a natural analogue for evaluating the consequences of CO_2 sequestration in basalt. The concentration of dissolved inorganic C in these groundwaters decreases from 3.88 to 0.746 mmol/kg with increasing basalt dissolution while the pH increases from 6.9 to 9.2. This observation provides direct evidence of the potential for basalt dissolution to sequester CO_2. Reaction path calculations suggest that dolomite and calcite precipitation is largely responsible for this drop in groundwater dissolved C concentration. The concentrations of toxic metal(loid)s in the waters are low, for example the maximum measured concentrations of Cd, As and Pb were 0.09, 22.8 and 0.06 nmol/kg, respectively. Reaction path modelling indicates that although many toxic metals may be initially liberated by the dissolution of basalt by acidic CO_2-rich solutions, these metals are reincorporated into solid phases as the groundwaters are neutralized by continued basalt dissolution. The identity of the secondary toxic metal bearing phases depends on the metal. For example, calculations suggest that Sr and Ba are incorporated into carbonates, while Pb, Zn and Cd are incorporated into Fe (oxy)hydroxide phases.

1. Introduction

A large current effort is being made to identify and optimize CO_2 sequestration technologies to address the potential dangers associated with increased atmospheric CO_2 content (IPCC, 2005; Oelkers and Schott, 2005; Oelkers and Cole, 2008). One such technology involves the injection of CO_2 into basaltic rocks (McGrail et al., 2006; Gislason et al., 2007; Matter et al., 2007; Oelkers et al., 2008). This method offers several potential advantages including the availability of divalent metal cations such as Ca^{2+} and Mg^{2+} which could provoke the precipitation of stable carbonate minerals (Walker and Hays, 1981; Gaillardet et al., 1999; Brady and Gislason, 1997; Wolff-Boenisch et al., 2006). One method to assess both the potential and the risks associated with CO_2 sequestration in basaltic rocks is through the study of natural analogues. One such analogue is the Mt. Hekla groundwater system. The groundwaters surrounding Mt. Hekla experience large inputs of magmatic gases dominated by CO_2 (Kjartansson, 1957; Gislason et al., 1992; Flaathen and Gislason, 2007). A study of the chemical composition of these groundwaters should, therefore, provide insight into the fate and consequences of injecting CO_2 into basaltic rocks. Taking advantage of this natural analogue, waters have been regularly sampled from 26 springs surrounding Mt. Hekla. Analyses of these waters, together with reaction path modelling, suggest that (1) CO_2 is readily sequestered, via fluid–basalt interaction through carbonate mineral precipitation and (2) although they may be liberated due to basalt dissolution, toxic metals are readily reincorporated into solid phases as the basalt neutralizes the initially CO_2-rich fluid. The purpose of this paper is to present the results of this combined field and modelling study providing insight into the consequences of injecting CO_2 into basaltic rocks.

2. Geological background: Hekla volcano and its groundwater system

The Mt. Hekla volcano (63.98°N, 19.70°W) is a ridge built up by repeated fissure eruptions. The volcano strikes N 65°E and is located where the eastern volcanic zone, meets the South Iceland seismic zone (Gudmundsson et al., 1992). It is one of Europe's most active volcanoes with 18 eruptions during the last 900 a (Gronvold et al., 1983). The most recent eruptions occurred during 1970, 1980, 1991 and 2000. The bulk of the erupted material during the last 900 a is of basaltic andesite composition (Sigvaldason, 1974; Gudmundsson et al. 1992; Moune et al., 2006). The main

* Corresponding author. Address: Université de Toulouse; UPS (OMP); LMTG; 14 Avenue Edouard Belin, F-31400 Toulouse, France. Fax: +33 0 5 61 33 25 60.
E-mail addresses: flaathen@gmail.com, therese@hi.is (T.K. Flaathen).

0883-2927/$ - see front matter © 2008 Elsevier Ltd. All rights reserved.
doi:10.1016/j.apgeochem.2008.12.031

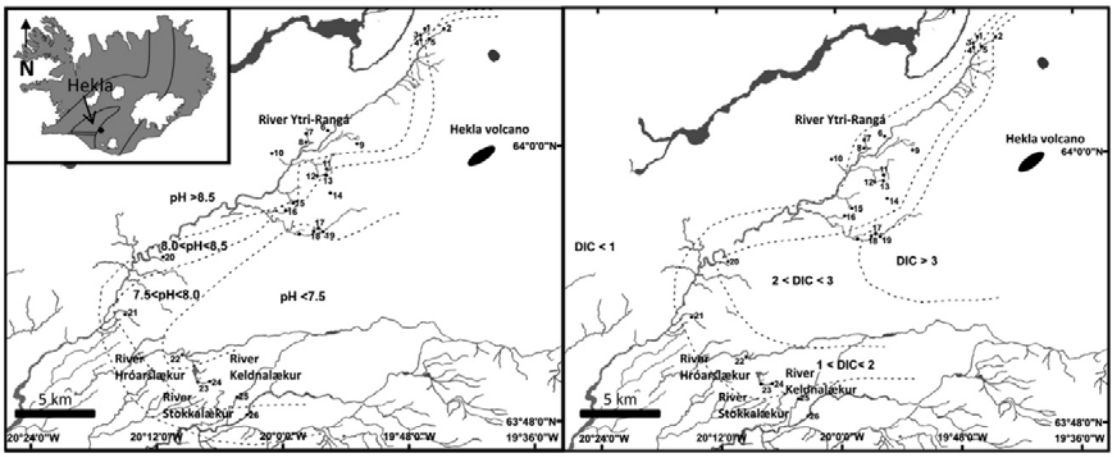

Fig. 1. Map showing the location of the Hekla volcano, the main springs, and the sample sites. Superimposed on the map is a) *in situ* pH in the spring water samples, and b) the dissolved inorganic C (DIC) concentration (meq/L) in the spring water samples.

rock forming phases of the basaltic andesitic tephra are glass (97.9%), plagioclase (1.6%), magnetite (0.2%), olivine (0.2%) and pyroxene (0.1%) (Sigvaldason, 1974). The basaltic andesite lava flows consist of dense dark rocks with relatively high viscosity upon extrusion, forming an aa or block type lava. Phenocrysts are rare in the 1970 lava flows (Sigvaldason, 1974).

The groundwater in the Mt. Hekla region flows from the NE to the SW along the volcanic zone. Groundwater discharge is observed at the source of the Ytri-Rangá River, NW of the volcano, as well as at springs west, south and SE of the volcano (Árnason, 1976). The surface hydrology of this system can be seen in Fig. 1. The post-glacial lava flows (<10 ka) and volcanic ash fallouts are very porous, preventing surface runoff in the vicinity of the volcano.

The groundwater chemistry of the Mt. Hekla system is strongly influenced by the input of magmatic gases and it is known for CO_2 degassing during eruptions (Kjartansson, 1957; Gislason et al., 1992; Flaathen and Gislason, 2007). During its 1947 eruption, several animals, birds, and sheep, were found suffocated due to high CO_2 concentrations in shallow depressions in the lava fields. Formation of Ca and Mg carbonates in discharging groundwater has been observed in the area (Kjartansson, 1957). The long-term influx of magmatic gases from the magma chamber and their interaction with basalt through the aqueous phase has lead to elevated concentrations of total dissolved solids (TDS) and high alkalinity in the Hekla groundwater (Gislason et al., 1992).

3. Materials and methods

3.1. Water samples from springs

A total of 111 samples from 26 springs surrounding Mt. Hekla were collected during 1988, 1991, 1992 and 2006. The locations of the sampling sites are shown in Fig. 1. Each spring was collected for 1–6 times except spring 18, which was sampled 19 times. The samples were taken during all seasons. The water samples were filtered immediately after sampling through 0.2 μm Millipore cellulose acetate membranes into high density polyethylene bottles. Samples taken for pH and dissolved inorganic C (DIC) measurement were collected in brown glass bottles with a special cap designed to eliminate air inside the bottles. Samples intended for major and trace element analyses were acidified using concentrated suprapur HNO_3. Alkalinity/dissolved inorganic C and pH were determined in the laboratory at ambient temperature 1–5 days after sampling.

Samples collected during 1988–1992 were analyzed at the University of Iceland. Fluorine and Cl were measured with ion-selective electrodes. Silica, Na, K, Ca, Mg, S, Fe, Mn, Ti, Al and Sr were measured by inductively coupled plasma atomic emission spectroscopy (ICP–AES). The detection limit for these analyses were 2.5×10^{-8}, 2.1×10^{-7}, 4.3×10^{-7}, 1.3×10^{-5}, 3.6×10^{-6}, 3.7×10^{-7}, 3.6×10^{-7}, 9.3×10^{-7}, 2.3×10^{-8} and 1.0×10^{-5} mol/kg, for Ca, Mg, Na, K, Si, Al, Fe, B, Sr and SO_4^{2-}, respectively. The uncertainty of these analyses was 3–5%.

For samples collected in 2006, F^-, Cl^- and $SO_4^{\ 2}$ were measured by ion-chromatography (IC) at the Institute of Earth Sciences, University of Iceland; these results have an uncertainty of 3–5% and the detection limit was 3.68×10^{-7}, 6.35×10^{-6} and 3.12×10^{-7} mol/kg, respectively. The cations, other than Fe, were analyzed at Analytica-SGAB, Luleå, Sweden. Calcium, K, Mg, Na, Si, Sr and V were measured with ICP-AES and Al, Ba, Cd, Co, Cr, Cu, Mn, Mo, Ni, total P, Pb and Zn together with As, B, Li, Ti and the lanthanides were measured using inductively coupled plasma field mass spectroscopy (ICP-SFMS). Mercury and Se were measured using atomic fluorescence spectroscopy (AFS). The detection limits for these latter analyses were 2.5×10^{-6}, 3.7×10^{-6}, 4.3×10^{-6}, 1.0×10^{-5}, 1.0×10^{-6} and 7.4×10^{-9} mol/kg for Ca, Mg, Na, K, Si and Al, respectively. The detection limits for the trace elements, Ba, Cd, Co, Cu, Mn, Pb, Sr and Zn, were 7.3×10^{-11}, 1.8×10^{-11}, 3.4×10^{-11}, 1.6×10^{-9}, 5.5×10^{-10}, 4.8×10^{-11}, 2.3×10^{-8} and 3.1×10^{-9} mol/kg, respectively. Iron was analyzed at Matís, Iceland by ICP-MS, with a detecion limit of 4.5×10^{-9} mol/kg. The measurements of these major elements together with Sr, P, Ba, Mo and V have an uncertainty between 12% and 15%. The uncertainty for the elements Al, Cr, Cu and Li varies between 15% and 25%, while the uncertainty of the other measured trace metals varies between 30% and 160%.

3.2. Thermodynamic calculations and reaction path modelling

3.2.1. Speciation and saturation state calculations

Speciation and saturation-state calculations were performed using the PHREEQC 2.14.2 computer code (Parkhurst and Appelo, 1999). The database llnl (The database used in the present study

Table 1
Secondary minerals assumed to precipitate during the reaction path modelling performed in the present study.

Mineral name	Formula
Calcite	$CaCO_3$
Cerussite	$PbCO_3$
Chalcedony	SiO_2
Clinochlore-14A	$Mg_5Al_2Si_3O_{10}(OH)_8$
	$CoFe_2O_4$
Delafossite	$CuFeO_2$
Ferrite–Zn	$ZnFe_2O_4$
Hematite	Fe_2O_3
Heulandite	$Ba_{0.65}Sr_{0.175}Ca_{0.585}K_{0.132}Na_{0.383}Al_{2.165}Si_{6.835}O_{18}{:}6H_2O$
Hydrozincite	$Zn_5(OH)_6(CO_3)_2$
Kaolinite	$Al_2Si_2O_5(OH)_4$
Laumontite	$CaAl_2Si_4O_{12}{:}4H_2O$
Magnesite	$MgCO_3$
Manganite	$MnO(OH)$
Otavite	$CdCO_3$
Rhodochrosite	$MnCO_3$
Siderite	$FeCO_3$
Smectite-high-Fe–Mg	$Ca_{0.025}Na_{0.1}K_{0.2}Fe_{0.7}Mg_{1.15}Al_{1.25}Si_{3.5}O_{10}(OH)_2$
Smectite-low-Fe–Mg	$Ca_{0.02}Na_{0.15}K_{0.2}Fe_{0.45}Mg_{0.9}Al_{1.25}Si_{3.75}O_{10}(OH)_{12}$
Smithsonite	$ZnCO_3$
Sphaerocobaltite	$CoCO_3$
Strontianite	$SrCO_3$
Witherite	$BaCO_3$

has the id: llnl.dat 85 2005-02-02. The data for this database were taken from 'thermo.com.V8.R6.230' prepared by Jim Johnson at Lawrence Livermore National Laboratory.) was used other than for the thermodynamic data for hydrated basaltic andesitic Hekla 2000 glass, which was taken from Wolff-Boenisch et al. (2004). The saturation state of the fluid is quantified in terms of the Gibbs free energy of reaction, ΔG_r, of the dissolving minerals or glass (Gislason and Arnórsson, 1990, 1993). The Gibbs free energy of reaction is equal to zero at equilibrium. If $\Delta G_r < 0$, the mineral is undersaturated. Dissolution rate equations for minerals and glasses are commonly written in terms of the ΔG_r (e.g. Gislason and Oelkers 2003).

3.2.2. Reaction path modelling

Reaction path modelling was performed to investigate the fate of metals and dissolved C in the Hekla groundwater using PHREEQC 2.14.2 and assuming the groundwater system is closed with respect to both CO_2 and secondary minerals. This modelling involves the dissolution of Hekla andesitic basalt (Moune et al., 2006) into CO_2-rich groundwater. The chemical composition of the Hekla lava has been constant during the last four eruptions (Gudmundsson et al., 1992; Moune et al., 2006). The 2000 lava has a chemical formula normalized to one Si consistent with Si $P_{0.01}$ $Ti_{0.03}$ $Al_{0.31}$ $Fe_{0.17}$ $Mg_{0.08}$ $Mn_{0.005}$ $Ca_{0.13}$ $Na_{0.16}$ $K_{0.03}$ $O_{3.13}$. The concentration of the trace metals, Ba, Cd, Co, Cu, Sr, Pb and Zn, are 2.50×10^{-3}, 1.65×10^{-6}, 7.86×10^{-4}, 4.12×10^{-4}, 4.58×10^{-3}, 1.57×10^{-5} and 3.23×10^{-3} mol/kg, respectively (Moune et al., 2006). The different constituents of the Hekla glass were added to the reaction fluid in the reaction path calculations as oxides and were forced to react with the solution in proportion to their composition in the glass. The temperature of the model was kept constant at 3.7 °C consistent with the average temperature of local groundwaters.

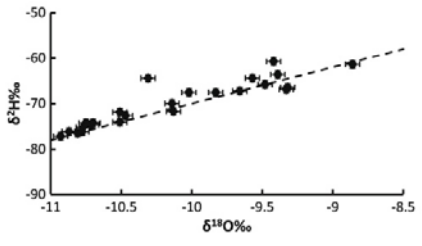

Fig. 2. $\delta^{18}O$ versus δ^2H values in the spring waters. The symbols represent the spring water samples and the line represents the meteoric water line (Craig, 1961). The coherence between the symbols and the line indicates a meteoric origin of the waters.

3.2.3. Initial modelling conditions and secondary mineral formation

The initial solution for the reaction path modelling performed in this study had the chemical composition of melted snow from SW Iceland (Gislason et al., 2000) equilibrated with 0.05 bar CO_2; this CO_2 pressure is 130 times that of the atmosphere. The resulting solution has a pH of 4.5. This CO_2 concentration was chosen to be consistent with the measured groundwater compositions such that the final Na concentration of the reaction path model matched that of the Na in the springs (see Fig. 8 below). The total aqueous concentration of Na was used for this purpose because it is negligibly incorporated into secondary phases during low temperature basalt alteration (Gislason et al., 1996); this choice is confirmed by the correspondence of measured fluid compositions with the model results presented below. Based on this concentration the total amount of solid, reactant was calculated to be 0.0098 mol of basaltic glass per kg of water to attain a final pH of 9.4.

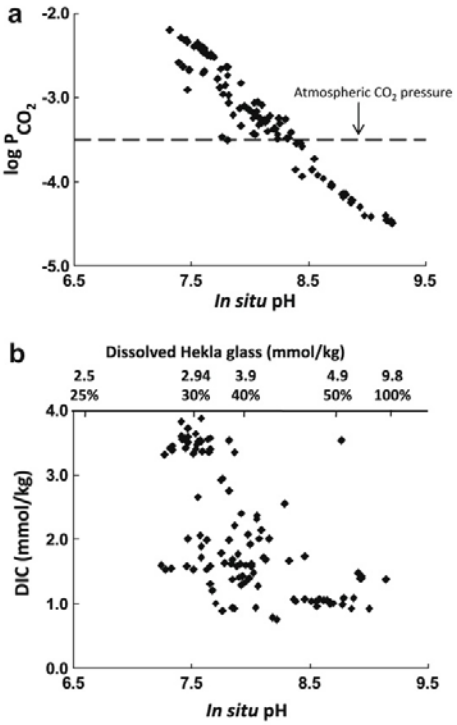

Fig. 3. (a) The symbols represent the partial pressure of CO_2 calculated using PHREEQC 2.14.2 in the springs plotted versus pH at the measured spring water temperature at the time of sampling (*in situ* pH). The stippled line is the atmospheric partial pressure of CO_2. The uncertainty of the measurements is approximated by the symbol size. (b) DIC concentrations in the spring water samples plotted versus *in situ* pH. The secondary *x*-axis shows the amount of Hekla glass dissolved in model calculation to reach the pH.

When Mt. Hekla andesitic basaltic volcanic glass dissolves in the initial CO_2-rich solution, the concentration of aqueous species increases and it eventually becomes supersaturated with respect to secondary minerals. The secondary minerals allowed to precipitate in the model calculations are those that are common in low-temperature alteration of basalt in Iceland (Mehegan et al., 1982; Kristmannsdóttir, 1982; Gislason et al., 1993; Neuhoff et al., 1999). A list of all secondary phases used in the model calculations are to be found in Table 1. Note that although allophane is a common clay mineral found in Iceland, it is not considered as a secondary phase in these calculations because this mineral is not in the llnl.dat database. Kaolinite is taken as a proxy for allophane in the calculations. In the same way, oxides and multiple oxide minerals such as hematite, delafossite, $CoFe_2O_4$ and $ZnFe_2O_4$ are essentially proxies

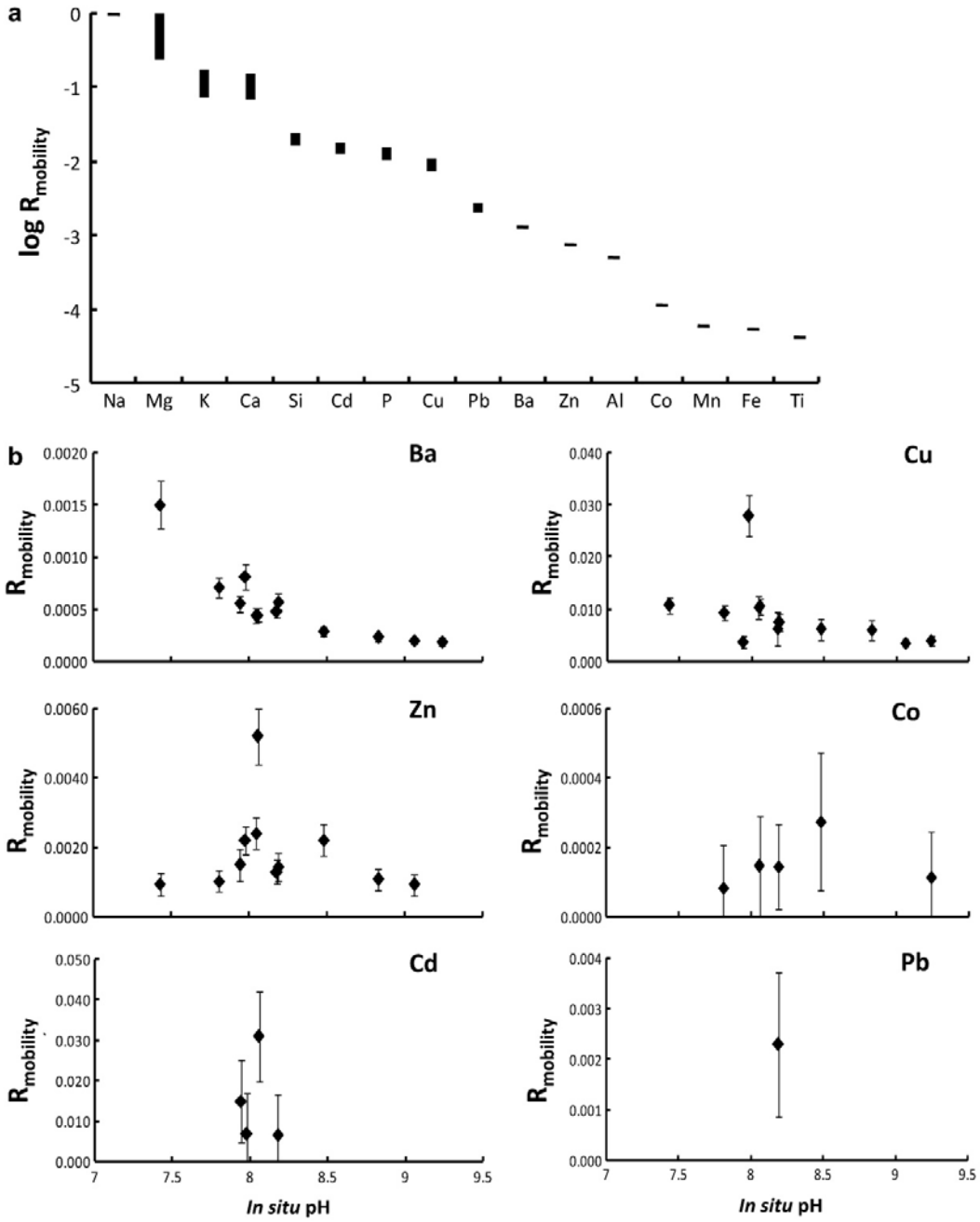

Fig. 4. (a) The logarithm of the relative mobility of major and trace elements in the spring waters. The concentration of Fe, Al, Mn, Cd, Co, Pb and Zn were in some samples below detection limit. (b) The mobility of the trace metals in the Hekla groundwater versus pH (see text).

Table 2
The annual discharge, DIC concentration and CO_2 flux in the rivers from the Hekla groundwater system.

Rivers	Annual discharge[a] (km^3/year)	DIC (mmol/kg)	Annual CO_2 flux (ton/year)
Ytri-Ranga	1.33[b]	1.57	8.89×10^4
Stokkalaekur	0.256	0.94	7.62×10^3
Hroarslaekur	0.394	0.94	1.33×10^4
Keldulaekur	0.429	0.94	1.48×10^4
Total	2.409		1.25×10^5

[a] The discharge of Stokkalaekur, Hroarslaekur and Keldnalaekur was obtained by a single measurement taken on each river on March 14th, 1992.
[b] The discharge of Ytri-Ranga is the mean annual discharge for the years 1996–1998 (Gislason et al., 1993).

for related oxy-hydroxide minerals absent from the database. In addition, due to similar database constraints, the zeolites heulandite and laumontite are considered in the model rather than the commonly found thomsonite and analcime.

4. Results

4.1. Main hydrogeochemical features

The aqueous concentrations of major elements of all samples can be seen in the Appendix. The pH and alkalinity/dissolved inorganic C (DIC) of these waters range from 7.3 to 9.2 and 0.75 to 3.88 meq/kg, respectively. The spatial distribution of these pH and DIC values are shown in Fig. 1. DIC decreases while pH increases with increased distance from the volcano. Total dissolved solids (TDS) range significantly with the highest concentrations close to the volcano.

$\delta^{18}O$ and δ^2H were measured in the groundwater samples collected in 1988. The results are plotted in Fig. 2 together with the meteoric water line according to Craig (1961). The uncertainty of the measurements is 0.05‰ and 0.8‰ for $\delta^{18}O$ and δ^2H, respectively. The coherence between the symbols and the line in Fig. 2 indicates a meteoric origin of the samples collected in this study. This observation coincides with earlier studies which concluded that all Icelandic ground waters are of meteoric origin (Árnason, 1976). According to Árnason (1976), the isotopically heaviest precipitation in Iceland is found along the southern coast with δ^2H of −50‰ while the isotopically lightest precipitation is in the central highlands at −106‰. Those measured in the Hekla waters analyzed in this study range between −60 ‰ and −77‰. Consistent with the general Icelandic precipitation trends, the lightest δ^2H waters measured in this study were found in the springs located to NE of the Hekla volcano, (springs 1, 3, 7 and 10) whereas the heaviest δ^2H waters are found in the springs to the south of Hekla (springs 20 and 21).

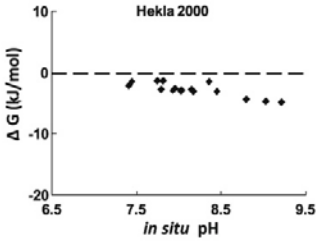

Fig. 5. The pH dependence of the saturation state of the hydrated Hekla basaltic andesitic glass, in the sampled spring waters. The symbols represent calculated saturation states and the dashed line shows equilibrium conditions: $\Delta_r G = 0$.

The partial pressure of CO_2, P_{CO2}, of the sampled spring waters is shown as a function of pH in Fig. 3a. P_{CO2} decreases systematically with pH. Carbon dioxide is supersaturated compared to the atmosphere at pH < 8.4 but undersaturated at higher pH. A direct comparison between DIC and pH, is shown Fig. 3b. DIC generally decreases as pH increases. Such a trend is consistent with CO_2 being precipitated as carbonate minerals, such as calcite, from these waters due to its interaction with basalts. Calcite precipitation is also suggested by the saturation state of these spring water samples as reported below.

4.1.1. Mobility of major ions

Bicarbonate is the major anion in the spring water samples with concentrations ranging from 0.0012 to 3.88 mmol/kg. Sulphate and Cl^- are 1 order and F^- 2 orders of magnitude less abundant than HCO_3^-. The most abundant cation is Na^+ with concentrations ranging from 0.42 to 2.50 mmol/kg. Sodium is reported to be the most mobile cation in SW Iceland (Gislason et al., 1996). The relative mobility of an element ($R_{mobility}$) in the ground water system during basalt weathering can be quantified relative to Na using (Gislason et al., 1996):

$$R_{mobility} = [X_{water}/Na_{water}]/[X_{rock}/Na_{rock}] \quad (1)$$

where $[X_{water}]$ and $[Na_{water}]$ are the average concentrations of the element X, and Na in the springs, and $[X_{rock}]$ and $[Na_{rock}]$ are the concentrations in the Hekla 2000 lava (Moune et al., 2006). Elemental concentrations were corrected for rainwater input prior to calculating $R_{mobility}$ in accord with Gislason et al. (2000). Fig. 4a shows the relative mobility ($R_{mobility}$) of major and selected trace elements in the springs. The sequence of mobility of the major elements from high to low mobility is Na > Mg > K > Ca > Si > P, which is roughly consistent with those of Gislason et al. (1996), who reported the weathering rates of southern Iceland, and of Aiuppa et al. (2000) who studied the composition of Mt. Etna groundwaters.

4.1.2. Mass flux of carbon

A number of studies have concluded that most of the CO_2 in magma of active volcanoes is lost to non-eruptive degassing (Allard et al., 1991; Aiuppa et al., 2004) and groundwaters (Federico et al., 2002) rather than via eruptive degassing. It seems likely, therefore, that much CO_2 is added to groundwater during dormant periods. To assess the CO_2 flux to groundwater in the dormant Mt. Hekla system, the DIC concentration of sampled springs was used to calculate the CO_2 flux emitted by the Hekla spring water. The studied springs source four rivers, the Ytri-Rangá (Gislason et al., 2003), Stokkalækur, Hróarslækur and Keldnalækur. The location of the rivers can be seen in Fig. 1; their annual discharge is listed in Table 2. The discharge, excluding snow melt events, are stable throughout the year. Gislason et al. (2003) reported 24 discharge measurements of Ytri-Rangá taken at various times throughout one year. The standard deviation of these discharge measurements is 8%. As some of the springs are supersaturated with respect to atmospheric CO_2 some will degas when they arrive at the surface (see Fig. 3). This degassing results in lower DIC concentrations and higher pH of the river samples taken at the discharge measuring station (see Table 2) versus those of the springs.

The annual CO_2 flux of the Mt. Hekla system to the surface can be estimated from the product of spring water DIC concentration and annual mean discharge of the four rivers draining the Mt. Hekla system. The total annual mean discharge of the four rivers draining this system is 2.41×10^9 m^3/a. The DIC concentrations in the springs range from 0.746 to 3.88 mmol/kg, indicating that the annual CO_2 discharge of the Mt Hekla system is between 99,380 and 257,500 ton/a. Note this estimate is based on the assumption that C originating (1) from vegetation and soil and, (2) directly from the atmosphere is negligible. The first assumption is validated by the

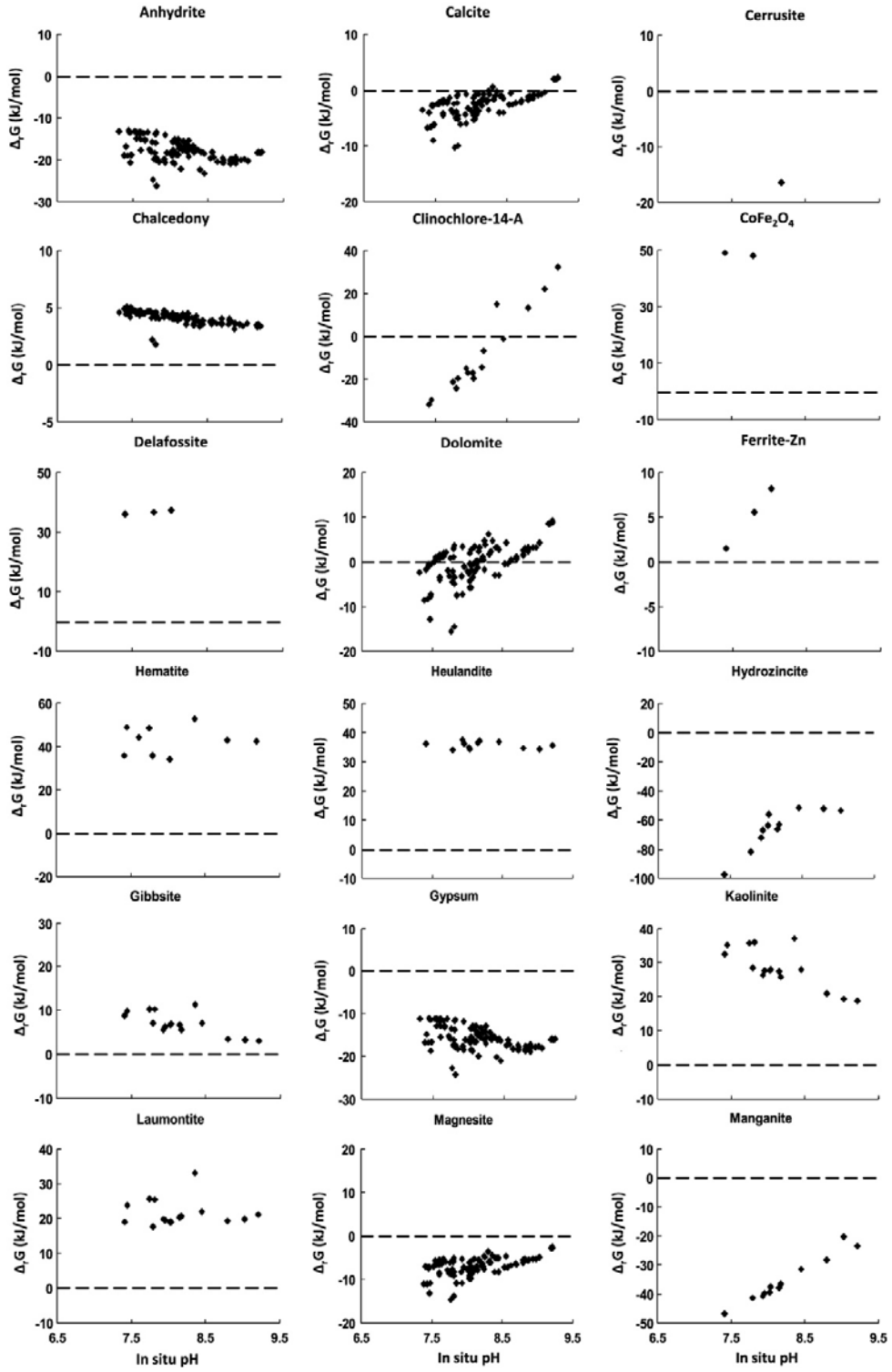

Fig. 6. The pH dependence of the saturation state of secondary minerals in the Hekla spring waters. The symbols represent calculated saturation states and the dashed line corresponds to equilibrium ($\Delta_r G = 0$).

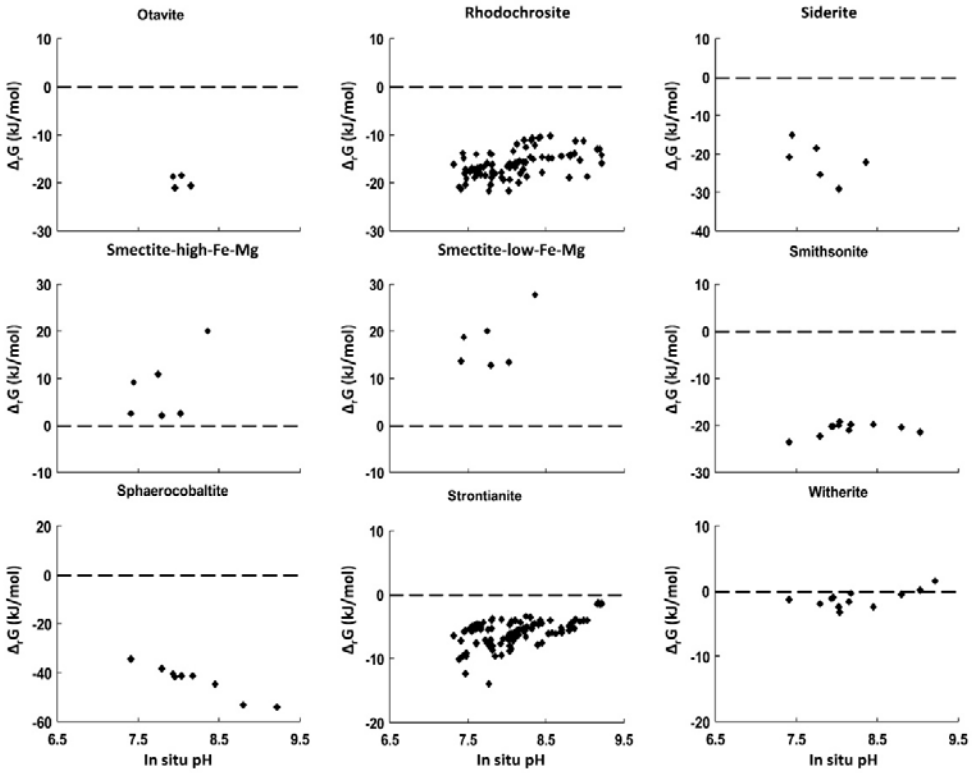

Fig. 6 (*continued*)

sparse vegetation and soil in the recharge area. The second assumption can be validated by comparing the CO_2 present in the Mt. Hekla spring waters with that of Icelandic rainwater. The average CO_2 content of Icelandic rainwater is 2.7×10^{-5} mol/kg (Gislason et al., 1996). This value is less than 3% of that dissolved in the spring waters. Nevertheless, this annual CO_2 discharge should only be taken as a minimum estimate. There are two other potentially significant CO_2 discharge pathways to the surface in this system: (1) CO_2 charged groundwater leaving the system through different rivers and (2) CO_2 degassing from the groundwater through the lavas.

4.1.3. Mobility of trace metals

Iron, Mn and Sr concentrations were measured in all ground water samples. Other trace element concentrations were measured in only the 12 samples collected in 2006 from the largest springs. These results are reported in the Appendix. The concentrations of Fe, Mn and Sr ranged from 6 to 115 nmol/kg, 0.42 to 11.7 nmol/kg and 117 to 407 nmol/kg, respectively. Most of the samples analyzed for Fe and Mn in the period 1988–1992 are below detection limits of the ICP-AES method used in this study. The concentrations of B, Ba, Co, Cr, Cu, Ni, Zn, Mo, Se, Li and V were low, slightly above the detection limits in more than half of the samples. The concentration of Cd, Pb and Hg together with As were below detection limits in most of the samples.

Moune et al. (2006) reported the concentrations of several trace elements in the Mt. Hekla 2000 lava. The concentrations were 11.26 wt% total Fe (expressed as FeO) and 46.3, 26.2, 211, 0.186, 344 and 3.25 ppm, respectively for Co, Cu, Zn, Cd, Ba and Pb. These values were used to calculate the relative mobility of these trace

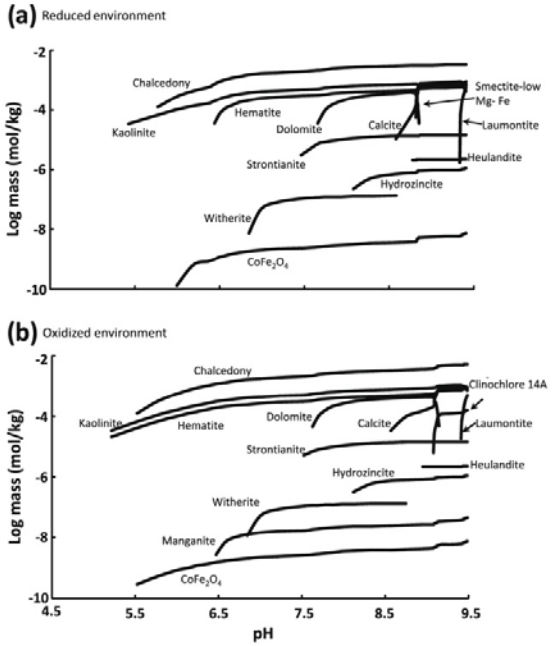

Fig. 7. Results of reaction path modelling. (a) Logarithm of the masses of secondary minerals precipitated during reaction path modelling for reduced environments. (b) Logarithm of the masses of secondary minerals precipitating during reaction path modelling for oxidized environments.

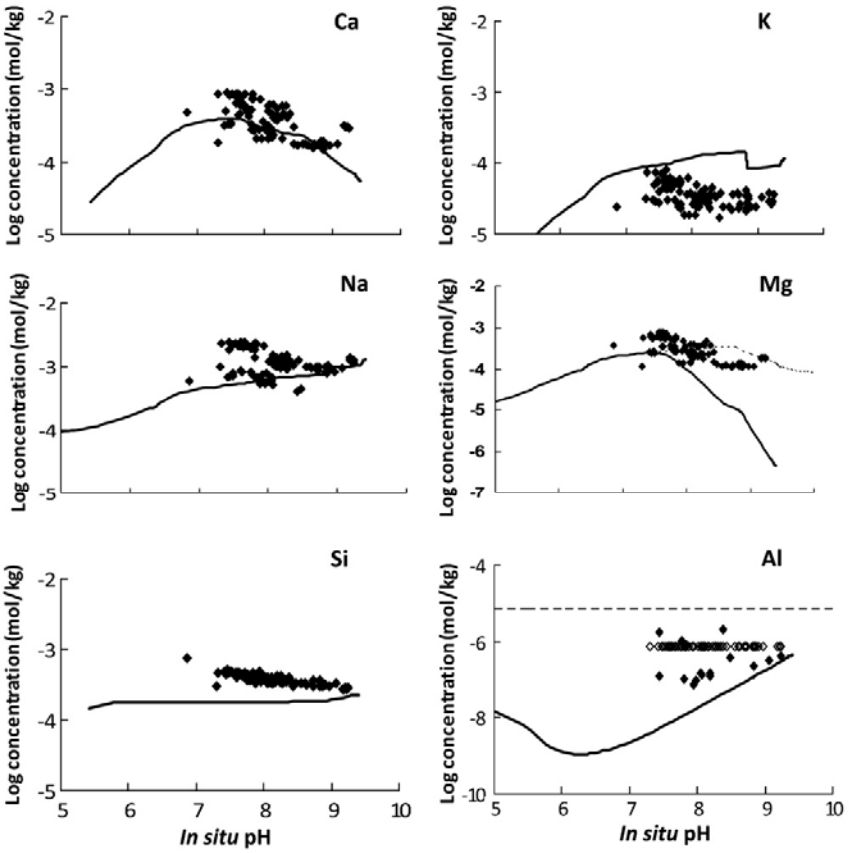

Fig. 8. A comparison of the concentration of major elements in the Hekla spring waters with those obtained by reaction path modelling. Closed symbols correspond to measured solution concentration and open symbols correspond to the maximum possible concentrations for samples below the detection limit. The solid curves represent the results of model calculations and the thin dotted line in the Mg diagram was obtained from reaction path modelling without allowing smectite and clinochlore to precipitate. The dotted line in the Al diagram is the drinking water guidelines given by the European Community (1998), and WHO (2006). The uncertainty in the analyses is approximated by the symbol size. 93 of 97 water samples collected between 1988 and 1992 had Al concentrations below the detection limit (7.4×10^{-7} mol/kg).

metals shown in Fig. 4a. The sequence of relative mobility is Cd > Cu > Zn > Ba > Al > Ti > Mn > Co > Fe. This is roughly consistent with results from Aiuppa et al. (2000), who reported the mobility of trace elements from the Mt. Etna volcano. The mobility of these trace elements versus in situ pH is shown in Fig. 4b. Barium is the only metal which shows a clear trend; its mobility decreases with increasing pH.

4.2. Saturation state ($\Delta_r G$) of minerals and volcanic glasses in the spring waters

The saturation states of minerals and glasses are quantitative constraints on their tendency to dissolve or precipitate in the water. The saturation states of various mineral phases in the spring waters were calculated using the computer code PHREEQC 2.14.2 (Parkhurst and Appelo, 1999). Results are shown in Fig. 5 for the primary phase and in Fig. 6 for secondary minerals.

Because calcite is the most common carbonate mineral, insight into the ability of the Mt. Hekla system to sequester CO_2 can be gained by considering the saturation state of Ca bearing solids. Hydrated Hekla 2000 glass is undersaturated in all the springs, as can be seen in Fig. 5, suggesting that the glass is an effective source for aqueous Ca^{2+} in this system. All primary minerals including anorthite, pyroxene and olivine are also undersaturated in the spring waters. Common secondary Ca-bearing phases in Iceland include carbonates, smectites, zeolites and sometimes anhydrite (Neuhoff et al., 1999; Mehegan et al., 1982; Kristmannsdóttir 1982; Gislason et al., 1993). The saturation indices of these minerals are shown in Fig. 6. The calculations show that smectites, laumontite and heulandite are saturated in all spring waters. Anhydrite and gypsum are highly undersaturated in the spring waters while calcite and dolomite are undersaturated at low pH but attain equilibrium in some springs at higher pH. These results suggest that although dolomite and calcite may form at elevated pH, providing mineralogical storage for dissolved CO_2, both clay minerals and zeolites can compete with carbonate minerals for Ca^{2+} ions, potentially limiting the Ca available for carbonate mineral precipitation. Other potential carbonate minerals including magnesite, siderite, cerrusite, hydrozincite, rhodochrosite, otavite, strontianite, smithsonite and sphaerocobaltite are undersaturated in all the springs while witherite is saturated at high pH.

4.3. Reaction path modelling

Reaction path modelling was performed using PHREEQC 2.14.2 (Parkhurst and Appelo, 1999) to simulate water–rock interaction in

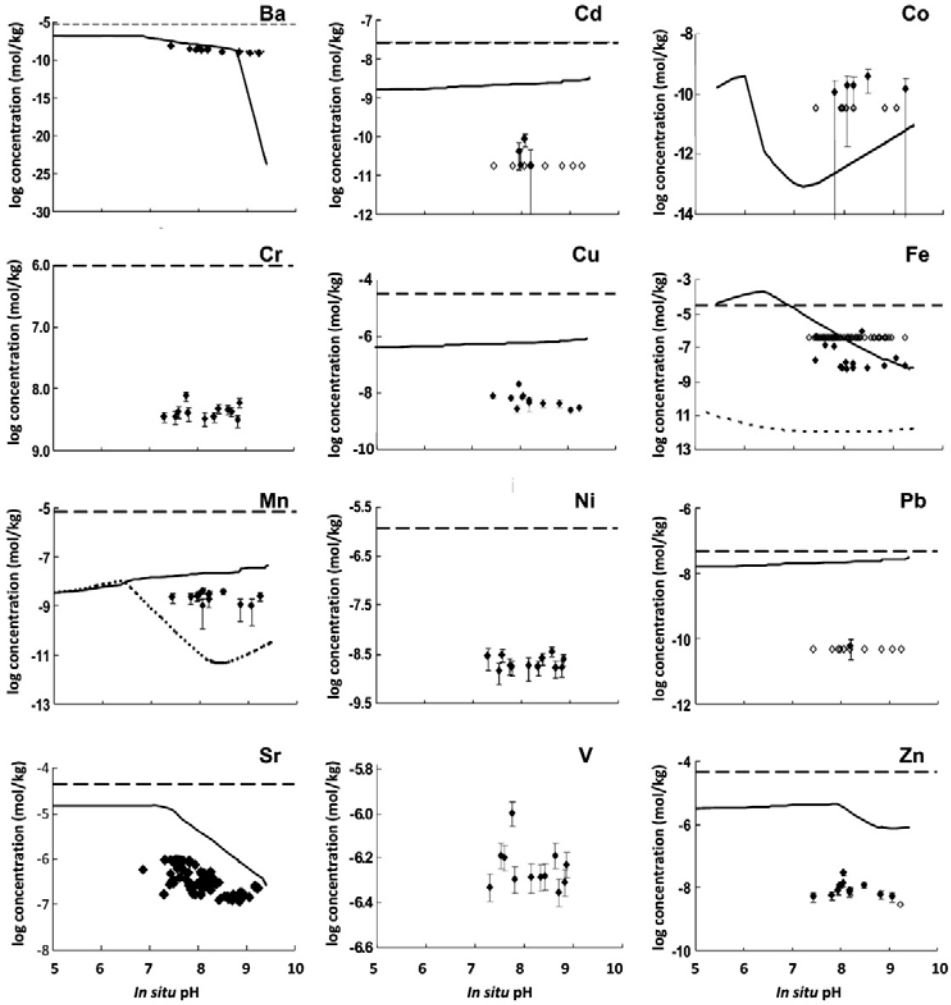

Fig. 9. Comparison between the trace element concentration of the Hekla spring waters with those obtained by reaction path modelling as a function of *in situ* pH. Closed symbols correspond to measured solution concentrations and open symbols correspond to the maximum possible concentrations for samples below the detection limit. The solid curves represent the results of reaction path modelling for reduced conditions and the dotted lines show the drinking water limits recommended by the European Community (1998), and WHO (2006). The thin dotted curve in the Ba diagram that fits all the samples including the three samples at the highest pH shows the concentration of Ba during reaction path modelling without heulandite precipitation. The thin dotted curve in the Fe and Mn diagrams stems from reaction path modelling during oxidized conditions (see text). When the errors bars are smaller than the symbol, the error bars are not shown.

the Hekla system. The modelling was performed under both reducing and oxidizing conditions. The O_2 fugacity in the reducing environment was set by Fe^{2+}/Fe^{3+} equilibrium fixed by the dissolving basalt coupled to hematite precipitation; that of the oxidizing environment was set by assuming the solution was constantly in equilibrium with atmospheric O_2. The groundwater initially had a 0.05 bar CO_2 partial pressure and pH = 4.5. As this solution reacts with Hekla glass, the pH increases and becomes supersaturated with respect to a number of secondary phases. The maximum pH attained during the modelling was 9.4. Within the model, secondary phases are assumed to precipitate and be in equilibrium with the fluid phase. The amount of the secondary minerals formed during the reaction path models are shown in Fig. 7. Modelling results for the reduced environment, illustrated in Fig. 7a, suggest that kaolinite is the first secondary mineral to precipitate at pH > 5.4. The oxides, chalcedony and $CoFe_2O_4$ reach saturation at pH > 5.8 and 6.0. Hematite attains saturation when pH reaches 6.3, and the carbonates, witherite, strontianite, dolomite and calcite attain saturation at pH > 6.8, 7.5, 7.7 and 8.6, respectively. Smectite precipitation begins at pH > 8.8. The zeolites heulandite and laumontite, attain saturation at pH 8.8 and 9.3, respectively. These modelling calculations suggest that the major alteration phases are chalcedony, kaolinite and hematite at 5.4 < pH < 8.0. At higher pH calcite, smectite, and eventually laumontite become important alteration phases. These results match the field observations reported by Kristmannsdóttir (1982), Mehegan et al. (1982), Neuhoff et al. (1999), which validates, in part, the model calculations. Model results for the oxidized system are shown in Fig. 7b. These results are similar to those of the reduced system other than (1) manganite, a mineral containing oxidized Mn is calculated to precipitate at pH > 6.5, and (2) clinochlore rather than smectite is calculated to precipitate at pH > 9. This latter result may be due to

lack of provision for solid-solutions in the thermodynamic database. The low Fe^{2+} concentration of the oxidized fluids destabilizes the Fe^{2+} bearing smectite in the model calculation.

5. Discussion

5.1. Controls on major element mobility

Insight into metal mobility can be obtained from the results of reaction path modelling. The concentrations of major elements in the springs are compared with those from the reaction path modelling in Fig. 8. As can be seen in Fig. 8, the concentrations of major elements tend to be close to those estimated from the model calculation. In some cases however, there are important difference between model calculations and spring water concentrations. For example, spring water Si concentrations are systematically higher than the model values. This suggests that the precipitation kinetics of chalcedony, which is the commonly observed SiO_2 phase in altered basalts, are sluggish. This observation is consistent with the results of Rogers et al. (2006), who reported that amorphous silica is the common silica phase formed via the low-temperature alteration of basalts by CO_2-rich fluids. Similar sluggish kinetics or the affect of allophane precipitation may be responsible for the scatter observed among the spring water Al concentrations. Note that allophane was not present in the thermodynamic database. Spring water Mg concentrations are significantly higher at pH > 7.5 than the modelled counterparts. This may be due to sluggish smectite and clinochlore precipitation kinetics; both of these minerals appear to be significantly supersaturated in the Hekla spring waters at this pH (see Fig. 6). By removing smectite and clinochlore precipitation from the reaction path model, the modelled Mg concentrations are equal to the spring water concentrations as can be seen in Fig. 8. Another factor that could lead to the underestimation of aqueous Mg concentrations in the model calculations is either sluggish dolomite kinetics or an overestimate of the stability of dolomite in the thermodynamic database. This possibility is suggested by the observation that, according to thermodynamic calculations, dolomite is supersaturated in many of the high pH spring waters (see Fig. 6). If dolomite was not allowed to precipitate in the reaction path modelling, the calculated quantity of calcite increased substantially.

5.2. Possible mobilization of toxic metals in groundwaters during CO_2 sequestration in basalt

The possible mobilization of toxic metals during injection of CO_2 rich water into basalt poses a potential risk for CO_2 sequestration in these rocks. The results presented above illuminate the limits on potential toxic metal mobility stemming from CO_2–basalt interaction. The concentrations of trace metals are very low in the spring waters, with concentrations ranging from 10^{-6} to 10^{-11} mol/kg (see Fig. 9). These concentrations are all below the drinking water guidelines given by the WHO (2006) and the European Community (1998). The degree to which measured spring water trace metal concentrations correspond to those generated from model calculations depends on the identity of the metal and are shown in Fig. 9. Barium spring water concentrations closely match those of model calculations at pH < 9. At this pH, aqueous Ba concentrations in the model calculations are controlled by witherite solubility. At higher pH, the modelled aqueous Ba concentration decreases rapidly with increasing pH due to heulandite precipitation. This decrease is not, however, reflected in the spring water concentration, and may be an artefact of the chemical composition of the heulandite present in the thermodynamic database. Spring water Co concentrations are significantly greater than their modelled counterparts. As Co concentrations in the model calculations are controlled by $CoFe_2O_4$ precipitation and the observation that the Hekla spring waters are highly supersaturated with respect to this phase it seems likely that $CoFe_2O_4$ does not precipitate in the natural system. Cobalt could, however, be incorporated in oxyhydroxides (as $Co(OH)_3$), as suggested by Marini et al. (2001). The modelled concentrations of Fe for the reduced conditions closely match those of the spring samples. In the reduced model calculation, Fe is controlled by hematite solubility. According to Stefánsson and Gislason (2001), surface waters in Iceland are close to saturation with amorphous FeOOH. Arnalds et al. (1995) identified three clay size phases in Icelandic soils: allophone, imogolite and poorly crystalline ferrihydrite. These phases are mostly amorphous to *X*-rays. In the model calculations, hematite appears in this calculation rather than either amorphous FeOOH or ferrihydrate because hematite is more stable. The corresponding calculation for the oxidized environment yields estimates of Fe and Mn concentrations that are far below those measured in the spring waters. This suggests that the redox state of the Hekla area groundwater is somewhat reduced and buffered by Fe(II) in the volcanic glass. Spring water Cu, Cd, Zn, Pb and Sr concentrations are far less than those estimated from the reaction path calculations, yet the calculations suggest that all Cu, Cd, Zn, Pb and Sr bearing solid phases are undersaturated except for hydrozincite at pH > 8.0. The reason for the large difference between certain trace metals in the model calculations and the spring water concentrations may stem from the adsorption of these metals on the surface of the precipitated secondary phases; such adsorption is not accounted for in the model. Iron(III) and Al(III) oxides are often used as coagulants in water and soil treatments because of their scavenging properties (Stumm and Morgan, 1996; Jackson and Bistricki, 1995; Kumpiene et al., 2008; Fatoki and Ogunfowokan, 2002). They readily scavenge metals like Cr, Ni, Cd, Mn, Zn and to a lesser extent Cu and As. The degree of scavenging normally increases with increasing pH (Fatoki and Ogunfowokan, 2002). Strontium is known to co-precipitate with aragonite, but thermodynamic data for the solid-solution of orthorhombic carbonates is not present in the model. The large

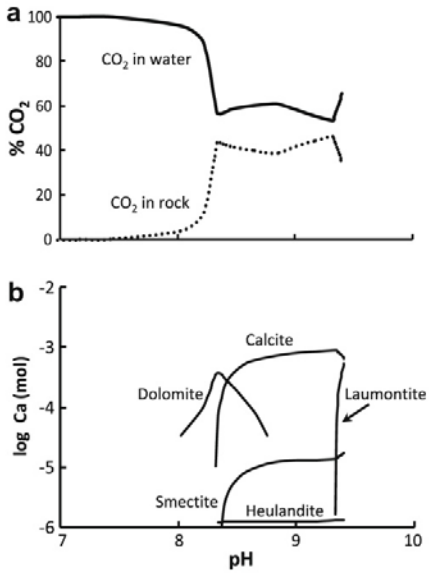

Fig. 10. (a) The distribution of inorganic C in the system between the aqueous and solid phase during the reaction path modelling. (b) The distribution of Ca^{2+} among secondary minerals forming during reaction path modelling.

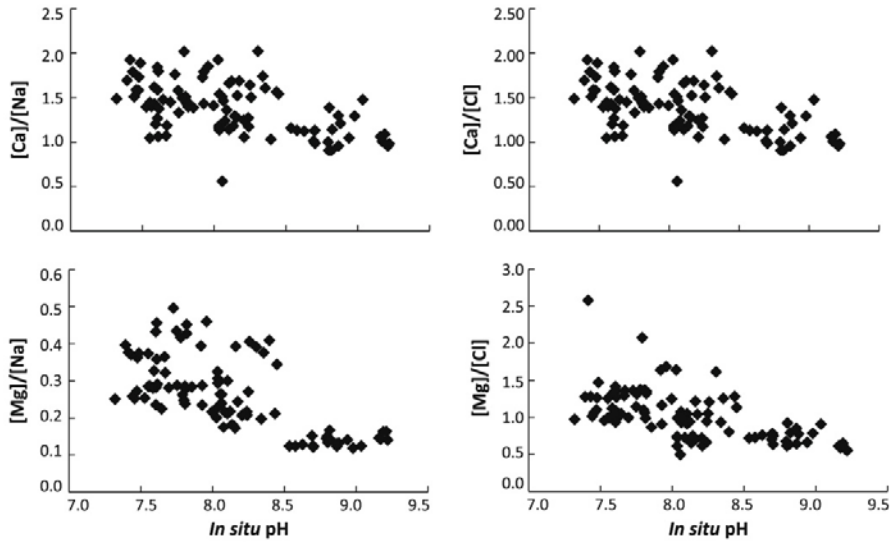

Fig. 11. Spring water Ca/Na, Mg/Na, Ca/Cl and Mg/Cl concentration ratios plotted as a function of *in situ* pH.

differences between measured and modelled trace metal concentrations illustrate the current limitations in quantifying trace element mobility using currently available thermodynamic databases.

5.3. CO_2 fixation in the Mt. Hekla ground water system

The variation of spring water DIC concentrations with pH, as illustrated in Fig. 3b, suggests that basalt–fluid interaction can fix dissolved CO_2 as carbonate minerals. Further insight into this process can be gained through the aid of Fig. 10. Fig. 10a shows the relative amount of C in the aqueous versus secondary minerals according to the model calculation, as a function of pH. At low pH, all C is present in the aqueous phase. When pH exceeds 7.7, dolomite precipitates fixing CO_2 into the solid phase followed by calcite at pH 8.6. The amount of calcite precipitation increases until pH 9.3 when 43% of all CO_2 is fixed in the solid. This result is roughly consistent with the field data shown in Fig. 4b where a pH increase from 7 to 9 decreases DIC concentration by roughly a factor of three. When the pH increases further in the model calculation, however, calcite dissolves and the amount of CO_2 in the water phase increases. The origin of this high pH behaviour can be deduced by considering Fig. 10b, which shows the distribution of Ca among the precipitated mineral phases. The first Ca-bearing mineral to attain saturation is dolomite followed by calcite, heulandite, smectite and laumontite. Since the amount of Ca consumed by smectite and heulandite formation is relatively small compared to calcite, they do not strongly affect the amount of calcite precipitating. In contrast, laumontite competes with calcite for Ca, limiting CO_2 fixation in the reaction path calculation at pH > 9.3. The consumption of divalent metal cations by carbonate precipitation during fluid–basalt interaction is also suggested by the measured source water compositions. The source water Ca/Na, Mg/Na, Ca/Cl and Mg/Cl concentration ratios are plotted as a function of pH in Fig. 11. Aqueous Ca and Mg concentrations decrease more strongly with pH than Na and Cl, consistent with both the reaction path calculations and the incorporation of these metals in precipitated carbonate minerals.

Further insight into the potential for CO_2 fixation as carbonate minerals in basaltic rocks can be attained by performing similar reaction path calculations for initial fluids containing higher CO_2 pressures. Such calculations have previously been presented by Marini (2007), Gysi and Stefánsson (2008).

6. Conclusions

The results presented above illuminate the fate of both CO_2 and dissolved metals during the interaction of CO_2-rich rainwater and basaltic rocks. The major conclusions of this study include:

1. Results indicate that the neutralization of CO_2-rich waters by their interactions with basalt in the subsurface may provide an effective means to fix CO_2 as carbonate minerals. This process proceeds by the combination of Ca and Mg liberated to solution through basalt dissolution driven by dissolved CO_2 to form calcite and perhaps dolomite. This process may be limited, however, by competition for dissolved Ca between precipitating carbonates and Ca-bearing aluminosilicate secondary phases such as zeolites and smectites.
2. Toxic metal mobility is limited during the movement of CO_2-rich water through basaltic rock. Reaction path calculations suggest that although these metals may be liberated by the initial dissolution of basalt in acidic CO_2 rich waters, these metals are incorporated, at least partly, in precipitating carbonates and Fe(III) (oxy)hydroxides as the fluid phase is neutralized by further basalt dissolution.

Acknowledgements

We thank Luigi Marini and Stefano Caliro for constructive reviews that led to significant improvements of the manuscript. We are grateful to many friends and colleagues for their help. Specifically we would like to thank Guðmundur B. Ingvarsson for helpful discussions and Rósa Ólafsdóttir for assisting with GIS. We would also like to thank the Carb-Fix consortium; Wallace S. Broecker, Juerg M. Matter, Hólmfriður Sigurðardóttir, Andri Stefánsson, Domenik Wolff-Boenisch, Einar Gunnlaugsson, Grímur Björnsson, Alexander Gysi, Edda Sif Aradóttir, Gabrielle J. Stockmann, Helgi Arnar Alfredsson and Snorri Gudbrandsson. This study was supported by The Nordic Volcanological Institute Fellowship, the

Science Institute of the University of Iceland and the MIN-GRO Research and Training Network (MRTN-CT-2006-035488).

Appendix A. Supplementary data

Supplementary data associated with this article can be found, in the online version, at doi:10.1016/j.apgeochem.2008.12.031.

References

Aiuppa, A., Allard, P., D'Alessandro, W., Michel, A., Parello, F., Treuil, M., Valenza, M., 2000. Mobility and fluxes of major, minor and trace metals during basalt weathering and groundwater transport at Mt. Etna volcano (Sicily). Geochim. Cosmochim. Acta 64, 1827–1841.

Aiuppa, A., Caleca, A., Federico, C., Gurrieri, S., Valenza, M., 2004. Diffuse degassing of carbon dioxide at Somma-Vesuvius volcanic complex (southern Italy) and its relation to regional tectonics. J. Volc. Geothermal Res. 133, 55–79.

Allard, P., Carbonelle, J., Dajlevic, D., Le Bronec, J., Morel, P., Robe, M.C., Maurenas, J.M., Faivre-Pierret, R., Martin, D., Sabroux, J.C., Zettwoog, P., 1991. Eruptive and diffusive emissions of CO_2 from Mount Etna. Nature 351, 387–391.

Arnalds, O., Hallmark, C.T., Wilding, L.P., 1995. Andisols from four different regions of Iceland. Soil. Sci. Soc. Am. J. 59, 161–169.

Árnason, B., 1976. Groundwater systems in Iceland traced by deuterium. Reykjavík, Societas Scientarium Islandica.

Brady, P.V., Gislason, S.R., 1997. Seafloor weathering controls on atmospheric CO_2 and global climate. Geochim. Cosmochim. Acta 61, 965–973.

Craig, H., 1961. Isotopic variations in meteoric waters. Science 133, 1702–1703.

European Community, 1998. Council directive 98/83 Official Journal of the European Community.

Fatoki, O.D., Ogunfowokan, A.O., 2002. Effect of coagulant treatment on the metal composition of raw water. Water SA 28, 293–298.

Federico, C., Aiuppa, A., Bellomo, S., Jean-Baptiste, P., Parello, Valenza M., 2002. Magma-derived gas influx and water–rock interactions in the volcanic aquifer of Mt. Vesuvius, Italy. Geochim. Cosmochim. Acta 66, 963–981.

Flaathen, T.K., Gislason, S.R., 2007. The effect of volcanic eruptions on the chemistry of surface waters: the 1991 and 2000 eruptions of Mt. Hekla, Iceland. J. Volc. Geothermal Res. 164, 293–316.

Gaillardet, J., Dupré, B., Allègre, C.J., 1999. Global silicate weathering and CO_2 consumption rates deduced from the chemistry of large rivers. Chem. Geol 159, 3–30.

Gislason, S.R., Arnórsson, S., 1990. Saturation state of natural waters in Iceland relative to primary and secondary minerals in basalts I. In: Spencer, R.J., I-Ming Chou (Eds.), Fluid–Mineral Interactions: a Tribute to H.P. Eugster. Geochemical Society, Special Publication No. 2, pp. 373–393.

Gislason, S.R., Arnórsson, S., 1993. Dissolution of primary basaltic minerals in natural waters: saturation state and kinetics. Chem. Geol. 105, 117–135.

Gislason, S.R., Oelkers, E., 2003. Mechanism, rates, and consequences of basaltic glass dissolution: II. An experimental study of the dissolution rates of basaltic glass as a function of pH and temperature. Geochim. Cosmochim. Acta 67, 3817–3832.

Gislason, S.R., Andrésdóttir, A., Sveinbjörnsdóttir, Á.E., Óskarsson, N., Thordarson, Th., Torssander, P., Novăk, M., Zăk, K., 1992. Local effects of volcanoes on the hydrosphere: example from Hekla, southern Iceland. In: Kharaka, Y.K., Maest, A.S. (Eds.), Water–Rock Interaction. Balkerna, Rotterdam, pp. 477–480.

Gislason, S.R., Arnórsson, S., Ármannsson, H., 1996. Chemical weathering of basalt in southwest Iceland: effect of runoff, age of rocks and vegetative/glacial cover. Am. J. Sci. 296, 837–907.

Gislason, S.R., Gunnlaugsson, E., Broeker, W.S., Oelkers, E.H., Matter, J.M., Stefánsson, A., Arnórsson, S., Björnsson, G., Fridriksson, T., Lackner, K., 2007. Permanent CO_2 sequestration into basalt: the Hellisheidi, Iceland project. Geophys. Res. Abstr. 9, 07153.

Gislason, S.R., Snorrason, Á., Eiríksdóttir, E.S., Sigfússon, B., Elefsen, S.O., Harðardóttir, J., Gunnarsson, Á., Torssander, P., 2003. Chemical composition, discharge and suspended material in rivers in South-Iceland, VI. Database of Science Institute and National Energy Authority. Science Institute, RH-03-2003 (in Icelandic).

Gislason, S.R., Stefánsdóttir, Á., Eiríksdóttir, E.S., 2000. ARCTIS, Regional Investigation of Arctic Snow Chemistry: Results from the Icelandic Expeditions, 1997–1999. Raunvisindastofnun, RH-05-2000.

Gislason, S.R., Veblen, D.R., Livi, K.J.T., 1993. Experimental meteoric water–basalt interactions: characterization and interpretation of alteration products. Geochim. Cosmochim. Acta 57, 1459–1471.

Gronvold, K., Larsen, G., Einarsson, P., Thorarinsson, S., Saemundsson, K., 1983. The Hekla eruption 1980–1981. Bull. Volcanol 46, 349–363.

Gudmundsson, A., Oskarsson, N., Gronvold, K., Saemundsson, K., Sigurdsson, O., Stefansson, R., Gislason, S.R., Einarsson, P., Brandsdottir, B., Larsen, G., Johannesson, H., Thordarson, T., 1992. The 1991 eruption of Hekla, Iceland. Bull. Volcanol. 54, 238–246.

Gysi, A.P., Stefánsson, A., 2008. Nomerical modelling of CO_2–water–basalt interaction. Mineral. Mag. 72, 55–59.

Intergovernmental Panel on Climate Change, 2005. Carbon dioxide capture and storage. Cambridge University Press, New York.

Jackson, A.J., Bistricki, T., 1995. Selective scavenging of copper, zinc, lead and arsenic by iron and manganese oxyhydroxide coatings on plankton in lakes polluted with mine and smelter wastes: results of energy dispersive X-ray micro-analysis. J. Geochem. Explor. 52, 97–125.

Kjartansson, G., 1957. Some secondary effects of the Hekla eruption. Exhalations of carbon dioxide, contamination of ground-water and lowering of water table. In: Einarsson, T., Kjartansson, G., Þorarinsson, S. (Eds.), The Eruption of Hekla 1947–1948 III. Societas Scientarum Islendica.

Kristmannsdóttir, H., 1982. Alteration in the IRDP Drill Hole compared with other drill holes in Iceland. J. Geophys. Res. 87, 6525–6531.

Kumpiene, J., Lagerkvist, A., Maurice, C., 2008. Stabilization of As, Cr, Cu, Pb and Zn in soil using amendments – a review. Waste Manage. 28, 215–225.

Marini, L., 2007. Geological Sequestration of Carbon-dioxide: Thermodynamics, Kinetics and Reaction Path Modeling. Elsevier, Amsterdam.

Marini, L., Canepa, M., Cipolli, F., Ottonello, G., Zuccolini, M.V., 2001. Use of stream sediment chemistry to predict trace element chemistry of groundwater. A case study from the Bisagno valley (Genoa, Italy). J. Hydrol. 241, 194–220.

Matter, J.M., Takahashi, T., Goldberg, D., 2007. Experimental evaluation of in situ CO_2–water–rock reactions during CO_2 injection in basaltic rocks: implications for geological CO_2 sequestration. Geochem. Geophys. Geosys. 8, doi: 10.1029/2006GC001427.

McGrail, B.P., Schaef, H.T., Ho, A.M., Chien, Y.J., Dooley, J., 2006. Potential for carbon dioxide sequestration in flood basalts. J. Geophys. Res. 111, B12201. doi:10.1029/2005JB004169.

Mehegan, J.M., Robinson, P.T., Delaney, J.R., 1982. Secondary mineralization and hydrothermal alteration in the Reydarfjordur drill core, Eastern Iceland. J. Geophys. Res. 87, 6511–6524.

Moune, S., Gauthier, P-J., Gislason, S.R., Sigmarsson, O., 2006. Trace elements degassing and enrichment in the eruptive plume of the 2000 eruption of Hekla volcano, Iceland. Geochim. Cosmochim. Acta 70, 461–479.

Neuhoff, P.S., Fridriksson, T., Arnórsson, S., Bird, D.K., 1999. Porosity evolution and mineral paragenesis during low-grade metamorphism of basaltic lavas at Teighathorn, Eastern Iceland. Am. J. Sci. 299, 467–501.

Oelkers, E.H., Cole, D.R., 2008. Carbon dioxide sequestration: a solution to a global problem. Elements 4, 305–310.

Oelkers, E.H., Schott, J., 2005. Geochemical Aspects of CO_2 sequestration. Chem. Geol. 217, 183–186.

Oelkers, E.H., Gislason, S.R., Matter, J., 2008. Mineral carbonation of CO_2. Elements 4, 333–337.

Parkhurst, D.L., Appelo, C.A.J., 1999. User's guide to PHREEQC (Version 2) – A computer program for speciation, batch-reaction, one-dimensional transport, and inverse geochemical calculations. U.S. Geol. Surv. Water Invest. Rep. 99-4259.

Rogers, K.L., Neuhoff, P.S., Pedersen, A.K., Bird, D.K., 2006. CO_2 metasomatism in a basalt hosted petroleum reservoir, Nuussuaq, West Greenland. Lithos 92, 55–82.

Sigvaldason, G.E., 1974. The eruption of Hekla 19471948. The pertrology of Hekla and origin of silicic rocks in Iceland. In: Einarsson, T., Kjartansson, G., Þorarinsson, S. (Eds.), The Eruption of Hekla 1947-1948 V. Societas Scientiarum Islandica.

Stefánsson, A., Gislason, S.R., 2001. Chemical weathering of basalts, southwest Iceland: effect of rock crystallinity and secondary minerals on chemical fluxes to the ocean. Am. J. Sci. 301, 513–556.

Stumm, W., Morgan, J.J., 1996. Aquatic Chemistry, Chemical Equilibria and Rates in Natural Waters. Wiley. Interscience publication, New York.

Walker, J.C.G., Hays, P.B., 1981. A negative feedback mechanism for the long-term stabilization of Earth's surface temperature. J. Geophys. Res. 86, 9776–9782.

WHO, 2006. Guidelines for Drinking-water Quality, 3rd ed., incorporating first addendum.

Wolff-Boenisch, D., Gislason, S.R., Oelkers, E.H., 2006. The effect of crystallinity on dissolution rates and CO_2 consumption capacity of silicates. Geochim. Cosmochim. Acta 70, 858–870.

Wolff-Boenisch, D., Gislason, S.R., Oelkers, E.H., Putnis, C.V., 2004. The dissolution rates of natural glasses as a function of their composition at pH 4 and 10.6, and temperatures from 25 to 74 °C. Geochim. Cosmochim. Acta 68, 4843–4858.

Chapter 4

Can sulphate enhance CO_2 mineralization in basalt? An experimental study of the effect of aqueous sulphate on basaltic glass dissolution rates

Flaathen, T.K., Oelkers, E.H., Gislason, S.R. (To be submitted to Geochimica et Cosmoschimica Acta).

4.1 Abstract

Steady-state dissolution rates of basaltic glass were measured in mixed-flow reactors at 50 °C and 3 < pH < 10 in HCl-NaCl-NH_4OH bearing solutions having an ionic strength of 0.01 M, or higher, as a function of aqueous sulphate concentration. Sulphate was added to reactive aqueous solutions in the form of Na_2SO_4. Measured dissolution rates increase with increased sulphate concentration in acid conditions, but no effect was found in basic conditions. At pH 5, the presence of 0.01 mol/kg sulphate doubled the dissolution rate while 0.05 mol/kg of sulphate triples the dissolution rate compared to that measured in sulphate-free solutions. This rate increase is found to be consistent with rates calculated using an equation previously proposed by Gislason and Oelkers (2003). Since the release of divalent cations is thought to be the rate limiting step for CO_2 mineralization in basalt, adding sulphate to the injected CO_2 might enhance the carbonization process in this rock.

4.2 Introduction

The concentration of CO_2 in the atmosphere has increased from ~280 ppm by volume at pre-industrial time to ~385 ppm today. Much of this increase is due to the combustion of fossil fuels which emits an estimated 29 Gt CO_2 annually into the Earth's atmosphere (Taylor, 1991; Manabe and Stouffer, 1993; Houghton et al., 1995; Retallack, 2002; ICPP, 2005; 2007; Broecker, 2008; Oelkers and Cole., 2008). A large current effort is being made to identify and optimize CO_2 sequestration technologies to address the potential dangers, such as global

warming and sea level rise, associated with increased atmospheric CO_2 content (Hitchon et al., 1999; Bachu and Adams, 2003; Arts et al., 2004; Chadwick et al., 2004; Emberley et al., 2004; IPCC, 2005; Oelkers and Schott, 2005; McGrail et al., 2006; Bachu et al., 2007; Marini, 2007; Matter et al., 2007; Oelkers and Cole, 2008; Broecker, 2008; Kelemen and Matter, 2008; Cantucci et al., 2009; Iding and Ringrose, 2009; Kharaka et al., 2009; Li et al., 2006; Audigane et al., 2007; Benson and Cole, 2008; Gislason et al., 2009; Hermanrud et al., 2009; Kharaka et al., 2009; Matter et al., 2009; Michael, et al., 2009; Schaef and McGrail, 2009; Stenhouse et al., 2009; Schaef et al., 2009). To reduce the emission of this greenhouse gas to the atmosphere, the possibility of sequester CO_2 in basaltic rocks is being investigated (McGrail et al., 2006; Gislason et al., 2009; Marini, 2007; Matter et al., 2007; Goldberg et al., 2008; Oelkers et al., 2008). This process involves dissolution of the basaltic rock and release of divalent metal cations such as Ca^{2+}, Mg^{2+} and Fe^{2+}. These ions then react with dissolved CO_2 and precipitate as carbonate minerals. The rate limiting step for this reaction is thought to be the release of divalent cations. As basalts are dominated by basaltic glass the release of divalent metals from basalt is closely related to the dissolution rates of this glass. Like all natural glasses, basaltic glasses are a mixture of oxides; basaltic glasses contain ~12% CaO, 10% FeO, and 9% MgO (Oelkers and Gislason, 2001). The mechanism and equations describing the rates of basaltic glass dissolution were reported by Oelkers and Gislason (2001) and Gislason and Oelkers (2003). These studies concluded that the rate limiting step for basaltic glass dissolution is the breaking of Si-O bonds when adjacent Al atoms had been removed from the glass structure. In accord with this equation, the logarithm of far-from-equilibrium basaltic glass dissolution rates were found to be proportional to the logarithm of the Al^{3+} activity of the reactive aqueous solution. Any process that lowers reactive fluid Al^{3+} activity including the presence of aqueous species that leads to Al-complex formation, will increase basaltic glass dissolution rates (c.f. Wolff-Boenisch et al., 2004.).

An application of the quantification of the effect of aqueous sulphate on mineral dissolution rates is that power plants emitting CO_2 often produce sulphuric gases as a byproduct. The high reactivity and oxidation capacity of sulphuric species make them difficult to store on land. By adding sulphate to the injected CO_2 solution, it may be possible to store the sulphate safely

underground. The purpose of this study was to investigate how much sulphate affects the dissolution rate of basaltic glass at subsurface conditions.

4.3 Theoretical background

The standard state adopted in this study is that of unit activity of pure minerals and H_2O at any temperature and pressure. For aqueous species other than H_2O, the standard state is unit activity of species in a hypothetical 1 molal solution referenced to infinite dilution at any temperature and pressure. The computer code PHREEQC (Parkhurst and Apello, 1999) was used to calculate aqueous activities and chemical affinities in the present study.

The quantification of the dissolution rate of a glass or mineral can be challenging because there are two distinct surface reactions that can affect rate variations with solution composition: 1) the inverse reaction, or the tendency to reprecipitate a solid as equilibrium is approached, and 2) the reaction forming the rate controlling precursor complex. Aagaard and Helgeson (1977; 1982), Lasaga (1981), Helgeson et al. (1984), Murphy and Helgeson (1987) and Oelkers (2001) quantified the effect of inverse reaction in terms of chemical affinity of the dissolving phase leading to an equation of the form

$$r = r_{+} (1 - \exp (-A^* / \sigma RT)), \quad (1)$$

where r designates the overall and r_{+} designates the forward dissolution rate, A^* refers to the chemical affinity for the solid surface layer hydrolyses reaction, which may differ from that of the bulk solid, σ stands for Temkin's average stoichiometric number equal to the ratio of the rate of destruction of the activated or precursor complex relative to the overall rate, R designates the gas constant and T represents the absolute temperature.

Dissolution of basaltic glass can be thought of as a two stage process. The first process involves the rapid removal of alkali and alkaline-earth metals, and the second process is the destruction of the tetrahedrally coordinated layer comprising Si, Al and Fe(III). The alkali and alkaline-earth metals, commonly referred to as modifying elements, are quickly removed from the basaltic glass surface through metal/proton exchange reactions (Thomassin and Touray, 1979; Berger et al., 1987; Guy and Schott, 1989; Crovisier et al., 1990). The removal of these

metals leads to a leached surface layer which consists of Si, Al and Fe(III). The thickness of this leached layer grows with time until the diffusion rate of the glass modifying elements through the leached surface layer is equal to the dissolution rate of the leached layer itself, which means that the long term dissolution rate is stoichiometric (Gíslason and Eugster, 1987; Crovisier et al., 1992). Basaltic glass reaches stoichiometric dissolution within several hours at acid, neutral and alkaline conditions (Guy and Schott, 1989; Crovisier et al., 1990; Gislason and Oelkers, 2003).

The metals comprising the leached layer are generally those found in tetrahedral coordination and have the same molar ratio as that of the glass; 1:0.36:0.02 for Si:Al:Fe(III), respectively. The role of Fe(III) on basaltic glass dissolution is not considered in the present study because of its low concentration in the leached layer and difficulties controlling Fe(III) concentration in solutions containing aqueous Fe(II) originating from glass dissolution.

Taking account of these observations, Daux et al. (1997), Oelkers and Gislason (2001) and Gislason and Oelkers (2003) concluded that the final and rate limiting step of basaltic glass dissolution is the destruction of this leached layer. The hydrolysis of this surface layer (in the absence of Fe(III)) can be expressed as

$$SiAl_{0.36}O_2(OH)_{1.08} + 1.08H^+ = SiO_2 + 0.36Al^{3+} + 1.08H_2O \quad (2)$$

Equilibrium constants for this reaction (K_2) were estimated by Bourcier et al. (1990) from the stoichiometrically weighted sum of the amorphous silica and gibbsite hydrolysis reactions. The chemical affinity of the surface layer hydrolysis reaction is thus given by

$$A^* = -RT\frac{Q_2}{K_2} = -RT\frac{a_{SiO_2}\, a_{Al^{3+}}^{0.36}}{K_2 a_{H^+}^{1.08}} \quad (3)$$

where Q_2 refers to the reaction quotient of reaction (2), and a_i designates the activity of the subscripted aqueous species. All basaltic glass dissolution experiments in this study were

performed at far from equilibrium conditions, which enable determination of the effect of activated or precursor complex formation reaction on rates independently of those stemming from the inverse reaction. According to Eqn. (1), the overall rates (r) equal forward rates (r_+) when $A^* >> \sigma RT$. As one approaches equilibrium, overall rates (r) decrease systematically and are equal to zero at equilibrium with the surface, where $A^* = 0$.

Similar to the dissolution of a number of aluminosilicate minerals (e.g. the alkali feldspars, Oelkers et al., 1994; Gautier et al., 1994), the dissolution of the Al-Si framework is proportional to the concentration of partially detached Si tetrehedra at the near surface. These partially detached Si are formed from the removal of adjacent Al atoms in accord with

$$3(\text{=Si-O-Al}) + 3H^+ = 3(\text{=Si-O-H}) + Al^{3+} \quad (4)$$

The law of mass action for reaction (4) is given by

$$K_4 = \frac{a_{Al^{3+}} X^3_{-Si-O-H}}{a^3_{H^+} X^3_{-Si-O-Al}} \quad (5)$$

where K_4 corresponds to the equilibrium constant of reaction (4) and X_i is the mole fraction of the subscripted surface species. Taking account of conservation of sites ($X_{\text{-Si-O-H}} + X_{\text{-Si-O-Al}} = 1$) it follows that when the basaltic glass surface still contains substantial Al,

$$X_{-Si-O-H} = \left(K_4 \frac{a^3_{H^+}}{a_{Al^{3+}}} \right)^{\frac{1}{3}} \quad (6)$$

and because r_+ is proportional to the concentration of =Si-O-H at groups at the surface (Gislason and Oelkers 2003):

$$r_+ = k_+ K_4^{1/3} \left(\frac{a_{H^+}^3}{a_{Al^{3+}}} \right)^{1/3} = k_+^{'} \left(\frac{a_{H^+}^3}{a_{Al^{3+}}} \right)^{1/3} \quad (7)$$

where r_+ again signifies the steady-state basaltic glass dissolution rate at far-from-equilibrium conditions, and k_+ refers to a rate constant calculated from Gislason and Oelkers (2003). Eqn. (7) suggests that decreasing the activity of Al^{3+} in the aqueous reactive solution increases far from equilibrium basaltic glass dissolution rates. A study performed by Wolff-Boenisch et al., (2004) showed that the dissolution rates of basaltic glass can be increased by an order of magnitude or more by complexing aqueous Al^{3+} ions with fluorine. Similarly Oelkers and Gislason (2001) observed a similar effect of the presence of aqueous oxalate on basaltic glass dissolution rates.

4.3.1 Aqueous sulphate speciation

Sulphate is an anion which can complex aluminum, forming aluminum-sulphate by the reactions:

$$Al^{3+} + SO_4^{2-} = Al(SO_4)^+ \quad (8)$$

$$Al^{3+} + 2SO_4^{2-} = Al(SO_4)_2^- \quad (9)$$

Figure 4.1 shows the aluminum speciation in a solution containing 0.1 M Na_2SO_4 and 10^{-6} M Al as a function of pH. The curves shown in this figure were calculated using PHREEQC (Parkhurst and Appelo, 1999). Aqueous sulphate only affects Al^{3+} speciation at $1 < pH < 6$. At highly acid conditions ($pH < 1.5$), Al^{3+} is the most common aluminum species in the solution.

Between pH 1.5 and 5, the aluminum-sulphate complexes, $Al(SO_4)_2^-$ and $Al(SO_4)^+$, are the most common species, while at higher pH, aluminum hydroxide complexes dominate the solution.

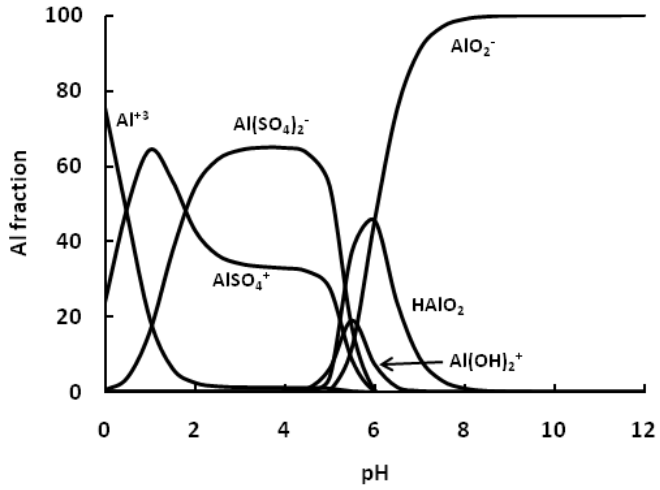

Figure 4.1 Distribution of aqueous Al in mole fraction units of an aqueous solution containing 0.1 M Na_2SO_4 and 10^{-6} M Al at 50 °C. Calculations performed using PHREEQC (Parkhurst and Appelo, 1999).

As basaltic glass dissolution rates increase with decreased aqueous Al^{3+} activity the dissolution rate should increase when sulphate is present in acid solutions. A calculation of the dissolution rate of the basaltic glass at these conditions can be seen in Figure 4.2, where an increase in the dissolution rate is predicted to occur between pH 1.5 and 6.

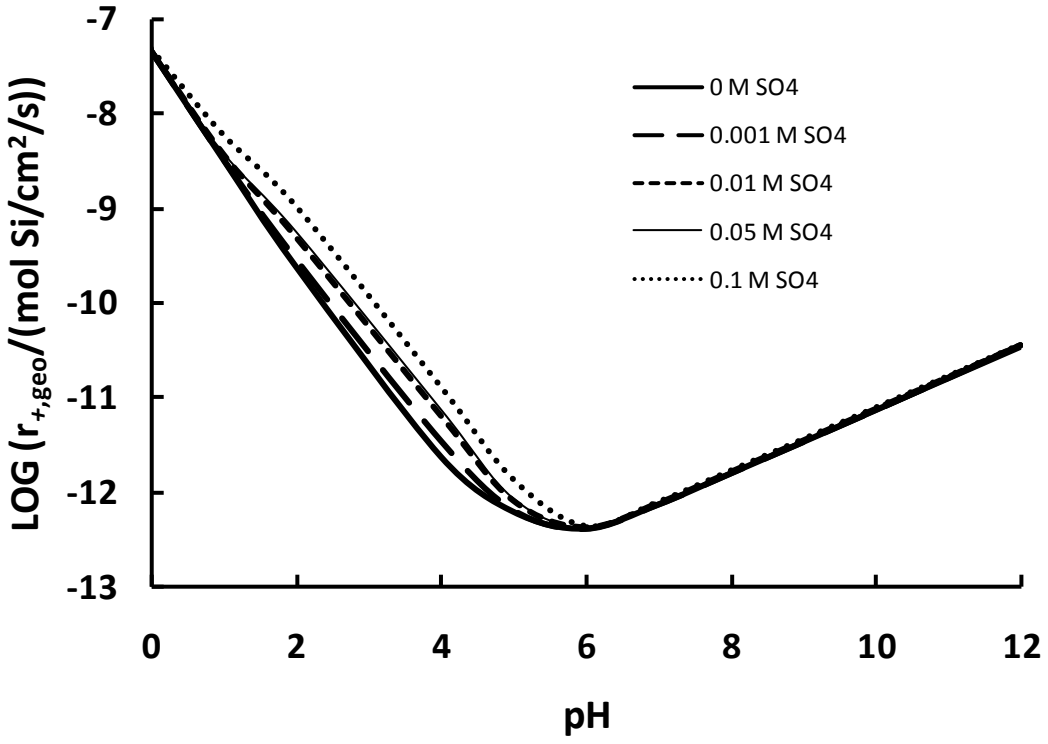

Figure 4.2 The logarithm of the dissolution rate vs. pH for basaltic glass at 50 °C in the system Na-Cl-H-OH-SO_4 in 0.1 m NaCl solutions and the indicated fixed concentration of SO_4, added to solution as Na_2SO_4 calculated using Eqn. (7). The aqueous activities used in this calculation were estimated using PHREEQC (Parkhurst and Appelo, 1999).

4.4 Materials and methods

The dissolution rate experiments were performed with Stapafell basaltic glass collected from a volcanic ash located at Stapafell Mountain, southwestern Iceland. This basaltic glass has been studied previously (Gislason and Oelkers, 2003; Oelkers and Gislason, 2001) and its chemical composition is consistent with $Na_{0.08}Ca_{0.263}Mg_{0.281}Fe_{0.188}Al_{0.358}SiO_{3.32}$ (Gislason and Oelkers, 2003). To obtain the 125-250 μm size fraction, the collected glass was ground and sieved after drying. This fraction was cleaned ultrasonically using first deionized water, then acetone to remove fine particles. The resulting basaltic glass powder was subsequently dried overnight at 110° C. The surface area, as determined using a three point BET method (Quantachrome Autosorb-1) using N_2 gas, was determined to be 1.524 m^2/g. The precision of the

measurements was ± 10%. The geometric surface area was estimated to be 106 cm^2/g assuming that the glass powder used comprised identical 187.5 µm cubes (c.f. Gislason and Oelkers, 2003).

Images of the basaltic glass powder were taken before and after dissolution rate experiments using a JEOL 6360 LV Scanning Electron Microscope (SEM). Figure 4.3 a) and b) shows the powder before experiments on a large and small scale, respectively. On a large scale, the basaltic glass appears to be smooth and free from fine particles. On a small scale, surface roughness is apparent. This roughness might help explain the big difference in BET and geometric surface area. After dissolution experiments (images c and d), there was no visible evidence of dissolution of the glass nor were any secondary minerals evident.

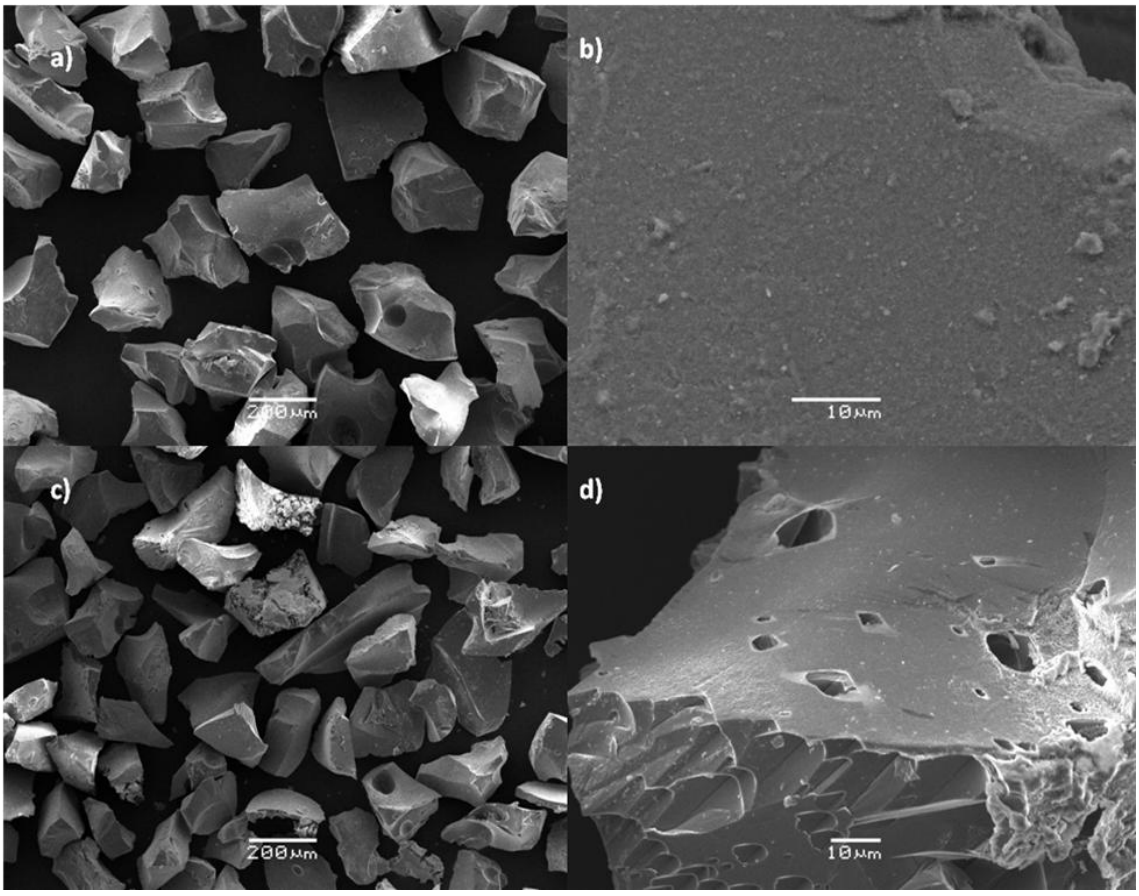

Figure 4.3. Scanning electron microscope images of the basaltic glass powder used in the present study. Images a) and b) are of the initial glass before the dissolution experiments. Image b) is an enlargement of

image a) showing fine scale surface roughness. Image c) and d) shows the glass after its dissolution in experiment in run BG 7 A.

All experiments were performed in titanium or polypropylene mixed flow reactor systems at selected pH and with solutions containing fixed amounts of aqueous sulphate. Such reactors have been used successfully in the determination of the dissolution rates of a large number of rock forming minerals and glasses (e.g Berger et al., 1994; Harouiya and Oelkers, 2004; Saldi et al., 2007, Chairat et al., 2007). All experiments were carried out at 50 ± 2 °C. For experiments performed in titanium reactors, a High Precision/High Pressure Liquid Chromatography Pump provided continuous fluid flow ranging from 0.1 to 10 g/min during the experiments. The precision of the fluid flow rates was ± 4 percent. The volume of the titanium reactor was 250 mL. The solution within the reactor was stirred by a Parr magnetically driven stirrer, the temperature controlled by a Parr controlled furnace, and elevated pressure was maintained using a back pressure regulator.

The volume of the polypropylene reactors used for the experiments were 30 mL and they were continuously stirred with floating Teflon stirring bars. These reactors were immersed in a water bath held at a constant temperature ± 2 °C. The fluid was injected using a Gilson peristaltic pump, which allows fluid flow rates from 0.01-10 g/min. The solution left the reactor through a 2.5 µm filter. No additional filtering was performed on outlet fluid sampled obtained from either reactor before chemical analysis.

Each experimental series comprised a sequence of experiments performed on a single basaltic glass powder. At the onset of each experimental series, the reactors were filled with glass powder and the inlet solution. The flow rate was held constant until the outlet solution contained a steady state Si concentration. Steady-state dissolution rates were obtained after 3-10 days depending on pH and flow rate. After steady state was verified with a minimum of three constant Si concentrations in the outlet fluid samples obtained over several residence times[1], inlet fluid composition, and/or fluid flow rate were changed to the next desired experimental condition.

Inlet fluids used in these experiments comprised demineralised H_2O, NaCl (99.5%) and Na_2SO_4 (99%) from Fluka, HCl from Merck, Prolabo rectopur NH_4Cl and Fluka BioUltra

[1] The residence time is defined as the volume of the reactor divided by the reactive fluid flow rate.

NH_4OH. Basic inlet solutions were bubbled with N_2 prior to their use in an attempt to minimize the dissolved CO_2 concentration. The compositions of all inlet solutions used in this study are listed in Table 4.1.

Table 4.1 Composition of the inlet fluids for all experiments performed in this study.

Experiment	pH (25°C)	SO_4 (mol/kg)	HCl (mol/kg)	NaCl (mol/kg)	NH_4Cl (mol/kg)	NH_4OH (mol/kg)
BG 6 D	3.06		9.44E-04	8.90E-03		
BG 7 A	2.85	1.00E-03	1.31E-03	8.00E-03		
BG 9 A	2.99	1.00E-02	1.43E-03			
BG 7 C	3.00	5.00E-02	2.45E-03			
BG 7 D	3.02	1.00E-01	3.32E-03			
BG 6 A	3.95		9.46E-05	9.89E-03		
BG 6 B	3.99	1.00E-03	1.03E-04	8.00E-03		
BG 6 C	4.04	1.00E-02	1.35E-04			
BG 6 E	4.01	5.00E-02	2.41E-04			
BG 6 F	3.96	1.00E-01	4.16E-04			
BG 17 E	5.02		9.80E-06	1.00E-02		
BG 8 F	5.03	1.00E-03	8.00E-06	8.00E-03		
BG 8 C	5.01	1.00E-02	1.40E-05			
BG 8 D	5.05	5.00E-02	2.20E-05			
BG 8 E	5.01	1.00E-01	3.10E-05			
BG 17 F	6.02	5.00E-02			1.00E-02	1.00E-05
BG 17 G	8.01	1.00E-01			1.01E-02	1.20E-05
BG 15 F	8.01				9.51E-03	4.40E-04
BG 15 A	8.07				9.51E-03	4.18E-04
BG 17 D	7.97				9.51E-03	4.00E-04
BG 15 B	8.07	1.00E-03			9.51E-03	4.50E-04
BG 15 C	8.04	1.00E-02			9.55E-03	3.80E-04
BG 15 D	8.02	5.00E-02			9.60E-03	3.60E-04
BG 15 E	7.97	1.00E-01			9.63E-03	3.00E-04
BG 14 A	9.01			3.40E-03	6.66E-03	2.94E-03
BG 14 F	8.99			3.40E-03	6.66E-03	2.94E-03
BG 17 A	9.03	1.00E-03		5.04E-04	6.59E-03	3.09E-03
BG 17 B	9.08	1.00E-02			6.76E-03	3.06E-03
BG 14 D	8.99	5.00E-02			7.05E-03	2.08E-03
BG 14 E	9.03	1.00E-01			7.20E-03	2.08E-03
BG 13 A	10.07			8.51E-03	1.44E-03	6.89E-03
BG 17 C	9.98			8.51E-03	1.52E-03	6.53E-03
BG 13 B	10.05	1.00E-03		5.51E-06	1.52E-03	7.50E-03
BG 13 C	10.08	1.00E-02			1.60E-03	7.70E-03
BG 13 E	10.09	5.00E-02			1.80E-03	7.07E-03
BG 13 D	10.07	1.00E-01			1.92E-03	7.35E-03

The silica and aluminum content in the inlet and outlet solutions were determined using the Molybate Blue method (Koroleff, 1976) and atomic absorption spectroscopy (Perkin Elmer

Zeeman 5000), respectively. The reproducibility of chemical analyses were ± 4% for Si and Al concentrations greater than 0.5 and 0.01 ppm, respectively, but of the order of ± 10% at lower concentrations. The pH of the outlet fluid was measured at 23 °C immediately after sampling. Outlet solutions for experiments run at 5 < pH < 9 were supersaturated with respect to gibbsite.

4.5 Results

Steady state dissolution rates (r) were computed from the measured steady-state Si concentration using

$$r = \frac{\Delta[\mathrm{Si}]\,\mathrm{F}}{\mathrm{s}\ \ \mathrm{M}} \qquad (9)$$

where Δ[Si] stands for the concentration difference between the inlet and outlet of silica in solution (mol/kg), F represents the fluid mass flow rate (g/s), s denotes the specific surface area of the initial glass (cm^2/g), and M signifies the initial mass of glass in the reactor (g). Both BET and geometric surface areas were used in these calculations yielding r_{BET} and r_{geo}, respectively. Dissolution rates obtained from all experiments are shown in Table 4.2 together with pH, flow rates, measured inlet and outlet concentrations of Si and Al, and the saturation state of hydrated basaltic glass (*A**, eqn. (1)) and gibbsite. The in-situ pH and saturation states were calculated using PHREEQC (Parkhurst and Appelo, 1999). The only other secondary minerals attaining saturation in these experiments were gibbsite and other Al oxy-hydroxide phases: boehmite, corundum and diaspore. The rates are given in units of moles of Si released per cm^2 of initial basaltic glass surface area per second. The saturation state of the hydrated basaltic glass was for all experiments less than -10 kJ/mole, which indicates that the experiments were performed at far from equilibrium conditions. Since several experiments were performed on the same glass powder, the surface area could potentially change and thereby affect the calculated rates. To make sure this was not the case, all series of runs ended with an experiment using the same conditions as at the beginning of each run. The repeated runs produced rates within ± 20% of that originally measured.

Table 4.2. Results of steady-state dissolution rate experiments as a function of pH and SO_4^{2-}

Experiment	Initial BET surface area (cm^2)	Flow rate (g/min)	Outlet pH (22 °C)	pH (50 °C) (PHREEQC)	Si concentrations			Al concentrations			Dissolution rates (mol/cm^2/s)		Stapafell hydrated basaltic glass (*A**) (kJ/mol)	Gibbsite (kJ/mol)
					Inlet (mol/kg)	Outlet (mol/kg)	ΔSi (mol/kg)	Inlet (mol/kg)	Outlet (mol/kg)	ΔAl (mol/kg)	$r_{+,BET}$	$r_{+,geo}$		
BG 6 D	6854	0.417	3.09	3.09	n.d	5.00E-05	5.00E-05	n.a.	n.a.		5.27E-14	7.54E-12	-24.63	-13.55
BG 7 A	7619	0.397	2.92	2.94	n.d	6.49E-05	6.49E-05	n.a.	n.a.		5.62E-14	8.03E-12	-24.94	-16.34
BG 9 A	7625	0.170	3.08	3.21	n.d	1.27E-04	1.27E-04	5.19E-07	3.14E-05	3.08E-05	5.21E-14	7.45E-12	-21.90	-12.93
BG 7 C	7614	0.371	3.05	3.26	n.d	6.35E-05	6.35E-05	n.a.	n.a.		5.12E-14	7.32E-12	-25.37	-17.26
BG 7 D	6854	0.380	3.08	3.31	n.d	6.39E-05	6.39E-05	n.a.	n.a.		6.08E-14	8.69E-12	-25.55	-17.88
BG 6 A	7631	0.377	4.05	4.05	n.d	8.43E-07	8.43E-07	n.a.	n.a.		1.68E-15	2.40E-13	-33.48	-7.61
BG 6 B	7624	0.401	4.02	4.10	n.d	3.39E-06	3.39E-06	n.a.	n.a.		3.13E-15	4.47E-13	-28.34	-3.71
BG 6 C	7614	0.405	4.05	4.19	n.d	3.96E-06	3.96E-06	5.19E-07	1.25E-06	7.31E-07	3.49E-15	4.99E-13	-28.22	-4.58
BG 6 E	7621	0.354	4.05	4.27	n.d	4.27E-06	4.27E-06	n.a.	n.a.		3.38E-15	4.83E-13	-28.59	-6.19
BG 6 F	7622	0.409	3.95	4.20	n.d	6.31E-06	6.31E-06	n.a.	n.a.		5.46E-15	7.81E-13	-28.09	-7.73
BG 17 E	30506	0.497	5.06	5.04	n.d	1.51E-06	1.51E-06	n.a.	n.a.		3.90E-16	5.58E-14	-26.67	6.99
BG 8 F	7624	0.174	5.13	5.14	n.d	1.04E-06	1.04E-06	n.a.	n.a.		4.03E-16	5.77E-14	-27.84	6.62
BG 8 C	7624	0.178	5.02	5.14	n.d	1.32E-06	1.32E-06	n.a.	n.a.		5.06E-16	7.23E-14	-27.16	6.56
BG 8 D	7625	0.206	5.05	5.25	n.d	2.79E-06	2.79E-06	n.a.	n.a.		1.28E-15	1.83E-13	-24.44	8.17
BG 8 E	7625	0.182	5.06	5.29	n.d	1.57E-06	1.57E-06	n.a.	n.a.		9.45E-16	1.35E-13	-26.79	6.37
BG 17 F	30506	0.501	6.01	5.68	n.d	1.67E-06	1.67E-06	n.a.	n.a.		3.77E-16	5.39E-14	-25.55	9.28
BG 17 G	30506	0.502	5.97	5.72	n.d	1.65E-06	1.65E-06	n.a.	n.a.		3.93E-16	5.63E-14	-25.68	9.10
BG 15 F	30506	0.500	8.01	7.25	9.26E-07	3.96E-06	3.04E-06	n.a.	n.a.		8.30E-16	1.19E-13	-25.43	5.20
BG 15 A	30506	0.498	7.99	7.23	4.63E-07	4.96E-06	4.50E-06	2.78E-08	6.84E-07	6.56E-07	1.22E-15	1.75E-13	-23.95	6.37
BG 17 D	30506	0.495	8.1	7.34	8.90E-07	4.81E-06	3.92E-06	n.a.	n.a.		1.06E-15	1.51E-13	-24.69	5.32
BG 15 B	30506	0.496	8.04	7.28	6.77E-07	4.42E-06	3.74E-06	2.78E-08	8.11E-07	7.83E-07	1.01E-15	1.45E-13	-24.75	5.51
BG 15 C	30506	0.496	8.02	7.26	7.12E-07	3.95E-06	3.24E-06	n.a.	n.a.		8.78E-16	1.26E-13	-25.31	5.07
BG 15 D	30506	0.500	7.99	7.23	1.10E-06	4.55E-06	3.44E-06	n.a.	n.a.		9.40E-16	1.34E-13	-25.18	5.07
BG 15 E	30506	0.508	7.97	7.21	1.03E-06	4.14E-06	3.11E-06	n.a.	n.a.		8.63E-16	1.23E-13	-25.55	4.70
BG 14 A	29836	0.497	9.02	8.26	4.06E-06	1.94E-05	1.53E-05	1.07E-07	7.18E-06	7.08E-06	4.24E-15	6.07E-13	-21.90	3.40
BG 14 F	29836	0.500	9.00	8.24	5.09E-06	1.02E-05	5.13E-06	n.a.	n.a.		2.85E-15	4.08E-13	-25.80	0.56
BG 17 A	30506	0.499	9.05	8.29	5.27E-06	1.40E-05	8.76E-06	n.a.	n.a.		2.39E-15	3.41E-13	-24.01	1.67
BG 17 B	30506	0.499	9.08	8.32	5.59E-06	1.32E-05	7.58E-06	n.a.	n.a.		2.07E-15	2.96E-13	-24.75	0.93
BG 14 D	29836	0.498	9.03	8.28	3.63E-06	9.21E-06	5.58E-06	n.a.	n.a.		2.56E-15	3.67E-13	-26.05	0.00
BG 14 E	29836	0.400	8.98	8.23	3.77E-06	9.40E-06	5.63E-06	n.a.	n.a.		2.62E-15	3.75E-13	-26.11	0.19
BG 13 A	30506	0.498	10.02	9.26	1.10E-05	5.44E-05	4.35E-05	2.15E-07	1.55E-05	1.53E-05	1.18E-14	1.69E-12	-21.41	0.00
BG 17 C	30506	0.497	9.98	9.22	1.12E-05	4.72E-05	3.59E-05	n.a.	n.a.	n.a.	9.75E-15	1.39E-12	-21.97	-0.25
BG 13 B	30506	0.496	10.08	9.32	1.07E-05	5.15E-05	4.08E-05	2.45E-07	1.41E-05	1.39E-05	1.11E-14	1.58E-12	-21.72	-0.43
BG 13 C	30506	0.495	10.07	9.31	1.20E-05	4.53E-05	3.33E-05	n.a.	n.a.		9.01E-15	1.29E-12	-22.96	-1.18
BG 13 E	30506	0.500	10.05	9.29	1.15E-05	4.05E-05	2.90E-05	n.a.	n.a.		7.92E-15	1.13E-12	-24.56	-1.79
BG 13 D	30506	0.503	10.06	9.30	1.43E-05	4.52E-05	3.09E-05	n.a.	n.a.		8.49E-15	1.21E-12	-25.25	-1.92

n.d. = not detected

n.a. = not analysed

An example of the approach of an experiment to steady state is illustrated in Figure 4.4. This figure shows the temporal evolution of measured dissolution rates during experiment BG 17 A. This experiment was performed at 50° C at pH 8.29 and with a fluid flow rate of 0.5 g/min. The residence time of this experiment, defined as the volume of the reactor divided by the fluid flow rate, is 8.3 h. All experiments were run until the Si concentration in the output solution had stayed unchanged for several residence times.

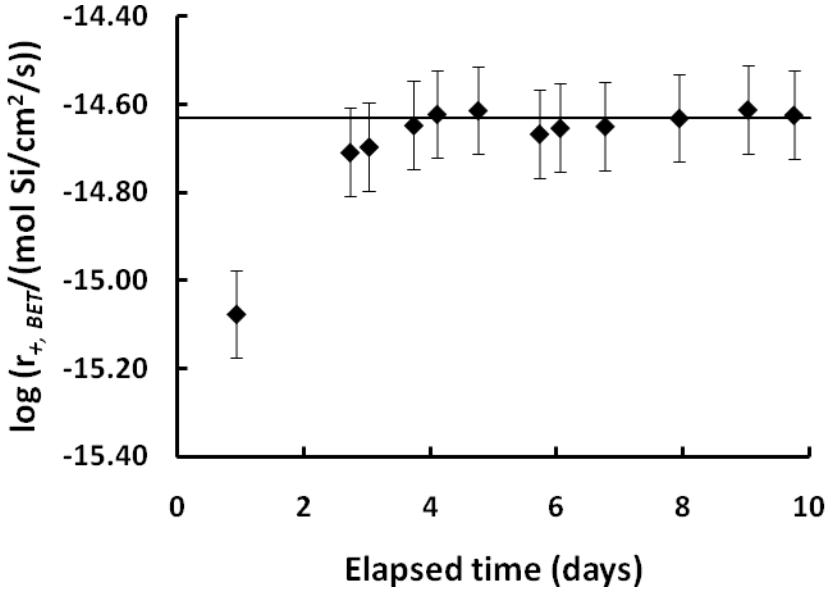

Figure 4.4. Temporal evolution of measured basaltic glass dissolution rates during experiment BG 17 A which was performed at pH 8.29 at 50 °C.

At pH less than ~2.5 and higher than ~10 basaltic glass dissolution is strongly influenced by the relatively slow diffusional transport of metals from the basaltic glass surfaces (Guy and Schott, 1989). Gislason and Oelkers (2003) demonstrated that the dissolution rates of basaltic glass are independent of stirring rates above 325 rpm at pH 3. Stirring rates of ~350 rpm were used in all experiments performed in this study and the dissolution rates obtained are believed to be surface reaction controlled since the basaltic glass dissolution rates are slower at higher pH.

The difference in input and output of Al and Si concentrations at steady state are shown in Figure 4.5, where the solid line corresponds to the Al/Si ratio of the dissolving basaltic glass. Note that Al has only been analyzed in a limited amount of samples. The solutions which were analyzed, however, showed close to stoichiometric dissolution. Two out of the three data points with the lowest Al concentrations, all of which plot below the stoichiometric dissolution line, were saturated with respect to gibbsite, which might explain the relatively low Al concentration.

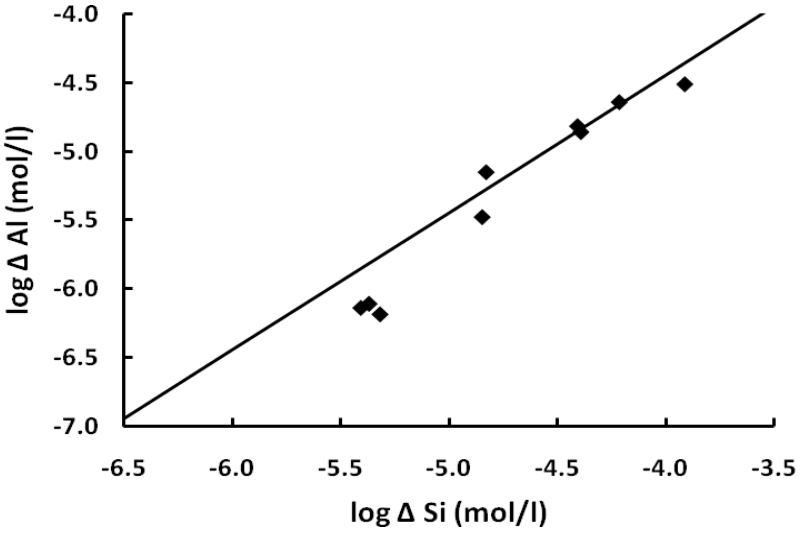

Figure 4.5. The logarithm of Δ[Al] concentration as a function of the corresponding logarithm of Δ[Si] concentration. The symbols represent measured solution compositions while the solid line corresponds to stoichiometric dissolution of the basaltic glass. The error bars of the measurements are hidden by the symbol.

The degree to which measured dissolution rates from this study are consistent with the multioxide dissolution mechanism described in Oelkers and Gislason (2001) and Gislason and Oelkers (2003) and illustrated in Figure 4.2, can be addressed in Figure 4.6. Figure 4.6 illustrates the logarithm of measured dissolution rates as a function of log (a^3_{H+}/a_{Al3+}). The filled diamonds correspond to experimental results where Al has been analyzed and the open

diamonds correspond to experimental results where the Al concentration has been calculated from the Δ[Si] concentration assuming stoichiometric dissolution. In accord with Eqn. (7), Gislason and Oelkers (2003) found that the logarithm of constant temperature far from equilibrium basaltic glass dissolution rates are a single linear function of log (a^3_{H+}/a_{Al3+}). This function is shown as a dashed line in Figure 4.6 while the linear regression of the data obtained in this study, consistent with log r_{BET}= 0.475 log (a^3_{H+}/a_{Al3+}) – 11.507, is shown as a solid line. As the figure shows, the data obtained from this study correspond closely to the behavior prescribed by the Gislason and Oelkers (2003) model.

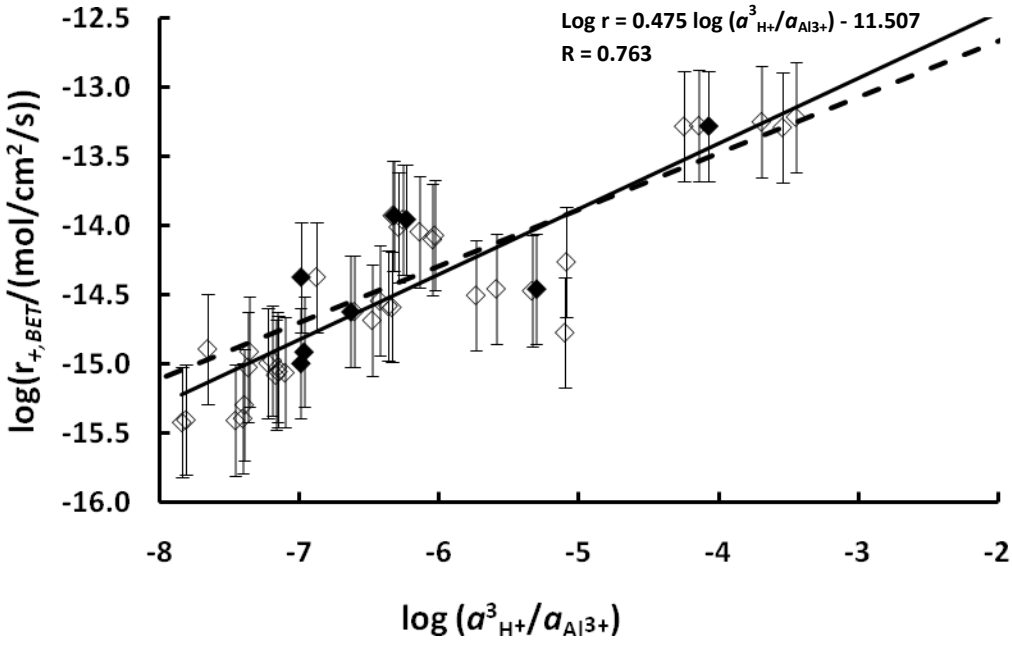

Figure 4.6. Variation of the logarithm of $r_{+,BET}$ obtained from the present study versus log(a^3_{H+}/a_{Al3+}). The filled diamonds correspond to experimental data with measured Al concentrations while the open diamonds correspond to experimental data where the Al concentrations have been calculated assuming stoichiometric dissolution. The solid line and the dashed line correspond to the tendency line from this study and Gislason and Oelkers (2003), respectively. The error bars correspond to a ± 0.4 log unit uncertainty.

Basaltic glass dissolution experiments were performed with solutions containing 0, 1, 10, 50 and 100 mM SO_4^{2-} and pH varying between 3 and 10. Figure 4.7 shows the effect of sulphate on the dissolution rate of basaltic glass at pH 5 where the diamonds represent measured rates and the line represents modeled rates using Eqn (7) normalized to the rate in sulphate free solution. The dissolution rate of the glass increases with rising sulphate concentrations. Even though the increase in dissolution rate is smaller than the estimated uncertainty (±0.4 log units), there is a clear trend, in acid conditions, that the dissolution rate increases with increasing amount of sulphate present, which is in agreement with the model. At pH 5, the dissolution rate doubles when 0.01 mol/kg of sulphate is added while it triples when adding 0.05 mol/kg compared with that of sulphate-free experiments.

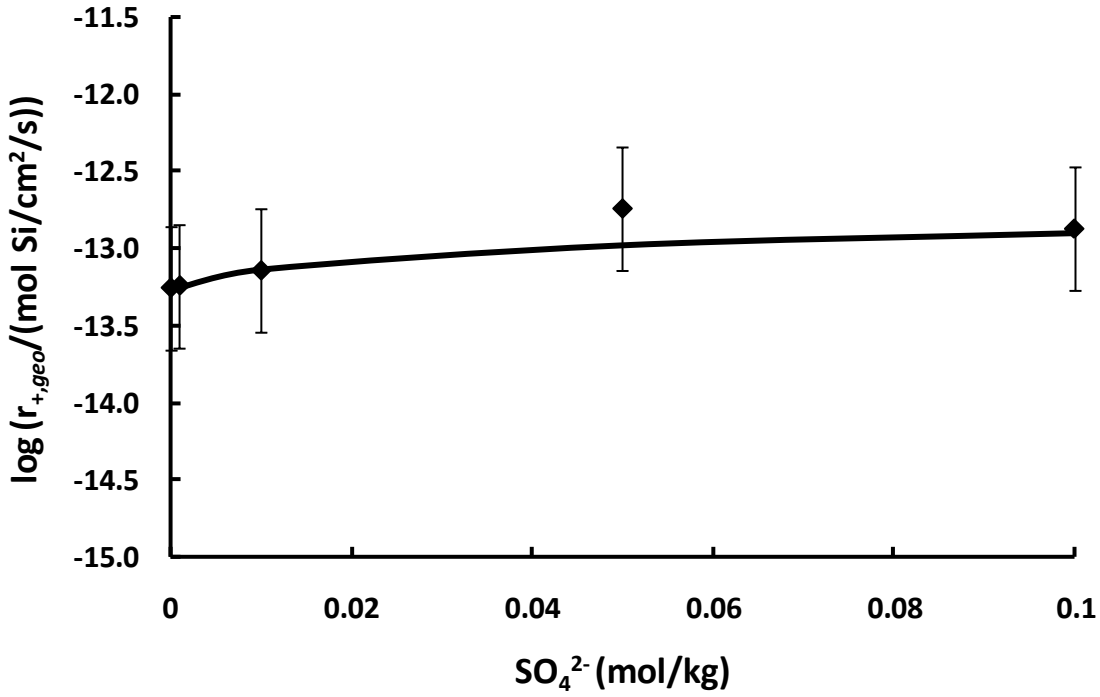

Figure 4.7 The diamonds shows the logarithm of $r_{+,geo}$ in experiments performed at pH 5 containing different amounts of SO_4^{2-} while the line corresponds to predicted rates using Eqn. (7) and a solution which contains 10^{-6} M Al at pH 5. The predicted rates where normalized to the rate in sulphate free solution.

The measured dissolution rates obtained from solution with different concentrations of SO_4^{2-} are plotted versus pH in Figure 4.8. The dissolution rates show the characteristic behavior as a function of pH which is common for Al-silicates (Gislason and Oelkers, 2003); dissolution rate decrease strongly with increasing pH in acid conditions, minimizing at near neutral condition (pH~6), and increasing again as pH increases. At pH 4 and 5, there is a tendency for the dissolution rate to increase with increased aqueous fluid SO_4^{2-} concentration. This might also be the case for pH 3. On the other hand, the dissolution rates in basic solutions, do not seem to be affected by the presence of SO_4^{2-}. The lines in Figure 4.8 show the predicted rates using Eqn. (7) normalized to the rate in sulphate free solutions.

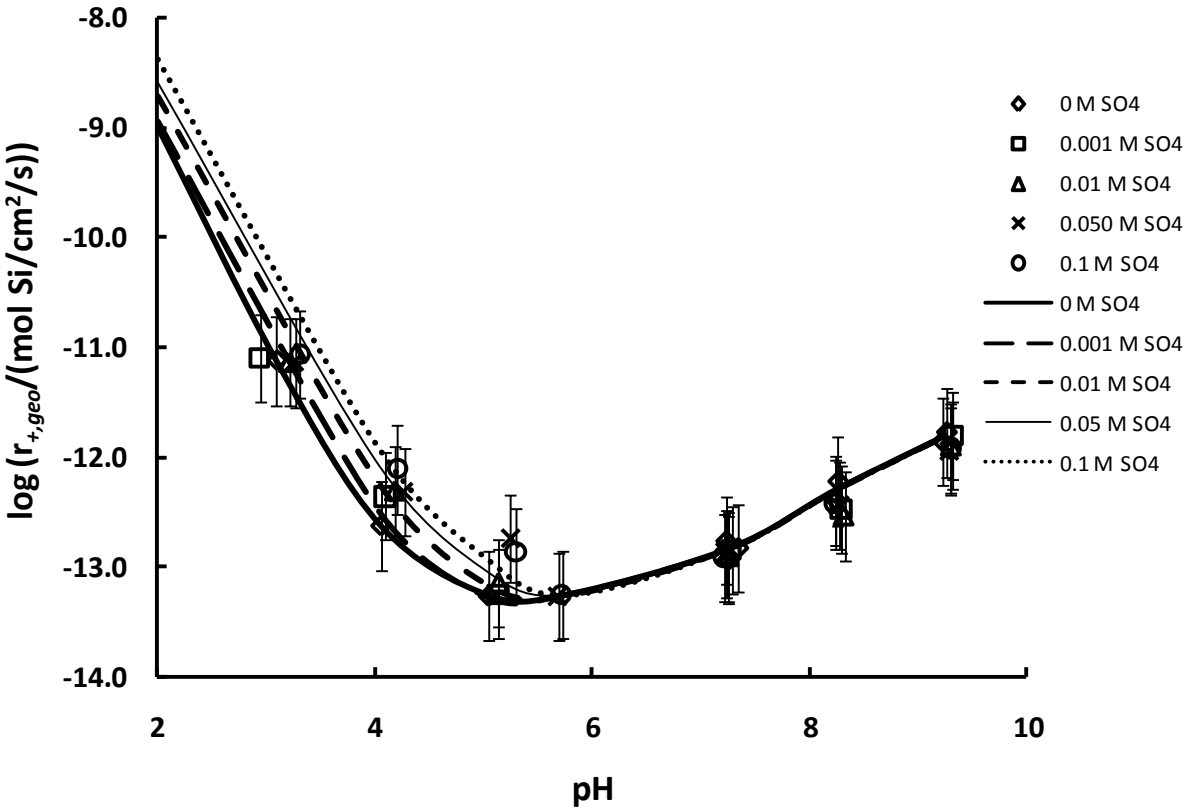

Figure 4.8. The logarithm of the dissolution rates with various concentrations of SO_4^{2-} versus pH for basaltic glass at 50 °C. The lines represents the predicted rates using the Eqn (7) normalized to the rate in sulphate free solutions.

A comparison of all measured rates with those calculated using the regression fit shown in Figure 4.6 is represented in Figure 4.9. The average difference between the absolute value of the difference between measured and calculated rates is 0.2 log units; all but 4 measured rates are reproduced to within 0.4 log units by this regression equation.

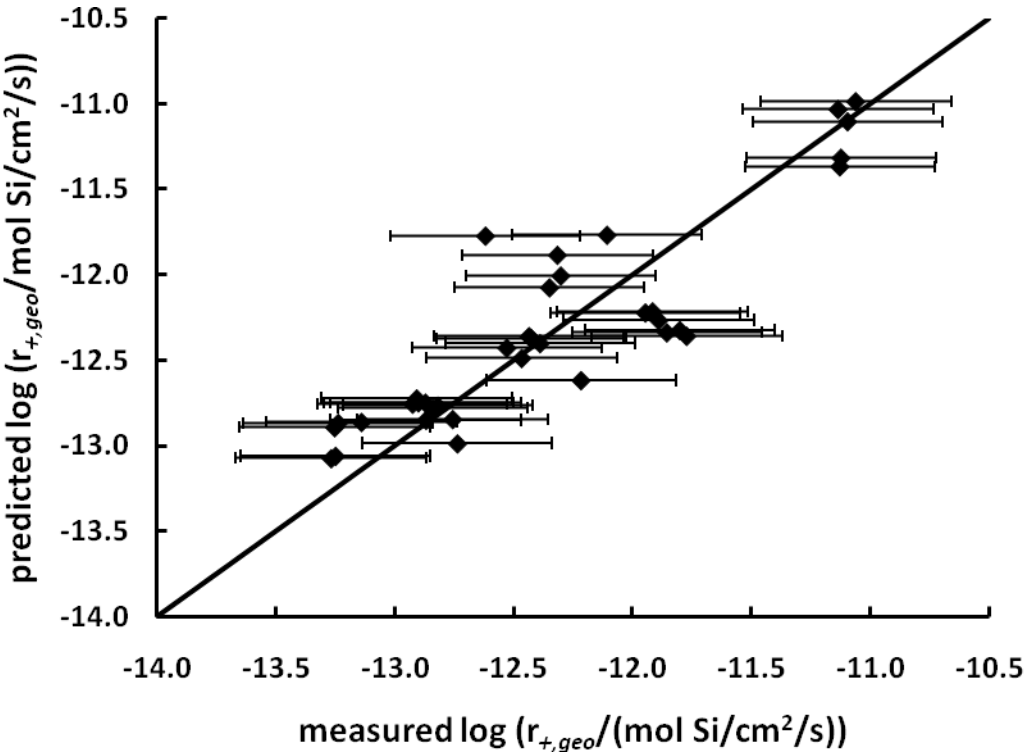

Figure 4.9. Predicted $r_{+,geo}$ versus their experimental counterparts. The solid diamonds corresponds to basaltic glass dissolution rates and the solid line corresponds to equal rates. The predicted rates were calculated using the linear function log $r_{,geo} = 0.475 \log(a^3_{H+}/a_{Al3+}) - 11.51$.

4.6 Conclusions

Experimental results from this study show that the effect of aqueous sulphate on basaltic glass dissolution rates using Eqn. (7) is approximately consistent with their experimentally

measured counterparts. This approximate coherence provides support for using this equation for the prediction of the reactive behavior of basaltic glass in complex natural systems.

Aqueous sulphate is found to increase basaltic glass dissolution rates in acid conditions. As such the addition of sulphate to injected CO_2 may enhance mineral sequestration in basaltic rocks. Such co-injection may prove to be an effective method for the safe storage of sulphur emitted from power plants and other types of industry.

References

Aagaard, P., Helgeson., H.C., 1977. Thermodynamic and kinetic constraints on hte dissolution of feldspars. Geological Society of America, Abstract 9, 873.

Aagaard, P., Helgeson, H.C., 1982. Thermodynamic and kinetic constraints on reaction rates among mineral and aqueous solutions: I. Theoretical considerations. American journal of Science 282, 237-285.

Arts, R., Eiken, O., Chadwick, A., Zweigel, P., ver der Meer, L., Zinszner, B., 2004. Monitoring of CO2 injected at Sleipner using time-lapse seismic data. Energy 29, 1383-1392.

Bachu, S., Adams, J.J., 2003. Sequestration of CO_2 in geological media in response to climate change: capacity of deep saline aquifers to sequester CO_2 in solution. Energy Conversion and Management 44, 3151-3175.

Bachu, S., Bonijoly, D., Bradshaw, J., Burruss, R., Holloway, S., Christensen, N.P., Mathiassen, O.M., 2007. CO_2 storage capacity estimation: Methodology and gaps. International Jouranla of Greenhouse Gas Control 1, 430-443.

Berger, G., Schott, J. and Loubet, M.,1987. Fundamental processes controlling the first stage of alteration of a basalt glass by seawater: an experimental study between 200 and 320° C. Earth Planet. Sci. Let. 84, 431-445.

Berger, G., Cadoré, E., Schott, J. and Dove, P.,1994. Dissolution rate of quartz in Pb and Na electrolyte solutions. Effect of the nature of surface complexes and reaction affinity. Geochim. Cosmochim. Acta, 58, 541-551.

Benson, S.M., Cole, D.R., 2008. CO_2 sequestration in Deep Sedimentary Formations. Elements 4, 325-331.

Bourcier W.L., Peiffer D.W., Knauss K.G., McKeegan K.D., and Smith D.K., 1990. A kinetic model for borosilicate glass dissolution based on the dissolution affinity of a surface altered layer. In *Scientific basis for nuclear waste Management XIII*. (eds. V.M. Oversby and P.Q. Brown) Mat. Res. Soc. SYmp. Proc. Pittsburgh Pa. 176, 120-128.

Broecker, W.S., 2008. CO_2 capture and storage: Possibilities and perspectives. Elements 4, 295-297.

Cantucci, B., Montegrossi, G., Vaselli, O., Tassi, F., Quattrocchi, F., Perkins, E.H., 2009. Geochemical modeling of CO_2 storage in deep reservoirs ; The Weyburn Project (Canada) case study. Chemical Geology. In Press.

Chadwick, R.A., Zweigel, P., Gregersen, U., Kirby, G.A., Holloway, S., Johannessen, P.N., 2004. Geological reservoir characterization of a CO_2 storage site: The Utsira Sand, Sleipner, northern North Sea. Energy 29, 1371-1381.

Chaïrat C., Schott, J., Oelkers E. H., Lartigue J.-E. and Harouiya N., 2007. Kinetics and mechanism of natural fluorapatite dissolution at 25°C and pH from 3 to 12. Geochimica et Cosmochimica Acta 71, 5901-5912.

Crovisier, J.L., Atassi, H, Daux, V. and Eberhart, J.P., 1990. Hydrolyse d'un verre basaltique tholéiitique à 60° C. Dissolution sélective puis congruent par élévation de pH. C.R. Acad. Sci. Paris, 310, II, 941-946.

Crovisier, J.L., Honnorez, J., Fritz, B., 1992. Dissolution of subglacial volcanic glasses from Iceland: laboratory study and modelling. Applied Geochemistry Supplement Issue 1, 55-81.

Daux, V., Guy, C., Advocat, T., Crovisier J-L., Stille, P., 1997. Kinetic Aspects of basaltic glass dissolution at 90° C: Role of silicon and aluminum. Chemical Geology 142, 109-128.

Emberley, S., Hutcheon, I., Shevalier, M., Durocher, K., Mayer, B., Gunter, W.D., Perkins, E.H., 2004. Geochemical monitoring of fluid-rock interaciton and CO_2 storage at the Weyburn CO_2-injection enhanced oil recovery site, Saskatchewan, Canada. Energy 29, 1393-1401.

Gautier, J.M., Oelkers, E.H., Schott, J., 1994. Experimental study of K-feldspar dissolution rates as a function of chemical affinity at 150 °C and pH 9. Geochimica et Cosmochimica Acta 58, 4549-4560.

Gislason, S.R., Eugster, H.P., 1987. Meteoric water-basalt interactions. I: A laboratory study. Geochimica et Cosmochimia Acta 51, 2827-2840.

Gislason, S.R., Oelkers, E.H., 2003. Mechanism, rates and consequences of basaltic glass dissolution: II. An experimental study of the dissolution rates of basaltic glass as a function of pH and temperature. Geochimica et Cosmochimica Acta 67, 3817-3832.

Gislason, S.R., Wolff-Boenisch, D., Stefansson, A., Oelkers, E., Gunnlaugsson, E., Sigurdardóttir, H., Sigfússon, Broecker, W., Matter, J., Stute, M., Axelsson, G., Fridriksson, T., 2009. Mineral sequeatration of carbon dioxide in basalt; The CarbFix project. International Journal of Greenhouse Gas (Submitted).

Goldberg, D.S., Takahashi, T., Slagle, A.L., 2008. Cabon dioxide sequestration in deep-sea basalt. Proceedings of the National Academy of Scienes 105: 9920-9925.

Guy C. and Schott J. , 1989. Multisite surface reaction versus transport control during hydrolysis of a complex oxide. Chemical Geology 78, 181-204.

Harouiya, N., Oelkers, E.H., 2004. An experimental study of the effect of aqueous fluoride on quartz and alkali-feldspar dissolution rates. Chemical Geology 205, 155-167.

Helgeson, H.C., Murphy, W.M., Aagaard, P., 1984. Thermodynamic and kinetic constraints on reaction rates among minerals and aqueous solutions: II. Rate constants, effective surface area, and the hydrolysis of feldspar. Geochimica et Cosmochimica Acta 48, 2405-2432.

Hitchon, B., Gunter, W.D., Gentzis, T., Bailey, R.T., 1999. Sedimentary basins and greenhouse gases; a serendipitous association. Energy Conversion & Management 40, 825-843.

Houghton, J.T., Meira Filho, L.G., Callander, B.A., Harris, N., Kattenberg, A., Maskell, K., 1996. Climate Change. The science of climate change, Cambridge University Press, UK, pp 572.

Iding, M., Ringrose, P., 2009. Evaluating the impact of fractures on the long-term performance od the In-Salah CO_2 storage site. Energy Procedia 1, 2021-2028.

Intergovernmental Panel on Climate Change (IPCC), 2005. Summary for Policymakers. In: Metz, B., Davidson, O., Coninck, H., Loos, M., Meyer, L. (eds) IPCC Special Report on Carbon Dioxide Capture and Storage, prepared by Working Group III of the Intergovernmental Panel on Climate Change. Cambridge University Press, Cambridge, UK, and New York, USA, pp 3-15.

Intergovernmental Panel on Climate Change (IPCC), 2007. Climate Change 2007; Synthesis Report. Contribution of working Groups I, II and III to the Fourth Assessment Report of the Intergovernmental Panel on Climate Change (Eds.) Pachauri, R.K., Reisinger, A. IPCC, Geneva, Switzerland, 104 pp.

Kelemen, P.B., Matter, J., 2008. In situ carbonation of peridotite for CO_2 storage. Proceedings of the National Academy of Science 105, 17295-17300.

Kharaka, Y.K., Thordsen, J.J., Hovorka, S.D., Nance, H.S., Cole, D.R., Phelps, T.J., Knauss, K.G., 2009. Potential environmental issues of CO_2 storage in deep saline aquifers: Geochemical results from the Frio-I Brine Pilot test, Texas, USA. Applied Geochemistry 24, 1106-1112.

Koroleff, F., 1976. Determination of silicon. In *Methods of seawater Analysis* (ed. K. Grasshoff). Springer Verlag, New York, pp 149-158.

Lasaga, A.C., 1981. Transition state theory. Reviews in Mineralogy 8, 135-169.

Manabe, S., Stouffer, R.J., 1993. Century-scale effects of increased atmospheric CO_2 on the ocean-atmosphere system. Nature 364, 215-218.

Marini, L., 2007. Geological Sequestration of Carbon Dioxide: Thermodynamics, Kinetics and Reaction Path modeling. Elsevier, Amsterdam, 470 pp.

Matter, J.M., Takahashi, T., Goldberg, D., 2007. Experimental evaluation of in situ CO_2-water-rock reactions during CO_2 injection in basaltic rocks: Implications for geological CO_2 sequestration. Geochemistry, Geophysics, Geosystems 8, Q02001, doi: 10.1029/2006GC001427.

Matter, J.M., Broecker, W.S., Stute, S., Gislason, S.R., Oelkers, E.H., Stefánsson, A., Wolff-Boenisch, D., Gunnlaugsson, E., Axelsson, G., Björnsson, G., 2009. Permanent Carbon Dioxide Storage into Basalt: The CarbFix Pilot Project, Iceland. Energy Procedia 1, 3641-3646.

McGrail, B.P., Schaef, H.T, Ho, A.M., Chien, Yi-Ju, Dooley, J.J., Davidson, C.L., 2006. Potential for carbon dioxide sequestration in flood basalts. Journal of Geophysical Research, vol 111. B12201, doi:10.1029/2005JB004169.

Michael, K., Arnot, M., Cook, P., Ennis-King, J., Funnell, R., Kaldi, J., Kirste, D., Paterson, L., 2009. CO_2 storage in saline aquifers I – current state of scientific knowledge. Energy Procedia 1, 3197-3204.

Murphy, W.M., Helgeson, H.C., 1987. Thermodynamics and kinetic constraints on reaction rates among minerals and aqueous solutions. III. Activated complexes and the pH-dependence of the rates of feldspar, pyroxene, wollastonite, and olivine hydrolysis. Geochimica et Cosmochimia Acta 51, 3137-3153.

Oelkers, E.H., Schott, J., Devidal, J.L., 1994. The effect of aluminum, pH, and chemical affinity on the rates of aluminosilicate dissolution reactions. Geochimica et Cosmochimica Acta 58, 2011-2024.

Oelkers, E.H., 2001. General kinetic description of multioxide silicate mineral and glass dissolution. Geochimica et Cosmochimica Acta 65, 3703-3719.

Oelkers, E.H., Gislason, S.R., 2001. The mechansim, rates and consequences of basaltic glass dissolution: I. An experimental study of the dissolution rates of basaltic glass as as function of aqueous Al, Si and oxalic acid concentration at 25 °C and pH = 3 and 11.

Oelkers, E.H., Schott, J., 2005. Geochemical aspects of CO_2 sequestration. Chemical Geology 217, 183-186.

Oelkers, E.H., Cole, D.R., 2008. Carbon dioxide sequestration: A solution to a global problem. Elements 4, 305-310.

Oelkers, E.H., Gislason, S.R., and Matter, J. (2008) Mineral carbonation of CO_2. Elements 4, 333-337.

Parkhurst D.L. and Appelo C.A.J. (1999). User's guide to PHREEQC (Version 2) – A computer program for speciation, batch-reaction, one-dimensional transport, and inverse geochemical calculations. USGS-Report 99-4259.

Retallack, G.J., 2002. Carbon dioxide and climate over the past 300 myr. Philosophical transactions. Series A, Mathematical, physical and engineering sciences 360, 659-673.

Saldi, G.D., Köhler, S.J., Marty, N., Oelkers, E.H., Dissolution rates of talc as a function of solution composition, pH and temperature. Geochimica et Cosmochimica Acta 71, 3446-3457.

Shaef, H.T., McGrail. B.P., Owen, A.T., 2009. Basalt-CO_2-H_2O Interactions and Variability in Carbonate Mineralization Rates. Energy Procedia 1, 4899-4906.

Schaef, H.T., McGrail. B.P,, 2009. Dissolution of Columbia River Basalt under mildly acidic conditions as a function of temperature: Experimental results relevant to the geological sequestration of carbon dioxide. Applied Geochemistry 24, 980-987.

Stenhouse, M., Arthur, R., Zhou, W., 2009. Assessing environmental impacts from geological CO_2 storage. Energy Procedia 1, 1895-1902.

Taylor, F.W., 1991. The Greenhouse effect and climate change. Reports on Progress in Physics 54, 881-918.

Thomassin, J.H. and Touret, J.C., 1979. Etude des premiers stades de l'interaction eau-verre basaltique: Donnés de la spectroscopie de photoélectrons et de ls microscopie électrinique a balayage. Bulletin of Mineralogy 102, 594-599.

Wolff-Boenisch, D., Gislason, S.R., Oelkers, E.H., 2004. The effect of fluoride on the dissolution rates of natural glasses at pH 4 and 25 °C. Geochimica et Cosmochimica Acta 68, 4571-4582.

Chapter 5

A preliminary study of the effect of aqueous sulphate on calcite precipitation rates.

Flaathen, T.K., Oelkers, E.H., Gislason, S.R. (To be submitted to Chemical Geology upon completion of study).

5.1 Abstract

The fourth chapter of this thesis is a detailed study of the effect of aqueous sulphate on the rates of basaltic glass dissolution. The conclusion of that chapter was that aqueous sulphate increases dissolution rates in acid conditions, but has little effect in basic conditions. This result suggests that co-injection of sulphate with CO_2 would not be detrimental to subsurface carbon sequestration efforts. This conclusion, however, is based on the assumption that the presence of aqueous sulphate does not dramatically slow down carbonate precipitation rates. To assess the potential effects of the presence of aqueous sulphate on calcite precipitation rates, steady-state precipitation rates of calcite were measured in mixed-flow reactors at 25 °C at pH 9.1 as a function of aqueous sulphate concentration. The results show that 0.005 M Na_2SO_4 decreases the precipitation rate of calcite with ~40%. This result suggests that co-injected sulphate could slow down calcite precipitation at the pH conditions typical of subsurface calcite precipitation. Further experiments are planned to completely define these effects at conditions expected at subsurface CO_2 injection sites.

5.2 Introduction

Calcite precipitation rates are a prerequsite for the understanding of the global carbon cycle, and to optimise the conditions for carbon sequestration and mineralization (e.g. Berner et al., 1983; Oelkers et al 2008). This preliminary study is aimed at determining the effect of the presence of dissolved sulphate on the rates of calcite precipitation at conditions present at subsurface carbon sequestration sites.

A large number of past studies have been aimed at quantifying the rates of calcite precipitaiton (e.g. Meyer, 1984; Zhong and Mucci, 1989, 1993; Dove and Hochella, 1993; Davis et al., 2000; Vavouraki et al., 2008). Many of these studies have revealed that the presence of aqueous trace metals and anions can strongly influence calcite growth rates. Vavouraki et al. (2008) suggested for example, that the presence of aqueous Na_2SO_4 increased calcite growth rates at basic pH. The presence of inorganic phosphate (Plant and House, 2002) and Mg^{2+} (Zhang and Dawe, 2000), have been reported to decrease calcite precipitation rates. The presence of polyphosphate (Lin and Singer, 2005) and other natural organic materials (Lin et al., 2005) have also been reported to inhibit calcite precipitation. These earlier results emphasize that the presence of trace species in solution can have dramatic effects on calcite precipitaiton and that such effects could strongly influence the success of carbon mineralization efforts.

Calcite is also known to co-precipitate with many different ions, such as Ni (Lakshtanov and Stipp, 2007), Fe, Sr, Ba and Mn (Ettler et al., 2005), U(VI), Cs(I), Sr(II), Ra(II) (Curti, 1999) and arsenite (Román-Ross et al., 2006). Calcite precipitaiton is therefore often used during water treatment to decrease the concentration of toxic metals in natural waters.

A major motivating factor in this study is to assess the potential effects of the co-injection of sulphur with CO_2 during carbon sequestration efforts. Sulphur is often present in the flue gases of power plants and their disposal also poses an environmental challenge. If possible, co-injection of sulphur with CO_2 could provide a novel cost effective disposal method for industrially generated sulphur. A prerequisite for this co-injection is that the presence of aqueous sulphur is not detrimental to the carbon sequestration effort. In chapter 4 of this thesis, the effect of the presence of aqueous sulphate on the availability of divalent cations needed for the mineral sequestration of CO_2 originating from the dissolution of basaltic glass was determined. Efforts described in this study are aimed at determining the effect of the presence of aqueous sulphate on the precipitation of calcite.

5.3 Theoretical Background

Calcite is one of the most common minerals on the face of the Earth, comprising about 4% by weight of the Earth's crust and is formed in many different geological environments. It readily precipitates out of solution when supersaturated by the reaction:

$$Ca^{2+} + CO_3^{2-} = CaCO_3 \quad (1)$$

Calcite dissolution and precipitation kinetics have traditionally been described as a function of the degree of disequilibrium in the aqueous solution by using the mechanistic model originally formulated by Plummer et al. (1978) for calcite dissolution, which describes the elementary reactions controlling dissolution in different pH regions. This approach generally employs the following empirical equation for precipitation reactions:

$$r = k\,(\Omega\text{-}1)^n \quad (2)$$

where r is the rate of precipitation normalized to the reacting surface, k is the apparent rate constant, (Ω-1) represents the degree of supersaturation of solution and n designates the empirical order of reaction, which is indicative of the growth mechanism of mineral surfaces . Ω defines the saturation state of solution, equal to the ratio of the ion activity product of dissolved mineral components (Q) to the thermodynamic solubility product (K_{sp}). For calcite, the saturation state is defined as:

$$\Omega = \frac{Q}{K_{sp}} = \frac{a_{Ca^{2+}} a_{CO_3^{2-}}}{K_{sp}} \quad (3)$$

The rate equation (3) was used to fit experimental data for precipitation of calcite (Nancollas and Reddy, 1971; Reddy et al., 1981; Mucci and Morse, 1983; Inskeep and Bloom, 1985; Busenberg and Plummer, 1986; Shiraki and Brantley, 1995), Mg-calcite (Mucci, 1986) and dolomite (Arvidson and Mackenzie, 1999). The published experimental data, together with the rate expressions generated to describe them, give a good representation of carbonate mineral behavior in aqueous solution at various conditions. This background provides a point of departure for describing the effect of solution composition on calcite precipitation rates.

5.4 Methods

Large transparent Iceland spar calcite crystals collected from hydrothermal veins in basaltic traps in Central Siberia as described in Pokrovsky et al. (2005), were used in this study.

Electron microprobe and total chemical analysis showed that the samples contained less than 0.5% impurities and no other phases were detected using XRD. These samples were ground with a pestle and an agate mortar. then sieved to obtain the 100 and 200 µm size fractions. This calcite powder was then reacted for several seconds in 1% HCl, ultrasonically cleaned in alcohol to remove adhering fine particles, rinsed repeatedly with distilled water, then dried overnight at 60 °C. The specific surface area of the resulting calcite powder was 334 cm^2/g as determined by multi-point krypton absorption using the B.E.T. method on a Quantachrome Autosorb-1.

Calcite precipitation experiments were performed on the calcite seeds described above in a mixed flow polypropylene reactor system at pH ~9.1. The experiments were all performed at 25 ± 2 °C. The volumes off the reactors were 30 mL and they were continuously stirred with floating Teflon stirring bars. The fluids were injected using a Gilson peristaltic pump, which allows fluid flow rates from 0.01-10 g/min. The solution left the reactor through a 2.5 µm filter. No additional filtering was performed on outlet fluid samples obtained from either reactor before chemical analysis. The two experiments were performed on a single calcite seed powder. The computer code PHREEQC (Parkhurst and Appelo, 1999) was used to calculate saturation states.

Calcite precipitation was induced by using two Gilson peristaltic pumps to inject simultaneously two distinct solutions into the reactor: a $NaHCO_3$-Na_2CO_3 mixed solution and a $CaCl_2$ solution at identical flow rates. This protocol was essential to avoid calcite precipitation prior to solution entry into the reactor. At the onset of each experiment, the reactor was filled with the calcite seed crystals and a 1:1 mixture of the two inlet solutions. The flow rate was held constant until the outlet solution contained a steady state Si concentration. Steady-state dissolution rates were obtained after 1-2 days. The sulphate was added to the $CaCl_2$ solution before experiment C started. Information about the composition of the various inlet solutions used in this study is listed in Table 5.1.

Table 5.1. Input solutions for calcite precipitation experiments.

Experiment	$NaHCO_3$ (mol/kg)	Na_2CO_3 (mol/kg)	$CaCl_2$ (mol/kg)	Na_2SO_4 (mol/kg)	ΔG_r Calcite (kJ/mol)	Ionic strength
A	1.69E-02	1.29E-03	1.42E-04	0	3.355	0.010
C	1.69E-02	1.29E-03	1.41E-04	0.01	2.450	0.025

The Ca content of the inlet and outlet solutions was determined using atomic absorption spectroscopy (Perkin Elmer Zeeman 5000). The reproducibility of chemical analyses was ± 2%. The outlet solution pH was measured at 23° C immediately after sampling. The pH was measured using a Metrohm© 744 pH meter coupled to a Metrohm© Pt1000/B/2 electrode with a 3 M KCl outer filling solution. The electrode was calibrated with NBS standards at pH 4.01, 6.86, and 9.22, with an average error of less than 0.05 pH units. Solution alkalinity was fixed by the large concentration of bicarbonate in the reactive solution and the solution pH. Inlet fluids used in these experiments comprised demineralised H_2O, $NaHCO_3$ (99,7%) from Riedel-de Haën, Na_2CO_3 (99,5%) from Fluka, $CaCl_2$ (1000 ppm standard) Merck and Na_2SO_4 (99%) from Fluka. The acidic $CaCl_2$ stock solution was neutralized using 1 M NaOH from Merck.

5.5 Results

The outlet concentrations of Ca, during the two experiments, are shown in Figure 5.1. During experiment A, which contained no sulphate, the concentration of Ca in the outlet fluid decreased quickly from $7.1x10^{-5}$ mol/kg to $4.7x10^{-5}$ mol/kg due to precipitation, as can be seen in Figure 1. When 0.005 mol/kg of sulphate were added to the $CaCl_2$ solution, the concentration of Ca in the outlet solution increased to $5.7x10^{-5}$ mol/kg.

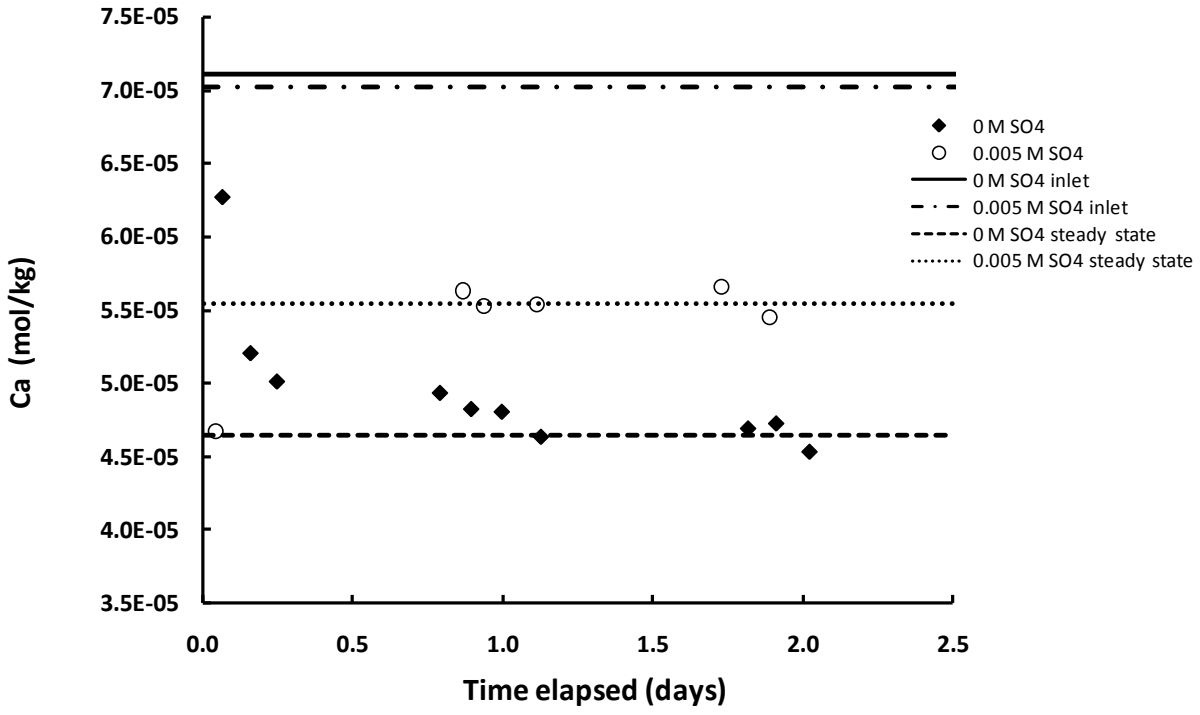

Figure 5.1. Results of calcite precipitation experiments with and without sulphate.

Steady state precipitation rates (r) were computed from the measured steady-state Ca concentration using

$$r = \frac{\Delta[\mathrm{Ca}] * F}{s_{BET} M} \qquad (4)$$

where Δ[Ca] stands for the concentration difference between the inlet and outlet of Ca in solution (mol/kg), F represents the fluid mass flow rate (g/s), s_{BET} denotes the BET specific surface area of the initial glass (cm^2/g), and M signifies the initial mass of glass in the reactor (g). Precipitation rates, given in units of moles of Ca per cm^2 of initial calcite surface area per second, obtained from our experiments are shown in Table 5.2 together with pH, flow rates, surface area, the difference in measured inlet and outlet concentrations of Ca (Δ[Ca]), and the saturation state of calcite, given as ΔG_r. The saturation states were calculated using the PHREEQC computer code (Parkhurst and Appelo, 1999).

Table 5.2 Results from the calcite precipitation experiments.

Experiment	pH (outlet)	Flow rate (g/min)	Surface area (cm^2)	Δ[Ca] (mol/kg)	r (mol $Ca/cm^2/s$)	ΔG_r Calcite (kJ/mol)
A	9.15	0.5603	94.2	2.47E-05	2.45E-12	2.397
C	9.05	0.5601	94.2	1.48E-05	1.47E-12	1.598

5.6 Conclusions

The results from this study show that aqueous SO_4^{2-} decreases the precipitation rate of calcite. By adding 0.005 M SO_4^{2-}, the precipitation rate is inhibited by ~40%. Additional experiments are planned, at various aqueous SO_4^{2-} concentrations, calcite saturation states and flow rates, to define in detail the effect of the presence of aqueous sulphate on calcite precipitation rates. It is anticipated that such results will enable accurate assessment of the degree to which the co-injection of sulfate with carbon dioxide during geological carbon sequestration efforts can simultaneously aid in mineral sequestration and the disposal of industrially generated sulfur.

5.7 References

Arvidson, R. S., Mackenzie, F. T., 1999. The dolomite problem: Control of precipitation kinetics by temperature and saturation state. American Journal of Science 299, 257-288.

Berner, R. A., Lasaga, A. C., Garrels, R. M. ,1983. The carbonate-silicate geochemical cycle and its effect on atmospheric carbon-dioxide over the past 100 million years. American Journal of Science 283, 641-683.

Busenberg, E., Plummer, L. N., 1986. A comparative study of the dissolution and crystal growth kinetics of calcite and aragonite, in Mumpton, F. A., editor, Studies in Diagenesis: U. S. Geological Survey Bulletin B 1578, pp. 139–168.

Curti, E., 1999. Coprecipitation of radionuclides with calcite: estimation of partition coefficients based on a review of laboratory investigations and geochemical data. Applied Geochemistry 14, 433-445.

Davis, K.J., Dove, P.M., De Yoreo, J.J., 2000. The role of Mg^{2+} as an impurity in calcite growth. Science, 290, 1134-1137.

Dove, P.M., Hochella M.F., 1993. Calcite precipitation mechanisms and inhibition by orthophosphate – In-Situ observations by scallnign force mincroscopy. Geochimica et Cosmochimica Acta, 57, 705-714.

Inskeep, W. P., Bloom, P. R., 1985. An evaluation of rate equations for calcite precipitation kinetics at pCO_2 less than 0.01 atm and pH greater than 8. Geochimica et Cosmochimica Acta 49, 2165-2180.

Ettler, V., Zelená, O., Mihaljevic, M., Sebek, O., Strnad, L., Coufal, P., Besdicka, P., 2003. Removal of trace elements from landfill leachate by calcite precipitation. Journal of Geochemical Exploration 88, 28-31.

Lakshtanov, L.Z., Stipp, S.L.S., 2007. Experimental study of nickel(II) interaction with calcite: Adsorption and coprecipitation. Geochimica et Cosmochimica Acta 71, 3686-3697.

Lin, Y.P., Singer, P.C., 2005. Inhibition of calcite crystal growth by polyphosphates. Water Research 39, 4835-4843.

Lin, Y.P., Singer, P-C., Aiken, R., 2005. Inhibition of calcite precipitaiton by natural organic material: Kinetic, mechanism and thermodynamics. Environmental Science and Technology 39, 6420-6428.

Meyer, H.J., 1984. The influence of impurities n the growth-rates of calcite. Journal of Crystal Growth, 66, 639-646.

Mucci, A., 1986. Growth kinetics and composition of magnesian calcite overgrowths precipitated from seawater: Quantitative influence of orthophosphate ions. Geochimica et Cosmochimica Acta 50, 2255-2265.

Mucci, A., Morse, J. W., 1983. The incorporation of Mg^{2+} and Sr^{2+} into calcite overgrowths: influences of growth rate and solution composition. Geochimica et Cosmochimica Acta 47, 217-233.

Nancollas, G. H., Reddy, M. M., 1971. The crystallization of calcium carbonate. II. Calcite growth mechanism. Journal of Colloid and Interface Science 37, 824-830.

Oelkers, E.H., Gislason, S.R., Matter, J., 2008. Mineral carbonation of CO_2. Elements 4, 333-337.

Parkhurst D.L., Appelo C.A.J., 1999. User's guide to PHREEQC (Version 2) – A computer program for speciation, batch-reaction, one-dimensional transport, and inverse geochemical calculations. USGS-Report 99-4259.

Plant, L.J., House, W.A., 2002. Precipitation of calcite in the presence of inorganic phosphate. Colloids and Surfaces A: Physiochemical and Engineering Aspects 203, 143-153.

Plummer, L. N., Wigley, T. M. L., and Parkhurst, D. L., 1978. Kinetics of calcite dissolution in CO_2-water system at 5 °C to 60 °C and 0.0 to 1.0 atm CO_2. American Journal of Science 278, 179-216.

Pokrovsky, O.S., Golubev, S.V., Schott, J. 2005. Dissolution kinetics of calcite, dolomite and magnesite at 25°C and 0 to 50 atm pCO_2. Chemical Geology 217, 239-255.

Reddy, M. M., Plummer, L. N., Busenberg, E., 1981. Crystal growth of calcite from calcium bicarbonate solutions at constant PCO_2 and 25 °C: a test of calcite dissolution model. Geochim. Cosmochim. Acta 45, 1281-1289.

Román-Ross, G., Cuello, G.J., Turillas, X., Fernández-Martínez, A., Charlet, L., 2006. Arsenite sorption and co-precipitation with calcite. Chemical Geology 233, 328-336.

Shiraki, R., Brantley, S. L., 1995. Kinetics of near-equilibrium calcite precipitation at 100°C: An evaluation of elementary reaction-based and affinity-based rate laws. Geochimica et Cosmochimica Acta 59, 1457-1471.

Vavouraki A.I., Putnis, C.V., Putnis, A., Koutsoukos P.G., 2008. An atomic force microscopy study of the growth of calcite in the presence of sodium sulfate. Chemical Geology, 253, 243-251.

Zhang, Y., Dawe, R.A., 2000. Influence of Mg2+ on the kinetics of calcite precipitation and calcite crystal morphology. Chemical Geology 163, 129-138.

Zhong S.J. and Mucci A., 1989. Calcite and aragonite precipitation from seawater solutions of various salinities – precipitation rates and overgrowth compositions. Chemical Geology, 78, 283-299.

Zhong S.J. and Mucci A., 1993. Calcite precipitation in seawater using a constant addition technique – A new overall reaction kinetic expression. Geochimica et Cosmochimica Acta, 57, 1409-1417.

6 Concluding remarks and perspectives

This thesis represents a series of related studies aimed at improving our understanding of the fate and consequences of CO_2 injected into basalts as a part of carbon sequestration efforts. Several significant questions have been addressed including:

1. Does basalt actually mineralize CO_2?
2. Is it environmentally safe, or will toxic metals be released into the environment during the operation?
3. How can we increase the release rate of divalent cations to solution so that the precipitation rate of carbonates can be enhanced?

The results from this study have shown that the neutralization of CO_2-rich waters by their interactions with subsurface basalt may provide an effective means to fix CO_2 as carbonate minerals. Since this process involves dissolution of the basalt, toxic metals will be released into the solution. However, analysis of the groundwater beneath the Hekla volcano, which has been used as a natural analogue to CO_2 sequestration, does not show any sign of being polluted with toxic elements. The concentrations of these elements are several orders of magnitude below the drinking water limits given by the World Health Organization in all water samples. From reactive transport modeling, it is clear that the mobility of these metals is limited by incorporation in carbonates and Fe(III) (oxy)hydroxides because the fluid is neutralized by basalt dissolution. The model calculations also suggest that this limited mobility stems from the high pH attained by aqueous fluids during their interaction with basalts. As the pH rises to 9 and higher, toxic metal bearing solids become less soluble and toxic metals adsorb more readily onto mineral surfaces. If CO_2 were injected into less basic rocks (e.g. sandstones) model calculations suggest that pH would not rise dramatically. In such cases toxic metal mobility could pose an environmental hazard.

The limiting step to mineralization of CO_2 in basalt is the release of divalent cations (Ca, Mg and Fe). One way to enhance the dissolution rate of the basaltic glass and thereby enhancing the release rate of these elements is adding a ligand which complexes aqueous Al^{3+}. The experimental results show that aqueous sulphate increases basaltic glass dissolution rates in acid conditions due to complexation of Al^{3+}, while adding 0.05 M SO_4^{2-} triples the dissolution rate of the basaltic glass at pH 5 at 50 °C. There was no effect of SO_4^{2-} in alkaline conditions.

The addition of SO_4^{2-} seems to have a negative effect on the precipitation rate of calcite, a concentration on 0.005M SO_4^{2-} inhibits the precipitation rate by ~40% at pH 9.1. The degree to which this degree of calcite precipitation inhibition effects the overall carbon mineralization process in basalts has yet to be assessed through comprehensive reactive transport model calculations.

The studies comprising this thesis, however, only represent a start to the development of the knowledge base necessary for supporting the successful sequestration of CO_2 in basalts via precipitation of carbonate minerals. Other critical laboratory studies need to focus on the dissolution rates of crystalline basalt containing olivines, plagioclase and pyroxenes because the dissolution rates of such rocks will be different from that of glass and thereby affect the geochemical modeling. As the carbonization process takes place, precipitation of secondary phases will, most likely, change the reactive surface area of the basalt, and thus decrease the dissolution rate. A better understanding of the effect of mineral coatings on the dissolution rate of basalt is needed. Besides, the thermodynamic effects of adsorption of trace elements on carbonates, Al oxides and Fe (oxy) hydroxides should be investigated to enable quantitative modeling of the behavior of these metals during carbon sequestration.

This thesis aimed in part at methods to optimize carbon sequestration efforts in basalts. As discussed above if it is possible to find a way to remove aqueous Al^{3+} from solution, divalent metal release to solution by silicates and thus CO_2 mineralization can be accelerated, since the rate limiting step of CO_2 mineralization in basalt is the release rate of divalent cations. This can be done either by 1) promoting the precipitation of Al-hydroxides, or any other Al-bearing phase which does not contain divalent cations, or 2) by adding a ligand which can complex aqueous Al^{3+} without decreasing the precipitation rate of carbonate minerals. For example, F^- has shown to strongly increase the basaltic glass dissolution rate (Wolff-Boenisch et al., 2004) while organics, like oxalic acid showed a smaller accelerating effect (Oelkers and Gislason, 2001).
Such efforts would have the additional benefit of avoiding precipitation of Ca- Fe- and Mg-bearing secondary minerals such as smectites, zeolites, and clays.

Carbon sequestration in basalts also involves the precipitation of carbonates, dominantly calcite. The precipitation rates of calcite are fast compared to basaltic glass dissolution, so accelerating calcite precipitation rates likely would have only a small affect on sequestration efforts. In contrast, maintaining solutions that are supersaturated with respect to calcite is

essential to assure its precipitation. Ways to increase or at least maintain supersaturation of calcite is by increasing pH or the amount of Ca^{2+} and carbonate in solution. The Ca^{2+} concentration can be increased by enhancing the basalt dissolution rate, while the amount of carbonate can be increased by raising the amount of CO_2 in the water. Anions that could complex calcite in aqueous solution should be avoided, as the precipitation of other calcium bearing phases.

Calcite, however, is not the only carbonate which might precipitate under these conditions. Iron and magnesium carbonates could also form if both thermodynamically favorable and not kinetically inhibited. Much work is ongoing in these areas. Recent work of Saldi et al, (2009) suggests that magnesite precipitation is inhibited at low temperature. In contrast, Gysi et al, (2008) found that Mg-Fe carbonates are the first carbonates to becomes saturated during CO_2 rich water-basalt interactions; some Mg-Fe carbonates have been found to precipitate during laboratory experiments of water-basalt interaction (Gysi et al, 2009).

Although laboratory studies, such as those described above provide insight into the behavior of processes on a small scale such information needs to be upscaled to provide industrial methods for the sequestration of carbon. Some challenges to upscaling laboratory observations to an industrial scale include quantifying 1) the reactive surface area of dissolving and precipitating minerals, 2) the subsurface hydrology, such as flow paths and permeability. Such information cannot be obtained without direct field observations. Field scale experiments with in-situ mineral carbonation are thus essential to understand and optimize the processes taking place when CO_2-rich fluid reacts with basalt towards the efficient and safe sequestration of carbon in these environments.

REFERENCES

Gysi, A., Stefánsson, A., 2008. Numerical modelling of CO_2-water-basalt interaction. Mineralogical Magazine 72, 55-59.

Gysi, A., Stefánsson, A., 2009. CO_2-water-basalt interaction: Geochemical modelling and experiments. Geochemica et Cosmochemica Acta 73, A483.

Oelkers, E.H., Gislason, S.R., 2001. The mechansim, rates and consequences of basaltic glass dissolution: I. An experimental study of the dissolution rates of basaltic glass as as function of aqueous Al, Si and oxalic acid concentration at 25 °C and pH = 3 and 11.

Saldi, G., Jordan, G., Schott, J., Oelkers, E.H., 2009. Magnesite growth rates as a function of temperature and saturation state. Geochimica et Cosmochimica Acta, In Press.

Wolff-Boenisch, D., Gislason, S.R., Oelkers, E.H., 2004. The effect of fluoride on the dissolution rates of natural glasses at pH 4 and 25 °C. Geochimica et Cosmochimica Acta 68, 4571-4582.

Appendices:

Appendix I – Flaathen et al., 2008. The effect of aqueous sulphate on basaltic glass dissolution rates. Mineralogical Magazine 72, 39-41.

Appendix II – Chemistry of springs water samples (Flaathen et al., 2009)

Mineralogical Magazine, February 2008, Vol. 72(1), pp. 39–41

The effect of aqueous sulphate on basaltic glass dissolution rates

T. K. FLAATHEN[1,*], E. H. OELKERS[1] AND S. GISLASON[2]

[1] LMTG-Université de Toulouse-CNRS-IRD-OMP, 14 Avenues Edouard Belin, 31400 Toulouse, France
[2] Institute of Earth Sciences, University of Iceland, Sturlugata 7, 101 Reykjavík, Iceland

ABSTRACT

Steady-state dissolution rates of basaltic glass were measured in mixed-flow reactors at 50ºC at pH 3 and 4 as a function of aqueous sulphate concentration. Dissolution rates in the presence of 0.1 moles/kg SO_4^{2-} were found to be ~3 times greater than those in corresponding SO_4^{2-} free solutions. This rate increase is found to be approximately consistent with that calculated using a rate equation previously proposed by Gislason and Oelkers (2003). These results suggest that the addition of sulphate to injected CO_2 may facilitate CO_2 sequestration in basalts by accelerating basaltic glass dissolution rates thus more rapidly releasing aqueous Ca and Mg to solution.

KEYWORDS: basaltic glass, dissolution rates, CO_2 sequestration, kinetics, aqueous sulphate.

Introduction

INCREASED CO_2 concentration in the atmosphere is thought to provoke climate change. To reduce the emission of this greenhouse gas to the atmosphere, the possibility of sequestrating CO_2 in basaltic rocks is being investigated (McGrail *et al.*, 2006; Gislason *et al.*, 2007; Matter *et al.*, 2007). This process involves dissolution of the basaltic rock and release of divalent metallic cations such as Ca^{2+}. The Ca^{2+} ions then react with dissolved CO_2 and precipitate as carbonate minerals. One way to enhance the amount of CO_2 that can be sequestered in this process is to increase the amount of Ca^{2+} ions available for carbonate precipitation. The dissolution rate of basaltic glass decreases with increased activity of Al^{3+} (Oelkers and Gislason, 2001; Gislason and Oelkers, 2001). By adding an aqueous species that leads to Al-complex formation, the dissolution rate of basaltic glass will increase (Wolff-Boenisch *et al.*, 2004.).

One other implication of this work is that power plants emitting CO_2 often produce sulphuric gases as a bi-product. The high reactivity and oxidation capacity of sulphuric species make them difficult to store on land. By adding sulphate to the injected CO_2 solution, it may be possible to store the sulphate safely underground. The purpose of this study was to investigate how much sulphate enhances the dissolution rate of basaltic glass.

* E-mail: flaathen@lmtg.obs-mip.fr
DOI: 10.1180/minmag.2008.072.1.39

Materials and methods

The dissolution-rate experiments were performed with Stapafell basaltic glass in titanium and polypropylene mixed-flow reactor systems at different pH and with solutions containing different amounts of sulphate (Oelkers and Gislason, 2001). The grain size was 125–250 μm and the BET surface area was measured at 1.524 m^2/g. The geometric surface area was estimated to be 120 cm^2/g assuming that the glass powder used consisted of identical 187.5 μm cubes. This method of estimating the geometric surface area was used in the work of Gislason and Oelkers (2003). The experiments were all performed at 50±2ºC. Information about flow rates and the composition of the various inlet solutions used in this study is given in Table 1.

The dissolution rate of basaltic glass was described by Gislason and Oelkers (2003) and can be written

TABLE 1. The composition of the solutions and flow rates used in the experiments.

Experiment	pH (25ºC) input	HCl (moles/kg)	NaCl (moles/kg)	Na_2SO_4 (moles/kg)	Ionic strength (moles/kg)	Flow rate (g/min)
BG6 D	3.05	0.00110	0.009	–	0.010	0.424
BG7 A	3.02	0.00132	0.008	0.001	0.012	0.401
BG7 B	3.02	0.00142	–	0.010	0.030	0.343
BG7 C	3.01	0.00245	–	0.050	0.136	0.371
BG7 D	3.03	0.00332	–	0.100	0.261	0.384
BG6 A	3.97	0.00009	0.010	–	0.010	0.382
BG6 B	3.96	0.00010	0.008	0.001	0.011	0.406
BG6 C	3.99	0.00014	–	0.010	0.029	0.402
BG6 E	4.01	0.00024	–	0.050	0.135	0.356
BG6 F	3.96	0.00042	–	0.100	0.259	0.408

$$r_{+,geo} = A_A \exp^{-(E_A/RT} \left(\frac{a^3_{H^+}}{a_{Al^{3+}}} \right)^{1/3} \quad (1)$$

where $r_{+,geo}$ signifies the geometric surface area normalized steady-state basaltic glass dissolution rate at far-from-equilibrium conditions, A_A refers to a constant equal to $10^{-5.6}$ (mol of Si) cm^2/s, E_A, designates a pH independent activation energy equal to 25.5 kJ/mol, R stands for the gas constant, T signifies temperature in K and a_i represents the activity of the subscripted aqueous species. By decreasing the activity of Al^{3+}, the dissolution rate increases. A study performed by Wolff-Boenisch *et al.* (2004) showed that by complexing Al^{3+} ions with fluorine, they could increase the dissolution rate of the basaltic glass by an order of magnitude or more.

Results

Surface-reaction controlled, far-from-equilibrium basaltic glass dissolution rates as a function of aqueous solution composition at 50ºC can be predicted using equation 1. Figure 1 shows the dissolution rates of basaltic glass with different amounts of sulphate. The curves in the figure were generated using aqueous activities computed with PHREEQC 2.12.5 (Parkhurst and Appelo, 1999) at a total Al concentration of 10^{-6} moles/kg. The basaltic glass dissolution rates increases by increased concentration of aqueous sulphate at acid to neutral conditions. Basaltic glass is calculated to dissolve 5.5 times faster in a 0.1 moles/kg SO_4 solution than in a SO_4-free solution at pH = 4. In contrast, there is no predicted effect of sulphate on basaltic glass dissolution rates at pH >7.5. The lack of effect at basic conditions can be explained by the lack of Al-SO_4 complexation at these pH values.

To further investigate the effect of sulphate on the dissolution rate of basaltic glass at far-from-equilibrium conditions, experiments using mixed-flow reactors were performed at pH 3 and 4. As shown in Fig. 2, a solution with 0.001 moles/kg sulphate almost doubles the dissolution rate while 0.1 moles/kg of sulphate triples the dissolution rate of basaltic glass. Calculations generated using equation 1 (Fig. 1) suggests that basaltic glass dissolution rates increase by a factor of 1.5 and 5.5 in 0.001 moles/kg and 0.1 moles/kg aqueous sulphate solutions, respectively, compared to that in sulphate-free solutions.

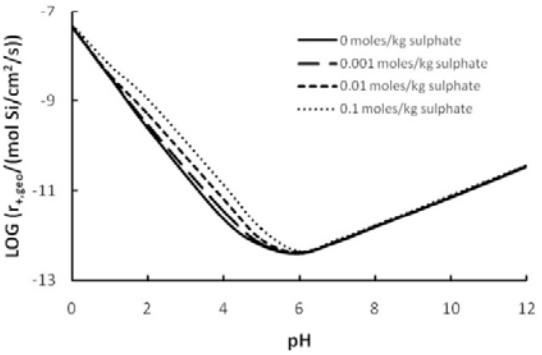

FIG. 1. The logarithm of the dissolution rate *vs.* pH for basaltic glass at 50ºC. The aqueous activities were computed using PHREEQC 2.12.5 and equation 1. The total Al concentration was 10^{-6} moles/kg and the sulphate concentration is given in the legend.

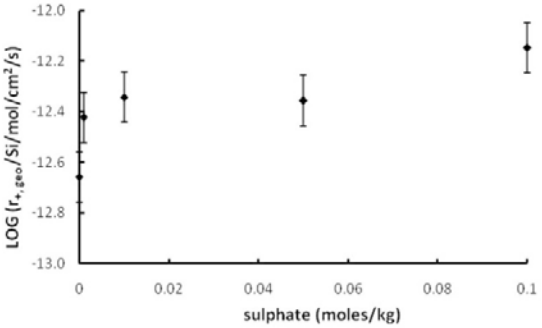

FIG. 2. Variation of measured steady-state basaltic glass dissolution rates obtained from Al and Si-free inlet solutions at pH 4 with aqueous SO_4^{2-} concentration at 50ºC. The error bars correspond to a 0.1 log unit uncertainty, which is consistent with the 20% uncertainty estimated for these data.

Discussion and conclusions

(1) Preliminary results show that the effect of aqueous sulphate on basaltic glass dissolution rates calculated using equation 1 is approximately consistent with their experimentally measured counterparts. This approximate coherence provides support for using this equation for the prediction of the reactive behaviour of basaltic glass in complex natural systems.

(2) Aqueous sulphate is found to increase basaltic glass dissolution rates. As such, the addition of sulphate to injected CO_2 may enhance carbonate mineral sequestration during carbon sequestration in basaltic rocks. Such co-injection may prove to be an effective method for the safe storage of sulphur emissions from power plants.

Acknowledgements

We are grateful to Oleg Pokrovsky, Jacques Schott, Per Aagaard and Guðmundur B. Ingvarsson for helpful discussions during the course of this study. Support from Reykjavik Energy and the European Community through the MIN-GRO Research and Training Network (MRTN-CT-2006-035488) is gratefully acknowledged.

References

Gislason, S.R. and Oelkers, E., (2003) Mechanism, rates, and consequences of basaltic glass dissolution; II. An experimental study of the dissolution rates of basaltic glass as a function of pH and temperature. *Geochimica et Cosmochimica Acta*, **67**, 3817–3832.

Gislason S. R., Gunnlaugsson E., Broeker W. S., Oelkers E. H., Matter J. M., Stefánsson A., Arnórsson S., Björnsson G., Fridriksson T. and Lackner K. (2007) Permanent CO_2 sequestration into basalt: the Hellisheidi, Iceland project. *Geophysical Research Abstracts*, **9**, 07153, 2007. European Geosciences Union General Assembly 2007 Vienna, Austria.

Matter, J.M., Takahashi, T. and Goldberg, D. (2007) Experimental evaluation of in situ CO_2-water-rock reactions during CO_2 injection in basaltic rocks: Implications for geological CO_2 sequestration. *Geochemistry Geophysics Geosystems*, **8**, Q02001, doi:10.1029/2006GC001427.

McGrail, B.P., Schaef, H.T., Ho, A.M., Chien, Y.J. and Dooley, J. (2006) Potential for carbon dioxide sequestration in flood basalts. *Journal of Geophysical Research*, **111**, B12201, doi: 10.1029/2005JB004169.

Oelkers, E.H. and Gislason, S.R. (2001) The mechanism, rates and consequences of basaltic glass dissolution: I. An experimental study of the dissolution rates of basaltic glass as a function of aqueous Al, Si and oxalic acid concentration at 25ºC and pH = 3 and 11. *Geochimica et Cosmochimica Acta*, **65**, 3671–3681.

Parkhurst, D.L. and Appelo, C.A.J. (1999) *User's guide to PHREEQC (Version 2) – A computer program for speciation, batch-reaction, one-dimensional transport, and inverse geochemical calculations*. USGS-Report 99-4259.

Wolff-Boenisch, D., Gislason, S.R. and Oelkers, E.H. (2004) The effect of fluoride on the dissolution rates of natural glasses at pH 4 and 25ºC. *Geochimica et Cosmochimica Acta*, **68**, 4571–4582.

Appendix II - Chemisty of spring water from the Hekla groundwater system (Flaathen et al., 2009)

Sample number	Spring number	Sampling Date and time	Sampling Location	T (°C) (in situ)	T (°C) (pH meas.)	pH (Electrode)	pH (in situ) (PHREEQC)[a]	Charge balance (% error) (PHREEQC)[a]
Drinking water guidelines[h]								
06HE010	1	02/08/2006 14:10	64.086° N, 19.744° W	4.9	23.1	8.78	9.04	5.4
88-3001	1	23/04/1988 12:47	64.085° N, 19.798° W	4.7	3.2	9.00	8.98	7.6
91-3014	1	20/01/1991 16:15	64.085° N, 19.798° W	4.6	18.8	8.36	8.54	-0.3
91-3096	1	13/02/1991 14:10	64.085° N, 19.714° W	4.7	21.5	8.65	8.88	0.0
91-3147	1	23/06/1991 14:05	64.085° N, 19.798° W	4.8	22.1	8.70	8.94	-3.4
06HE012	2	02/08/2006 15:35	64.085° N, 19.714° W	4.7	23.1	7.27	7.41	5.5
88-3013	2	29/06/1988 14:15	64.085° N, 19.714° W	4.3	5.5	7.58	7.59	1.0
91-3013	2	20/01/1991 15:17	64.085° N, 19.714° W	4.1	19.4	7.54	7.67	0.7
91-3143	2	23/06/1991 12:55	64.085° N, 19.714° W	4.5	22.0	7.41	7.55	0.0
91-3172	2	17/07/1991 23:20	64.085° N, 19.714° W	4.3	20.4	7.53	7.67	-1.2
91-3173	2	17/07/1991 23:30	64.085° N, 19.714° W	4.3	21.4	7.47	7.61	-0.2
92-3026	2	19/10/1992 19:00	64.085° N, 19.714° W	4.2	21.2	7.86		
06HE009	3	02/08/2006 13:30	64.082° N, 19.744° W	3.8	23.4	7.85	8.03	7.9
88-3002	3	23/04/1988 14:30	64.082° N, 19.751° W	3.9	3.50	8.87	8.86	3.5
91-3015	3	20/01/1991 16:30	64.082° N, 19.751° W	3.8	19.5	8.38	8.58	-0.4
91-3095	3	13/02/1991 13:50	64.082° N, 19.751° W	3.9	22.2	8.55	8.79	-5.8
91-3146	3	23/06/1991 14:00	64.082° N, 19.751° W	4.1	22.1	8.46	8.69	-5.3
88-3003	4	23/04/1988 14:57	64.079° N, 19.754° W	4.0	2.0	8.46	8.43	0.2
91-3016	4	20/01/1991 16:52	64.079° N, 19.754° W	3.3	19.7	7.92	8.08	-0.5
91-3094	4	13/02/1991 13:30	64.079° N, 19.754° W	3.4	21.0	8.06	8.24	-4.4
91-3145	4	23/06/1991 13:45	64.079° N, 19.754° W	3.7	22.1	7.93	8.10	-3.5
06HE011	5	02/08/2006 15:00	64.079° N, 19.738° W	3.8	23.1	7.63	7.79	5.9
88-3004	5	23/04/1988 16:30	64.079° N, 19.743° W	4.0	2.8	7.82	7.81	2.7
88-3005	5	23/04/1988 17:33	64.079° N, 19.743° W					
88-3014	5	29/06/1988 17:15	64.079° N, 19.743° W	4.0	4.3	7.75	7.75	1.9
91-3017	5	30/01/1991 17:30	64.079° N, 19.743° W	3.2	20.2	7.84	8.00	0.7
91-3093	5	13/02/1991 13:15	64.079° N, 19.743° W	3.3	22.5	7.88	8.06	-8.6
91-3144	5	23/06/1991 13:30	64.079° N, 19.743° W	3.7	22.3	7.89	8.06	-2.9
88-3015	6	29/06/1988 23:00	64.013° N, 19.913° W	5.0	5.5	8.62	8.63	1.6
88-3016	7	30/06/1988 11:45	64.012° N, 19.955° W	5.2	7.5	8.67	8.70	2.0
88-3018	8	30/06/1988 17:00	64.006° N, 19.955° W	5.0	7.0	8.67	8.70	3.6
88-3020	9	01/07/1988 10:55	64.001° N, 19.866° W	4.5	6.8	8.79	8.82	3.5
91-3012	9	20/01/1991 14:00	64.001° N, 19.866° W	4.3	18.8	8.51	8.70	2.1
91-3084	9	12/02/1991 17:52	64.001° N, 19.866° W	4.4	22.0	8.56	8.80	-1.1
91-3148	9	23/06/1991 15:10	64.001° N, 19.866° W	4.7	22.2	8.58	8.81	-5.1
88-3017	10	30/06/1988 14:20	63.998° N, 20.010° W	8.0	9.1	8.85	8.87	1.9
88-3022	11	01/07/1988 15:35	63.986° N, 19.915° W	3.5	4.2	8.33	8.34	1.0
88-3032	12	06/07/1988 13:35	63.965° N, 19.909° W	1.9	2.9	8.11	8.12	-0.1
91-3010	12	20/01/1991 11:55	63.965° N, 19.909° W	2.0	20.1	7.91	8.09	0.6
88-3021	12	01/07/1988 13:45	63.981° N, 19.932° W	2.5	3.6	8.13	8.14	9.7
91-3011	12	20/01/1991 12:35	63.981° N, 19.932° W	2.3	19.6	7.96	8.13	0.3
91-3083	12	12/02/1991 17:07	63.981° N, 19.932° W	2.3	21.3	8.01	8.21	-0.1
91-3142	12	22/06/1991 21:00	63.981° N, 19.932° W	2.8	22.3	8.01	8.21	-2.5
06HE007	13	02/08/2006 10:25	63.981° N, 19.915° W	2.3	23.2	7.95	8.16	5.4
91-3082	14	12/02/1991 16:40	63.965° N, 19.909° W	1.9	22.7	8.02	8.24	0.1
91-3141	14	22/06/1991 20:25	63.965° N, 19.909° W	2.3	21.9	7.85	8.03	-1.4
06HE005	15	01/08/2006 13:50	63.961° N, 19.963° W	3.4	23.1	8.94	9.22	1.8
88-3031	15	06/07/1988 10:05	63.961° N, 19.968° W	3.0	4.4	9.15	9.17	6.5
91-3002	15	19/01/1991 10:22	63.961° N, 19.968° W	2.9	20.5	8.91	9.16	1.4
91-3085	15	12/02/1991 18:45	63.961° N, 19.968° W	2.9	21.0	8.93	9.19	2.8
91-3140	15	22/06/1991 19:15	63.961° N, 19.968° W	3.3	22.3	8.94	9.21	0.5
92-3010	15	15/03/1992 14:00	63.961° N, 19.968° W	3.0	22.0	8.77		
06HE004	16	01/08/2006 12:40	63.957° N, 19.977° W	3.9	23.2	7.98	8.17	2.1
88-3033	16	06/07/1988 17:20	63.956° N, 19.981° W	3.2	4.4	8.05	8.06	0.3
91-3001	16	19/01/1991 09:55	63.956° N, 19.981° W	3.0	21.5	8.05	8.25	0.5
91-3086	16	12/02/1991 19:17	63.956° N, 19.981° W	2.9	21.5	7.86	8.04	-0.1
91-3139	16	22/06/1991 18:55	63.956° N, 19.981° W	3.4	22.2	7.92	8.10	-2.0
92-3009	16	15/03/1992 13:30	63.955° N, 19.980° W	2.8	22.4	7.99		
06HE006	17	01/08/2006 14:50	63.942° N, 19.931° W	4.5	23.4	7.76	7.93	1.6

Sample number	Spring number	Sampling Date and time	Sampling Location	T (°C) (in situ)	T (°C) (pH meas.)	pH (Electrode)	pH (in situ) (PHREEQC)[a]	Charge balance (% error) (PHREEQC)[a]
88-3023	18	02/07/1988 21:00	63.941° N, 19.938° W	4.2	4.9	7.52	7.53	1.2
90-3001	18	01/09/1990	63.941° N, 19.938° W	4.5	3.8	7.45	7.44	2.1
90-3027	18	25/04/1990	63.941° N, 19.938° W	4.6	4.6	7.32	7.32	2.6
91-3008	18	20/01/1991	63.941° N, 19.938° W	4.2	18.0	7.34	7.46	-0.5
91-3088	18	13/02/1991 09:30	63.941° N, 19.938° W	4.9	21.4	7.47	7.61	-1.7
91-3124	18	24/02/1991 13:32	63.941° N, 19.938° W	4.5	22.1	7.42	7.56	-3.2
91-3125	18	09/03/1991 11:16	63.941° N, 19.938° W	4.3	22.0	7.47	7.62	-4.6
91-3126	18	01/04/1991 07:44	63.941° N, 19.938° W	4.3	21.6	7.55	7.70	-2.1
91-3127	18	16/04/1991 08:55	63.941° N, 19.938° W	4.3	22.0	7.44	7.58	-2.3
91-3128	18	09/05/1991 17:00	63.941° N, 19.938° W	4.3	21.8	7.41	7.55	-2.4
91-3129	18	01/06/1991 11:14	63.941° N, 19.938° W	4.3	22.1	7.66	7.81	-2.6
91-3138	18	22/06/1991 18:10	63.941° N, 19.938° W	4.6	22.1	7.44	7.58	-1.9
91-3213	18		63.941° N, 19.938° W	4.3	20.4	7.34	7.47	0.7
92-3011	18	15/03/1992 14:30	63.941° N, 19.938° W	4.2	22.2	7.55		
92-3012	18	15/03/1992 15:00	63.941° N, 19.938° W	4.6	21.3	7.82		
92-3013	18	01/11/1991 09:25	63.941° N, 19.938° W	4.3	22.0	7.57		
92-3014	18	10/11/1991 10:25	63.941° N, 19.938° W	4.3	22.0	7.58		
92-3015	18	25/12/1991 16:15	63.941° N, 19.938° W	4.3	21.9	7.64		
92-3016	18	25/01/1992 16:40	63.941° N, 19.938° W	4.3	21.5	7.52		
88-3024	19	03/07/1988 12:15	63.940° N, 19.920° W	4.7	6.2	7.59	7.60	-0.1
91-3009	19	20/01/1991 09:23	63.940° N, 19.920° W	4.5	17.8	7.53	7.64	0.5
91-3089	19	13/02/1991 09:56	63.940° N, 19.920° W	4.9	22.7	7.65	7.80	-0.5
91-3137	19	22/06/1991 17:55	63.940° N, 19.920° W	4.8	22.2	7.66	7.81	-1.9
06HE008	20	02/08/2006 11:20	64.009° N, 19.883° W	5.0	23.0	8.56	8.80	5.8
88-3030	20	05/07/1988 15:55	63.924° N, 20.186° W	3.8	5.0	8.29	8.30	1.5
91-3003	20	19/01/1991 11:05	63.924° N, 20.186° W	3.8	19.6	8.00	8.16	0.3
91-3081	20	12/02/1991 15:00	63.924° N, 20.186° W	3.8	21.0	8.16	8.36	0.4
91-3136	20	22/06/1991 16:35	63.924° N, 20.186° W	4.3	21.9	8.07	8.26	-0.5
92-3008	20	15/03/1992 12:30	63.924° N, 20.186° W	3.8	22.5	8.09		
88-3029	21	05/07/1988 13:25	63.883° N, 20.248° W	2.9	5.3	7.58	7.60	1.8
91-3004	21	19/01/1991 11:47	63.883° N, 20.248° W	3.0	19.5	7.47	7.61	-0.4
91-3080	21	12/02/1991 14:23	63.883° N, 20.248° W	3.0	22.4	7.58	7.75	0.3
91-3135	21	22/06/1991 16:00	63.883° N, 20.248° W	3.4	22.0	7.57	7.73	-2.2
92-3007	21	15/03/1992 12:00	63.883° N, 20.248° W	3.0	22.0	7.82		
88-3028	22	05/07/1988 10:00	63.853° N, 20.158° W	2.7	5.3	7.46	7.49	2.8
91-3005	22	19/01/1991 13:20	63.853° N, 20.158° W	2.7	20.1	7.33	7.48	0.1
91-3079	22	12/02/1991 13:30	63.853° N, 20.158° W	2.6	21.0	7.28	7.43	0.5
91-3134	22	22/06/1991 15:05	63.853° N, 20.158° W	3.0	21.8	7.24	7.39	-2.2
88-3027	23	04/07/1988 17:45	63.833° N, 20.133° W	2.9	4.7	7.90	7.92	2.2
91-3006	23	19/01/1991 14:38	63.833° N, 20.133° W	2.9	19.9	7.63	7.78	-3.4
91-3078	23	12/02/1991 12:23	63.833° N, 20.133° W	2.9	20.7	7.66	7.82	0.8
91-3133	23	22/06/1991 14:25	63.833° N, 20.133° W	3.4	22.0	7.66	7.82	-2.9
92-3006	23	15/03/1992 11:15	63.833° N, 20.133° W	3.0	22.4	7.75		
06HE003	24	01/08/2006 10:40	63.833° N, 20.114° W	3.3	23.2	7.78	7.96	2.0
06HE002	25	31/07/2006 17:00	63.822° N, 20.067° W	2.8	22.3	7.85	8.03	2.9
88-3026	25	04/07/1988 13:55	63.822° N, 20.071° W	2.5	3.7	8.04	8.05	0.6
91-3007	25	19/01/1991	63.822° N, 20.071° W	2.5	20.0	7.70	7.85	-5.2
91-3076	25	12/02/1991 11:25	63.822° N, 20.071° W	2.5	21.0	7.76	7.93	0.2
91-3132	25	22/06/1991 14:00	63.822° N, 20.071° W	2.8	21.6	7.86	8.04	-3.3
92-3005	25	14/03/1992 18:30	63.822° N, 20.071° W	2.6	22.0	7.68		
06HE001	26	31/07/2006 15:25	63.809° N, 20.052° W	3.2	22.1	8.22	8.45	3.7
91-3130	26	22/06/1991 12:00	63.809° N, 20.056° W	3.0	21.5	8.18	8.40	-1.6

[a] PHREEQC2 computer program (Parkhurst and Appelo, 1999)

[b] Inductively coupled plasma atomic emission spectroscopy

[c] The samples were titrated with 0.1 N HCl and 0.1 M NaOH

[d] Ionchromatography

[e] Inductively coupled plasma field mass spectroscopy

[f] Atomic fluorescence spectroscopy

[g] Mass spectrometry

[h] Drinking water guidelines are from WHO 2006.

[i] Drinking water guideline from Counsil Directive 98/83/EC, 1998

b.d. = beneath detection limit

Sample number	SiO2 (mmol/kg) (ICP-AES)[b]	Na (mmol/kg) (ICP-AES)[b]	K (mmol/kg) (ICP-AES)[b]	Ca (mmol/kg) (ICP-AES)[b]	Mg (mmol/kg) (ICP-AES)[b]	DIC (mmol/kg) (PHREEQC)[a]	Alk (meq./kg) (Titration)[c]	S (mmol/kg) (ICP-AES)[b]	SO4-2 (mmol/kg) (IC)[d]	Cl (mmol/kg) (Ion-selective electrode)	F (mmol/kg) (Ion-selective electrode)
Drinking water guidelines[h]											0.0790
06HE010	0.329	0.974	0.0330	0.180	0.120	0.991	0.982	0.123	0.109	0.213[d]	0.0304[d]
88-3001	0.296	1.02	0.0320	0.184	0.121	0.916	0.901	0.133		0.233	0.029
91-3014	0.325	0.979	0.0240	0.180	0.120	1.07	1.05	0.139		0.246	0.0
91-3096	0.318	0.944	0.0241	0.178	0.123	1.06	1.05	0.123		0.238	0.029
91-3147	0.305	0.837	0.0242	0.169	0.116	1.01	1.00	0.131		0.253	0.030
06HE012	0.438	1.84	0.0501	0.494	0.671	3.32	2.95	0.221	0.218	0.348[d]	0.0548[d]
88-3013	0.408	2.35	0.0616	0.668	0.752	3.88	3.57	0.439		0.646	0.0557
91-3013	0.431	2.14	0.0478	0.577	0.671	3.46	3.23	0.383		0.577	0.0530
91-3143	0.437	2.17	0.0453	0.652	0.791	3.82	3.50	0.419		0.714	0.0518
91-3172	0.437	2.09	0.0427	0.609	0.743	3.64	3.40	0.416		0.659	0.0499
91-3173	0.424	2.17	0.0436	0.626	0.758	3.72	3.44	0.424		0.680	0.0495
92-3026						3.34					
06HE009	0.377	1.18	0.0353	0.259	0.230	1.39	1.34	0.150	0.134	0.226[d]	0.0381[d]
88-3002	0.308	1.06	0.031	0.194	0.137	1.09	1.069	0.147		0.241	0.0341
91-3015	0.328	0.99	0.0225	0.176	0.122	1.04	1.02	0.159		0.246	0.0322
91-3095	0.303	0.84	0.0212	0.163	0.119	1.041	1.03	0.141		0.254	0.0311
91-3146	0.308	0.86	0.0234	0.172	0.128	1.07	1.05	0.148		0.261	0.0318
88-3003	0.332	1.25	0.0379	0.303	0.258	1.74	1.71	0.182		0.285	0.0377
91-3016	0.347	1.06	0.0243	0.219	0.181	1.29	1.25	0.173		0.268	0.0370
91-3094	0.326	0.90	0.0233	0.212	0.180	1.28	1.25	0.148		0.271	0.0354
91-3145	0.333	0.99	0.0282	0.241	0.202	1.42	1.38	0.156		0.302	0.0357
06HE011	0.384	1.39	0.0391	0.334	0.353	1.99	1.88	0.161	0.157	0.257[d]	0.0426[d]
88-3004	0.366	1.82	0.0496	0.521	0.506	2.75	2.61	0.310		0.454	0.0364
88-3005	0.386	2.22	0.0573	0.647	0.687			0.424		0.623	0.0432
88-3014	0.369	1.90	0.0527	0.532	0.535	2.92	2.75	0.329		0.491	0.0417
91-3017	0.357	1.20	0.0264	0.274	0.252	1.63	1.57	0.174		0.285	0.0395
91-3093	0.348	1.06	0.0245	0.261	0.241	1.58	1.53	0.169		0.559	0.038
91-3144	0.347	1.16	0.0290	0.295	0.270	1.77	1.72	0.177		0.333	0.038
88-3015	0.323	0.96	0.0371	0.167	0.122	1.05	1.040	0.108		0.240	0.0280
88-3016	0.314	0.93	0.0368	0.156	0.112	0.99	0.98	0.103		0.229	0.0278
88-3018	0.320	0.98	0.0379	0.161	0.121	1.02	1.00	0.103		0.234	0.0278
88-3020	0.341	1.01	0.0417	0.190	0.141	1.08	1.07	0.122		0.258	0.0302
91-3012	0.371	1.01	0.0264	0.180	0.125	1.04	1.03	0.120		0.274	0.0337
91-3084	0.371	0.82	0.0230	0.163	0.120	0.96	0.95	0.088		0.271	0.0295
91-3148	0.343	0.81	0.0274	0.174	0.131	1.07	1.06	0.112		0.283	0.0317
88-3017	0.311	0.89	0.0348	0.149	0.109	0.93	0.91	0.101		0.246	0.0252
88-3022	0.348	1.17	0.0350	0.399	0.224	1.67	1.64	0.187		0.321	0.0626
88-3032	0.339	1.14	0.0361	0.412	0.240	1.72	1.67	0.199		0.336	0.0748
91-3010	0.367	1.21	0.0280	0.458	0.253	1.61	1.57	0.279		0.428	0.0653
88-3021	0.333	1.31	0.0396	0.386	0.232	1.69	1.64	0.023		0.389	0.0551
91-3011	0.341	1.29	0.0300	0.398	0.229	1.60	1.56	0.257		0.428	0.0554
91-3083	0.348	1.19	0.0269	0.399	0.239	1.58	1.54	0.248		0.411	0.0520
91-3142	0.343	1.19	0.0305	0.4019	0.242	1.62	1.58	0.261		0.471	0.0540
06HE007	0.352	1.23	0.0368	0.367	0.208	1.34	1.30	0.230	0.216	0.378[d]	0.0599[d]
91-3082	0.356	1.11	0.0274	0.432	0.233	1.48	1.45	0.258		0.431	0.0569
91-3141	0.359	1.20	0.0290	0.4902	0.267	1.68	1.63	0.313		0.513	0.0653
06HE005	0.289	1.27	0.0358	0.297	0.176	1.39	1.36	0.204	0.192	0.393[d]	0.0383[d]
88-3031	0.268	1.36	0.0381	0.313	0.191	1.37	1.33	0.175		0.401	0.0382
91-3002	0.277	1.28	0.029	0.304	0.184	1.484	1.45	0.165		0.377	0.0365
91-3085	0.291	1.19	0.0270	0.303	0.189	1.39	1.36	0.156		0.369	0.0345
91-3140	0.277	1.18	0.0293	0.3061	0.188	1.44	1.40	0.173		0.410	0.0367
92-3010	0.269	1.14	0.0233	0.2796	0.178	3.53	3.46	0.151			
06HE004	0.417	1.46	0.0437	0.546	0.347	2.08	2.02	0.346	0.327	0.415[d]	0.0662[d]
88-3033	0.390	1.56	0.0491	0.615	0.400	2.37	2.29	0.374		0.511	0.0693
91-3001	0.415	1.50	0.037	0.601	0.395	2.320	2.27	0.361		0.457	0.0584
91-3086	0.407	1.36	0.0334	0.582	0.385	2.20	2.13	0.329		0.4690	0.0563
91-3139	0.400	1.37	0.0360	0.6127	0.396	2.40	2.33	0.356		0.460	0.0595
92-3009	0.382	1.28	0.0291	0.5313	0.350	1.40	1.35	0.298			
06HE006	0.491	2.11	0.0629	0.731	0.485	2.93	2.82	0.552	0.531	0.500[d]	0.0822[d]

Sample number	SiO2 (mmol/kg) (ICP-AES)[b]	Na (mmol/kg) (ICP-AES)[b]	K (mmol/kg) (ICP-AES)[b]	Ca (mmol/kg) (ICP-AES)[b]	Mg (mmol/kg) (ICP-AES)[b]	DIC (mmol/kg) (PHREEQC)[a]	Alk (meq./kg) (Titration)[c]	S (mmol/kg) (ICP-AES)[b]	SO4-2 (mmol/kg) (IC)[d]	Cl (mmol/kg) (Ion-selective electrode)	F (mmol/kg) (Ion-selective electrode)
88-3023	0.480	2.37	0.0726	0.846	0.590	3.33	3.03	0.692		0.697	0.0728
90-3001	0.479	2.39	0.0760	0.886	0.606	3.41	3.04	0.726		0.678	0.0742
90-3027	0.459	2.32	0.0755	0.861	0.573	3.41	2.94	0.661		0.670	0.0721
91-3008	0.479	2.23	0.0575	0.810	0.554	3.46	3.10	0.642		0.602	0.0754
91-3088	0.472	2.13	0.055	0.845	0.589	3.50	3.23	0.652		0.623	0.0716
91-3124	0.455	2.08	0.0564	0.8059	0.581	3.54	3.25	0.615		0.666	0.0747
91-3125	0.451	2.05	0.0557	0.7992	0.583	3.59	3.32	0.629		0.671	0.0745
91-3126	0.469	2.15	0.0570	0.8455	0.591	3.52	3.30	0.627		0.674	0.0747
91-3127	0.469	2.14	0.0550	0.8436	0.587	3.57	3.29	0.621		0.681	0.0745
91-3128	0.465	2.13	0.0555	0.8493	0.594	3.60	3.30	0.631		0.678	0.0742
91-3129	0.464	2.18	0.0550	0.8530	0.596	3.57	3.39	0.631		0.683	0.0737
91-3138	0.458	2.13	0.0523	0.8337	0.588	3.56	3.28	0.619		0.606	0.0745
91-3213	0.454	2.19	0.0554	0.8246	0.584	3.38	3.04	0.626		0.612	0.0759
92-3011	0.448	2.16	0.0539	0.8402	0.591	2.65	2.42	0.599			
92-3012	0.410	1.72	0.0415	0.5879	0.417	3.54	3.36	0.438			
92-3013	0.476	2.09	0.0540	0.8173	0.572	3.53	3.23	0.637			
92-3014	0.466	2.04	0.0532	0.8235	0.569	3.52	3.23	0.611			
92-3015	0.468	2.08	0.0545	0.8298	0.570	3.56	3.30	0.591			
92-3016	0.477	2.05	0.0535	0.8021	0.571	1.53	1.39	0.585			
88-3024	0.440	2.50	0.0806	0.771	0.579	3.37	3.11	0.702		0.700	0.0763
91-3009	0.438	2.46	0.0617	0.755	0.545	3.40	3.16	0.633		0.602	0.0705
91-3089	0.426	2.325	0.0582	0.764	0.566	3.36	3.19	0.623		0.597	0.0684
91-3137	0.421	2.31	0.0550	0.7288	0.540	3.39	3.22	0.596		0.590	0.0724
06HE008	0.367	1.01	0.0345	0.187	0.134	1.05	1.04	0.109	0.102	0.226[d]	0.0326[d]
88-3030	0.369	1.26	0.0463	0.580	0.472	2.54	2.49	0.206		0.378	0.0340
91-3003	0.400	0.965	0.0311	0.435	0.357	1.918	1.87	0.147		0.377	0.0314
91-3081	0.393	1.04	0.0333	0.460	0.369	2.00	1.96	0.166		0.377	0.0331
91-3136	0.369	0.984	0.0326	0.4569	0.376	2.02	1.97	0.160		0.395	0.0330
92-3008	0.377	0.939	0.0275	0.4425	0.379	2.14	2.08	0.154			
88-3029	0.460	0.86	0.0427	0.440	0.347	1.89	1.74	0.145		0.330	0.0315
91-3004	0.464	0.841	0.0304	0.457	0.357	2.008	1.85	0.150		0.346	0.0305
91-3080	0.440	0.77	0.0293	0.415	0.310	1.71	1.61	0.134		0.354	0.0277
91-3135	0.447	0.817	0.0301	0.4729	0.375	2.05	1.93	0.155		0.360	0.0300
92-3007	0.408	0.730	0.0242	0.397	0.331	1.99	1.89	0.131			
88-3028	0.495	0.79	0.0391	0.343	0.277	1.58	1.42	0.117		0.273	0.0358
91-3005	0.498	0.736	0.0279	0.326	0.247	1.550	1.39	0.113		0.279	0.0372
91-3079	0.509	0.72	0.0289	0.334	0.248	1.53	1.36	0.112		0.278	0.0346
91-3134	0.487	0.691	0.0299	0.322	0.252	1.60	1.41	0.113		0.281	0.0351
88-3027	0.398	0.75	0.0368	0.280	0.275	1.42	1.36	0.084		0.253	0.0366
91-3006	0.412	0.70	0.0244	0.282	0.268	1.54	1.45	0.087		0.279	0.0352
91-3078	0.427	0.67	0.0238	0.266	0.261	1.32	1.25	0.084		0.278	0.0329
91-3133	0.402	0.700	0.0270	0.296	0.289	1.58	1.51	0.0879		0.303	0.0345
92-3006	0.398	0.585	0.0198	0.224	0.226	1.78	1.68	0.0751			
06HE003	0.441	0.800	0.0381	0.364	0.341	1.63	1.57	0.139	0.135	0.288[d]	0.0283[d]
06HE002	0.344	0.683	0.0312	0.314	0.205	0.931	0.902	0.204	0.187	0.357[d]	0.0235[d]
88-3026	0.347	0.58	0.0292	0.206	0.143	0.94	0.909	0.0661		0.228	0.0249
91-3007	0.332	0.54	0.0189	0.207	0.139	1.01	0.967	0.0753		0.241	0.0266
91-3076	0.347	0.54	0.0189	0.211	0.143	0.880	0.85	0.0699		0.238	0.0249
91-3132	0.327	0.523	0.0184	0.2148	0.145	0.928	0.898	0.0709		0.280	0.0255
92-3005	0.320	0.496	0.0172	0.2116	0.150	1.21	1.13	0.0586			
06HE001	0.324	0.448	0.0248	0.172	0.136	0.746	0.736	0.0337	0.0292	0.203[d]	0.0134[d]
91-3130	0.299	0.417	0.0170	0.1777	0.147	0.788	0.776	0.0406		0.263	0.0157

Sample number	Al (µmol/kg) (ICP-AES)[b]	Fe (µmol/kg) (ICP-AES)[b]	P (µmol/kg) (ICP-SFMS)[e]	PO4 (µmol/kg) (Spectro-photometer)	Sr (µmol/kg) (ICP-AES)[b]	Mn (nmol/kg) (ICP-SFMS)[e]	Ti (nmol/kg) (ICP-AES)	B µmol/kg (ICP-SFMS)[e]	As µmol/kg (ICP-SFMS)[e]	Ba nmol/kg (ICP-SFMS)[e]
Drinking water guidelines[h]	7.43	3.58				7291		46.3	0.133	5980
06HE010	0.326	0.0240	2.644		0.143	1.11	1.19	2.06	b.d	0.874
88-3001	b.d	b.d		2.63	0.1674		28.8			
91-3014	b.d	b.d		2.43	0.153		36.7			
91-3096	b.d	b.d		2.65	0.191		57.9			
91-3147	b.d	b.d		1.90	0.159		123			
06HE012	0.123	0.018	1.840		0.490	2.44	9.12	3.12	0.0228	6.61
88-3013	b.d	b.d		2.06	0.663		8.25			
91-3013	b.d	b.d		2.07	0.577		26.7			
91-3143	b.d	b.d		1.51	0.622		35.5			
91-3172	b.d	b.d		1.49	0.628		17.4			
91-3173	b.d	b.d		1.69	0.650		22.7			
92-3026										
06HE009	0.143	0.014	2.079		0.251	1.09	2.28	1.74	b.d	1.93
88-3002	b.d	b.d		2.14	0.1899		b.d.			
91-3015	b.d	b.d		2.79	0.155		29.5			
91-3095	b.d	b.d		2.61	0.159		20.3			
91-3146	b.d	b.d		2.98	0.171		49.8			
88-3003	b.d	b.d		1.88	0.310		b.d			
91-3016	b.d	b.d		2.70	0.226		46.8			
91-3094	b.d	b.d		2.45	0.206		11.2			
91-3145	b.d	b.d		1.81	0.239		74.0			
06HE011	0.101	0.115	1.595		0.323	2.28	3.72	2.06	b.d	3.11
88-3004	b.d	b.d		1.77	0.514		22.6			
88-3005	b.d	b.d		1.85	0.650		32.0			
88-3014	b.d	b.d		1.87	0.531		23.2			
91-3017	b.d	b.d		2.27	0.268		39.0			
91-3093	b.d	b.d		2.19	0.249		13.8			
91-3144	b.d	b.d		1.45	0.289		26.3			
88-3015	b.d	b.d		3.06	0.135		3.81			
88-3016	b.d	b.d		3.12	0.123		9.60			
88-3018	b.d	b.d		2.74	0.134		b.d			
88-3020	b.d	b.d		2.68	0.163		b.d			
91-3012	b.d	b.d		2.46	0.142		18			
91-3084	b.d	0.104		2.81	0.124		20.3			
91-3148	b.d	b.d		2.88	0.146		22.8			
88-3017	b.d	b.d		2.93	0.118		b.d			
88-3022	b.d	b.d		3.54	0.296		b.d			
88-3032	b.d	b.d		3.30	0.305		5.53			
91-3010	b.d	b.d		2.72	0.330		26.2			
88-3021	b.d	b.d		2.37	0.344		b.d			
91-3011	b.d	b.d		2.10	0.352		48.2			
91-3083	b.d	b.d		2.10	0.326		46.3			
91-3142	b.d	b.d		2.12	0.321		92.9			
06HE007	0.152	0.007	2.58		0.289	1.93	0.188	1.11	b.d	2.13
91-3082	b.d	b.d		2.29	0.303		46.1			
91-3141	b.d	b.d		2.42	0.346		48.1			
06HE005	0.408	0.009	1.81		0.227	2.64	1.06	b.d	b.d	0.837
88-3031	b.d	b.d		1.81	0.267		b.d			
91-3002	b.d	b.d		1.68	0.243		19.0			
91-3085	b.d	0.139		1.64	0.233		94.9			
91-3140	b.d	b.d		1.95	0.241		41.4			
92-3010	b.d	b.d		2.46	0.226		3.91			
06HE004	0.123	0.0119	2.20		0.445	3.09	1.17	b.d	b.d	2.53
88-3033	b.d	b.d		2.08	0.538		b.d			
91-3001	b.d	b.d		2.11	0.526		23.8			
91-3086	b.d	b.d		1.92	0.488		14.5			
91-3139	b.d	b.d		2.01	0.512		22.8			
92-3009	b.d	b.d		1.97	0.452		6.63			
06HE006	0.0764	0.00759	2.13		0.735	2.73	0.180	2.78	b.d	2.44

Sample number	Al (µmol/kg) (ICP-AES)[b]	Fe (µmol/kg) (ICP-AES)[b]	P (µmol/kg) (ICP-SFMS)[e]	PO4 (µmol/kg) (Spectro-photometer)	Sr (µmol/kg) (ICP-AES)[b]	Mn (nmol/kg) (ICP-SFMS)[e]	Ti (nmol/kg) (ICP-AES)	B µmol/kg (ICP-SFMS)[e]	As µmol/kg (ICP-SFMS)[e]	Ba nmol/kg (ICP-SFMS)[e]
88-3023	b.d	b.d		3.55	0.938		b.d			
90-3001	1.70	0.458		2.06	0.961		209			
90-3027	b.d	b.d		1.82	0.947		62.6			
91-3008	b.d	b.d		2.23	0.888		19.0			
91-3088	b.d	0.133		2.14	0.953		275			
91-3124	b.d	b.d		1.60	0.948		14.2			
91-3125	b.d	b.d		1.57	0.934		b.d			
91-3126	b.d	b.d		1.69	0.919		24.9			
91-3127	b.d	b.d		1.34	0.914		8.40			
91-3128	b.d	b.d		2.02	0.910		131			
91-3129	b.d	b.d		1.09	0.903		14.9			
91-3138	b.d	b.d		1.27	0.820		b.d			
91-3213	b.d	b.d		1.24	0.918		59.4			
92-3011	b.d	b.d		1.83	0.884		9.08			
92-3012	b.d	b.d		2.04	0.675		64.0			
92-3013	b.d	b.d		1.87	0.880		88.0			
92-3014	b.d	b.d		1.75	0.872		35.8			
92-3015	b.d	b.d		1.88	0.870		45.6			
92-3016	b.d	b.d		1.48	0.876		139			
88-3024	b.d	b.d		2.22	0.957		b.d			
91-3009	b.d	b.d		2.20	0.899		48.5			
91-3089	b.d	b.d		2.09	0.908		54.8			
91-3137	b.d	b.d		1.96	0.807		b.d			
06HE008	0.229	0.00886	2.693		0.143	1.19	0.537	2.17	b.d	1.02
88-3030	b.d	b.d		2.58	0.369		b.d			
91-3003	b.d	b.d		3.06	0.294		19.5			
91-3081	2.19	0.863		2.93	0.285		60.1			
91-3136	b.d	b.d		2.22	0.277		32.2			
92-3008	b.d	b.d		2.49	0.289		8.04			
88-3029	b.d	b.d		1.26	0.397		b.d			
91-3004				1.30	0.397		26.4			
91-3080	1.04	0.401		1.23	0.342		44.5			
91-3135	b.d	b.d		0.795	0.378		74.5			
92-3007	b.d	b.d		1.39	0.351		51.7			
88-3028	b.d	b.d		1.21	0.331		b.d			
91-3005	b.d	b.d		1.22	0.294		11.3			
91-3079	b.d	b.d		1.04	0.319		114			
91-3134	b.d	b.d		0.369	0.275		24.2			
88-3027	b.d	b.d		1.47	0.249		b.d			
91-3006	b.d	b.d		1.25	0.263		31.9			
91-3078	0.791	b.d		0.975	0.220		59.4			
91-3133	b.d	b.d		0.594	0.235		53.0			
92-3006	b.d	b.d		1.06	0.198		91.0			
06HE003	0.0956	0.00618	1.19		0.290	3.02	2.03	0.882	b.d	3.57
06HE002	0.139	0.00562	1.52		0.240	4.40	0.850	0.588	b.d	1.94
88-3026	b.d	b.d		1.38	0.180		b.d			
91-3007	b.d	b.d		1.88	0.174		26.2			
91-3076	b.d	b.d		1.93	0.167		35.3			
91-3132	b.d	b.d		1.35	0.164		16.9			
92-3005	b.d	b.d		1.23	0.177		26.7			
06HE001	0.393	0.00634	2.25		0.138	4.08	0.451	0.517	b.d	1.26
91-3130	b.d	b.d		1.87	0.126	b.d	13.0			

Sample number	Cd nmol/kg (ICP-SFMS)[e]	Co nmol/kg (ICP-SFMS)[e]	Cr nmol/kg (ICP-SFMS)[e]	Cu nmol/kg (ICP-SFMS)[e]	Ni nmol/kg (ICP-SFMS)[e]	Pb nmol/kg (ICP-SFMS)[e]	Zn nmol/kg (ICP-SFMS)[e]	Hg nmol/kg (ICP-SFMS)[e]	Mo µmol/kg (ICP-SFMS)[e]
Drinking water guidelines[h]	26.7		962	31473	1193	48.3	45886	30.0	0.730
06HE010	b.d		3.37	2.55	1.86	b.d	5.29	b.d	0.0169
88-3001									
91-3014									
91-3096									
91-3147									
06HE012	b.d	b.d	3.54	7.79	1.49		5.37	0.0130	0.0278
88-3013									
91-3013									
91-3143									
91-3172									
91-3173									
92-3026									
06HE009	b.d	b.d	3.13	7.52	1.75	b.d	13.6	b.d	0.0175
88-3002									
91-3015									
91-3095									
91-3146									
88-3003									
91-3016									
91-3094									
91-3145									
06HE011	b.d	0.115	3.54	6.78	1.79	b.d	5.86	b.d	0.0198
88-3004									
88-3005									
88-3014									
91-3017									
91-3093									
91-3144									
88-3015									
88-3016									
88-3018									
88-3020									
91-3012									
91-3084									
91-3148									
88-3017									
88-3022									
88-3032									
91-3010									
88-3021									
91-3011									
91-3083									
91-3142									
06HE007	0.02	b.d	6.06	4.56	2.57	b.d	7.31	b.d	0.0624
91-3082									
91-3141									
06HE005	b.d	0.156	7.65	2.91	1.94	b.d	b.d	b.d	0.0458
88-3031									
91-3002									
91-3085									
91-3140									
92-3010									
06HE004	b.d	0.200	4.33	5.43	3.17	0.0632	8.14	b.d	0.0753
88-3033									
91-3001									
91-3086									
91-3139									
92-3009									
06HE006	0.04	b.d	4.67	2.75	3.70	b.d	8.47	b.d	0.0818

Sample number	Cd nmol/kg (ICP-SFMS)[e]	Co nmol/kg (ICP-SFMS)[e]	Cr nmol/kg (ICP-SFMS)[e]	Cu nmol/kg (ICP-SFMS)[e]	Ni nmol/kg (ICP-SFMS)[e]	Pb nmol/kg (ICP-SFMS)[e]	Zn nmol/kg (ICP-SFMS)[e]	Hg nmol/kg (ICP-SFMS)[e]	Mo µmol/kg (ICP-SFMS)[e]
88-3023									
90-3001									
90-3027									
91-3008									
91-3088									
91-3124									
91-3125									
91-3126									
91-3127									
91-3128									
91-3129									
91-3138									
91-3213									
92-3011									
92-3012									
92-3013									
92-3014									
92-3015									
92-3016									
88-3024									
91-3009									
91-3089									
91-3137									
06HE008	b.d	b.d	4.35	4.34	1.72	b.d	6.13	<0.00997	0.0166
88-3030									
91-3003									
91-3081									
91-3136									
92-3008									
88-3029									
91-3004									
91-3080									
91-3135									
92-3007									
88-3028									
91-3005									
91-3079									
91-3134									
88-3027									
91-3006									
91-3078									
91-3133									
92-3006									
06HE003	0.0196	b.d	4.06	20.1	1.79	b.d	12.5	<0.00997	0.0167
06HE002	0.0898	0.202	4.87	7.63	2.62	b.d	29.5	<0.00997	0.0254
88-3026									
91-3007									
91-3076									
91-3132									
92-3005									
06HE001	b.d	0.378	3.58	4.47	2.98	b.d	12.5	<0.00997	0.00664
91-3130									

Sample number	Li µmol/kg (ICP-SFMS)[e]	Se nmol/kg (AFS)[f]	V µmol/kg (ICP-AES)[b]	δ^2H (MS)[g]	$\delta^{18}O$ (MS)[g]
Drinking water guidelines[h]		127			
06HE010	<0.576	b.d	0.518		
88-3001				-77.15	-10.93
91-3014					
91-3096					
91-3147					
06HE012	2.56	b.d	0.650		
88-3013				-71.86	-10.51
91-3013					
91-3143					
91-3172					
91-3173					
92-3026					
06HE009	0.599	b.d	0.493		
88-3002				-76.12	-10.87
91-3015					
91-3095					
91-3146					
88-3003				-74.05	-10.51
91-3016					
91-3094					
91-3145					
06HE011	0.906	b.d	0.520		
88-3004				-74.55	-10.71
88-3005					
88-3014				-74.23	-10.7
91-3017					
91-3093					
91-3144					
88-3015				-74.23	-10.75
88-3016				-76.15	-10.78
88-3018					
88-3020				-72.62	-10.47
91-3012					
91-3084					
91-3148					
88-3017				-76.44	-10.81
88-3022					
88-3032				-67.56	-9.83
91-3010					
88-3021				-66.89	-9.33
91-3011					
91-3083					
91-3142					
06HE007	2.90	b.d	0.591		
91-3082					
91-3141					
06HE005	b.d	b.d	1.01		
88-3031				-66.89	-9.33
91-3002					
91-3085					
91-3140					
92-3010					
06HE004	1.70	b.d	0.636		
88-3033				-65.8	-9.48
91-3001					
91-3086					
91-3139					
92-3009					
06HE006	1.44	b.d	0.648		

Sample number	Li µmol/kg (ICP-SFMS)[e]	Se nmol/kg (AFS)[f]	V µmol/kg (ICP-AES)[b]	δ^2H (MS)[g]	$\delta^{18}O$ (MS)[g]
88-3023				-64.42	-9.57
90-3001					
90-3027					
91-3008					
91-3088					
91-3124					
91-3125					
91-3126					
91-3127					
91-3128					
91-3129					
91-3138					
91-3213					
92-3011					
92-3012					
92-3013					
92-3014					
92-3015					
92-3016					
88-3024				-63.61	-9.39
91-3009					
91-3089					
91-3137					
06HE008	b.d	b.d	0.446		
88-3030				-61.37	-8.86
91-3003					
91-3081					
91-3136					
92-3008					
88-3029				-60.73	-9.42
91-3004					
91-3080					
91-3135					
92-3007					
88-3028				-69.96	-10.14
91-3005					
91-3079					
91-3134					
88-3027					
91-3006					
91-3078					
91-3133					
92-3006					
06HE003	0.744	b.d	0.506		
06HE002	0.895	b.d	0.524		
88-3026				-67.55	-10.02
91-3007					
91-3076					
91-3132					
92-3005					
06HE001	0.303	b.d	0.469		
91-3130					